EXPERIMENTAL AND NUMERICAL INVESTIGATION OF THERMOCAPILLARY EFFECTS IN THIN LIQUID LAYERS

A Dissertation
Presented to
The Academic Faculty
By
Timothy Philip Koehler

In Partial Fulfillment
of the Requirements for the Degree
Doctor of Philosophy in Mechanical Engineering

Georgia Institute of Technology

December 2007

EXPERIMENTAL AND NUMERICAL INVESTIGATION OF THERMOCAPILLARY EFFECTS IN THIN LIQUID LAYERS

Approved By:

Dr. Minami Yoda, Co-Advisor
School of Mechanical Engineering
Georgia Institute of Technology

Dr. Said Abdel-Khalik, Co-Advisor
Woodruff School of Mechanical Engineering
Georgia Institute of Technology

Dr. S. Mostafa Ghiaasiaan
Woodruff School of Mechanical Engineering
Georgia Institute of Technology

Dr. Cyrus Aidun
School of Mechanical Engineering
Georgia Institute of Technology

Dr. Roman Grigoriev
School of Physics
Georgia Institute of Technology

Dr. Karl Jacob
School of Polymers, Textile, & Fabric Engineering
Georgia Institute of Technology

Date Approved: September 17, 2007

ACKNOWLEDGEMENTS

I am sincerely grateful to all those who have made this work possible. I would like to thank my co-advisors, Dr. Minami Yoda and Dr. Said Abdel-Khalik, for their continual guidance and support. Additionally, the assistance of the remaining members of my committee, Dr. Cyrus Aidun, Dr. S. Mostafa Ghiaasiaan, Dr. Roman Grigoriev, and Dr. Karl Jacob, was greatly appreciated.

I would especially like to thank Mr. Dennis Sadowski for his endless help and support in the design and construction of the experimental apparatus. Dr. Seungwon Shin also deserves special recognition for his effort and assistance with the numerical model.

My laboratory colleagues and friends have provided me with invaluable support and camaraderie and I would like to thank them for their assistance and encouragement: Lorenzo Crosatti, Samuel Durbin, Tracie Durbin, Donavon Gerty, C.C. Hu, Charlotte Kotas, Celine Lascar, and Haifeng Li.

Most importantly, I am deeply grateful for the love and support my family. I would especially like to thank my girlfriend, Thao Le, for her love, patience, and understanding.

TABLE OF CONTENTS

LIST OF TABLES

LIST OF FIGURES

NOMENCLATURE

Symbols

A	aspect ratio
Bo	Bond number
Bo_D	Dynamic Bond number
C	Capillary number
c_p	specific heat (J/g·K)
g	gravitational acceleration (m/s^2)
h	local film height (mm)
h_o	initial film height (mm)
k	thermal conductivity (W/m·K)
M	Marangoni number
r	r-coordinate, radial direction (mm)
R	Rayleigh number
Re	Reynolds number
Pr	Prandtl number
u	velocity (m/s)
z	z-coordinate, vertical direction (mm)
R_o	film radius (mm)
T	temperature (°C)
t	time (s)

Greek Letters

α	thermal diffusivity ()
β	thermal expansion coefficient (1/°C)
ΔT	radial surface temperature difference (°C)
γ	surface tension temperature coefficient (N/(m·°C))
θ	θ-coordinate, azimuthal direction (°)
μ	dynamic viscosity ($N \cdot s/m^2$)
ρ	density (g/cm^3)
σ	surface tension (N/m)

Subscripts

c	center
m	minimum
o	initial
r	*r* component
s	surface
z	*z* component

SUMMARY

Thin liquid layers have been proposed for heat extraction and protection of the solid surfaces of divertors in magnetic fusion reactors. A number of conceptual designs for plasma-facing components (PFC) use stationary and flowing liquid layers as a renewable first wall for reactor chambers to remove heat and shield solid surfaces from damaging radiation while maintaining acceptable plasma purity levels. Such liquid-protected PFC have the potential to make fusion more commercially attractive by increasing reactor lifetimes and decreasing failure rates. The results of this research will help identify the parameter ranges for successful operation of such protection schemes.

This thesis investigates the thermocapillary behavior of axisymmetric horizontal liquid layers with initial heights from 0.27 to 3.0 mm. A negative radial temperature gradient is imposed at the bottom of the liquid layer. Experimental, numerical and asymptotic analyses were carried out for "thin" layers where buoyancy forces are negligible. A novel asymptotic solution for this axisymmetric geometry was derived from the previous two-dimensional long-wave analysis by Sen *et al*. (1982). A numerical simulation using the level contour reconstruction method was used to follow the evolution of the liquid-gas interface above an axisymmetric non-isothermal solid surface. Experimental validation of the theoretical and numerical studies was performed using silicone oils of various viscosities ($\mu = 0.48 \times 10^{-2} - 9.6 \times 10^{-2}$ N·s/m^2). Two measurement techniques, a needle contact method and laser-confocal displacement method, were employed to obtain height profiles for applied temperature differences up to 65°C. Finally, reflectance shadowgraphy was used to visualize free-surface deformation and classify flow regimes in "thick" layers, where the assumptions of

negligible buoyancy and axisymmetric flow are no longer valid. The results of this investigation will allow designers to determine operating windows for successful implementation of liquid-protected PFC.

CHAPTER 1

INTRODUCTION

A thin film is a layer of liquid of small aspect ratio, defined as the ratio of the film thickness to its lateral extent, bounded on both sides by media of different densities. Instabilities of thin liquid films can be caused by several phenomena, including gravitational forces, surface tension, van der Waals forces, and interfacial shear stresses. Although thin liquid films have been extensively studied in a wide variety of applications, the promise of using thin liquid protection in fusion reactors has motivated our research in this area. Thin liquid layers have been proposed for plasma-facing components (PFC) in magnetic fusion energy (MFE) reactors to shield solid surfaces from damaging radiation and to extract heat for use in a power cycle. In particular, liquid-protected divertors could significantly increase the power density, reactor lifetime, and efficiency of MFE reactors while enabling safe operation by minimizing plasma impurities.

Although a fusion reactor capable of producing net power has yet to be built, the international community has recognized the need for new reliable sources of energy and has dedicated a significant amount of resources to develop fusion technology. Fusion is potentially a nearly limitless source of energy free of greenhouse gases. With appropriate technological development, fusion energy should also be economically competitive with fossil fuels and fission.

This chapter introduces fusion energy and the use of liquids to protect plasma-facing components. The objectives of this investigation are given at the end of the chapter.

1.1. Background

In this section, MFE is introduced with an emphasis on the protection of plasma-facing components. Liquid-protection schemes are discussed for these components and specific criteria for safe operation are given based on previous investigations.

1.1.1. Magnetic Fusion Energy

Fusion is the most abundant source of energy in the universe. It is what powers the Sun and the stars, and could meet many of our energy needs on Earth. A fusion reaction consists of the combination two lighter atomic nuclei to produce a heavier nucleus and a large amount of energy according to Einstein's famous equation, $E = mc^2$, where E, m, and c represent energy, mass, and the speed of light, respectively. An example of such a reaction is shown in Figure 1.1, where the ions of two isotopes of hydrogen, deuterium (D) and tritium (T), fuse to form helium (He^4) and a highly energetic neutron.

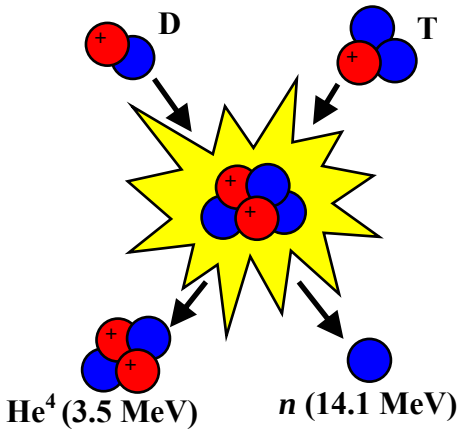

Figure 1.1: Schematic representation showing the fusion of deuterium and tritium

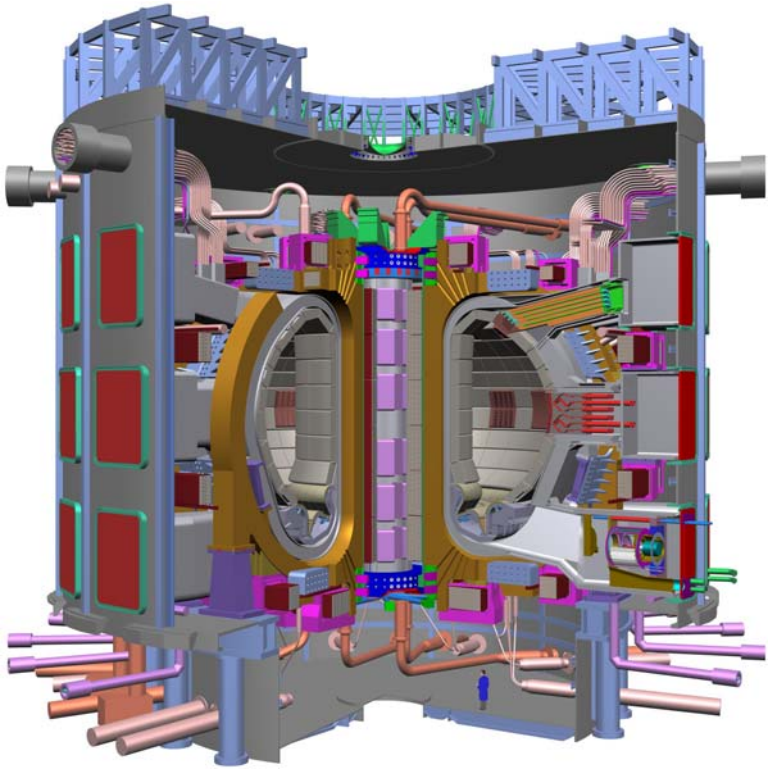

Figure 1.2: Schematic of ITER reactor with 2 m person at bottom to indicate scale

Fusion reactions occur in high-temperature and pressure plasmas and can only be sustained if enough of the resultant energy maintains, or confines, the plasma under these conditions. In the stars, strong gravitational fields confine the fusion plasma to allow reactions to continuously burn. Other methods of plasma confinement are required to harness that power here on Earth. Over the last half century, several concepts have been studied to produce controlled fusion energy. In inertial fusion energy (IFE), high-power laser beams compress and heat fuel pellets to cause a fusion reaction that occurs so quickly that the atoms cannot separate. Confinement of the plasma is thus provided by the inertia of the fuel itself and must only last long enough for the reaction to take place.

IFE reactions would have to occur several times per second to provide up to 1 GW of power in a commercial plant.

Much more work has been performed on MFE reactors, which use magnetic fields to confine the plasma at temperatures and pressures high enough to create and sustain fusion. While several concepts for MFE confinement geometries have been proposed, the most common configuration in large-scale experimental reactors is the tokamak, a reactor where the plasma is mainly confined in a toroidal field generated by external magnets surrounding the plasma. The newest demonstration of this concept is the toroidal magnetic fusion test reactor called ITER, currently under development by a consortium of researchers from the European Union, Japan, China, Korea, Russia, and the United States of America. ITER (Figure 1.2), to be built in Cadarache, France, will be capable of producing 500 MW power and will be used to demonstrate fusion as a safe and economical source of power over its projected lifetime of two decades. ITER will also investigate plasma confinement, stability, and impurity issues. Building upon the expected success and findings of ITER, a demonstration fusion reactor (DEMO) will be constructed to show that fusion energy can produce electric power on the scales necessary for a commercial reactor. The proposed reactor is expected to be approximately 15% larger than ITER and should be capable of maintaining a continuous fusion burn for several hours as opposed to the goal of 500 s in ITER. Successful operation of DEMO will prove the feasibility of commercial fusion reactors.

Toroidal reactors like ITER are complex devices consisting of several systems and components serving different purposes operating in extreme environments. This thesis focuses on the plasma-facing components (PFC) like the divertor, a high heat flux

component located along the bottom of the reactor chamber which interacts directly with the plasma. The divertor extracts impurities from the plasma, maintaining the plasma purity high enough to sustain fusion. The main source of plasma impurities is helium "ash," *i.e.*, the charged helium products from the fusion reaction. Capturing these particles in a magnetic field by depositing them upon the divertor prolongs the plasma confinement time. The divertor also extracts heat from the plasma in the form of high-energy neutrons exiting the plasma randomly or energetic impurity removal, contributing nearly 15% of the heat used in the power cycle. Divertors are hence subject to extremely high heat fluxes in excess of 10 MW/m^2.

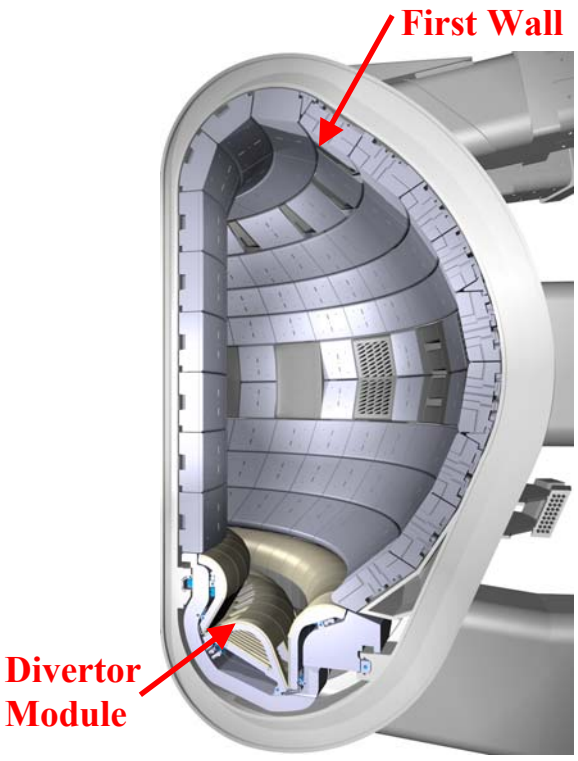

Figure 1.3: Cross-section of the ITER reactor chamber with solid first wall and divertor.

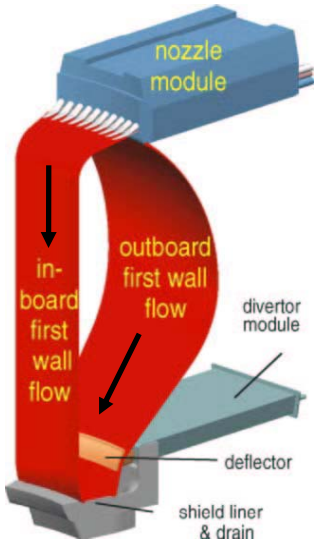

Figure 1.4: Proposed liquid-protection scheme utilizing a flowing liquid sheet along reactor chamber wall and divertor surfaces, from Nygren, *et al*. (2004) [38]

In current divertor designs, particles are deposited upon a solid metal surface in direct contact with the plasma, as shown in Figure 1.3. Radiation, erosion, and thermal stresses are major issues in divertor design and significantly limit reactor lifetimes. A economically viable commercial reactor should operate for at least 30–40 years, a period much longer than current divertor design lifetimes (~20 years). In addition, divertors must be capable of extracting heat with a high power conversion efficiency [33]. To achieve these requirements, recent conceptual designs have proposed using liquid metals and molten salts to protect the solid surfaces of PFC from the damage and degradation due to soft radiation. These designs use stationary and flowing thin liquid films to provide adequate protection of the solid surface and more efficient heat removal. An example of a proposed liquid-protected reactor chamber is shown in Figure 1.4, where the entire reactor chamber is protected by a flowing liquid sheet. Here, a molten salt sheet is injected through the nozzle module from which it flows along the walls and to the

divertor where it is pumped to a power conversion cycle and a filtration system to recover tritium before being recirculated back to the reactor chamber.

1.1.2. Liquid Protection of Plasma-Facing Components

The idea of protecting PFC with liquids is nearly 25 years old [80]. However, two research programs have recently revived interest in the implementation of liquid protection. The Advanced Power Extraction (APEX) and Advanced Limiter-Divertor Plasma Facing Systems (ALPS) programs have performed studies on liquid-protected PFC and plasma surface interactions [1, 34, 38]. The advantages of this concept lie in the liquid protecting the solid surfaces from erosion, radiation, and thermal stress, while extracting the useful incident heat for high power conversion efficiency.

Liquid protection schemes for fusion reactors propose to use renewable liquid first walls which also eliminate the need for a secondary coolant and the additional infrastructure required to handle this secondary coolant to cool the plasma-facing components. In a typical solid divertor, the heat absorbed at the divertor surface is removed by a coolant and transferred to a standard power generation cycle. However, in a liquid-protected divertor, the liquid layer can both act as the coolant and protect the underlying solid components from thermal stresses by transferring heat directly to the power cycle.

Liquid protection can also aid in fueling the fusion reaction which requires both deuterium and tritium. Deuterium, a stable isotope of hydrogen, is naturally abundant, making up 1 part in 5000 of the hydrogen in seawater. Tritium, on the other hand, is a radioactive isotope of hydrogen with a half-life of 12.3 years. Thus, breeding tritium,

preferably on-site to minimize handling issues, is required to generate fuel for fusion reactors. Tritium is most commonly generated by bombarding lithium with energetic neutrons. Using a lithium-containing molten salt as the divertor coolant would have the additional advantage of breeding the tritium required to run the reactor.

Liquid metals and molten salts have been considered in the APEX study for a liquid first wall and divertor in a fusion reactor design incorporating liquid wall technology [38] with liquid layer thicknesses ranging from 0.5 mm to 2 cm. Plasma interactions with walls of liquid lithium (Li), gallium (Ga), tin-lithium (Sn-Li), and molten Flibe (Li_2BeF_4) have been investigated with an emphasis on sputtering, evaporation, retention and release of incident particles to place operational limits on the respective fluids [5]. Two-dimensional numerical simulations were used to study plasma impurity levels derived from evaporation of liquid walls [49]. Maximum allowable surface temperatures for several candidate liquids were established based on evaporation limits. Other recent studies have actually tested plasma-facing liquid surfaces in experimental reactors. Experiments were conducted at the Princeton Plasma Physics Laboratory using a Li pool limiter with an average depth of 0.5 cm [31, 32]. The experiments demonstrated that plasma-facing liquid surfaces can improve plasma performance in terms of reducing impurities, increasing the electron temperature, and decreasing plasma resistivity. These studies claim that energy confinement times were improved by up to six times. A Li capillary pore system (Li-CPS) was investigated in the Russian T-11M reactor and was determined to be stable under pulsed and steady-state heating loads [26].

Another key issue regarding liquid-protected PFC is the possibility of dry-spot formation in regions of high temperature gradients. Spatial non-uniformities in wall and free-surface temperatures can create surface tension gradients in thin liquid films and thus induce instability in the liquid layer that could lead to rupture. Shin *et al*. (2005) used a two-dimensional level contour reconstruction method to follow the evolution of the free surface above a non-uniformly heated surface for a "non-flowing" thin liquid film [65]. A set of generalized non-dimensional charts for the maximum allowable surface temperature gradient were developed and applied to various candidate coolants including Li, lithium-lead (Li-Pb), Flibe, Sn, and Ga.

1.2. Objectives

The goal of this doctoral thesis is to understand the behavior of thin liquid layers exposed to a non-uniform surface temperature using experimental and numerical studies. The three main objectives are to:

1. Understand the influence of the important dimensionless parameters (*i.e*., the film aspect ratio A, capillary number C, and Bond number Bo) on the steady state free-surface profile of thin axisymmetric liquid layers on a horizontal flat solid surface bounded above by ambient air and subject to an axisymmetric radial temperature difference. The liquid layer is considered to be an open cylinder constrained by a wall at R_o, the radial/lateral extent of the liquid film. These dimensionless parameters are defined as follows:

$$A = \frac{h_o}{R_o},\ C = \frac{\gamma_o \Delta T_s}{\sigma_o} A,\ Bo = \frac{\rho_L g h_o^{\,2}}{\sigma_o} \qquad (1.1)$$

Here, ΔT is the temperature difference; σ_o is the surface tension; γ_o is the surface tension temperature coefficient; ρ_L is the liquid density; h_o is the initial height; p is the pressure and g is the gravitational acceleration. The properties of the liquid therefore determine the free-surface geometry.

2. Derive and validate the axisymmetric asymptotic solution for a thin liquid layer and numerical simulation predictions for a thicker liquid layer with a spatially varying surface temperature by comparing the steady state free-surface profiles to experimental data.
3. Investigate flow patterns for liquid layers of higher aspect ratio when the free surface becomes three-dimensional and thereby determine the limits on the validity of the thin-film approximation The important parameters for thicker films are the Marangoni number M and dynamic Bond number Bo_D, defined as follows:

$$M = \frac{\gamma_o \Delta T_s h_o}{\alpha \mu} A, \qquad Bo_D = \frac{\rho g \beta h_o^2}{\gamma_o} \tag{1.2}$$

Here μ, α and β are the viscosity, thermal diffusivity, and thermal expansion coefficient of the liquid, respectively.

This work will contribute to our fundamental understanding of thin liquid layers subject to a temperature gradient and provide design guidance for liquid-protected PFC.

The remainder of this thesis is organized as follows. A review of relevant literature regarding thermocapillary flows in thin liquid layers is presented in Chapter 2. Chapter 3 describes of the experimental apparatus and investigation techniques used in these studies. The axisymmetric thin film theoretical and numerical investigations are detailed in Chapter 4. Results from all studies characterizing the behavior of liquid layer subjected to non-uniform heating are presented and discussed in Chapter 5. Chapter 6

summarizes the conclusions of this research and suggests future work in thermocapillary flows for fusion energy. Details of the thermocouple calibration are explained in Appendix A. The error analysis, experimental repeatability, and axisymmetry are examined in Appendix B. Finally, Appendix C contains additional experimental and numerical results.

CHAPTER 2

LITERATURE REVIEW

Thermocapillary flows in liquid layers can arise in a wide variety of problems, and have thus been studied quite extensively. Past applications of thermocapillary flows include crystal growth, arc-welding, and thin-film heat transfer. There has, however, been little consideration of thermocapillary effects in liquid-protected plasma-facing components.

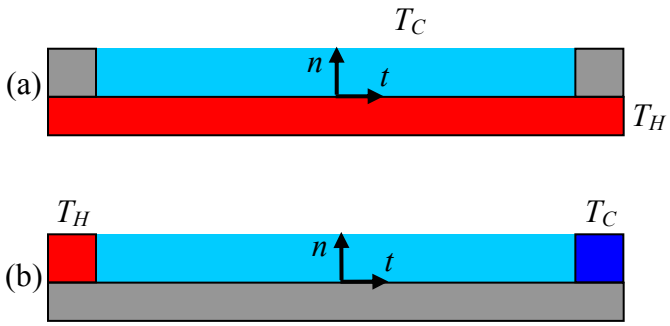

Figure 2.1: Two-dimensional test configuration schematics used to study (a) Marangoni convection and (b) thermocapillary convection. Colors indicate heated (red), cooled (dark blue), and adiabatic (grey) walls. The liquid film is shown in light blue.

Common to all these applications is a liquid-gas interface subject to an externally-imposed temperature difference, ΔT. The resulting spatial gradient in surface tension must be balanced by the shear stress at the interface, creating a flow within the liquid layer. This phenomenon is known as the Marangoni effect [56]. Thermocapillary instabilities can appear when ΔT is either applied normal [Marangoni convection, Figure

2.1(a)] or parallel [thermocapillary convection, Figure 2.1(b)] to the interface. This chapter reviews the pertinent literature on thermocapillary flows. [12]

2.1. Marangoni Convection

When a liquid layer is heated from below and cooled from above, a flow may be driven by thermocapillary stresses whose magnitude is characterized by the Marangoni number, $M = \gamma_o \Delta T_\perp h_o / \mu\alpha$, where $\Delta T_\perp$ is the imposed temperature difference along *n*, as shown in Figure 2.1(b). Thermocapillary flows in this situation are often accompanied by buoyancy effects, characterized by the Rayleigh number $R = \rho g \beta_o \Delta T_\perp h_o^3 / \mu\alpha$, where β_o is the thermal expansion coefficient. The ratio of buoyancy to thermocapillary forces is characterized by the dynamic Bond number, $Bo_D = R/M$. This section describes previous research on uniformly-heated thin films for the cases when thermocapillary effects are dominant, or $Bo_D < 1$. Although Marangoni convection occurs in a geometry that is inherently different from that studied in this thesis, the flow within a single cell resembles the basic flow in axisymmetric thermocapillary convection. In addition, because the experimental configuration considered in this thesis heats the liquid layer from below (albeit in a non-uniform fashion), Marangoni convection may occur in the flows studied here.

The onset of cellular Marangoni convection was first experimentally observed in 1900 by Bénard [6] in uniformly-heated thin films. These observations and the stability analysis of Lord Rayleigh [47] incorrectly attributed the formation of hexagonal convective cells to buoyancy and gave a critical minimum temperature gradient across the fluid layer required for cell formation. In 1956, Block [7] identified convective cells

formed for temperature gradients well below Rayleigh's criterion and concluded that surface tension must also play a role in the formation of these cells. Pearson [41], who extended the analysis of Rayleigh, showed that an instability mechanism based on thermocapillary forces could also drive cellular convection. Pearson's model considered a hot spot on the liquid surface with thermocapillary-driven flow away from this spot towards the surrounding cooler liquid. This radial outflow is balanced by a vertical upflow of warm fluid from the bottom of the liquid layer towards the hot spot on the free surface. The resultant flow is then sustainable if the temperature gradient in the liquid layer is large enough to balance conductive cooling. Though Pearson's model neglected deformation of the fluid interface and considered only surface forces, it is nevertheless the first description of Marangoni convection.

Our understanding of Marangoni convection was improved upon by adding gravitational effects [37] and free-surface deformation [57] to Pearson's model,. The results of independent experimental investigations [28] are in good agreement with the predictions of these theoretical analyses. In silicone oil liquid films of h_o = 0.72 – 2.57 mm, the onset of cell formation occurred at M = 7.17 – 76.8, respectively. In addition, Scriven and Sternling [57] noted that the kinematic boundary condition at the liquid-gas interface requires an up- and downflow in the shallow and deep regions (compared with the average height), respectively, of the thin film, where the return flow is driven by the resultant pressure gradient. This flow is hence quite distinct from buoyancy-driven flows where there is upflow in the deeper regions of the film.

The physical mechanism that leads to the onset of Marangoni convection is a destabilizing thermocapillary stress that is caused by either long-wave or short-wave

disturbances as shown by linear stability analyses [21, 50, 71]. Long-wavelength disturbances arise when the temperature field within the liquid layer is modified by free-surface deformations, while short-wavelength disturbances occur when interfacial perturbations are damped by diffusion. Thus, the stability of thin films is strongly dependent on the Bond number *Bo* [50] and for extremely thin liquid films (thickness below several hundred Å), the growth of free-surface perturbations can lead to film rupture [71]. Marangoni convection has been studied more recently using nonlinear stability analyses [4, 13, 81]. Nonlinearities have been shown by Williams and Davis [81] to accelerate long-wavelength film rupture and reduce the preferred wavelength. Burelbach, *et al*. [9] found that rupture is delayed and accelerated by thermocapillary effects in condensing and evaporating films, respectively. Oron, *et al*. [39] reviews theoretical studies on the long-scale evolution of thin liquid films while Davis [14] provides a thorough review of experiments on Marangoni convection for water and silicone oil films of $M = 0 - 200$ and $Pr = 7 - 500$.

2.2. Thermocapillary Convection

Thermocapillary convection refers to the flows that result in a thin liquid layer with a temperature difference along the liquid-gas interface. Typically, the temperature difference along t at the liquid surface, denoted by ΔT_S, is imposed by placing the liquid layer between hot and cold end walls as shown in Figure 2.1(b). Unlike Marangoni convection in uniformly heated thin films, surface temperature perturbations are not required to initiate thermocapillary flows. The imposed surface temperature gradient, regardless of magnitude, is the driving mechanism. There is hence no critical

temperature difference or Marangoni number in thermocapillary convection—thermocapillary convection occurs at any nonzero temperature gradient.

The literature on thermocapillary convection is mainly motivated by crystal growth applications, where thermocapillary flows affect the homogeneity and quality of the crystal [53]. Most of the relevant work has thus considered the liquid bridge or float-zone configuration, or simplified the problem to a flow in a rectangular slot, although a few studies have considered annular geometries. Very little is known about axisymmetric discs of fluid in which the hot end wall effects are eliminated.

The basic thermocapillary convective flow consists of a steady, unicellular cell and is fairly robust regardless of the geometry of the film. Transitions from this basic state occur for temperature differences exceeding a certain magnitude, and many studies have been interested in classifying the flow regime transition. For small dynamic Bond numbers ($Bo_D < 0.2$), a transition from the basic flow to one characterized by hydrothermal waves occurs. For larger Bo_D, steady multi-cellular or oscillatory will arise when a critical temperature difference is exceeded. This section reviews studies of thermocapillary convection in thin liquid layers.

2.2.1. Steady Unicellular Thermocapillary Convection

The basic state of a thin film exposed to an external temperature gradient is a single, steady-state convective cell driven by the thermocapillary stresses along the fluid-gas interface. In many theoretical investigations, the liquid is confined in an infinitely long rectangular slot with hot and cold end walls as depicted in Figure 2.1(b). Sen and Davis [58, 59], for example, use an asymptotic ($A \rightarrow 0$) theory to approximate the

interface shape and velocity profile within the liquid layer for steady solutions. In this investigation, long-wave evolution equations accounting for variable surface tension and are derived for the case where gravitational effects are negligible and the core flow is treated separately from the flow near the end walls. The core flow is found to be similar to that inside a Marangoni convection cell, where the surface-tension driven flow drives liquid from the hot wall toward the cold wall, deforming the liquid-gas interface and creating a hydrostatically driven return flow along the bottom of the liquid layer. The end walls form either one or two recirculating cells in the liquid, depending on whether the liquid at the end walls has a zero contact angle or a pinned contact line, respectively.

Other heating configurations have been studied for the purpose of investigating thermocapillary-driven rupture of thin films. Experimentally, the liquid film is typically contained between cold end walls with heating applied from above [46] or below [10]. Most of the theoretical studies assume that the film is infinite with a temperature difference applied along the free surface [72, 82]. Other analytical investigations consider liquid metal films heated at the free surface by radiation [22] and pulsed laser beams [2, 3]. In these studies, the conditions for steady, unicellular flow to occur were determined in terms of the operating M and Bo for liquids of various Pr.

The theoretical investigation performed by Tan, *et al*. [72] studied the effects of van der Waals forces, surface tension, and gravity on the local film deformation in steady flows. A two-dimensional nonlinear long-wave evolution equation was used to track the liquid-gas interface of 0.1 μm films of water ($M = 2.36$, $Pr = 7$, and $Bo = 1.31\times10^{-9}$), sodium ($M = 3.74\times10^{-3}$, $Pr = 0.005$, and $Bo = 4.96\times10^{-10}$) and silicone oil ($M = 3.74\times10^{-3}$, $Pr = 48$, and $Bo = 4.52\times10^{-9}$) subjected to a spatially periodic temperature gradient. It

was also found that steady continuous flow in the thin liquid layer was attainable only below a critical temperature gradient. The theoretical model of Tan, *et al.* was validated by Burelbach, *et al*. [10]. Their film thickness measurements using a needle contact technique for steady flows in silicone oils (h_o = 0.125 – 1.684 mm, M = 6 – 4100, Pr = 480, and Bo = 120) on a wide rectangular plate exposed to a non-uniform spatial temperature gradient from below were in good agreement with the theoretical predictions for films of thickness less than 0.5 mm. For thicker films, *i.e.* $h_o > 0.5$ mm, the experimental data were not in agreement with the theory; this discrepancy was attributed to inertial effects becoming non-negligible as the initial height increases. Burelbach, *et al.* also reported that films of $h_o > 1.0$ mm could not be ruptured although the steady unicellular thermocapillary flow remained robust for the liquid heights studied.

The behavior of thermocapillary flows leading to film rupture is well-understood for two-dimensional rectangular geometries; axisymmetric liquid layers have not been as thoroughly investigated, however. Experimental investigations in axisymmetric geometries have typically used molten metals such as lead and gallium ($Pr << 1$) and in Reference [46], for example, suffered from inverse thermocapillary convection. The inverse thermocapillary flow was explained by surface contamination from impurities in the liquid metal which caused an inverse surface tension dependence on temperature. Other investigations have considered annular geometries, but this geometry requires a meniscus or pinned contact line at the inner radial end wall to prevent film rupture. The asymptotic studies of Vrane [79] on annuli did produce rupture for a non-zero slope contact line at the inner heated wall, however, the rupture did not occur at the hot end

wall. Instead, the boundary condition imposed at the end wall forced rupture to appear at a location inside the annulus.

2.2.2. Steady Multi-Cellular Thermocapillary Convection

As the temperature difference across the liquid layer (*i.e.*, M) exceeds a critical value, the steady thermocapillary flow is no longer stable and transitions to other flow regimes. The stability of thermocapillary flows was first investigated by Smith and Davis [68-70] in infinite thin films with negligible buoyancy effects. In the study, an instability mechanism called hydrothermal waves was discovered to exist in thin films as a temperature disturbance wave that propagates through the liquid film. The direction of propagation of the hydrothermal waves was found to depend on Pr for return flow. Flows of intermediate Pr, like those studied in this thesis, were shown to produce hydrothermal waves that travel obliquely to the basic flow. Davis [14] reviews hydrodynamic stability analyses for planar liquid layers with externally applied temperature gradients.

Riley and Neitzel [48] verified the existence of hydrothermal waves in rectangular channels and suggested that they only occur in more shallow layers ($Bo_D < 0.22$). Laser-Doppler velocimetry (LDV), shadowgraphy, particle tracking, and thermography were used to determine the flow structure in silicone oil layers (30 mm $\times$ 50 mm) of 0.75 mm $< h_o <$ 2.5 mm. The study reported four distinct flow regimes, shown in Figure 2.2 for M *vs.* Bo_D: steady, unicellular flow, hydrothermal waves, steady, multi-cellular flow, and oscillatory flow. Steady, multi-cellular flow and oscillatory flow occurred for thicker layers (*i.e.*, $Bo_D > 0.22$). The Bo_D represents the ratio of thermocapillary to buoyancy

effects and this study shows that as buoyancy effects become more important, the assumption of negligible gravity in the stability analysis of Smith and Davis becomes invalid and thus the appearance of hydrothermal waves cannot be expected.

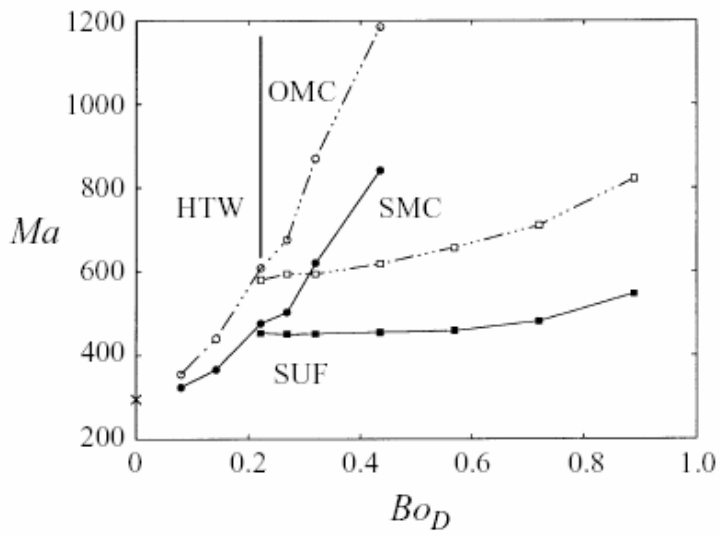

Figure 2.2: Transition map of experimental results from Riley and Neitzel [48] where $Ma = M$. The data is shown for Ma calculated using $\partial T/\partial x$ between the end walls (open symbols) and $\partial T/\partial x$ in the "core" region of the flow. Regimes are denoted as steady, unicellular flow (SUF), hydrothermal waves (HTW), steady, multi-cells (SMC), and oscillatory multi-cells (OMC).

Experimental investigations in rectangular [8, 12, 15, 20, 27, 48, 77] and annular [17, 19, 23, 29, 30, 53] liquid films of 1 mm $\leq h_o \leq$ 10 mm have been conducted to study the stability of thermocapillary flows. The transition from steady unicellular flow to more complex flows was first observed by Kirdyashkin [27] in a two-dimensional rectangular ethyl alcohol layer for which velocity and temperature profiles were acquired inside the liquid layer via visualization of suspended aluminum particles in the liquid and an intrusive thermocouple probe, respectively. These measurements were in good

agreement with analytically-derived profiles for return flow and indicated that for flows below a critical M, the flow is steady and unicellular, but become more complex when this critical M is exceeded. Kirdyashkin's observations, however, disagreed with the studies of Smith and Davis because the basic flow transitioned first to steady multi-cellular convective rolls rather than hydrothermal waves. Kirdyashkin was among many other researchers [12, 15-17, 20, 53, 77] to experimentally observe a transition from steady, unicellular flow to steady, multi-cellular flow instead of to hydrothermal waves, as predicted by Smith and Davis.

Early studies in rectangular geometries were very interested in experimentally verifying the transition of steady, unicellular flow to hydrothermal waves. However, this was rarely the case, as observed in the experiments of Villers and Platten [77], conducted on acetone layers of $h_o > 9$ mm for $8 \times 10^3 < M < 2.2 \times 10^5$. Here the transition was first to steady, multi-cellular structures and two explanations were given for the disagreement between theory and experiment; buoyancy in the liquid layer acts against the formation hydrothermal waves and the end walls, which were not included in the theoretical work of Smith and Davis, change the preferred instability mode. In a rectangular slot (200 mm $\times$ 10 mm), Daviaud and Vince [12] used shadowgraphy to visualize thermocapillary convection in silicone oil layers of 0 mm $< h_o <$ 10 mm. Above a critical M, the appearance of stationary rolls occurred for $h_o > 2.8$ mm and was attributed to gravitational effects.

De Saedeeleer, *et al*. [15] used LDV to characterize the flow structures in the basic flow as well as in the instability modes for rectangular liquid layers of 10 mm width and lengths up to 74 mm. In all their experiments, the decane layer first transitioned to

steady, multi-cellular rolls prior to the initiation of oscillatory flow. Gillon and Homsy [20] also used LDV to characterize the convective flow in a rectangular (1 cm × 3.8 cm) cavity filled with silicone oil (Pr = 8.4) of h_o = 6.8 mm. The temperature difference ΔT across the short dimension of the cavity was varied between 0.3°C < ΔT < 20°C, corresponding to $6 \times 10^3 < M < 4.2 \times 10^5$. The transition from steady, two-dimensional flow to steady three-dimensional convection was found to occur at $M = 1.5 \times 10^5$. Schatz and Neitzel [51] summarize many of the above experiments and other work performed on thermocapillary instabilities.

The mechanism that drives the transition to the steady, multi-cellular flow remains unknown; localized instabilities due to buoyancy and end wall effects are often suggested as possible causes for instability. Mercier and Normand [35] claim that a thermal boundary layer at the free surface affects the vertical temperature profile in the upper portion of the liquid layer where the velocity profile is nearly linear. The liquid layer would then be unstable to thermal perturbations that would develop into stationary longitudinal counter-rotating cells as described by Smith and Davis for linear flow. However, other studies [15, 53, 77] have shown that the stationary cells are co-rotating. Shevtsova and Legros [62] suggest that thermal boundary layers along the end walls have also been thought to affect the stability of the unicellular flow. Perez-Garcia *et al*. [43] further explain that the thermal boundary layer at the end wall acts as a perturbation to the basic flow and may spread throughout the layer disrupting basic flow.

Side walls are inherent to experimental studies in rectangular geometries and thus many researchers have conducted investigations in annuli to remove the effects of sidewalls. Schwabe, *et al*. [53] heated the inner wall and cooled the outer wall of an

annular slot to study thermocapillary instabilities using shadowgraphy. Multi-cellular stationary rolls were also observed for $M = 690$ in a layer of $h_o = 2.0$ mm. Garnier and Chiffaudel [19] discuss the results of silicone oil (1.2 mm < h_o < 1.9 mm) experiments in an annulus of 8 mm inner diameter and 135 mm outer diameter. Hoyas, *et al*. [23] investigated silicone oil films ($0.019 < A < 0.030$) in an annulus of 63.5 mm radial extent using a numerical analysis and experiments. Their experimental shadowgraph images showed good qualitative agreement with the numerical simulations, capturing flow patterns appearing in the following sequence as ΔT increases: stationary co-rotating rolls, flower-like standing waves, oscillating flower-like structures, and spiral traveling waves. Other investigations [18, 42, 54, 55] observed the same types of flow structures in annular geometries. Peng, *et al*. [42] suggests that the steady multi-cellular flows are an effect of thermal boundary layers at the end walls. The vertical temperature profile near the end walls develops an inverse gradient as a result of buoyancy-driven flows carrying fluid of lower temperature to regions near the free surface of a higher temperature. This explanation is very similar to that of Perez-Garcia *et al*. [43] for rectangular geometries. The studies of Schwabe, *et al*. [54, 55], however indicate that buoyancy cannot be a factor in the development of the steady, multi-cellular rolls because they also appear in microgravity environments.

2.2.3. Oscillatory Multicellular Thermocapillary Convection

The steady thermocapillary flow eventually transitions to an oscillatory state as the temperature difference is increased beyond a second critical value, as shown by the

experiments of Riley and Neitzel [48]. Many other studies have observed this transition in rectangular [8, 12, 15, 20, 27, 48, 77] and annular [17, 19, 23, 29, 30, 53] geometries.

Braunsfurth and Homsy [8] performed experiments similar to Reference [20] using particle tracking velocimetry on an acetone (Pr = 4.44) layer, and discovered that for $M > 6.8 \times 10^5$ oscillatory flow appears in the liquid layer, possibly due to an eddy near the free surface that oscillates in both size and strength. Three-dimensional numerical investigations using the volume-of-fluid method have been performed by Li, *et al*. to simulate thermocapillary flows in annuli for silicone oil [29] and silicon melt [30] layers. The layers investigated were cooled at the inner wall and heated at the outer wall. In [29], thermocapillary flow in liquid layers (1 mm < h_o < 17 mm) contained in annuli (20 mm inner diameter, 40 mm outer diameter) became oscillatory when M exceeded critical values ranging from 4×10^4 to 6×10^4. Two oscillatory flow patterns were observed depending on the aspect ratio. For $A < 0.075$, roll cells that traveled radially in "fan-blade-shaped" sections were formed, while thicker layers were characterized by spokes that traveled azimuthally. For the studies of low-Pr silicon melt layers [30], the numerical simulations neglected gravity to remove the influence of buoyancy. The annular layers investigated were had an inner diameter of 15 mm and outer diameter of 50 mm with depths of h_o = 1.5, 3 and 8 mm. The critical M for transition to oscillatory flow depended on the liquid depth and vertical heat flux. Each layer depth exhibited a different pattern of oscillatory flow. For h_o = 1.5 mm, hydrothermal waves were dominant and traveled azimuthally, while straight spoke-like patterns with standing wave oscillations appear for h_o = 8 mm. A combination of these patterns occur when h_o = 3 mm.

There has also been a large interest in cylindrical liquid layers of $A = 1$ especially regarding the transition to oscillatory flow for applications in material processing in reduced-gravity environments. In these studies [25, 66, 67], free-surface deformation is neglected due to the large aspect ratio. Kamotani *et al*. [25] maintained $A = 1$ while varying the diameter of the liquid layer from 1.2 to 3.0 cm. The critical M for the initiation of oscillatory flow depends on the diameter, indicating that using M is insufficient to predict oscillatory flow. The authors claim that free-surface deformation is partially responsible for the transition to oscillatory flow and therefore suggest a non-dimensional parameter characterizing the surface deformation in a liquid layer. However, Sim and Zebib [66] used both non-deformable flat and curved free surfaces in two- and three-dimensional numerical simulations and obtained time-periodic flows that varied with the surface curvature. Azimuthal waves generated oscillations in thermocapillary convection and therefore only three-dimensional simulations are capable of predicting oscillatory flows. This conclusion was further supported by a subsequent study [67] in which the two-dimensional model was improved to allow for surface deformation, and still observed no oscillatory flow.

There is very little existing literature on axisymmetric geometries other than the studies on annuli discussed in the previous section. Ezersky, *et al*. [16, 17] have performed the only experiments to our knowledge on a axisymmetric disc of liquid—a geometry that has only one (outer) end wall. In these studies, hydrothermal waves were studied using shadowgraphy to determine the frequency of hydrothermal and surface waves. For their 100 mm diameter (2 mm $< h_o <$ 8 mm) liquid layers, Ezersky *et al*. determined the frequency of surface waves as a function of the temperature difference

across the liquid layer, and found that liquid layers of $h_o < 3.0$ mm underwent a sequence of transitions from steady, unicellular flow to steady, concentric rolls, and then to traveling waves. The critical M at each transition, however, was not characterized. Film rupture was not reported for any of these experiments.

In summary, the transitions of thermocapillary flows are well known for rectangular and annular geometries, but little is known about the stability of axisymmetric discs of liquid. There has been little comparison of the transitional behavior and resulting flow patterns in axisymmetric thermocapillary flow with those observed in other geometries. In addition, the mechanism behind the initiation of steady, multi-cellular flow regimes is still not entirely known. Given the marked role of end walls in rectangular and annular geometries, comparison of the results in this thesis for a circular film of liquid, which has only one outer end wall, with the results for annular geometries with two (inner and outer) end walls may give insight into how the presence or absence of end walls affect the flow regimes and transitions in thermocapillary flows.

CHAPTER 3

EXPERIMENTAL APPARATUS AND PROCEDURE

The experiments to characterize thermocapillary flows in non-uniformly heated thin liquid layers are described in this chapter. The following sections discuss the design of the experimental test section as well as the shadowgraph and film height measurement systems. The components of each system are detailed, followed by a description of the operating procedure.

3.1. Experimental Test Apparatus

This section describes the table-top experimental apparatus used to impose a radial temperature gradient on a thin axisymmetric liquid layer. The heating and cooling systems, the support structure, and the temperature measurement system are detailed.

3.1.1. Experimental Setup

An experimental test section was designed and constructed to create a temperature radial temperature gradient across a thin axisymmetric liquid layer. The cylindrical polar coordinate system for these experiments is defined with the origin located at the center of the test section as shown in Figure 3.1. The radial coordinate r is along the radius of the liquid layer, the axial coordinate z is normal to and measured from the solid surface at the base of the liquid layer, and the azimuthal coordinate $\theta \equiv 0$ is defined to be along the radial line of thermocouples (TCs) embedded below the solid surface. The liquid layer has a radial extent $R_o = 76.2$ mm and a height h_o ranging from 0.5 mm–3.0 mm.

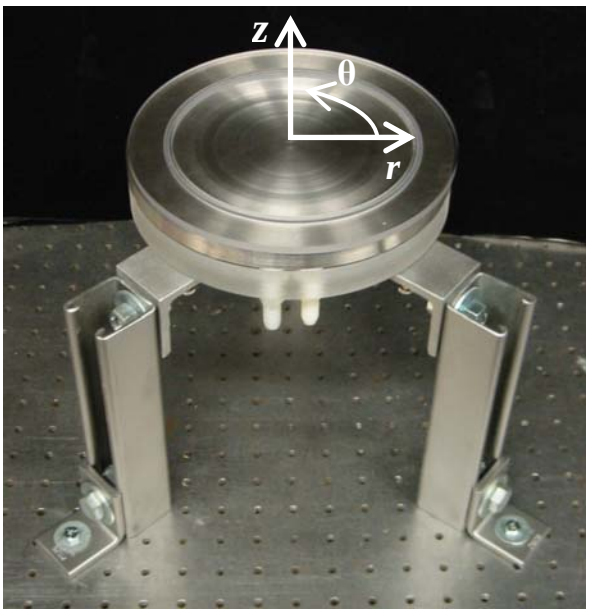

Figure 3.1: Photograph of test section showing cylindrical coordinate system

Figure 3.2 shows the experimental setup. The liquid layer, which rests upon a 203 mm diameter stainless steel plate, is contained by an acrylic ring of inner radius R_o = 76.2 mm. Table 3.1 lists the hardware components used in this experimental setup. The steel plate lies on top of a polycarbonate cooling channel; the acrylic ring, the steel plate and the cooling channel are held together by eight stainless steel C-clamps evenly spaced around the perimeter of the experimental apparatus. The clamps apply pressure on O-rings embedded in the containment ring and the cooling channel that seal the system against leaks. The entire apparatus rests atop three Unistrut support posts (B) that can be leveled using #8-32 threaded inserts of ½" length.

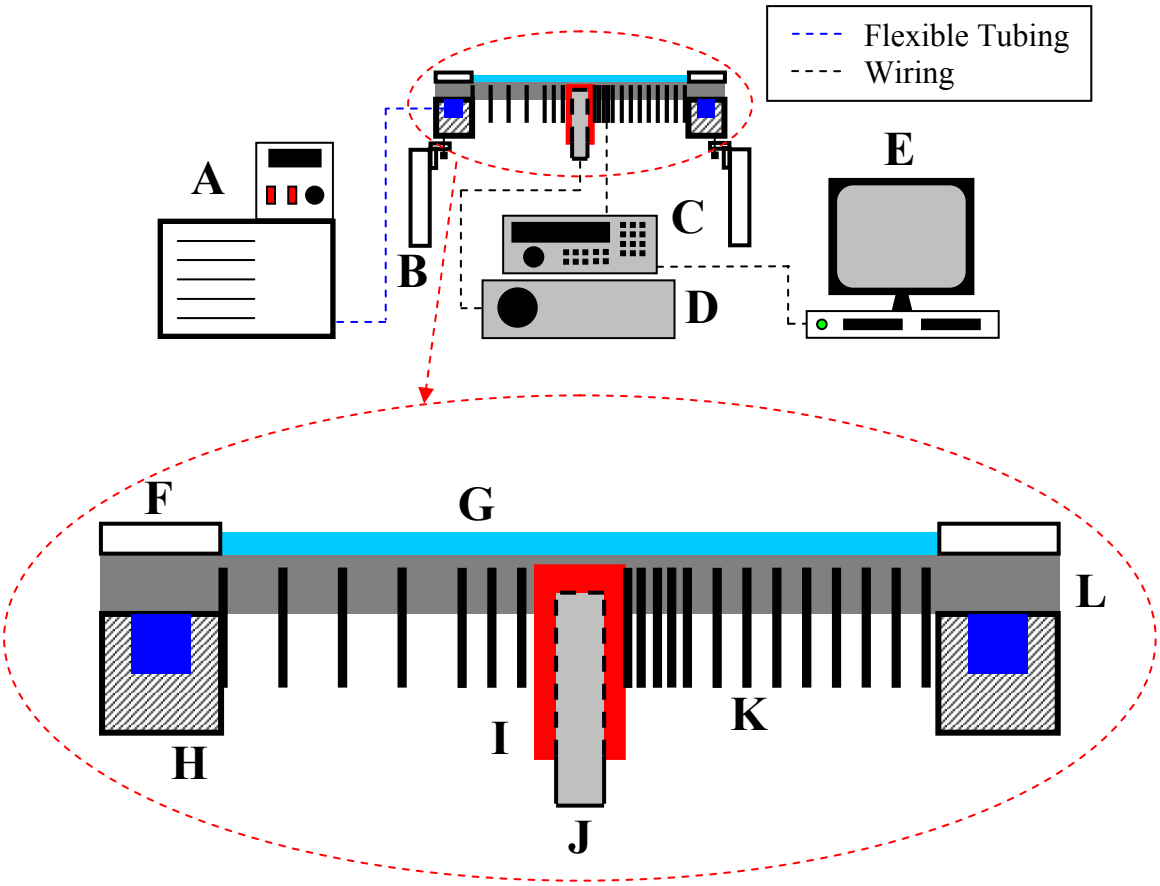

Figure 3.2: Schematic of experimental setup and closeup of test section.

The temperature profile at the upper surface of the steel plate is controlled by heating the plate at its center and cooling along the perimeter of the liquid layer. The plate is heated at the center by a 400 W maximum capacity electrical cartridge heater (J) encased in a 19 mm diameter copper plug (I) located 2.5 mm below the upper surface of the steel plate. A VARIAC transformer (D) supplies power to the heater and is monitored by a multimeter (Fluke 77) that measures both the voltage across and the current passing through the heater. The perimeter of the liquid layer is cooled by flowing water chilled to a temperature of 15.4°C continuously through a polycarbonate channel with an inner diameter of 165.1 mm, a width of 25.4 mm, and a depth of 12.7 mm. The

water is kept at 15.4°C using a constant-temperature bath (A) and pumped through flexible tubing to the cooling channel; the water is then returned to the constant-temperature bath after making a single pass around the perimeter of the liquid film. Two sheathed K-type thermocouples (Omega KMQXL-125U-6) are used to measure the temperature at the inlet and outlet of the cooling channel and verify that the film temperature remains constant over its perimeter. In all experiments, the temperature difference between the chilled water at the inlet and outlet of the cooling channel did not exceed 0.1°C as determined by a handheld TC reader (Omega HH23).

Table 3.1: Detailed list of the experimental apparatus hardware components

Label	Description	Manufacturer	Model
A	Iso-Temp Refrigerated Ciculator	Fisher Scientific	9000
B	Unistrut Support Posts	In house construction	-
C	Data Acquistion Unit	HP Agilent	34970A
D	VARIAC Power Supply	In house construction	-
E	Workstation PC	Dell	Precision 410
F	Acrylic Containment Ring 203.2 mm OD 6.4 mm thick 152.4 mm ID	In-house construction	-
G	Silicone Oil Layer	See Table 3.2	-
H	Polycarbonate Ring 203.2 mm OD 25.4 mm thick 152.4 mm ID	In house construction	-
I	Copper Insert 19 mm OD 38.1 mm long	In house construction	-
J	High-Temperature Cartridge Heater 9.5 mm dia. 400 W max. 50.8 mm long	McMaster-Carr	35025K191
K	20 K-type Thermocouples	Omega	CHAL-010
L	Steel Plate 203.2 mm dia. 12.7 mm thick	In house construction	-

The radial temperature distribution near the plate surface is measured using 20 bare-wire K-type thermocouples (Omega CHAL-010) located 2.5 mm below the upper surface. The 0.005" TC wires are fed through a 1" long ceramic two-bore tube with an outer diameter of 1/16". The bare TC wires are coated with enamel paint everywhere except at the thermocouple bead for electrical isolation. The thermocouples in their ceramic tubes are pressed into pre-drilled 1/16" holes in the steel plate and secured in place by thermal epoxy (OMEGABOND 200) to maintain good thermal contact with the steel plate. The azimuthal coordinate $\theta \equiv 0°$ is along the radius defined by 13 TCs located at r' = 0.16, 0.20, 0.24, 0.28, 0.32, 0.41, 0.49, 0.57, 0.66, 0.74, 0.82, 0.91, and 0.99. Seven more thermocouples at $\theta = 180°$ and r' = 0.16, 0.24, 0.32, 0.49, 0.66, 0.82, and 0.99 are used to verify the axisymmetry of the temperature distribution. The temperatures from each TC are obtained through a data acquisition system (C) directly connected to a PC (E). The TC channels were scanned at 1 Hz and an average of 1000 samples taken at 1 kHz was recorded for each channel. Before installation, the TCs were calibrated using a block calibrator (Techne Laboratory Equipment DB-35L) and a platinum resistance temperature detector (RTD) with manufacturer-supplied uncertainty of 0.005°C (ASL T100-250, SN 440037). Appendix B gives further details on TC calibration.

The working fluid in these experiments was silicone oil (polydimethylsiloxanes). Silicone oils are commonly used for thermocapillary flow experiments [51] because silicone oil-air interfaces have a fairly low surface tension and are hence relatively unaffected by most surfactants; and silicone oils have almost no evaporation due to their low volatility [10]. In order to investigate a wider parameter space, silicone oils of four

different dynamic viscosities (μ = 4.8 × 10^{-3}, 1.9 × 10^{-2}, 4.8 × 10^{-2}, and 9.6 × 10^{-1} N·s/m^2) were used. The relevant properties of these oils, as specified by the manufacturers, are summarized in Table 3.2; γ_o was taken to be 6.8×10^{-5} N/(m·K) for all four silicone oils.

Table 3.2: Silicone oil material properties

Manufacturer	Gelest	Gelest	Dow-Corning	Dow-Corning
μ (10^{-2}N·s/m^2)	0.48	1.9	4.8	96
ρ (g/cm^3)	0.92	0.95	0.97	0.97
k (W/m·K)	0.12	0.14	0.15	0.16
c_p (J/g·K)	1.46	1.46	1.47	1.46
σ (10^{-2}N/m)	1.92	2.06	2.08	2.12

3.1.2. Experimental Procedures

The experimental apparatus was prepared for each experiment by cleaning, leveling, and filling the test section. The steel plate was first washed with soap and water to remove any residual oil and contaminants from the steel surface. The test section was then leveled within 0.025° of horizontal based on a graduated bubble level (Starrett 98-6) using the threaded inserts attached to the three support posts for the plate. Finally, the silicone oil was placed on the steel plate after selecting a viscosity and initial film height to match design parameters. The initial film height was determined by the mass of the silicone oil removed from the stock container and placed directly in the test section as measured by a digital scale (Ohaus GT8000) with an accuracy of 0.1g. This measurement was verified by measuring the volume of the silicone oil using a pipette (Fisher-Scientific Finnpipette 2-10 mL) with an accuracy of 0.1 mL. Because the volume

of the liquid layer often exceeded 10 mL, multiple extractions of silicone oil were made from the manufacturer's container.

A radial temperature gradient was imposed across the liquid film as follows. The experimental test section, initially at room temperature, is first cooled to 15.4°C by activating the water chiller. A constant power input is then supplied to the heater and the system is allowed to reach thermal equilibrium. This procedure ensures that all local temperatures increase monotonically, eliminating any effects due to intermittent heating and cooling. Figure 3.3 shows the typical evolution of surface temperature (measured by the thermocouples) at five different locations: r' = 0.16 (thick solid), 0.28 (thick dashed), 0.49 (thick dotted), 0.74 (thin solid), and 0.99 (thin dashed) where the time t is measured from the instant when the heater is turned on. In all cases, no experimental data were obtained until the readings had achieved their steady-state values, defined to be a variation for all 20 TC readings of less than 0.1°C over 1 min. Figure 3.3 shows that this occurs at t greater than about 20 min.

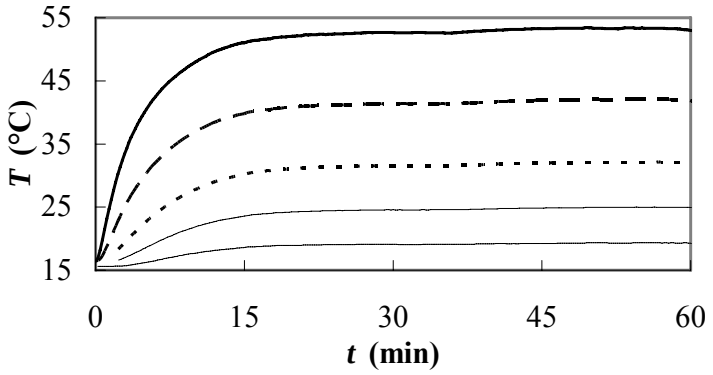

Figure 3.3: Temperature history of TC readings at r' = 0.16 (thick solid), 0.28 (thick dashed), 0.49 (thick dotted), 0.74 (thin solid), and 0.99 (thin dashed) for a liquid layer with A = 0.014, Bo = 0.48, and $C = 1.7 \times 10^{-3}$.

3.2. Data Acquisition and Analysis

Thermocapillary effects on liquid layers subject to a radial temperature gradient were studied experimentally by measuring the free-surface geometry and the thickness of the liquid layer. The objective of these investigations was to determine the flow regime maps in terms of the relevant dimensionless parameters. The following sections describe the reflectance shadowgraphy technique used to visualize the free surface and two methods for determining liquid layer thickness.

3.2.1. Free-Surface Visualization

The free-surface geometry of non-uniformly heated liquid layers was examined using a reflectance shadowgraph technique. The principles of shadowgraphy are reviewed by Settles [60] and Merzkirch [36], among others. A standard double-pass shadowgraph system was modified slightly for these studies by replacing the mirror with the liquid free surface, similar to the setup used by Ezersky [16] to study hydrothermal waves. In this application of the shadowgraph technique, the path of the incident light is modified by the contour of the liquid free surface. An undisturbed free surface will reflect most of the incident light back along the same optical path, resulting in an image of the light source. Otherwise, disturbances on the free surface will alter the image by deflecting the light from its original path. The reflectance shadowgraph system used in these investigations is shown in Figure 3.4 and listed in Table 3.3.

A standard 12" long, ½" diameter fiber optic light guide (Edmund Optics NT38-659) directs white light from a 500W source (LS). The light is passed through an iris diaphragm (I) used to create a 0.8 mm point source of light at the focal length of the

achromatic anti-reflection (AR) coated lens (L). Before reaching the lens, the light expands from the diaphragm through an AR coated beamsplitter cube (BS). The interference coating of the beamsplitter reflects and transmits 50% of the incident light, directing the reflected portion away from the optical system.

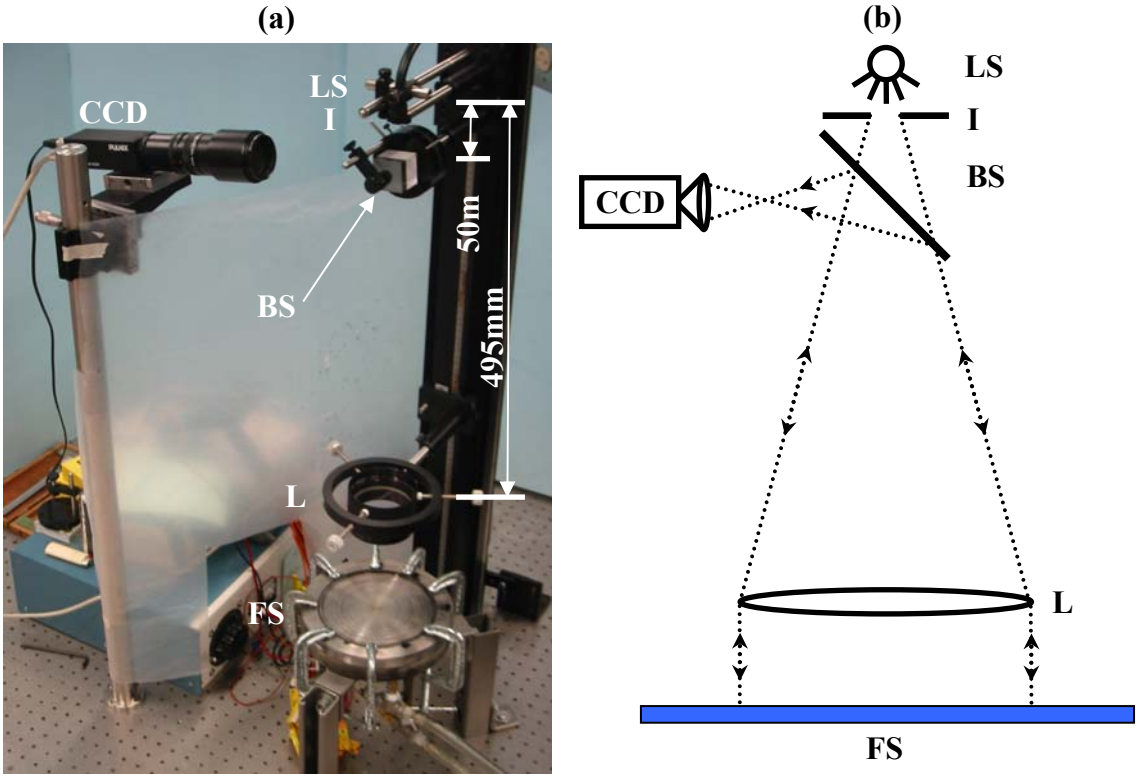

Figure 3.4: Reflectance shadowgraph system shown (a) in a photograph and (b) schematically with light paths.

The light is collimated by the lens, illuminating only a 50 mm diameter region at the center of the liquid film, or the region of the film with the highest temperature gradient. The collimated light is then reflected from the liquid free surface back to the lens. The deformations of the free surface deflect the light away from the incident path; this deflected light returns through the optical system, through the converging lens back

to the beamsplitter where the light is again evenly split, with the reflected 50% directed into the image capture system. At most, only 25% of the total illumination images the free-surface geometry.

Table 3.3: List of optical components in the shadowgraph setup

Label	Description	Manufacturer	Model
CCD	Charge-Coupled Device	Pulnix	TM-6710
LS	Fiber Optic Light Source 500 W max. intensity	Dolan-Jenner	Fiber-Lite PL900
I	Iris Diaphragm 0.8 mm min. aperature	Edmund Optics	NT32-621
BS	Beamsplitter Cube 35 mm × 35 mm	Edmund Optics	NT32-702
L	Achromatic Lens 495 mm focal length 80 mm dia.	A. Jaegers	#1158
FS	Liquid Free Surface	-	-

The shadowgraph images of the liquid free surface are captured by a progressive scanning B/W digital output camera (CCD) at 120 Hz with a close-focusing macro video lens (Navitar Zoom 7000). The digital images were acquired on the HD of a PC (DELL Precision 410) using a PCI framegrabber card (Bitflow Inc. Road Runner R3-PCI-CL-23-L). The non-interlaced images were captured in scanning mode at a spatial resolution of 540 × 480 pixels. Sequences of 300 images were captured and saved as AVI movie files, which were later distilled into individual JPEG images. These image sequences were used to qualify the temporal and symmetric behavior of the liquid layer.

Prior to imaging differentially heated layers, two images are taken to provide quantitative information about the shadowgraphs. First, a sharpened steel pointer (1.27 mm max. dia.) is positioned between the lens and the liquid free surface such that its tip lies directly over the center of the experimental test section. An image of this pointer

provides the pixel location of the center of the test section as shown in Figure 3.5(a). Second, a 30 × 30 fine screen mesh (37.1% open area and 0.25 mm wire diameter) is laid across the top of the test section between the lens and the free surface. A single image of this mesh, like that shown in Figure 3.5(b), is used to determine the magnification of the shadowgraph images. Note that the brighter regions visible in Figure 3.5, which are due to the reflection of the incident light inside the beamsplitter cube, could not be entirely removed from the shadowgraph image during alignment.

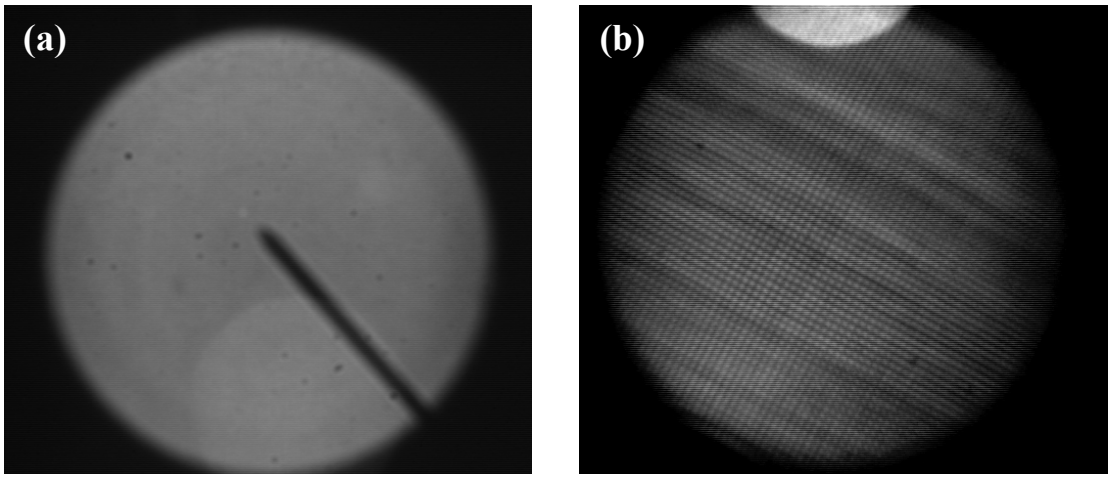

Figure 3.5: Shadowgraph images of (a) indicator marking the center of the plate and (b) fine mesh screen used to provide scale.

Preliminary shadowgraph images showed that the liquid free surface was subject to low frequency surface waves starting at the outer containment ring and propagating towards the center of the plate with a frequency of about 5 Hz as shown in Figure 3.6. These waves, which were found to occur even for isothermal liquid layers, were found to be due to building vibrations. The experimental test section was therefore vibration-isolated from the structure for the shadowgraph experiments.

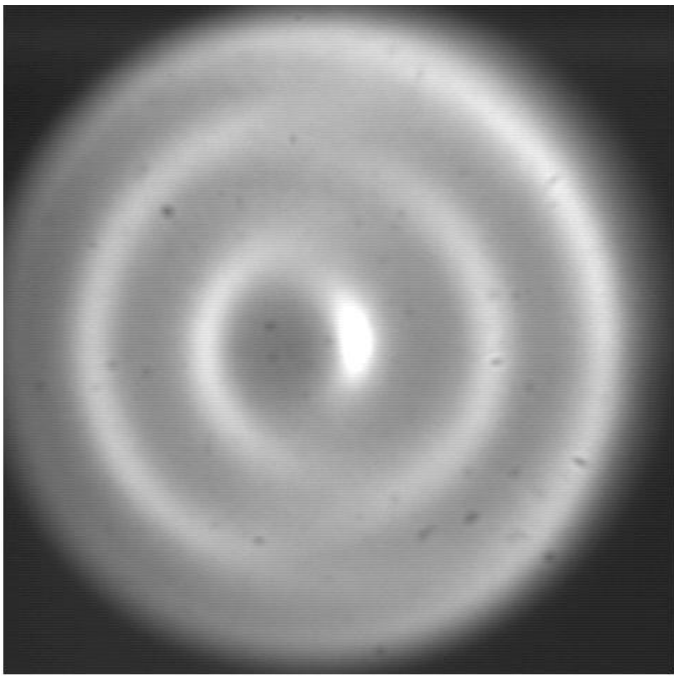

Figure 3.6: Shadowgraph image showing surface waves caused by structural vibrations. The bright regions move toward the center of the image arriving with a frequency on the order of 5 Hz.

The vibration isolation system setup used in these studies is shown in Figure 3.7 and its components are listed in Table 3.4. The experimental apparatus is situated on a laboratory table (A) supported by vibration isolators (B) inflated with compressed air from the house line. Compressed air at ~100 psi from the house line enters a pressure regulator with gage (C) where it is regulated to 40 psi. The union cross (E) divides the inlet air into three paths that direct the air to additional pressure regulators (F) used to control the pressure in the isolators thereby adjusting the floating height of the table. The air pressures in two of the isolators are set individually while the remaining two isolators are controlled by a single pressure regulator. For these latter isolators, the air flows from the regulator (F) through a union tee (D) before reaching the isolators. This arrangement,

based on more recent vibration isolation table designs, simulates a three-point support to ease the leveling process.

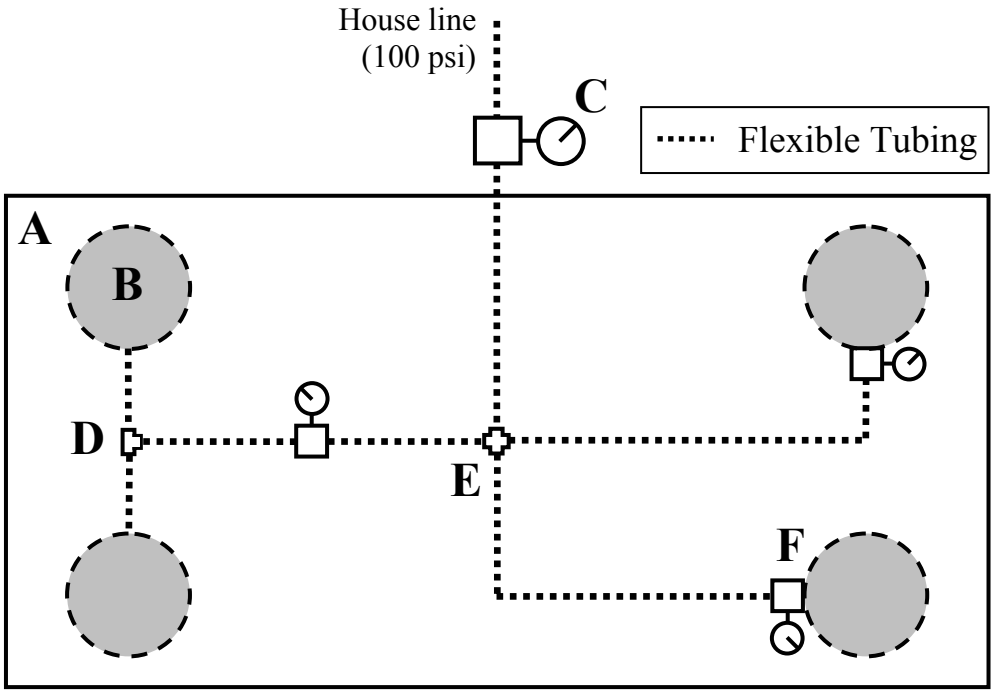

Figure 3.7: Schematic of vibration isolation system hardware setup

Table 3.4: List of hardware components used in the vibration isolation system.

Label	Description	Manufacturer	Model
A	Laboratory Table 4’ × 8’ × 12”	Newport	RS4000-48-12
B	Isolator	NRC, Inc.	XL-B
C	150 psi max. pressure regulator w/ gauge	SpeedAire	42029
D	¼” NPT union tee	Swagelok	B-810-3
E	¼” NPT union cross	Swagelok	B-810-4
F	5–100 psi pressure regulator w/ gauge	Norgren	07-119-RGKA

Before any data collection, the optical system was positioned and aligned. First, the isolation legs of the laboratory table were inflated such that the table top was

horizontal as measured by a SmartTool digital level with an accuracy of 0.1°. Second, the experimental test section was leveled as explained in Section 3.1.2. Third, the light source, beamsplitter, and lens were mounted and aligned. The light source was initially mounted with the iris directly over the center of the liquid layer. The lens was then placed at a focal length from the light source so that the illumination of the liquid layer was centered on the free surface and was horizontally aligned using the Starrett bubble level to guarantee that the collimated light beam was perpendicular to the initially flat liquid surface. The beamsplitter was then positioned to ensure direct illumination of the free surface. Fourth, the camera was positioned, leveled, and aligned. Two linear stages (Newport UMR8.25) with a maximum travel of 50 mm were used to control the vertical and horizontal positions of the camera, while an L-bracket was rotated to change the camera angle. The two stages were mounted perpendicular to each other using a square. A SmartTool digital level was used to verify the horizontal tilt of the camera matched that of the experimental test section. The camera was then positioned such that the shadowgraph image of the free surface was centered on the CCD.

Once the system was aligned, experiments were performed as described in Section 3.1.2. After reaching thermal equilibrium, the laboratory lights and water chiller were turned off while acquiring shadowgraph images. Turning off the overhead lights ensured that the free surface was only illuminated by the fiber optic light source. The flow through the cooling channel was found to create vibrations that led to surface waves similar to those shown in Figure 3.6. Images were acquired over about 15 s; the plate surface temperatures increased by no more than 0.5°F over this period at the maximum power input of 100 W.

3.2.2. Needle Contact Technique

The thermocapillary behavior of thin liquid layers was further characterized by experimental measurements of the local layer thickness from a needle contact method. The needle method used in these studies is similar to that employed by Burelbach, *et al*. [10] in their investigations of thermocapillary effects in rectangular films. In this method, the z-positions of the film free surface and the solid surface were measured at a given radial position r. The actual height $h(r)$ of the liquid layer is then the difference between these two values.

The experimental setup for the needle contact investigations is shown in Figure 3.2 and detailed in Table 3.5. The steel needle (C) was mounted by a bracket (D) vertically to two linear stages, a screw-driven long-travel stage (A) with an accuracy of 0.025 cm and a precision stage (B) equipped with a Newport SM-50 Vernier micrometer with an accuracy of 1 μm, to adjust the r- and z-positions, respectively, of the needle. The location of the free surface was determined by visual inspection to be the position at which the needle tip is wetted by the liquid. The location of the solid steel surface was found by translating the rod towards the plate until an electrical connection was established, as determined using a multimeter (E). The uncertainty in these measurements of film height is estimated to be ±0.02mm.

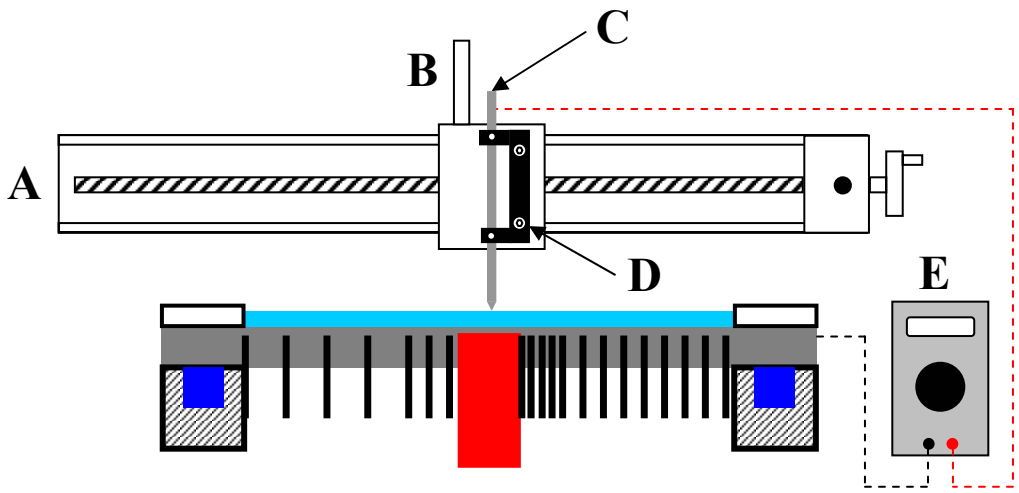

Figure 3.8: Experimental setup for needle contact measurements of local film height.

Table 3.5: List of components in the needle contact measurement experimental setup.

Label	Description	Manufacturer	Model
A	Screw-driven linear stage 355 mm max. travel	Velmex	Unislide A400
B	Precision linear stage with Vernier actuator (Newport SM-50) 50 mm max. travel	Newport	433
C	Sharpened steel needle 1.27 mm max. dia.	In house construction	-
D	Mounting bracket	In house construction	-
E	Multimeter	Omega	Omegaette HHM93

Before thickness measurements can be acquired using the needle contact technique, it is necessary to mount, align, and center the steel needle and translation stages. First, the linear stages are positioned perpendicular to each another using a handheld square and the steel needle and its mounting bracket are secured to the face of the vertical translation stage such that the needle is aligned with the direction of travel, again using the handheld square. Second, the SmartTool digital level is used to verify

that the face of the vertical translation stage is within 0.1° of vertical. Third, the location of the center of the test section is found on the *r*-axis stage by positioning the needle such that it points directly at a mark on the center of the surface of the steel plate. This center mark is located at the intersection of three arcs with a radius identical to that of the steel plate drawn by placing a compass at three different θ positions at the edge of the steel plate. The center point coincided with small "bump" on the surface remaining from the initial machining of the steel plate. Finally, the horizontal translation is adjusted to be parallel with the surface of the steel plate by finding the location of the steel surface at two radial locations and adjusting the horizontal position of the translation stage until the angle of the line intersecting those points is less than 0.05°.

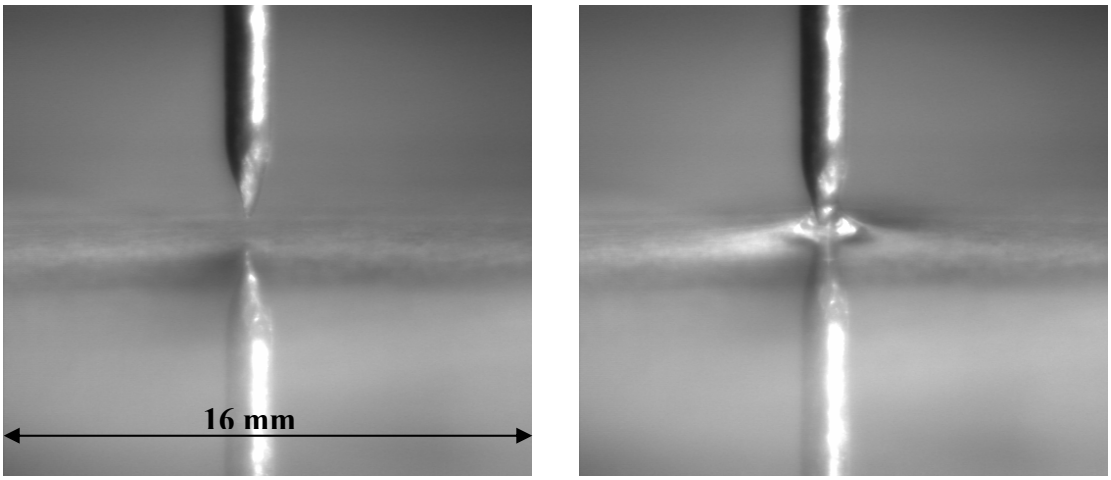

Figure 3.9: Photographs showing the wetting of the steel needle at the point of contact with the liquid free surface.

A profile of the liquid layer thickness is obtained starting at $r' = 0$ over radial increments of $\Delta r = 5.08\,\text{mm}$ after reaching thermal equilibrium (see Section 3.1.2) for a given set of experimental parameters. At each radial location, the needle is translated down toward the liquid free surface using the precision linear stage. When the liquid

wets the needle, as determined visually by the appearance of a meniscus on the needle tip (Figure 3.9), the *z*-position is recorded. The needle is then translated further into the liquid layer until it contacts the solid steel surface at $z' = 0$. An electrical connection between the steel needle and the steel plate registers on the multimeter when contact is made and the *z*-position is recorded. The local thickness of the liquid layer is then the difference between the two recorded *z*-positions. The needle is extracted from the liquid layer and moved to the next radial location. To avoid any backlash in the translation stage, the micrometer was only turned in one direction during the entire thickness measurement. Similarly the *r*-axis translation stage was only moved in one direction during a single profile measurement. An initial layer thickness profile is acquired for each temperature gradient to verify the average film height and the horizontal level of the apparatus.

3.2.3. Confocal Laser Displacement Measurements

For more precise measurements of the free-surface geometry for comparison with the shadowgraph visualizations, a non-intrusive confocal laser displacement measurement system was used. The measurement system, manufactured by Keyence Inc. (LT-9030M), determines displacement from the reference working distance of 30 mm by correlating the focal point with the maximum intensity of light reflected from a surface. The confocal laser sensor, shown in Figure 3.10, uses a 170 μW semiconductor laser with a wavelength of 670 nm. The laser is guided through an objective lens mounted to a vibrating tuning fork and is then reflected from the liquid free surface back to a pinhole element atop a light-receiving sensor. When the light is precisely focused on the liquid

free surface, a maximum intensity of the reflected beam passes through the pinhole and triggers a detection signal in the light sensor. This signal is sent to the tuning fork to record the position of the lens at the instant the laser is focused on the liquid free surface. The focused laser beam has a spot diameter of 7 μm and is vibrated vertically by the tuning fork across 2 mm at 10 Hz. The measurement resolution of this system is 0.1 μm.

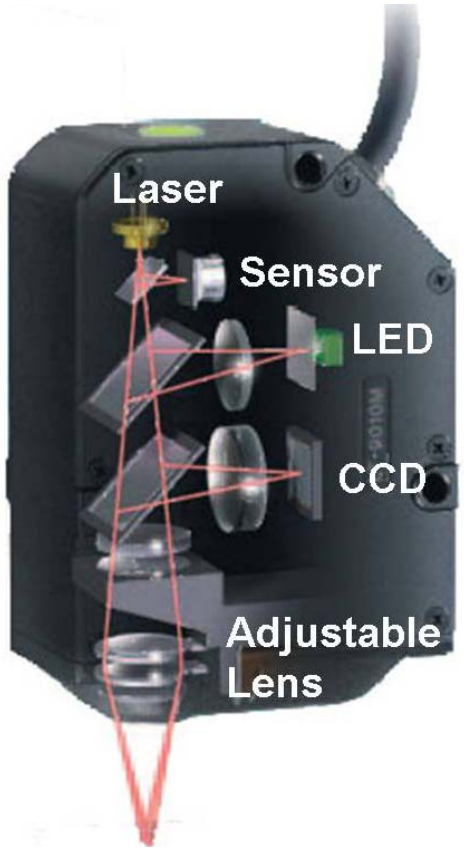

Figure 3.10: Diagram of the internal components of the Keyence LT-9030M laser confocal displacement sensor (Laser, Sensor, and Lens) and infrared microscope (LED and CCD).

To help position the laser confocal system, an infrared (IR) confocal microscope consisting of an IR LED and CCD is included in the optical system as shown in Figure

3.10. The microscope uses an 870 nm LED light source to illuminate the target surface. A CCD camera captures a 2.5 mm × 2.0 mm image of the target surface. The microscope was used to center the laser over the test section by visualizing machining flaws on the steel surface.

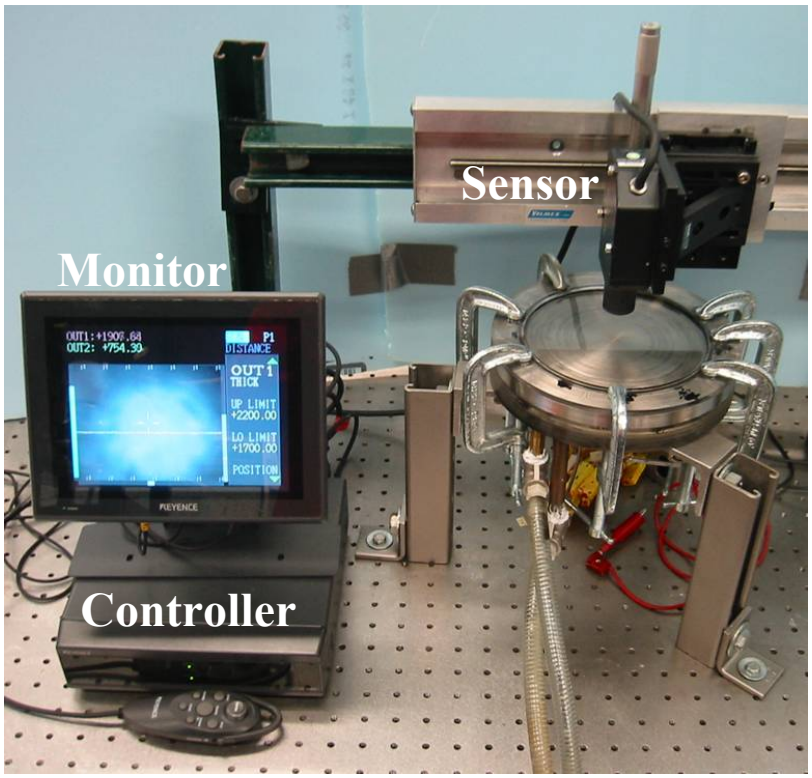

Figure 3.11: Experimental setup for measurement of the free surface displacement.

Table 3.6: List of equipment used in the displacement measurement experiments

Description	Manufacturer	Model
Laser Sensor Unit	Keyence	LT-9030M
Laser Controller	Keyence	LT-9501
LCD Monitor	Keyence	CA-MN80
Workstation PC	Gateway	E-3200

The laser sensor is mounted to the same positioning apparatus described in Section 3.2.2 consisting of the Velmex Unislide A400 and Newport 433 translation stages

to acquire an accurate characterization of the steady-state liquid free surface. The sensor can thus be precisely positioned along the radius and vertical axis to determine the steady-state height profile. The displacement measurement apparatus setup is shown in Figure 3.11 and detailed in Table 3.6. The signal from the laser sensor is sent to a controller module which processes and displays the signal on an LCD monitor as either an intensity peak or a quantified displacement. The image from the microscope is also depicted as the background of the displacement graph on the monitor. The processed signal, consisting of the displacement of the free surface from the reference height and the thickness of the liquid layer (for liquid layers of $h_o \geq 2\,\text{mm}$), is recorded to a text file on a PC HD using software developed in MATLAB 6.0.

Before displacement measurements of the free surface, the sensor head was mounted and aligned. The SmartTool digital level was used to ensure the sensor unit was within 0.1° of vertical. The visible laser beam was visible was focused on the the central bump on the plate surface ($r' = 0$) following a procedure similar to that used in the needle contact method. The Velmex translation stage used for horizontal positioning was aligned parallel to the steel plate by taking displacement measurements of the dry steel plate at two radial locations and adjusting the level of the stage until the slope between the points was less than 0.05°. It was also necessary to acquire a calibration profile of the surface of the dry steel plate before placing the liquid layer on the experimental test section.

The procedure used in the laser confocal displacement measurements is very similar to that used in the needle contact method. The liquid viscosity, the liquid mass, and the heating power are selected to achieve a particular set of design parameters as

described in Section 3.1.2. The test apparatus is allowed to reach thermal equilibrium and the laser sensor is positioned at $r' = 0$ using the Velmex translation stage. The vertical height of the sensor is adjusted by the Newport 433 linear stage such that the displacements shown on the LCD monitor are approximately zero. The displacement profile is then acquired, moving the laser unit by $\Delta r = 1.27\,\text{mm}$ between the first 20 radial locations. Steps of $\Delta r = 2.54\,\text{mm}$, then 5.08 mm are then used between the next ten and five radial locations, respectively. A finer radial spatial resolution is used near the center of the plate because the free-surface deformation is greatest there; a coarser resolution is used to determine the relatively flat profile near the edge of the film. At each radial location, 100 measurements are recorded at 10 Hz.

CHAPTER 4

THEORETICAL AND NUMERICAL ANALYSES

Details of the theoretical and numerical investigations of thermocapillary effects in thin liquid layers are presented in this chapter. For each method, the mathematical formulation is first developed, followed by a description of the solution technique.

4.1. Derivation of Theoretical Model

In this section, an axisymmetric asymptotic solution of the steady-state film height for very thin films over a non-isothermal surface is presented. The theoretical analysis applies an asymptotic assumption to the full set of governing equations and boundary conditions. The resulting nonlinear evolution equation, formulated in terms of the initial liquid height, h_o, is solved using a simple shooting method.

4.1.1. Axisymmetric Evolution Equation

An initially quiescent thin liquid film of average height (z-dimension) h_o with a non-uniform temperature distribution $T(r)$ at the horizontal solid-liquid interface, or $z = 0$ is considered as shown in Figure 4.1. The viscous liquid film is bounded above by the liquid-gas interface and below by the solid-liquid interface. Gravitational forces are included in the analysis. The three-dimensional mass, momentum, and energy equations in polar cylindrical coordinates, are as follows for a constant density and viscosity fluid:

$$\frac{1}{r}\frac{\partial}{\partial r}\left(rv_r\right)+\frac{1}{r}\frac{\partial}{\partial \theta}\left(v_\theta\right)+\frac{\partial}{\partial z}\left(v_z\right)=0 \tag{4.1}$$

$$\rho\left(\frac{\partial v_r}{\partial t}+v_r\frac{\partial v_r}{\partial r}+\frac{v_\theta}{r}\frac{\partial v_r}{\partial \theta}-\frac{{v_\theta}^2}{r}+v_z\frac{\partial v_r}{\partial z}\right)=-\frac{\partial p}{\partial r}+\mu\left[\begin{array}{l}\frac{\partial}{\partial r}\left(\frac{1}{r}\frac{\partial}{\partial r}\left(rv_r\right)\right)+\frac{1}{r^2}\frac{\partial^2 v_r}{\partial \theta^2}\\+\frac{\partial^2 v_r}{\partial z^2}-\frac{2}{r^2}\frac{\partial v_\theta}{\partial \theta}\end{array}\right] \quad (4.2)$$

$$\rho\left(\frac{\partial v_\theta}{\partial t}+v_r\frac{\partial v_\theta}{\partial r}+\frac{v_\theta}{r}\frac{\partial v_\theta}{\partial \theta}-\frac{v_r v_\theta}{r}+v_z\frac{\partial v_\theta}{\partial z}\right)=-\frac{1}{r}\frac{\partial p}{\partial \theta}+\mu\left[\begin{array}{l}\frac{\partial}{\partial r}\left(\frac{1}{r}\frac{\partial}{\partial r}\left(rv_\theta\right)\right)+\frac{1}{r^2}\frac{\partial^2 v_\theta}{\partial \theta^2}\\+\frac{\partial^2 v_\theta}{\partial z^2}-\frac{2}{r^2}\frac{\partial v_r}{\partial \theta}\end{array}\right] \quad (4.3)$$

$$\rho\left(\frac{\partial v_z}{\partial t}+v_r\frac{\partial v_z}{\partial r}+\frac{v_\theta}{r}\frac{\partial v_z}{\partial \theta}+v_z\frac{\partial v_z}{\partial z}\right)=-\frac{\partial p}{\partial z}+\mu\left[\frac{1}{r}\frac{\partial}{\partial r}\left(r\frac{\partial v_z}{\partial r}\right)+\frac{1}{r^2}\frac{\partial^2 v_z}{\partial \theta^2}+\frac{\partial^2 v_z}{\partial z^2}\right]+\rho g \quad (4.4)$$

$$\rho c_p\left(\frac{\partial T}{\partial t}+v_r\frac{\partial T}{\partial r}+\frac{v_\theta}{r}\frac{\partial T}{\partial \theta}+v_z\frac{\partial T}{\partial z}\right)=k\left[\frac{1}{r}\frac{\partial}{\partial r}\left(r\frac{\partial T}{\partial r}\right)+\frac{1}{r^2}\frac{\partial^2 T}{\partial \theta^2}+\frac{\partial^2 T}{\partial z^2}\right] \quad (4.5)$$

Here, r, θ, and z are the radial, azimuthal, and axial coordinates, respectively. The r, θ, and z velocity components are denoted by v_r, v_θ, and v_z, respectively. The absolute temperature is T, pressure is p, and the gravitational acceleration is g. The liquid material properties are the density, ρ, the viscosity, μ, the specific heat, c_p, and the thermal conductivity, k. For steady-state and axisymmetric flow:

$$\frac{\partial v_r}{\partial t}=\frac{\partial v_z}{\partial t}=\frac{\partial T}{\partial t}=\frac{\partial v_r}{\partial \theta}=\frac{\partial v_z}{\partial \theta}=\frac{\partial T}{\partial \theta}=\frac{\partial p}{\partial \theta}=\frac{\partial^2 v_r}{\partial \theta^2}=\frac{\partial^2 v_z}{\partial \theta^2}=\frac{\partial^2 T}{\partial \theta^2}=v_\theta=0 \quad (4.6)$$

Note that these assumptions obviate Equation 4.3. The remaining equations (4.1, 4.2, 4.4, and 4.5) reduce to:

$$\frac{1}{r}\frac{\partial}{\partial r}\left(rv_r\right)+\frac{\partial}{\partial z}\left(v_z\right)=0 \quad (4.7)$$

$$\rho\left(v_r\frac{\partial v_r}{\partial r}+v_z\frac{\partial v_r}{\partial z}\right)=-\frac{\partial p}{\partial r}+\mu\left[\frac{\partial}{\partial r}\left(\frac{1}{r}\frac{\partial}{\partial r}\left(rv_r\right)\right)+\frac{\partial^2 v_r}{\partial z^2}\right] \quad (4.8)$$

$$\rho\left(v_r\frac{\partial v_z}{\partial r}+v_z\frac{\partial v_z}{\partial z}\right)=-\frac{\partial p}{\partial z}+\mu\left[\frac{1}{r}\frac{\partial}{\partial r}\left(r\frac{\partial v_z}{\partial r}\right)+\frac{\partial^2 v_z}{\partial z^2}\right]+\rho g \tag{4.9}$$

$$\rho c_p\left(v_r\frac{\partial T}{\partial r}+v_z\frac{\partial T}{\partial z}\right)=k\left[\frac{1}{r}\frac{\partial}{\partial r}\left(r\frac{\partial T}{\partial r}\right)+\frac{\partial^2 T}{\partial z^2}\right] \tag{4.10}$$

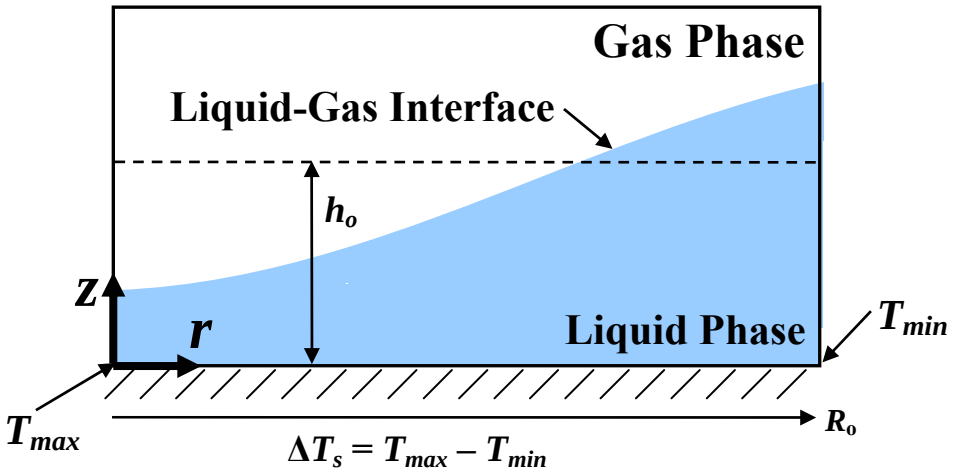

Figure 4.1: Schematic of the axisymmetric liquid layer subjected to a radial temperature gradient for the numerical model and asymptotic analysis.

The relevant boundary conditions for an axisymmetric, thin liquid layer exposed to an passive bounding gas, and a zero slope condition at the end wall located at $r = R_o$, are given in the following equations for the normal and tangential stress balances, the kinematic condition, the energy balance at the interface ($z = h(r)$), as well as the solid wall boundary conditions at $r = R_o$ and the symmetry conditions at $r = 0$.

Normal stress balance at liquid-gas interface ($z = h$):

$$\left(\sigma_{ij}\boldsymbol{n}_i\boldsymbol{n}_j\right)\cdot\overline{\boldsymbol{N}}=\left(\boldsymbol{p}+\sigma\kappa\right)\cdot\overline{\boldsymbol{N}} \tag{4.11}$$

Here, the viscous stress tensor σ_{ij} represents:

$$\sigma_{ij} = \begin{pmatrix} 2\mu\dfrac{\partial v_r}{\partial r} & \mu\dfrac{\partial v_r}{\partial z} + \mu\dfrac{\partial v_z}{\partial r} \\ \mu\dfrac{\partial v_r}{\partial z} + \mu\dfrac{\partial v_z}{\partial r} & 2\mu\dfrac{\partial v_z}{\partial z} \end{pmatrix} \tag{4.12}$$

and the unit normal vector directed from the liquid to the gas is defined as:

$$\overrightarrow{\boldsymbol{N}} = \frac{-\dfrac{\partial h}{dr}}{\left[1+\left(\dfrac{\partial h}{dr}\right)^2\right]^{\frac{1}{2}}}\boldsymbol{e}_r + \frac{1}{\left[1+\left(\dfrac{\partial h}{dr}\right)^2\right]^{\frac{1}{2}}}\boldsymbol{e}_z \tag{4.13}$$

where $\boldsymbol{e}_r$ and $\boldsymbol{e}_z$ are unit vectors in the r and z directions, respectively, and h is a function of r describing the height of the liquid layer. The curvature of the interface, κ, is given by:

$$\kappa = \frac{\dfrac{\partial^2 h}{\partial r^2} + \left[\dfrac{\partial h}{\partial r} + \dfrac{1}{r}\left(\dfrac{\partial h}{\partial r}\right)^3\right]}{\left[1+\left(\dfrac{\partial h}{\partial r}\right)^2\right]^{\frac{3}{2}}} \tag{4.14}$$

The surface tension, σ, is assumed to be a linear function of temperature and is thus to the following relation:

$$\sigma = \sigma_o + \gamma_o[T(r) - T_{ref}] \tag{4.15}$$

where σ_o is the surface tension at a reference temperature T_{ref}, and γ_o is the surface tension temperature coefficient. The normal stress condition at the liquid-gas interface can be re-written as:

$$2\mu\left[1+\left(\frac{\partial h}{\partial r}\right)^2\right]^{\frac{1}{2}}\begin{bmatrix} \dfrac{\partial v_r}{\partial r}\left(\dfrac{\partial h}{\partial r}\right)^2 - \dfrac{\partial h}{\partial r}\dfrac{\partial v_r}{\partial z} \\ -\dfrac{\partial h}{\partial r}\dfrac{\partial v_z}{\partial r} + \dfrac{\partial v_z}{\partial z} \end{bmatrix} = p\left[1+\left(\frac{\partial h}{\partial r}\right)^2\right]^{\frac{3}{2}} + \sigma\frac{\partial^2 h}{\partial r^2} + \frac{\sigma}{r}\frac{\partial h}{\partial r} + \frac{\sigma}{r}\left(\frac{\partial h}{\partial r}\right)^3 \tag{4.16}$$

Tangential stress balance at liquid-gas interface ($z = h$):

$$\left(\sigma_{ij}\boldsymbol{n}_i\boldsymbol{n}_j\right)\cdot\vec{\boldsymbol{t}} = \left\{\frac{\dfrac{\partial\sigma}{\partial T}\left(\dfrac{\partial T}{\partial r}+\dfrac{\partial h}{\partial r}\dfrac{\partial T}{\partial z}\right)}{\left[1+\left(\dfrac{\partial h}{\partial r}\right)^2\right]^{\frac{1}{2}}}\right\}\cdot\vec{\boldsymbol{t}} \tag{4.17}$$

In this equation, $\boldsymbol{t}_j$ is the tangential unit vector in the radial direction from the interface directed away from the origin. The tangential unit vector is given by:

$$\boldsymbol{t}_j = \frac{1}{\left[1+\left(\dfrac{\partial h}{dr}\right)^2\right]^{\frac{1}{2}}}\boldsymbol{e}_r + \frac{\dfrac{\partial h}{dr}}{\left[1+\left(\dfrac{\partial h}{dr}\right)^2\right]^{\frac{1}{2}}}\boldsymbol{e}_z \tag{4.18}$$

Therefore, the tangential stress condition at the liquid-gas interface can be represented by the following formulation:

$$\mu\left[1+\left(\frac{\partial h}{\partial r}\right)^2\right]^{-\frac{1}{2}}\left[\begin{array}{l}-2\dfrac{\partial h}{\partial r}\dfrac{\partial v_r}{\partial r}+\dfrac{\partial v_r}{\partial z}+\dfrac{\partial v_z}{\partial r}-\dfrac{\partial v_r}{\partial z}\left(\dfrac{\partial h}{\partial r}\right)^2 \\ -\dfrac{\partial v_z}{\partial r}\left(\dfrac{\partial h}{\partial r}\right)^2+2\dfrac{\partial h}{\partial r}\dfrac{\partial v_z}{\partial z}\end{array}\right] = \gamma_o\left(\frac{\partial T}{\partial r}+\frac{\partial h}{\partial r}\frac{\partial T}{\partial z}\right) \tag{4. 19}$$

Kinematic condition at interface ($z = h$):

$$v_r\frac{\partial h}{\partial r} - v_z = 0 \tag{4.20}$$

Energy balance at interface ($z = h$):

$$k\nabla T\cdot n_i = -h_g\left(T - T_g\right) \tag{4.21}$$

Here, h_g refers to the heat transfer coefficient for the cooling of the liquid surface by the surrounding gas. Substituting from Equation 4.13 and simplifying:

$$k\left[1+\left(\frac{\partial h}{\partial r}\right)^2\right]^{-\frac{1}{2}}\left[\frac{\partial T}{\partial z}-\frac{\partial h}{\partial r}\frac{\partial T}{\partial r}\right]=h_g\left(T-T_g\right) \tag{4.22}$$

Solid wall boundary conditions at $z=0$:

$$v_r=v_z=0 \tag{4.23}$$

$$T=T_s \tag{4.24}$$

Here, the no-slip condition along the solid wall is specified and the fluid is assumed to take the surface temperature of the wall, T_s.

Solid wall boundary conditions at $r=R_o$:

$$v_r=v_z=\frac{\partial h}{\partial r}=0 \tag{4.25}$$

At this boundary, the no-slip condition is assumed once again. We also impose the arbitrary boundary condition at the outer edge of the liquid film that the slope of the free-surface be zero.

Symmetry conditions at $r=0$:

$$\frac{\partial h}{\partial r}=\frac{\partial^3 h}{\partial r^3}=0 \tag{4.26}$$

Assuming symmetric height across the center of the cylindrical film, the first and third derivatives must be zero.

The governing equations (Equations 4.7–4.10) and boundary conditions (Equations 4.16, 4.19, and 4.22–4.26) can be non-dimensionalized using appropriate scales. Non-dimensional quantities are shown with primes.

$$r = R_o r' \tag{4.27}$$

$$z = h_o z' \tag{4.28}$$

$$v_r = U v_r' \tag{4.29}$$

$$v_z = \frac{h_o U}{R_o} v_z' \tag{4.30}$$

$$p = \frac{\mu U R_o}{h_o^2} p' \tag{4.31}$$

$$t = \frac{R_o}{U} t' \tag{4.32}$$

$$h = h_o h' \tag{4.33}$$

$$T_s = \Delta T_s T_s' + T_{min} \tag{4.34}$$

$$T = \Delta T_s \left(T' + T_s' \right) + T_{min} \tag{4.35}$$

$$T_g = \Delta T_s T_g' + T_{min} \tag{4.36}$$

Here, R_o is the radius of the liquid layer, h_o is the initial height of the liquid layer, U is a yet undetermined velocity scale, ΔT_s is the radial temperature difference across the liquid layer, and T_{min} is the minimum temperature of the solid surface. Substituting these into Equations 4.7–4.10, the resulting non-dimensional governing equations are:

$$\frac{1}{r'} \frac{\partial}{\partial r'} \left(r v_r' \right) + \frac{\partial}{\partial z'} \left(v_z' \right) = 0 \tag{4.37}$$

$$\frac{\rho U h_o^2}{\mu R_o} \left(v_r \frac{\partial v_r}{\partial r} + v_z \frac{\partial v_r'}{\partial z'} \right) = -\frac{\partial p'}{\partial r'} + \frac{\partial^2 v_r'}{\partial z'^2} + \left(\frac{h_o}{R_o} \right)^2 \frac{\partial}{\partial r'} \left(\frac{1}{r'} \frac{\partial}{\partial r'} \left(r' v_r' \right) \right) \tag{4.38}$$

$$\frac{\rho U h_o^4}{\mu R_o^3}\left(v_r'\frac{\partial v_z'}{\partial r'}+v_z'\frac{\partial v_z'}{\partial z'}\right)=-\frac{\partial p'}{\partial z'}+\frac{h_o^4}{R_o^4}\left[\frac{1}{r'}\frac{\partial}{\partial r'}\left(r'\frac{\partial v_z'}{\partial r'}\right)\right]+\frac{h_o^2}{R_o^2}\left(\frac{\partial^2 v_z'}{\partial z'^2}\right)+\frac{\rho g h_o^3}{\mu U R_o} \quad (4.39)$$

$$\frac{\rho c_p U h_o^2}{k R_o}\left[v_r'\left(\frac{\partial T'}{\partial r'}+\frac{\partial T_s'}{\partial r'}\right)+v_z'\frac{\partial T'}{\partial z'}\right]=\frac{h_o^2}{R_o^2}\left\{\frac{1}{r'}\frac{\partial}{\partial r'}\left[r'\left(\frac{\partial T'}{\partial r'}+\frac{\partial T_s'}{\partial r'}\right)\right]\right\}+\frac{\partial^2 T'}{\partial z'^2} \quad (4.40)$$

The interface conditions are also scaled utilizing the surface tension based on the non-dimensional temperature:

$$\sigma=\sigma_o+\gamma_o\Delta T\left(T'+T_s'\right) \quad (4.41)$$

Normal stress at $z'=h'$*:*

$$2\left[1+\left(\frac{h_o}{R_o}\right)^2\left(\frac{\partial h'}{\partial r'}\right)^2\right]^{\frac{1}{2}}\left\{\begin{array}{l}\left(\frac{h_o}{R_o}\right)^4\left[\frac{\partial v_r'}{\partial r'}\left(\frac{\partial h'}{\partial r'}\right)^2-\frac{\partial h'}{\partial r'}\frac{\partial v_z'}{\partial r'}\right]\\ +\left(\frac{h_o}{R_o}\right)^2\left[\frac{\partial v_z'}{\partial z'}-\frac{\partial h'}{\partial r'}\frac{\partial v_r'}{\partial z'}\right]\end{array}\right\}=$$

$$p\left[1+\left(\frac{h_o}{R_o}\right)^2\left(\frac{\partial h'}{\partial r'}\right)^2\right]^{\frac{3}{2}}+\left[\frac{\sigma_o}{\mu U}-\frac{\gamma_o\Delta T}{\mu U}\left(T'+T_s'\right)\right]\left(\frac{h_o}{R_o}\right)^5\left[\frac{1}{r'}\left(\frac{\partial h'}{\partial r'}\right)^3\right] \quad (4.42)$$

$$+\left[\frac{\sigma_o}{\mu U}-\frac{\gamma_o\Delta T}{\mu U}\left(T'+T_s'\right)\right]\left(\frac{h_o}{R_o}\right)^3\left[\frac{\partial^2 h'}{\partial r'^2}+\frac{1}{r'}\frac{\partial h'}{\partial r'}\right]$$

Tangential stress at $z'=h'$*:*

$$\left[1+\left(\frac{h_o}{R_o}\right)^2\left(\frac{\partial h'}{\partial r'}\right)^2\right]^{-\frac{1}{2}}\left[\begin{array}{l}-2\left(\frac{h_o}{R_o}\right)^2\left[\frac{\partial h'}{\partial r'}\frac{\partial v_r'}{\partial r'}-\frac{\partial v_z'}{\partial r'}\left(\frac{\partial h'}{\partial r'}\right)^2+\frac{\partial v_z'}{\partial r'}+2\frac{\partial h'}{\partial r'}\frac{\partial v_z'}{\partial z'}\right]\\ -\left(\frac{h_o}{R_o}\right)^4\frac{\partial v_r'}{\partial z'}\left(\frac{\partial h'}{\partial r'}\right)^2+\frac{\partial v_r'}{\partial z'}\end{array}\right]= \quad (4.43)$$

$$\frac{\gamma_o\Delta T}{\mu U}\left(\frac{h_o}{R_o}\right)\left[\left(\frac{\partial T'}{\partial r'}+\frac{\partial T_s'}{\partial r'}\right)+\frac{\partial h'}{\partial r'}\frac{\partial T'}{\partial z'}\right]$$

Kinematic condition at $z'=h'$:

$$v_r'\frac{\partial h'}{\partial r'}-v_z'=0 \quad (4.44)$$

Energy balance at $z' = h'$:

$$\left[1+\left(\frac{h_o}{R_o}\right)^2\left(\frac{\partial h}{\partial r}\right)^2\right]^{-\frac{1}{2}}\left[\frac{\partial T}{\partial z}-\left(\frac{h_o}{R_o}\right)^2\frac{\partial h'}{\partial r'}\left(\frac{\partial T'}{\partial r'}+\frac{\partial T_s'}{\partial r'}\right)\right]=-\frac{h_g h_o}{k}\left(T'+T_s'-T_g'\right) \quad (4.45)$$

Solid wall boundary conditions at $z' = 0$:

$$v_r' = v_z' = 0 \quad (4.46)$$

$$T' = 0 \quad (4.47)$$

Solid wall boundary conditions at $r' = 1$:

$$v_r' = v_z' = \frac{\partial h'}{\partial r'} = 0 \quad (4.48)$$

Symmetric boundary conditions at $r' = 0$:

$$\frac{\partial h'}{\partial r'} = \frac{\partial^3 h'}{\partial r'^3} = 0 \quad (4.49)$$

From inspection of Equations 4.37–4.40 and the conditions 4.42–4.45, several dimensionless parameters describing the relative importance of various effects can be distinguished.

Aspect ratio: $$A = \frac{h_o}{R_o} = \frac{\text{height of liquid layer}}{\text{radius of liquid layer}}$$

Reynolds number: $$Re = \frac{\rho U h_o}{\mu} = \frac{\text{inertial forces}}{\text{viscous forces}}$$

Bond number: $$Bo = \frac{\rho g h_o^2}{\sigma_o} = \frac{\text{gravitational forces}}{\text{surface tension forces}}$$

Capillary number: $$C = \frac{\mu U}{\sigma_o} = \frac{\text{thermocapillarity}}{\text{mean surface tension}}$$

Prandtl number: $$Pr = \frac{c_p \mu}{k} = \frac{\text{momentum}}{\text{thermal diffusivity}}$$

Marangoni number: $$M = \frac{U h_o}{\alpha} = \frac{\text{thermal convection}}{\text{thermal diffusion}}$$

Biot number: $$Bi = \frac{h_g h_o}{k} = \frac{\text{surface convection}}{\text{bulk conduction}}$$

The Marangoni number can be considered to be a modified Peclet number where $M = Re\,Pr$. For further analysis, a velocity scale must be chosen. One possibility, based on the analysis of Shin, *et al*. [65], can be obtained by balancing the viscous and inertial forces in the liquid layer, requiring *Re* to be unity:

$$U = \frac{\mu}{\rho R_o} \tag{4.50}$$

However, as pointed out by Ostrach [40], this scaling is actually inappropriate for an asymptotic analysis for a thin liquid film. The flow is primarily driven by shear stress induced at the free surface by surface tension gradients. The correct scaling, described below, arises from the tangential stress condition at the interface. Here it is necessary to balance the viscous shear stress at the liquid-gas interface with the surface tension gradient. This choice is made by requiring the non-dimensional coefficient on the right hand side of the tangential stress condition, Equation 4.43, to be exactly one. The velocity scale then is of a typical lubrication type, as used by Sen and Davis [58] and Vrane [78]:

$$U = \frac{\gamma_o \Delta T}{\mu} A \tag{4.51}$$

Note that in this form the Reynolds, Marangoni, and capillary numbers take the following forms:

$$Re = \frac{\rho \gamma_o \Delta T_s h_o}{\mu^2} A, \qquad M = \frac{\gamma_o \Delta T_s h_o}{\alpha \mu} A, \qquad C = \frac{\gamma_o \Delta T_s}{\sigma_o} A \tag{4.52}$$

This lubrication type analysis has been performed such that all of the terms in the governing equations can be expressed as dimensionless quantities. The set of governing equations (Equations 4.37–4.40) and the corresponding boundary conditions (Equations 4.42–4.49) can now be reduced to:

$$\frac{1}{r'}\frac{\partial}{\partial r'}\left(r' v_r'\right)+\frac{\partial}{\partial z'}\left(v_z'\right)=0 \tag{4.53}$$

$$Re\,A\left(v_r'\frac{\partial v_r'}{\partial r'}+v_z'\frac{\partial v_r'}{\partial z'}\right)=-\frac{\partial p'}{\partial r'}+\frac{\partial^2 v_r'}{\partial z'^2}+A^2\frac{\partial}{\partial r'}\left(\frac{1}{r'}\frac{\partial}{\partial r'}\left(r' v_r'\right)\right) \tag{4.54}$$

$$ReA^3\left(v_r'\frac{\partial v_z'}{\partial r'}+v_z'\frac{\partial v_z'}{\partial z'}\right)=-\frac{\partial p'}{\partial z'}+A^4\left[\frac{1}{r'}\frac{\partial}{\partial r'}\left(r'\frac{\partial v_z'}{\partial r'}\right)\right]+A^2\left(\frac{\partial^2 v_z'}{\partial z'^2}\right)+\frac{Bo\,A}{C} \tag{4.55}$$

$$M\,A\left[v_r'\left(\frac{\partial T'}{\partial r'}+\frac{\partial T_s'}{\partial r'}\right)+v_z'\frac{\partial T'}{\partial z'}\right]=A^2\left\{\frac{1}{r'}\frac{\partial}{\partial r'}\left[r'\left(\frac{\partial T'}{\partial r'}+\frac{\partial T_s'}{\partial r'}\right)\right]\right\}+\frac{\partial^2 T'}{\partial z'^2} \tag{4.56}$$

At $z'=h'$:

$$2\left[1+A^2\left(\frac{\partial h'}{\partial r'}\right)^2\right]^{\frac{1}{2}}\left\{A^4\left[\frac{\partial v_r'}{\partial r'}\left(\frac{\partial h'}{\partial r'}\right)^2-\frac{\partial h'}{\partial r'}\frac{\partial v_z'}{\partial r'}\right]+A^2\left[\frac{\partial v_z'}{\partial z'}-\frac{\partial h'}{\partial r'}\frac{\partial v_r'}{\partial z'}\right]\right\}=$$
$$p\left[1+A^2\left(\frac{\partial h'}{\partial r'}\right)^2\right]^{\frac{3}{2}}+\frac{A^3}{C}\left[1-\frac{C}{A}\left(T'+T_s'\right)\right]\left[\frac{\partial^2 h'}{\partial r'^2}+\frac{1}{r'}\frac{\partial h'}{\partial r'}\right] \tag{4.57}$$
$$+\frac{A^5}{C}\left[1-\frac{C}{A}\left(T'+T_s'\right)\right]\left[\frac{1}{r'}\left(\frac{\partial h'}{\partial r'}\right)^3\right]$$

$$\left[1+A^2\left(\frac{\partial h'}{\partial r'}\right)^2\right]^{-\frac{1}{2}}\left[\begin{array}{l}-2A^2\left[\begin{array}{l}\frac{\partial h'}{\partial r'}\frac{\partial v_r'}{\partial r'}+\frac{\partial v_z'}{\partial r'}-\\ \frac{\partial v_z}{\partial r}\left(\frac{\partial h'}{\partial r'}\right)^2+2\frac{\partial h'}{\partial r'}\frac{\partial v_z'}{\partial z'}\end{array}\right]\\ -A^4\frac{\partial v_r'}{\partial z'}\left(\frac{\partial h'}{\partial r'}\right)^2+\frac{\partial v_r'}{\partial z'}\end{array}\right]=\frac{\partial T'}{\partial r'}+\frac{\partial T_s'}{\partial r'}+\frac{\partial h'}{\partial r'}\frac{\partial T'}{\partial z'} \tag{4.58}$$

$$v_r'\frac{\partial h'}{\partial r'}-v_z'=0 \tag{4.59}$$

$$\left[1+A^2\left(\frac{\partial h'}{\partial r'}\right)^2\right]^{-\frac{1}{2}}\left[\frac{\partial T'}{\partial z'}-A^2\frac{\partial h'}{\partial r'}\left(\frac{\partial T'}{\partial r'}+\frac{\partial T_s'}{\partial r'}\right)\right]=-Bi\left(T'+T_s'-T_g'\right) \tag{4.60}$$

At $z'=0$:

$$v_r'=v_z'=0 \tag{4.61}$$

$$T'=0 \tag{4.62}$$

For $r'=1$:

$$v_r'=v_z'=\frac{\partial h'}{\partial r'}=0 \tag{4.63}$$

At $r'=0$:

$$\frac{\partial h'}{\partial r'}=\frac{\partial^3 h'}{\partial r'^3}=0 \tag{4.64}$$

Seeking an asymptotic solution for Equations 4.53–4.64 in the limit of a very thin film, or $A\to 0$, the system of equations reduces to the following:

$$\frac{1}{r'}\frac{\partial}{\partial r'}\left(r'v_r'\right)+\frac{\partial}{\partial z'}\left(v_z'\right)=0 \tag{4.65}$$

$$\frac{\partial^2 v_r'}{\partial z'^2}=\frac{\partial p'}{\partial r'} \tag{4.66}$$

$$\frac{\partial p'}{\partial z'}=\frac{Bo\,A}{C} \tag{4.67}$$

$$\frac{\partial^2 T'}{\partial z'^2}=0 \tag{4.68}$$

At $z'=h'$:

$$p'=-\frac{A^3}{C}\left[\frac{\partial^2 h'}{\partial r'^2}+\frac{1}{r'}\frac{\partial h'}{\partial r'}\right] \tag{4.69}$$

$$\frac{\partial v_r'}{\partial z'}=\frac{\partial T'}{\partial r'}+\frac{\partial T_s'}{\partial r'}+\frac{\partial h'}{\partial r'}\frac{\partial T'}{\partial z'} \tag{4.70}$$

$$v_r' \frac{\partial h'}{\partial r'} - v_z' = 0 \tag{4.71}$$

$$\frac{\partial T'}{\partial z'} = -Bi\left(T' + T_s' - T_g'\right) \tag{4.72}$$

At $z' = 0$:

$$v_r' = v_z' = 0 \tag{4.73}$$

$$T' = 0 \tag{4.74}$$

For $r' = 1$:

$$v_r' = v_z' = \frac{\partial h'}{\partial r'} = 0 \tag{4.75}$$

For $r' = 0$:

$$\frac{\partial h'}{\partial r'} = \frac{\partial^3 h'}{\partial r'^3} = 0 \tag{4.76}$$

The system of Equations 4.65–4.76 can be reduced to a single nonlinear equation for the height of the liquid layer. Noting that the energy balance, Equation 4.68, indicates that the liquid layer is in a state of pure conduction, the temperature distribution can first be determined from Equations 4.68, 4.72, 4.73, and 4.74.

$$T' = \frac{Bi\left(T_g' - T_s'\right)}{1 + Bi\, h'} z' \tag{4.77}$$

The partial derivatives with respect to r' and z' are then:

$$\frac{\partial T'}{\partial r'} = \left[\frac{Bi\left(T_g' - T_s'\right)}{1 + Bi\, h'}\right]_{r'} z' \tag{4.78}$$

$$\frac{\partial T'}{\partial z'} = \frac{Bi\left(T_g' - T_s'\right)}{1 + Bi\, h'} \tag{4.79}$$

After some algebra, Equations 4.67 and 4.69 are solved for the pressure distribution:

$$p' = \frac{Bo\,A}{C} z' - \left[\frac{Bo\,A}{C} h' + \frac{A^3}{C} \left(\frac{\partial^2 h'}{\partial r'^2} + \frac{1}{r'} \frac{\partial h'}{\partial r'} \right) \right] \tag{4.80}$$

The partial derivative of the pressure distribution with respect to r is then:

$$\frac{\partial p'}{\partial r'} = -\left[\frac{Bo\,A}{C} h'_{r'} + \frac{A^3}{C} \frac{\partial}{\partial r'} \left(\frac{\partial^2 h'}{\partial r'^2} + \frac{1}{r'} \frac{\partial h'}{\partial r'} \right) \right] \tag{4.81}$$

Using the r-momentum equation, the tangential stress condition at the interface, and the solid surface boundary conditions (Equations 4.66, 4.70, 4.73, and 4.74), an expression is found for the horizontal velocity component.

$$v_r' = -\left[\frac{Bo\,A}{C} \frac{\partial h'}{\partial r'} + \frac{A^3}{C} \frac{\partial}{\partial r'} \left(\frac{\partial^2 h'}{\partial r'^2} + \frac{1}{r'} \frac{\partial h'}{\partial r'} \right) \right] \left(\frac{z'^2}{2} - h' z' \right) + \frac{\partial}{\partial r'} \left[\frac{Bi\,h' T_g' + T_s'}{1 + Bi\,h'} \right] z' \tag{4.82}$$

The vertical velocity component can likewise be determined from the continuity equation and the solid surface boundary condition (Equations 4.65, 4.73, and 4.74). After substitution and simplification, the vertical velocity is given by:

$$v_z' = -\frac{1}{r'} \frac{\partial}{\partial r'} \left\{ \begin{array}{l} -\left[\frac{Bo\,A}{C} \frac{\partial h'}{\partial r'} + \frac{A^3}{C} \frac{\partial}{\partial r'} \left(\frac{\partial^2 h'}{\partial r'^2} + \frac{1}{r'} \frac{\partial h'}{\partial r'} \right) \right] \left(\frac{z'^3}{6} - h' \frac{z'^2}{2} \right) \\ + \frac{\partial}{\partial r'} \left[\frac{Bi\,h' T_g' + T_s'}{1 + Bi\,h'} \right] \frac{z'^2}{2} \end{array} \right\} \tag{4.83}$$

Now applying the kinematic condition at the interface, the leading order asymptotic expansion gives the following expression for steady-state, axisymmetric thermocapillary flow in a thin liquid layer:

$$\frac{\partial}{\partial r'} \left\{ \left[\frac{Bo\,A}{C} \frac{\partial h'}{\partial r'} + \frac{A^3}{C} \frac{\partial}{\partial r'} \left(\frac{\partial^2 h'}{\partial r'^2} + \frac{1}{r'} \frac{\partial h'}{\partial r'} \right) \right] \left(\frac{h'^3}{3} \right) + \frac{\partial}{\partial r'} \left[\frac{Bi\,h' T_g' + T_s'}{1 + Bi\,h'} \right] \frac{h'^2}{2} \right\} = 0 \tag{4.84}$$

This equation is the equivalent of an axisymmetric, steady-state volume flux balance for the thin liquid layer.

$$q_r' = 0 \tag{4.85}$$

where q_r' is the volume flux. However, the axisymmetric assumption at $r' = 0$ and the solid wall boundary at $r' = 1$ require that q = 0 at these locations. Thus, Equation 4.84 can be reduced to the following:

$$\frac{\partial^3 h'}{\partial r'^3} h' + \frac{\partial^2 h'}{\partial r'^2} \frac{h'}{r'} + \left(\frac{Bo}{A^2} - \frac{1}{r'^2} \right) \frac{\partial h'}{\partial r'} h' + \frac{3}{2} \frac{C}{A^3} \frac{\partial}{\partial r'} \left[\frac{Bi\, h' T_g' + T_s'}{1 + Bi\, h'} \right] = 0 \tag{4.86}$$

If the convective cooling by the air above the liquid is assumed to be negligible, $Bi = 0$. Then, Equation 4.86 becomes:

$$\frac{\partial^3 h'}{\partial r'^3} h' + \frac{\partial^2 h'}{\partial r'^2} \frac{h'}{r'} + \left(\frac{Bo}{A^2} - \frac{1}{r'^2} \right) \frac{\partial h'}{\partial r'} h' + \frac{3}{2} \frac{C}{A^3} \frac{\partial T_s'}{\partial r'} = 0 \tag{4.87}$$

One final simplification can be made, based upon the work of Tan, *et al*. (1990). If the application of the asymptotic analysis is limited to cases in which $A^3 \ll C$, Equation 4.87 is further reduced to the following nonlinear equation for the nondimensional steady-state, axisymmetric height of a thin liquid layer, h', resting atop a non-isothermal solid surface with a known radial temperature distribution T_s'.

$$\frac{\partial h'}{\partial r'} h' + \frac{3}{2} \frac{C}{Bo\, A} \frac{\partial T_s'}{\partial r'} = 0 \tag{4.88}$$

4.1.2. Shooting Method Solution

A numerical solution to Equation 4.88 was developed using a shooting method implemented in MATLAB v7.0 to determine the nondimensional steady-state film height h'. The method utilizes a function called "ode45" in MATLAB 7.0 that finds the solution of a system of ordinary differential equations for a specified interval. Rearranging Equation 4.88, the slope of the profile can be determined at a particular

radial location given some knowledge of the temperature distribution and the height of the film at that point.

$$\frac{\partial h'}{\partial r'} = -\frac{3}{2}\frac{C}{Bo\,A}\frac{1}{h'}\frac{\partial T_s'}{\partial r'} \tag{4.89}$$

The non-dimensional temperature distribution, T_s, should be a monotonic function of r' with its maximum at $r' = 0$ and its minimum at $r' = 1$. For these studies, the dimensional temperature along the solid wall was taken to be a Gaussian distribution as defined in Equation 4.90.

$$T_s = C_1 \exp\{-r'^2 / C_2\} + C_3 \tag{4.90}$$

The amplitude, width, and offset of this Gaussian temperature profile are denoted by C_1, C_2, and C_3, respectively. According to Equation 4.34, the non-dimensional temperature distribution along the solid wall is then:

$$T_s' = \frac{\exp\left(-r'^2 / C_2\right) - \exp\left(-1/C_2\right)}{1 - \exp\left(-1/C_2\right)} \tag{4.91}$$

In this formulation, it is only necessary to specify a width to the distribution, and for consistency, $C_2 = 0.2$ in all cases. The choice of this value is not entirely arbitrary. A Gaussian curve-fit was applied to the experimental temperature measurements from several trials, and from these data, it was determined that the best curve-fits had a width of 0.2. An example of this curve-fit is shown in Figure 4.2 for the experimental case of $A = 0.014$, $Bo = 0.48$, and $C = 1.7 \times 10^{-3}$; the curve-fit has a $R^2 > 0.95$.

To find the solution of the differential equation in Equation 4.89, the steady-state height h' at $r' = 0$ must also be specified. Because the solution is dependent on the chosen value of h' at $r' = 0$, it may not provide a physically significant result. It is thus

necessary to verify the solution by comparing the dimensionless volume under the resultant profile h' with its initial value of π. The volume of fluid is determined by simple numerical integration under the axisymmetric height profile. The solution of Equation 4.89 is determined using the following procedure. First, the steady-state height at $r' = 0$ is chosen to be $h' = 0$. Second, the shooting method is used to obtain the steady-state free-surface profile from $r' = 0$ to $r' = 1$. Third, the absolute difference in volume is calculated and if it exceeds 0.1%, the initial value of h' is incremented. These steps are repeated until volume under the profile found by the shooting method is within 0.1% of the dimensionless volume.

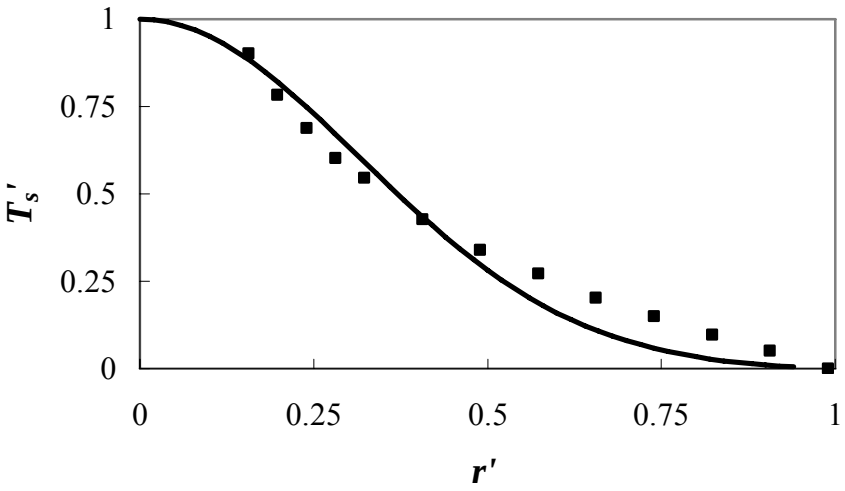

Figure 4.2: Comparison of dimensionless experimentally measured temperature data (■) with a Gaussian curve-fit with a width $C_2 = 0.2$ (solid line) for a liquid film of $A = 0.014$, $Bo = 0.48$, and $C = 1.7 \times 10^{-3}$ with $R^2 > 0.95$.

4.2. Numerical Modeling

In this section, the full numerical simulation of an axisymmetric liquid layer exposed to a spatially-varying surface temperature is described. The simulations utilize

the level contour reconstruction method developed by Shin [63, 65] based on in the finite difference/front tracking code of Unverdi and Tryggvason [74, 75] for two-dimensional multi-fluid flows.

4.2.1. Level Contour Reconstruction Method

The level contour reconstruction method is a front-tracking technique that has been simplified by removing logical connectivity and thus eliminating much of the associated computational load. The accuracy and advantages of typical Lagrangian surface tracking are still maintained. This front-tracking method employs two grids: a two-dimensional Eulerian mesh and a one-dimensional discretized Lagrangian mesh. The level contour method uses a Heaviside indicator function to assign elements within one fluid the value of unity while elements in the other fluid have the value zero. In contrast with other front-tracking methods, the liquid-gas interface is thus constructed with physical but not logical connections obviating the need for computationally intensive operations like element addition and deletion with connectivity and resorting. The element areas and interface normals are automatically defined following the construction of the interface making it possible to compute surface tension forces directly on the interface elements. The physics at the interface is determined prior to the distribution of information to the stationary grid.

4.2.2. Mathematical Development

This section outlines the derivation of the governing equations used in the full direct numerical simulations and the corresponding boundary conditions. Because the

problem is formulated for multiple fluids, the governing equations are written such that a single set of two-dimensional equations is valid for both the thin liquid layer and the bounding gas.

4.2.2.1. *Governing Equations*

The assumptions used in this formulation include that the heating of the solid surface is axisymmetric and variations in the toroidal direction are negligible. The interface effects are incorporated by using delta-function source terms in the local single-field formulation. By assuming the bulk fluids to be incompressible, the material properties are thus considered to be constant although not necessarily equal for the two fluids. The material property fields can be defined over the entire domain using the Heaviside indicator function $I(\mathbf{r}, t)$ as exemplified in Equation 4.92 for density.

$$\rho(\mathbf{r},t) = \rho_L + (\rho_G - \rho_L) I(\mathbf{r},t) \tag{4.92}$$

The indicator function is determined by solving the Poisson equation.

$$\nabla^2 I = \nabla \cdot \int_{\Gamma(t)} \mathbf{n}\delta(\mathbf{r} - \mathbf{r}_f)\, ds \tag{4.93}$$

where $\mathbf{n}$ is the unit normal to the interface, $\mathbf{r}_f$ is a parameterization of the interface and $\delta(\mathbf{r}\text{-}\mathbf{r}_f)$ is a delta function that is only nonzero when $\mathbf{r} = \mathbf{r}_f$. The interface is advected in a Lagrangian manner by integration:

$$\frac{d\,\mathbf{r}_f}{dt} \cdot \mathbf{n} = \mathbf{v}_f \cdot \mathbf{n} \tag{4.94}$$

where $\mathbf{v}_f$ is the interface velocity vector and will be equal to the fluid velocity at the interface in the absence of any phase change. As shown above, the physics at the interface only accounts for the normal component of the interface motion. Because the

tangential component does not appear, it is assumed that the interface and the fluid at the interface have the same tangential velocity component.

In order to simulate the deformation of a thin layer of liquid subjected to a non-uniform surface temperature, the mass, momentum, and energy equations are written for the entire flow field neglecting mass transfer at the interface due to evaporation and condensation. Following the derivation of Shin, *et al*. [65] and using the velocity scaling in Equation 4.50, the dimensionless variables indicated with primes take the following values:

$$r' = \frac{r}{R_o} \tag{4.95}$$

$$z' = \frac{z}{h_o} \tag{4.96}$$

$$v_r' = \frac{\rho_L R_o}{\mu_L} v_r \tag{4.97}$$

$$v_z' = \frac{\rho_L R_o}{a \mu_L} v_z \tag{4.98}$$

$$t' = \frac{\mu_L}{\rho_L R_o^2} t \tag{4.99}$$

$$T' = \frac{\left(T - T_{min}\right)}{\Delta T} \tag{4.100}$$

$$p' = \frac{\rho_L h_o^2}{\mu_L} p \tag{4.101}$$

Because of the multi-fluid domain, subscripts of L and G have been introduced to indicate whether the material property is evaluated for the liquid or gas phase,

respectively. The single field formulation also requires the following terms to specify the local material properties in the governing equations.

$$\rho^+ = \frac{\rho(\mathbf{r},t)}{\rho_L} \tag{4.102}$$

$$\mu^+ = \frac{\mu(\mathbf{r},t)}{\mu_L} \tag{4.103}$$

$$k^+ = \frac{k(\mathbf{r},t)}{k_L} \tag{4.104}$$

$$c^+ = \frac{c(\mathbf{r},t)}{c_L} \tag{4.105}$$

The non-dimensional governing equations (Equations 4.8–4.10) can be written as follows for the axisymmetric, transient case using the scales of Equations 4.95–4.101 and the material property ratios of Equations 4.102–4.105:

$$\frac{\partial v_r'}{\partial r'} + \frac{v_r'}{r'} + \frac{\partial v_z'}{\partial z'} = 0 \tag{4.106}$$

$$\begin{aligned} &A^2\rho^+\left(\frac{\partial v_r'}{\partial t'} + v_r'\frac{\partial v_r'}{\partial r'} + v_z\frac{\partial v_r'}{\partial z'}\right) = \\ &-\frac{\partial p'}{\partial r'} + A^2\frac{1}{r'}\frac{\partial}{\partial r'}\left(2\mu^+\frac{1}{r'}\frac{\partial v_r'}{\partial r'}\right) + A^2\frac{\partial}{\partial z'}\left(\mu^+\frac{\partial v_z'}{\partial r'}\right) \\ &-2A^2\mu^+\frac{v_r'}{r'^2} + \frac{\partial}{\partial z'}\left(\mu^+\frac{\partial v_r'}{\partial z'}\right) + \int\left(\sigma'\kappa\mathbf{n} + \frac{\partial\sigma'}{\partial s}\mathbf{t}\right)\delta\, ds\cdot\mathbf{i} \end{aligned} \tag{4.107}$$

$$\begin{aligned} &A^4\rho^+\left(\frac{\partial v_z'}{\partial t'} + v_r'\frac{\partial v_z'}{\partial r'} + v_z'\frac{\partial u_z'}{\partial z'}\right) = -\frac{\partial p'}{\partial z'} + \frac{BoM}{Pr\,C}\rho^+ \\ &+A^4\frac{1}{r'}\frac{\partial}{\partial r'}\left[\mu^+ r'\left(\frac{\partial v_z'}{\partial r'} + \frac{\partial v_r'}{\partial z'}\right)\right] + A^2\frac{\partial}{\partial z'}\left(2\mu^+\frac{\partial v_z'}{\partial z'}\right) + \int\left(\sigma'\kappa\mathbf{n} + \frac{\partial\sigma'}{\partial s}\mathbf{t}\right)\delta\, ds\cdot\mathbf{i} \end{aligned} \tag{4.108}$$

$$A^2\rho^+\left(\frac{\partial\left(c^+T'\right)}{\partial t'}+v_r'\frac{\partial\left(c^+T'\right)}{\partial r'}+v_z'\frac{\partial\left(c^+T'\right)}{\partial z'}\right)= \frac{a^2}{\mathrm{Pr}}\frac{1}{r'}\frac{\partial}{\partial r'}\left(k^+r'\frac{\partial T'}{\partial r'}\right)+\frac{1}{\mathrm{Pr}}\frac{\partial}{\partial z'}\left(k^+\frac{\partial T'}{\partial z'}\right) \tag{4.109}$$

The surface tension forces that act solely at the interface have been included as delta-function source terms in the momentum Equations 4.106 and 4.107. The dimensionless surface tension is assumed to vary linearly with temperature T' as before and becomes:

$$\sigma'=\frac{M\,A}{Pr\,C}-\frac{M}{Pr\,A}T' \tag{4.110}$$

Thus, the normal surface tension force and thermocapillary forces are incorporated while automatically satisfying the boundary conditions at the interface.

4.2.2.2. *Boundary Conditions*

Figure 4.3 depicts the initial surface configuration and boundary conditions used to model a horizontal surface subjected to a temperature gradient. The investigation window used in these simulations spans $0\le r'\le 1$ and $0\le z'\le 3$. The thin liquid layer and bounding gas are initially quiescent atop a solid surface and are assigned a temperature $T_{min}'=0$. Along the edge of the domain at $r'=0$, the symmetric boundary conditions from Equation 4.49 are once again applied. Along the boundary at $r'=1$, it is assumed in these simulations that $A\ll 1$, and that a periodic set of conditions will suffice. These conditions require symmetry in the local film height about $r'=1$, so again Equation 4.49 applies. At the liquid-solid interface $z'=0$, no-slip and perfect conduction are assumed as before in Equation 4.47. The final set of boundary conditions occurs at $z'=3$ where the bounding gas is left open to the atmosphere.

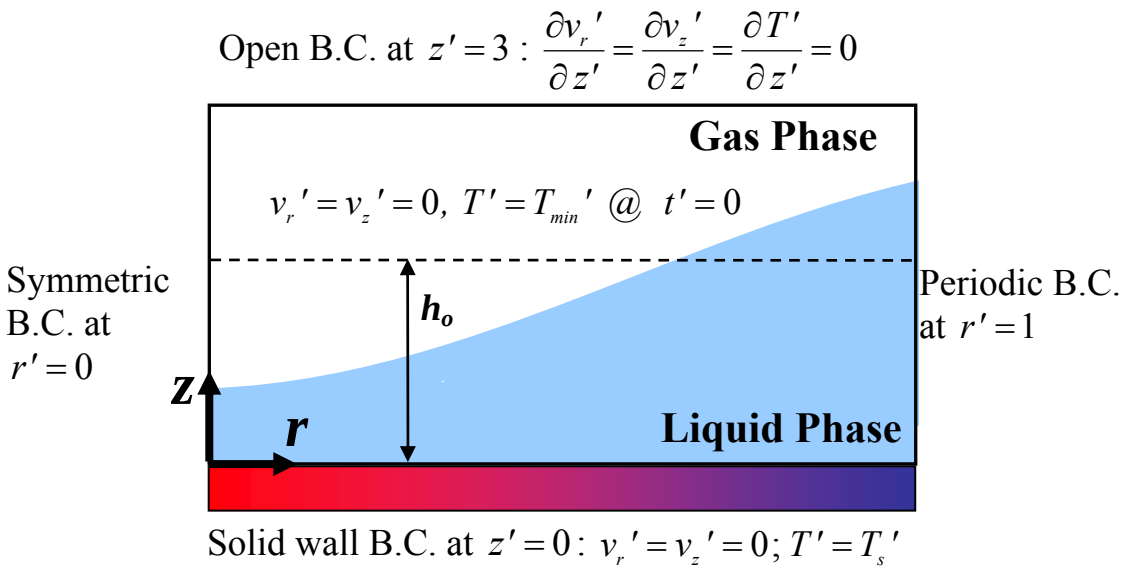

Figure 4.3: Initial surface configuration and boundary conditions for a non-uniformly heated liquid layer above a horizontal solid surface.

4.2.3. Numerical Method

The numerical techniques employed in the novel front-tracking method developed by Shin [63] are detailed in this section. The reconstruction of the interface, the transfer of information between grids, the calculation of the source terms, and the finite differencing scheme are all discussed.

4.2.3.1. *Front Tracking*

As previously mentioned, the level contour reconstruction method utilizes a front tracking scheme with two grids. Figure 4.4 depicts the front-tracking concept using the Lagrangian grid to determine the interfacial geometry and physics to be used in the local calculations on the Eulerian grid. This technique is common to the numerical investigations in Refs. [45, 61, 73]. The front-tracking technique used here differs from

the original studies because the Lagrangian grid is not a linked list that retains connectivity between neighboring interface nodes. Instead, the inherent computational burden associated with addition and deletion of elements in linked lists is eliminated by representing the interface with an indicator function in addition to the Lagrangian grid as developed by Shin [63].

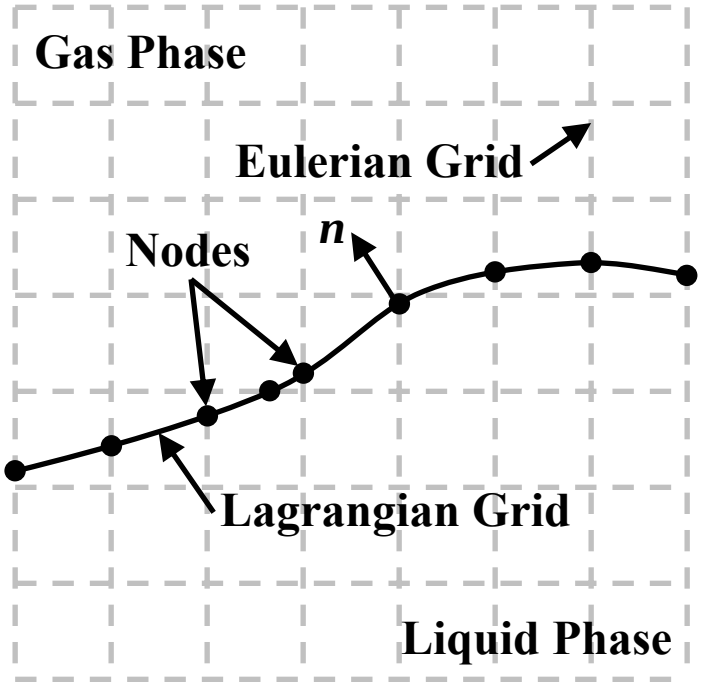

Figure 4.4: Schematic of the two grids used in the numerical tracking of the interface.

With two representations of the interface, it is possible to reconstruct one while retaining knowledge of the interface position. For example, if the indicator function is known, a series of interface elements can be placed along the $I(\mathbf{r}, t) = 0.5$ contour. Similarly, the indicator function can be found using the Poisson equation (Equation 4.93) if the interface element locations are known. To construct the interface elements from the indicator function, a linear contour line of $I(\mathbf{r}, t) = 0.5$ is drawn across each cell in

the stationary grid as shown in Figure 4.5(a). Using linear interpolation to construct these elements ensures that the endpoints of neighboring elements have exactly the same location, meaning that they are physically linked and logical connection of elements is not necessary. Orienting the interface is simply a matter of directing the surface normal such that it points in the direction of the maximum value of the indicator function as shown in Figure 4.5(b).

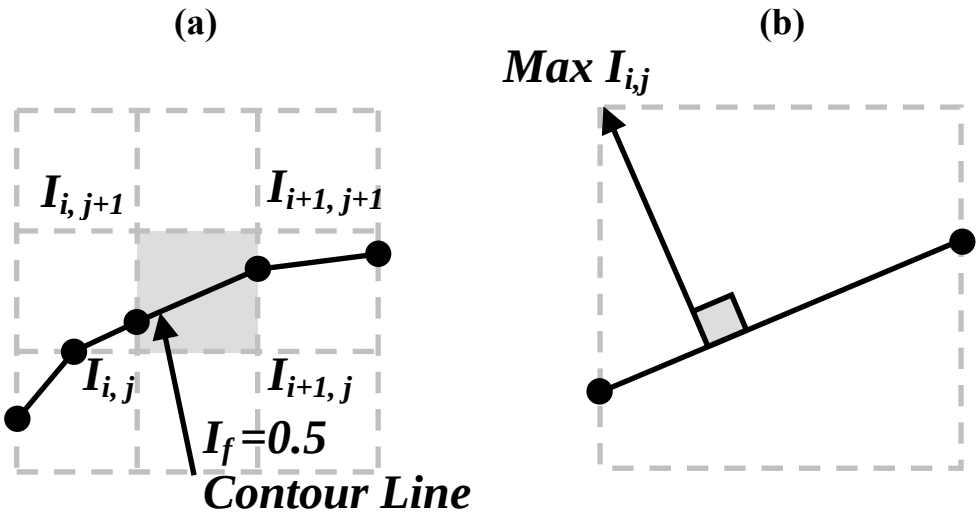

Figure 4.5: (a) Construction of interfacial elements using the $I(\mathbf{r}, t) = 0.5$ contour line. (b) Orientation of surface normal for an individual surface element.

Reconstruction of the interface is necessary to ensure a smooth topology especially in regions of high surface curvature. The procedure described above is used to reconstruct the interface every 100 time steps, a frequency that is sufficient to maintain a smooth interface in this application. For the time steps in which reconstruction does not occur, the interface is tracked by integration of Equation 4.94. Interface reconstruction can result in small discrepancies in the global mass due to coarse grid resolution.

Therefore, the reconstruction step is slightly modified such that an optimum indicator function value is chosen to conserve the mass of the liquid film. The optimum value of $I(\mathbf{r}, t)$ varies only slightly from 0.5 and was shown by Shin [63] to approach 0.5 as the grid resolution was increased.

4.2.3.2. *Information Exchange between Grids*

Passing of information between the two grids occurs at every time step and is performed using Peskin's Immersed Boundary Method [44]. Source terms must be calculated along the interface and distributed to the stationary grid. Conversely, field variables must be transferred from the stationary grid to the interface. The immersed boundary method assigns a finite thickness to the infinitely thin interface by means of a distribution function that places sources at several grid points near the interface. Typically, the thickness of the interface is on the order of the stationary grid size and remains constant throughout the simulation to avoid numerical diffusion.

In the formulation of Equations 4.93, 4.107, and 4.108, the general form of the source term integrals is:

$$\Phi = \int_{\Gamma(t)} \phi \, \delta\left(\mathbf{r} - \mathbf{r}_f\right) ds \tag{4.111}$$

where ϕ represents the source (*i.e.*, surface tension) and can be represented discretely as the following summation:

$$\Phi_{ij} = \sum_p \phi_p \, D_{ij}\left(\mathbf{r}_p\right) \Delta s \tag{4.112}$$

Here, Δs represents the element length as shown in Figure 4.6 and the Dirac delta function is approximated as the following for a grid point $\mathbf{r}_p = \left(r_p, z_p\right)$:

$$D_{ij}(\mathbf{r}) = \frac{\delta(r_p/d_r - i)\delta(z_p/d_z - j)}{d_r d_z} \tag{4.113}$$

Here, d_r and d_z represent the distance components of an element from a grid point and $\delta(r)$ can be determined from:

$$\delta(r) = \begin{cases} \delta_1(r), & |r| \le 1 \\ 1/2 - \delta_1(2 - |r|), & 1 < |r| < 2 \\ 0, & |r| \ge 2 \end{cases} \tag{4.114}$$

where:

$$\delta_1(r) = \frac{3 - 2|r| + \sqrt{1 + 4|r| - 4r^2}}{8} \tag{4.115}$$

Discrete fluid variables, R_{ij}, can likewise be transferred to the interface through interpolation:

$$R_p = \sum_{ij} d_r\, d_z\, R_{ij}\, D_{ij}(\mathbf{r}_p) \tag{4.116}$$

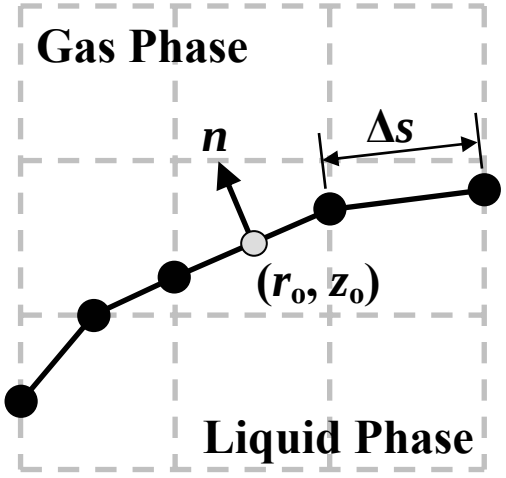

Figure 4.6: Schematic showing the definition of the normal vector *n* and element length Δs for each interface element.

4.2.3.3. *Calculation of Source Terms*

In the governing equations, surface integral source terms appear for the Heaviside indicator function and for the surface tension force. The right hand side of the Poisson equation (Equation 4.93) is determined using the surface normal and element length for each element as defined in Figure 4.6. Peskin's Immersed Boundary Method, described above, is then used to distribute this indicator function over the element centroids.

The integral source term for surface tension appears in the two momentum equations (4.107 and 4.108). The force is calculated directly on the interface making use of the tracked surface elements.

$$\delta F_e = \int_{\Delta s} \left[\sigma \kappa \mathbf{n} + \frac{\partial \sigma}{\partial s} \mathbf{t} \right] \mathrm{d}s \tag{4.117}$$

Using the Frenet relationship, $\kappa \mathbf{n} = d\mathbf{t}/ds$, the calculation of higher order derivatives to find the curvature is avoided and results in:

$$\delta F_e = = \int_B^A \frac{\partial (\sigma \mathbf{t})}{\partial s} \mathrm{d}s = \left(\sigma_A \mathbf{t}_A - \sigma_B \mathbf{t}_B \right) \tag{4.118}$$

Here, *A* and *B* refer to two neighboring elements between which the surface tension force is being evaluated. The tangents of these elements are known and the force is applied at the endpoints of each element and is directed inward toward the element center.

4.2.3.4. *Finite Differencing Scheme*

A projection method is used to calculate the fluid variables of **v**, *P*, and *T* using a first-order Euler time integration similar to that in Chorin [11] and Juric and Tryggvasson [24]. Equation 4.106 can be written discretely at time step *n* as:

. (4.119)

Similarly, Equations 4.107 and 4.108 become:

$$\frac{\mathbf{w}^{n+1}-\mathbf{w}^{n}}{\Delta t}=\mathbf{A}^{n}+\mathbf{F}^{n+1}-\nabla P \tag{4.120}$$

where the mass flux $\mathbf{w}=\rho\mathbf{v}$. The advection, diffusion, and gravitational terms from the momentum equations (4.106 and 4.107) are lumped into the parameter **A** while **F** contains the surface forces. Chorin's original projection method [11] breaks Equation 4.120 into two parts by introducing $\widetilde{\mathbf{w}}$ to represent the mass flux that would occur without the effect of pressure.

$$\frac{\widetilde{\mathbf{w}}-\mathbf{w}^{n}}{\Delta t}=\mathbf{A}^{n}+\mathbf{F}^{n+1} \tag{4.121}$$

$$\frac{\mathbf{w}^{n+1}-\widetilde{\mathbf{w}}}{\Delta t}=\nabla P \tag{4.122}$$

Equation 4.121 can be evaluated for the mass flux $\widetilde{\mathbf{w}}$. The pressure *P* can be found by taking the divergence of Equation 4.122 and can be solved applying Equation 4.119 and using a standard fast Poisson solver.

$$\nabla^{2}P=\frac{\nabla\cdot\widetilde{\mathbf{w}}}{\Delta t} \tag{4.123}$$

The values of $\widetilde{\mathbf{w}}$ and *P* can then be used to find the velocity at the next time step, v^{n+1}, from Equation 4.122 by dividing $\mathbf{w}^{n+1}$ by the fluid density

CHAPTER 5

RESULTS AND DISCUSSION

This chapter presents and discusses the experimental, numerical, and theoretical results on the free-surface behavior of thermocapillary flows. Reflectance shadowgraphy of the free surface is used to qualitatively map out flow regimes in a parameter space described by the Marangoni and dynamic Bond numbers. Measurements of the free-surface height obtained using the needle contact method and the laser-confocal displacement sensor are then presented and compared to both numerical and theoretical predictions.

The parameter space investigated in this thesis spans aspect ratios $0.007 < A < 0.039$, dynamic Bond numbers $0.04 < Bo_D < 1.32$, Bond numbers $0.11 < Bo < 4.10$, capillary numbers $0 < C < 8.0\times10^{-3}$, and Marangoni numbers $0 < M < 990$. Thermocapillary effects are significant in all of these cases; buoyancy effects are also significant for the thicker liquid layers (*i.e.*, larger Bo_D). Riley and Neitzel [48] found in their investigation of thermocapillary flows in 2D geometries that thermocapillary and buoyancy effects are non-negligible at $Bo_D > 0.22$. Our results (see Section 5.2.1) suggest that the critical dynamic Bond number for axisymmetric layers is about 0.19. We therefore classify layers based on their dynamic Bond number as:

- thin ($Bo_D < 0.19$), where thermocapillary effects dominate, deforming the liquid free surface and leading to film rupture as ΔT (*i.e.*, M or C) increases; or
- thick ($Bo_D > 0.19$), where inertia and buoyancy also affect the thermocapillary flow.

Horizontal liquid layers heated non-uniformly from below, as studied in this thesis, are subject to thermocapillary, hydrostatic, buoyancy, inertial, and surface tension effects. For thin films, heat transfer across the film thickness is primarily due to conduction, making buoyancy negligible. The hot spot at the center of the free surface creates thermocapillary stresses that shear the liquid and through viscous drag move fluid from the "hot" center outwards to the "cold" perimeter. This outward flow deforms the free surface, reducing and increasing the film thickness at the hot spot and cold perimeter, respectively. The presence of an end wall at the perimeter, as is the case here, creates capillary pressures that drive a return flow of colder fluid to the center, where it will be heated, repeating the cycle. The difference in film thickness due to the outward thermocapillary flow also imparts hydrostatic forces that can drive a return flow along the bottom of the liquid layer. If thermocapillary effects dominate the opposing capillary and hydrostatic pressures, the film will rupture. Near the point of rupture, small radii of curvature lead to capillary pressure dominating thermocapillary stresses [76].

For thick films, buoyancy and inertial effects also become significant. Buoyancy, or natural convection, is strongest at the center of the liquid layer (directly above the copper heater plug), where the fluid is heated from below and rises vertically toward the free surface. Thus, buoyancy and thermocapillary effects together drive the "outflow" towards the perimeter [48]. The marked velocity gradients created by these effects, along with capillary pressure, drive the return flow [79].

5.1. Reflectance Shadowgraphy Results

Reflectance shadowgraph images of the liquid free surface were acquired for dynamic Bond numbers ranging from 0.15 to 1.32. At each Bo_D, shadowgraphs were captured for several Marangoni numbers $0 < M < 990$. The small changes in free-surface height ($O(1\ \mu m)$) visualized with shadowgraphy were used to classify different flow regimes for thermocapillary flow. This section presents and discusses typical shadowgraph images that characterize each type of flow. The flow transitions are presented in a flow regime map in the M–Bo_D plane.

5.1.1. Flow Regime Descriptions

Thermocapillary flow instabilities have been the subject of many previous investigations, as detailed in Sec. 2.2. In contrast with previous studies, we focus here on axisymmetric discs of silicone oils. It is well-known that any nonzero radial temperature difference ΔT (*i.e.*, M) will create a thermocapillary flow. Once M exceeds a critical value, however, the flow becomes unstable so that any small perturbations cause transition to a new and different flow pattern. Three such flow regimes, similar to those seen in annular layers [1, 2, 4, 5], were observed in these experiments, namely steady, unicellular flow; steady, multi-cellular flow; and unsteady, three-dimensional flow.

5.1.1.1. *Steady, Unicellular Flow*

The basic flow state in the axisymmetric geometry studied in this thesis is pure thermocapillary convection where the radial temperature difference creates a surface tension gradient that drives a radial outflow near the top of the liquid layer so that the

layer “thins” over the hot center and “thickens” along the cool edges. This deformation causes a return flow driven by hydrostatic pressure differences along the bottom of the liquid layer, as shown schematically in Figure 5.1.

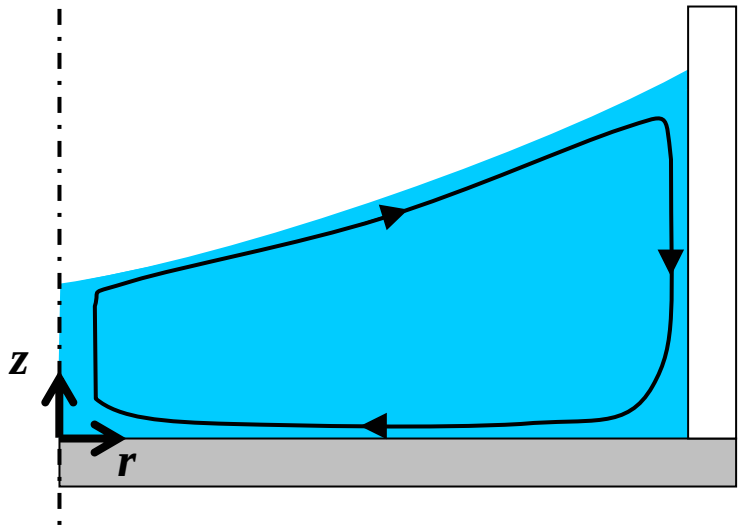

Figure 5.1: Schematic showing the typical flow pattern for steady unicellular thermocapillary flow.

In thin films, steady, unicellular thermocapillary flow drives global deformation of the liquid free surface. In these experiments, the center of the liquid is heated and the perimeter cooled, leading to a concave free surface that condenses light reflected back to the CCD. Typical shadowgraph images of thin liquid layers (Bo_D = 0.15) are shown for M = 0, 13 and 23 in Figure 5.2(a), along with corresponding ray-tracing diagrams illustrating how a decrease in the radius of curvature of the free surface qualitatively affects these shadowgraphs in Figure 5.2(b). At M = 0, the flat free surface is essentially a planar mirror. As M increases, the free surface becomes a parabolic reflector, focusing incident light into a smaller region near the center of the shadowgraph and making it

practically impossible to visualize the outer portions of the illuminated region. Although not shown here, dry-out occurs at $M = 28$.

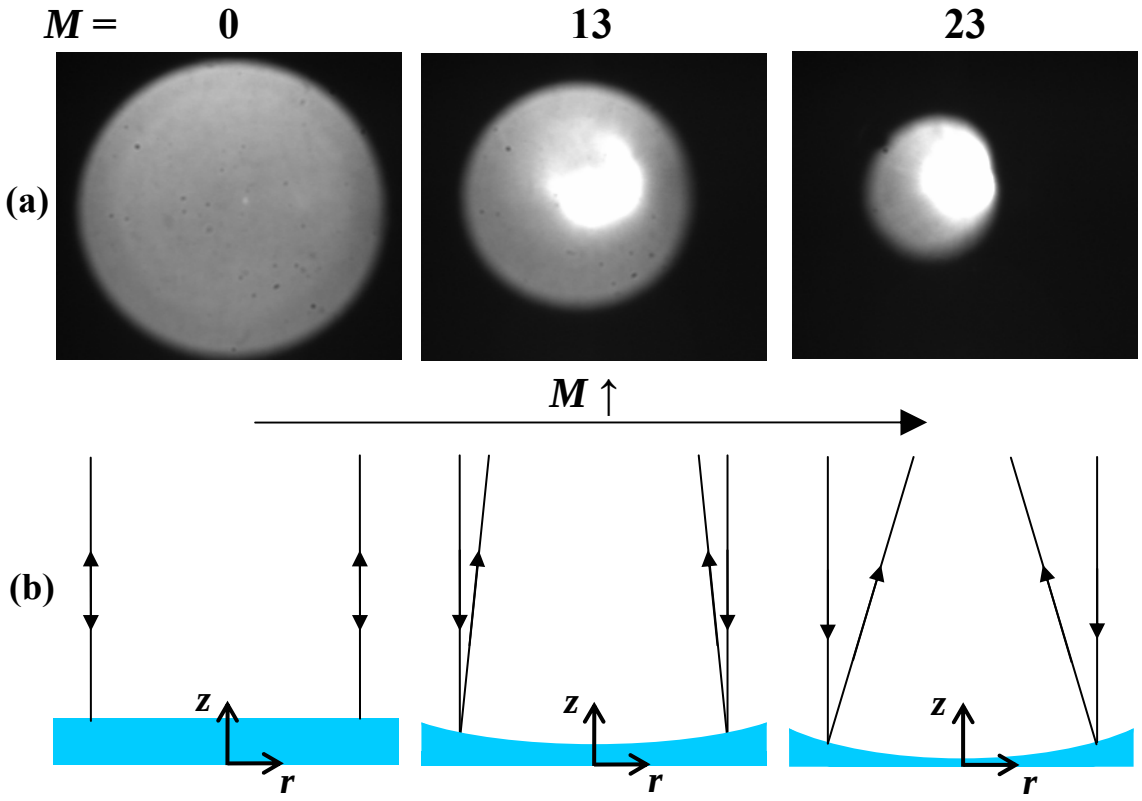

Figure 5.2: (a) Shadowgraphs of a thin film ($A = 0.013$, $Bo = 0.47$, and $Bo_D = 0.15$) and (b) diagrams showing the reflected light paths at the free surface as M increases.

Unlike previous studies in annular or 2D geometries [1, 8, 12], there is no solid surface to "pin" the contact line in the hot center of the film. The free-surface deformations observed here are hence significantly greater than those observed previously; these large deformations make it difficult to use shadowgraphy techniques to visualize the free surface of the thin-layer cases. Reflectance shadowgraphy, which can visualize a minimum free-surface deformation of about 1 μm (compared with a flat surface) [51], suggests that unicellular flow is maintained in thin layers until the layer

ruptures. Thermocapillary effects can rupture layers of $h_o < 1$ mm. Hydrothermal waves were not observed using this technique, because rupture of the film occurred prior to the initiation of hydrothermal waves.

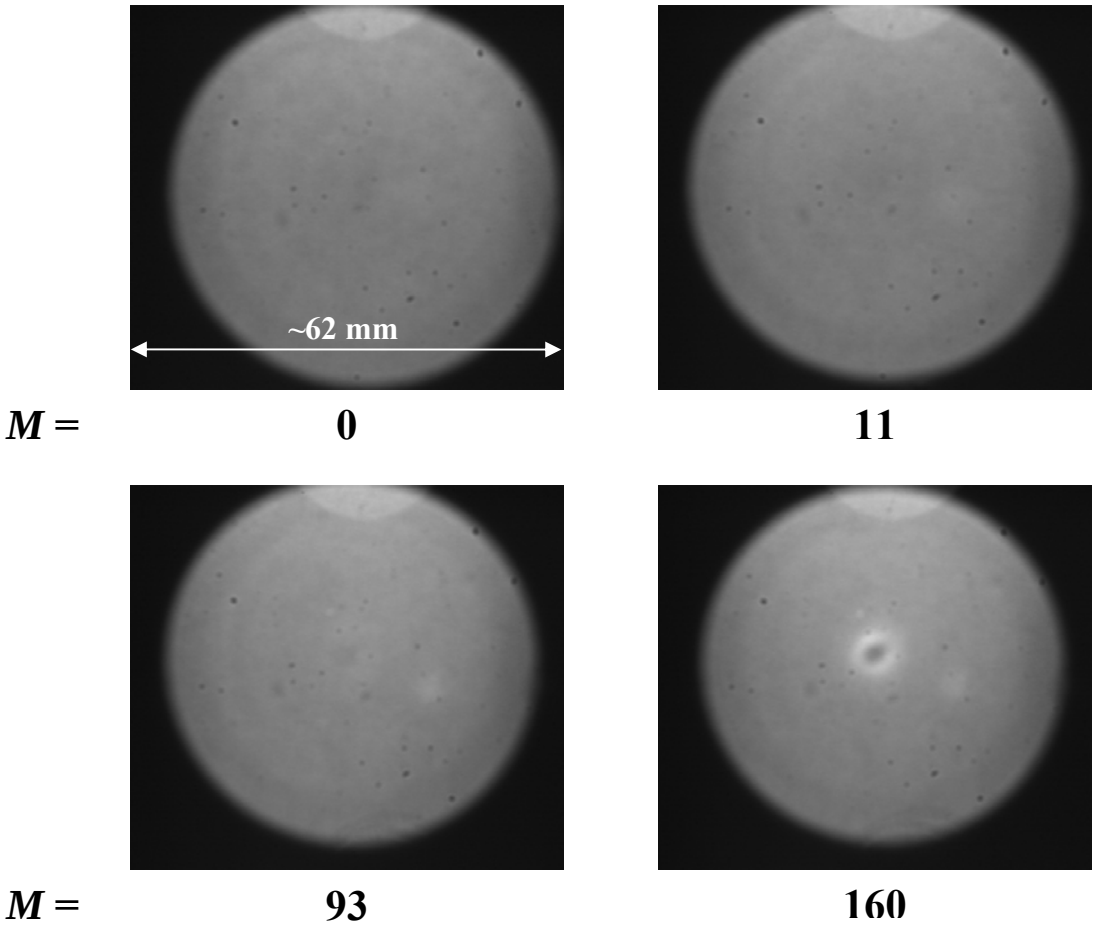

Figure 5.3: Shadowgraph images showing steady, unicellular thermocapillary convection for a liquid layer of $Bo_D = 1.10$ and $0 < M < 160$.

Free-surface deformation in thick layers is reduced to a degree where shadowgraphs can be used to visualize the free surface over most of the illuminated region. Figure 5.3 shows four shadowgraphs of a thick layer at $Bo_D = 1.10$ for $M = 0$, 11, 93 and 160. The illuminated region contracts slightly at higher M due to free-surface

deformation. Although this deformation increases the intensity at the center of the film, the shadowgraphs show a steady flow with a smoothly concave free surface representative of unicellular thermocapillary flow at all M values.

5.1.1.2. *Steady Multicellular Flow*

Transition from unicellular flow to a steady-state flow with several co-rotating, concentric cells occurs in thick liquid layers above a critical value of M. As pictured in Figure 5.4, the concentric, co-rotating cells lead to small (O(1 μm)) deformations of the free surface. Although this steady, multi-cellular flow has been previously observed in experiments of buoyant-thermocapillary liquid layers in 2D [27] and annular [53] geometries, the stability analysis of Smith and Davis [17, 18] does not predict the existence of such a flow state. Further studies show that steady, multi-cellular flows are created by the interaction of thermal boundary layers along the end walls with the basic thermocapillary flow; thus both buoyancy and thermocapillary effects must be significant for the onset of this flow regime.

The axisymmetric disc of liquid studied in this thesis eliminates the hot (usually inner) end wall which previous investigators found to be critical in the development of multi-cellular flows. Thus, the onset of the cells must be due to some other disturbance to the thermocapillary flow. The possibility of a Kelvin-Helmholtz instability leading to co-rotating cells was considered, since temperature differences along z in thicker films could lead to density stratification. According to Schlichting [52], viscous shear flows are unstable to cross-stream perturbations when $Ri < 0.0417$, where the Richardson number Ri is determined by $Ri = -\dfrac{g\beta\left(\partial T/\partial z\right)}{\rho\left(\partial u/\partial z\right)^2}$. Following Kirdyashkin's analysis [27],

the Richardson number in thermocapillary flows reduces to $Ri = 3\,Pr/2$, and therefore a Kelvin-Helmholtz instability can only arise in films of $Pr \ll 1$. Re-writing *Ri* in terms of the Prandtl number, however, assumes that the vertical temperature gradient is constant across the entire liquid film—which cannot be the case here, given the thermal boundary layers immediately above and below the solid and free surfaces, respectively. A local Richardson number based upon the temperature difference across such thermal boundary layers would clearly be much greater than that obtained by Kirdyashkin's analysis. Unfortunately, temperature measurements were not obtained within the liquid film, and the cell size of the numerical simulations is far too large to capture the thermal boundary layers. It is therefore impossible to estimate a local Richardson number in these experiments to characterize the onset of Kelvin-Helmholtz instabilities.

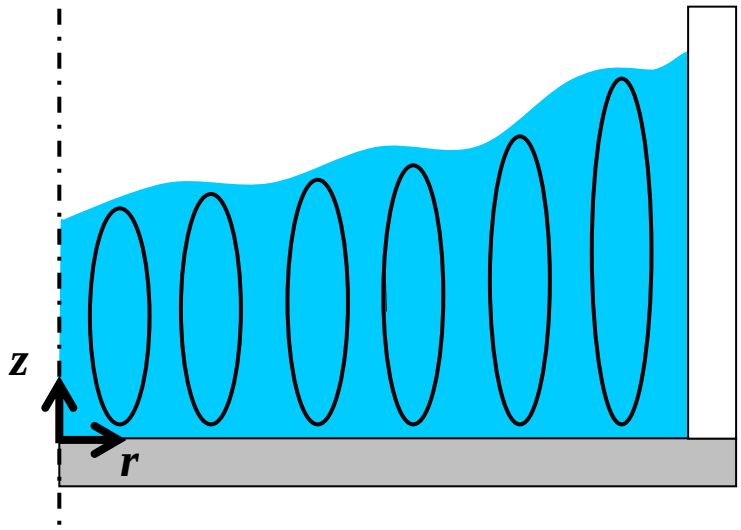

Figure 5.4: Schematic of co-rotating cells in steady, multi-cellular thermocapillary flow.

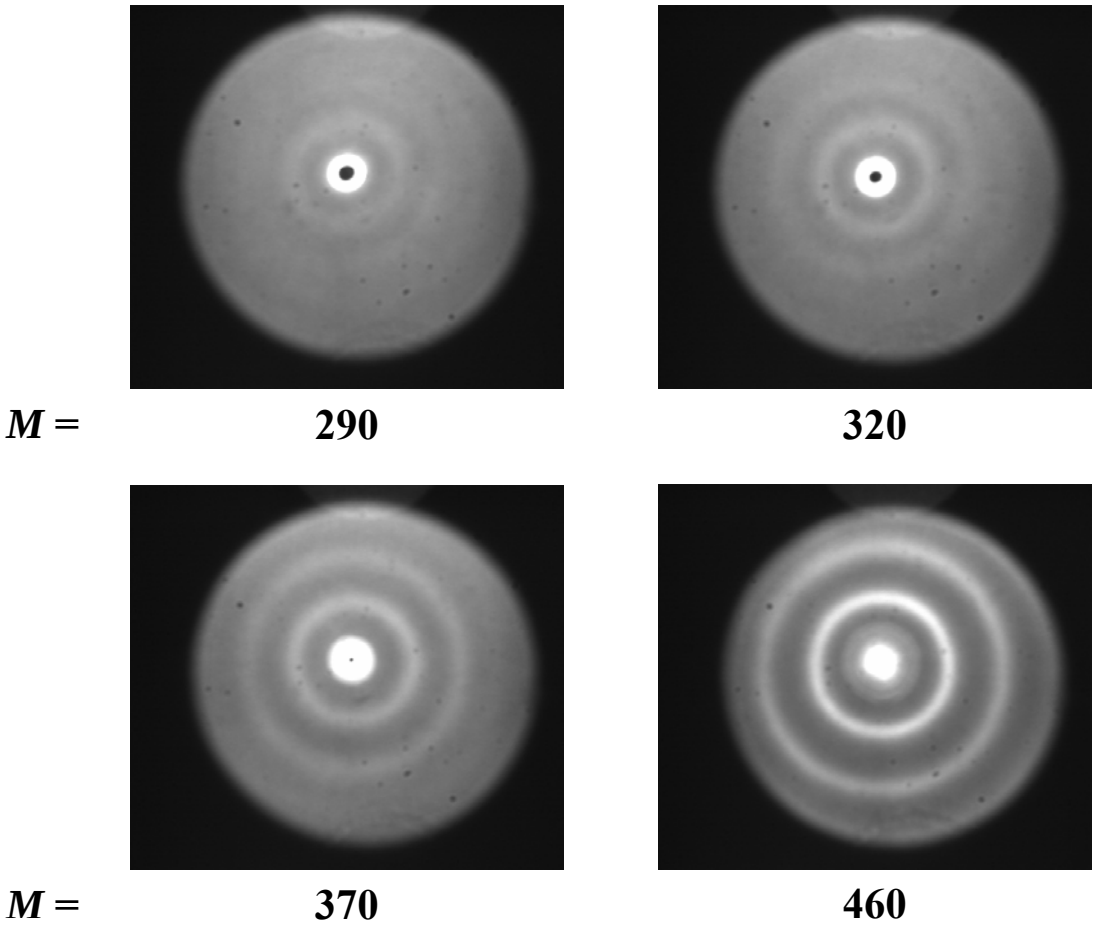

Figure 5.5: Shadowgraph images showing steady, multi-cellular thermocapillary convection for a liquid layer of Bo_D = 1.10 and 290 < M < 460.

Given the relatively small free-surface perturbations typical of this flow regime, shadowgraphs clearly show the steady, multi-cellular flow. Figure 5.5 shows steady, multi-cellular flow for a liquid layer of Bo_D = 1.10 at M = 290, 320, 370 and 460. Because concave regions of the interface condense the light and reflect it back through the lens, the brighter rings in the shadowgraph represent depressions in the free-surface (*i.e.*, thin regions). Conversely, incident light is likely to be scattered away from the lens by convex free-surface geometries and thus the darker circles in the shadowgraph correspond to thick regions. The position and dimensions of the concentric rolls are

time-independent, but the contrast between the brighter and darker regions increases with M, corresponding to larger velocity magnitudes in the cells and larger free-surface deformation. The temporal behavior of the multi-cellular flow is pictured in Figure 5.6, where the intensities of the shadowgraph along a line of pixels crossing $r' = 0$ are monitored for Bo_D = 1.10 and M = 460. The bright and dark bands in this Figure remain fixed in radial position, verifying the steadiness of the free-surface patterns under these conditions.

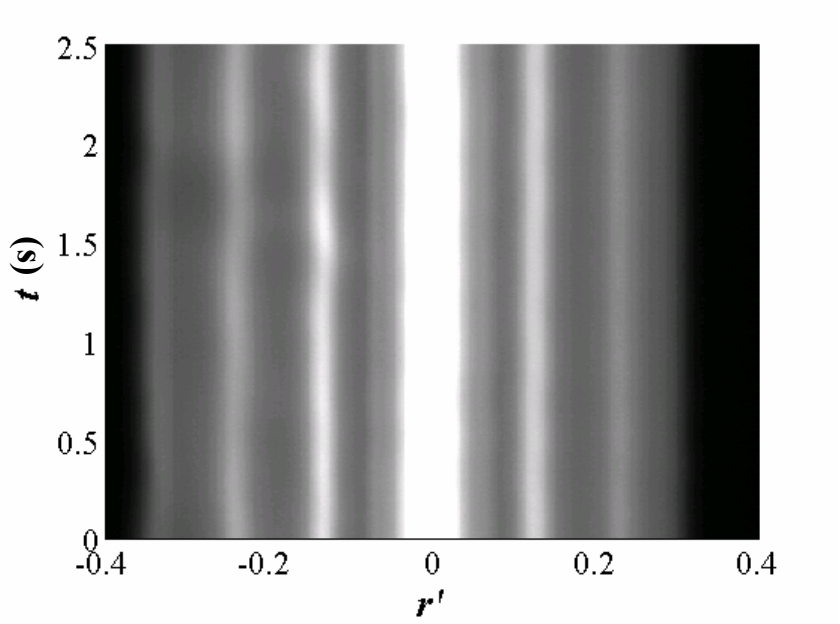

Figure 5.6: Temporal plot of shadowgraph intensities for Bo_D = 1.10 and M = 460.

5.1.1.3. *Oscillatory Multicellular Flow*

As M continues to increase, the steady, multi-cellular thermocapillary flow becomes unsteady and loses its axisymmetry, resulting in a fully 3D oscillatory flow. Previous investigations of thermocapillary flow in annular geometries [3, 6] have

observed “spoke-like” structures with surface waves that travel from the hot towards the cold wall. These investigations also observed similar flow patterns, as illustrated by the shadowgraphs in Figure 5.7 for a thick liquid layer of Bo_D = 1.10 and M = 500, 640, 750 and 830.

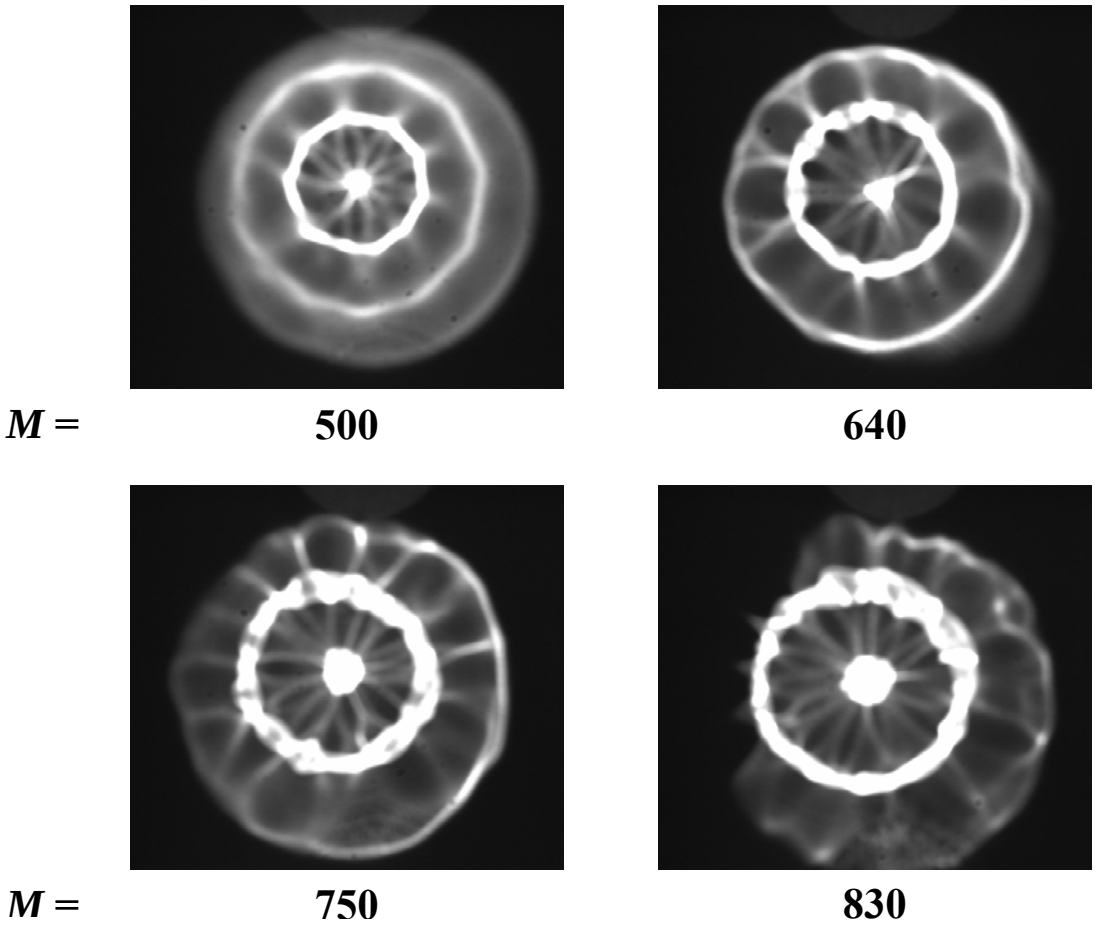

Figure 5.7: Shadowgraph images showing unsteady, three-dimensional thermocapillary convection for a liquid layer of Bo_D = 1.10 and 500 < M < 830.

Although the shadowgraphs suggest that the originally steady, concentric convective rolls still exist at these M, they also show the onset of new azimuthal “spoke-like” structures—or structures similar to Rayleigh-Benard cells, albeit constrained within

a single roll. Although the shadowgraph technique is used in many cases only to visualize free-surface deflections, it is possible that the "spokes" observed here are actually density variations within the liquid layer. The index of refraction of the silicone oil varies with temperature, and can therefore affect the shadowgraph image if reflections from the steel surface as well as those from the liquid free-surface are imaged.

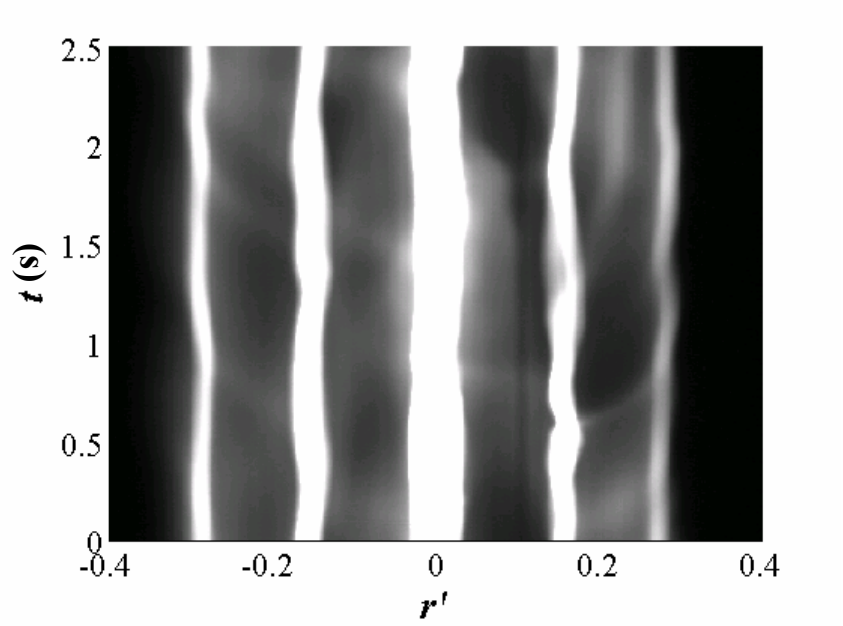

Figure 5.8: Temporal plot of shadowgraph intensities for Bo_D = 1.10 and M = 500.

Azimuthal surface waves appear inside the convective cells between the bounding "spokes," and travel radially outwards (*i.e.*, from the hot to the cold side of the roll) within the spokes, suggesting that the convection has become unsteady. A plot of pixel intensities (Figure 5.8) along a line crossing through $r' = 0$ shows the time-dependent behavior of a thick film; the concentric cells oscillate radially and surface waves propagate radially between concentric cells. As M increases within this flow regime, the free-surface structures become more pronounced; surface waves appear more frequently,

apparently with increasingly larger amplitudes. Eventually, the free surface becomes so perturbed that shadowgraphy cannot be used to visualize the free surface. In all experiments, the surface waves were observed to appear simultaneously with the onset of azimuthal "spokes." Hence we conclude that steady, multi-cellular flow transitions directly to unsteady, 3D flow.

5.1.2. Flow Regimes

As discussed previously, these thermocapillary flow regimes are determined by the dynamic Bond and the Marangoni numbers. In thick films, shadowgraph images of the liquid free surface revealed three distinct regimes. Figure 5.9 maps out these flow regimes in the Bo_D-M plane based on 165 independent experiments for silicone oils of three different viscosities, namely $\mu = 5\times10^{-3}$ N·s/m^2 (□), 2×10^{-2} N·s/m^2 (◊) and 5×10^{-2} N·s/m^2 (Δ). The boundaries between the three types of thermocapillary-buoyant convection (steady, unicellular flow (I), steady, multi-cellular flow (II) and oscillatory, multicellular flow (III)) are indicated by the dashed lines. The solid line shows the vaporization limit of the liquid, based on our experimental tests; experiments at Marangoni numbers above this line are those for a volatile liquid film where evaporative effects are significant. For the case of a thin film ($Bo_D = 0.15$) in which neither vaporization nor flow transitions occur, shadowgraphy could not detect film rupture. The rupture limit shown in this Figure is based upon the film height measurements discussed in 5.2.1.1. The boundary between thin films and thick films is represented by the dotted vertical line at $Bo_D = 0.19$.

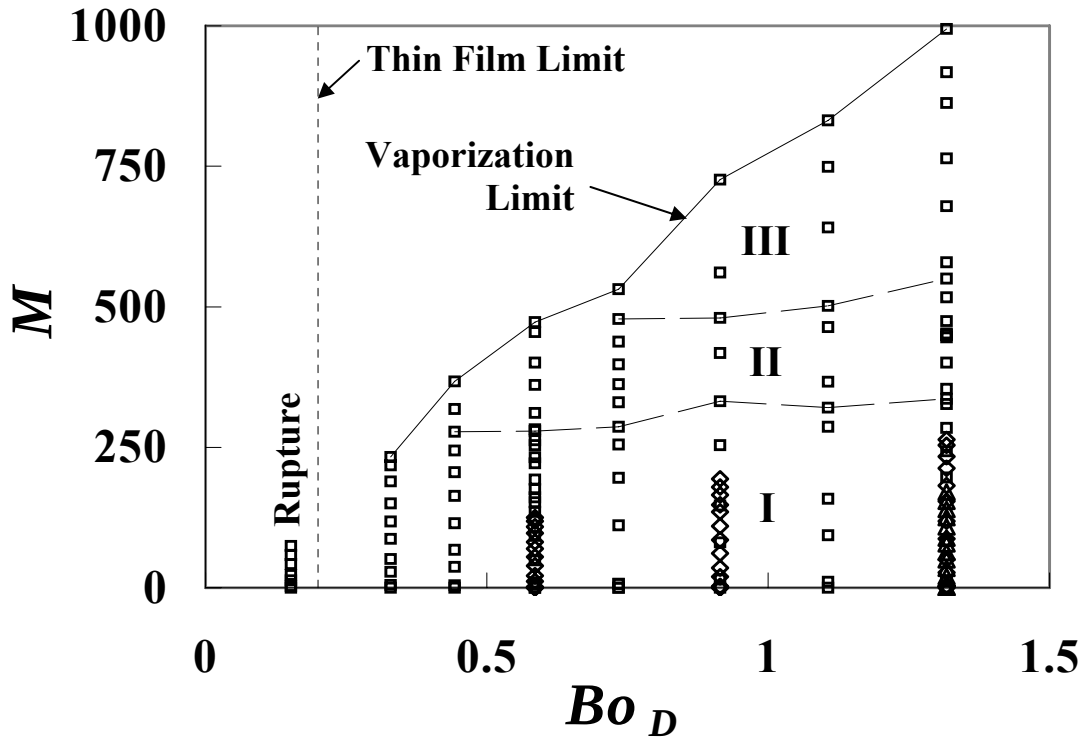

Figure 5.9: Flow regime map for silicone oil films of viscosities 5×10^{-3} N·s/m^2 (□), 2×10^{-2} N·s/m^2 (◊), and 5×10^{-2} N·s/m^2 (Δ). Dashed lines denote the limits between steady, unicellular flow (I), steady, multi-cellular flow (II) and oscillatory, multicellular flow (III). The solid line represents the vaporization limit of the liquid. The boundary between thin films and thick films is represented by the dotted vertical line at $Bo_D = 0.19$.

The flow regime map suggests that the flow transitions in thick films are mainly governed by Marangoni number. In the open axisymmetric configuration of these experiments, transition from steady, unicellular to steady, multi-cellular flow occurs for layers of $0.44 < Bo_D < 1.32$ at M between 280 and 330. Likewise, steady, multi-cellular flow was observed to transition to oscillatory, multicellular flow for $480 < M < 550$ in layers of $0.73 < Bo_D < 1.32$ in silicone oils of 5×10^{-3} N·s/m^2. Shadowgraph images were only acquired for M below the vaporization limit. For this reason, steady, multi-cellular flow and unsteady, 3D flow were not observed for $Bo_D < 0.44$ and $Bo_D < 0.73$, respectively, because vaporization of the film occurred before the transitional M was

reached. The critical M for each transition varies slightly with Bo_D, and seems to increase with Bo_D. Thick films of higher-viscosity (and hence higher Bo_D) oils remain in the steady unicellular flow regime, reaching the vaporization limit before they exceed the critical M for transition to steady multi-cellular flow.

5.2. Film Height Studies of Steady Thermocapillary Flows

This section summarizes results on film thickness from asymptotic analysis, numerical simulations and experimental measurements for both thin and thick films. Results from the asymptotic analyses and numerical simulations based on the level contour reconstruction method are only presented for thin films; the simplifying assumptions used for our analyses and simulations could not be extended to thick films, where thermocapillary and/or buoyancy effects become non-negligible. Local film height and free-surface displacements were experimentally measured using both needle contact and non-intrusive optical methods to quantify and further characterize the structure of steady, unicellular flows in non-uniformly heated thin and thick liquid layers. Although unsteady flows occur in thick films for $M > 480$, the techniques used here to determine film height in these experiments are unable to temporally resolve the free-surface geometry.

5.2.1. Thin Films

The shadowgraph visualizations showed that these thin liquid layers, which are dominated by thermocapillary stresses, exhibit only a steady, unicellular flow where free-surface deformation increases with M until dry-out occurs, or the layer ruptures. The

results presented in this section quantify local film heights for thin films using experimental, numerical and analytical methods. The important nondimensional parameters for thin films are A, Bo, and C based upon the scaling arguments of Ostrach [40] and Sen and Davis [59]. As mentioned previously, thin films are defined to have aspects ratios $A < 0.016$ and Bond numbers $Bo < 0.56$.

5.2.1.1. *Experimental Investigations*

Experiments measuring the height of thin liquid layers were conducted for heights $h_o = 0.27 - 1.2$ mm and radial surface temperature differences $\Delta T_s = 5.4 - 90°C$, corresponding to $A = 0.0035 - 0.016$, $Bo = 0.03 - 0.65$, and $C = 0 - 4.67\times10{-}3$. Steady-state free-surface profiles for a Dow-Corning silicone oil ($\mu = 5\times10^{-3}$ N·s/m^2) determined using the needle contact method are shown in Figure 5.10 in terms of the non-dimensional film thickness h' for $A = 1.17 \times 10^{-2}$, $Bo = 0.36$, and $C = 0$ (×), 9.34×10^{-4} (●), 1.32×10^{-3}(▲), 1.70×10^{-3} (◆), 2.08×10^{-3} (■). The experimental uncertainty in these data is less than the size of the symbols (*cf.* Appendix A). The Capillary number C is adjusted by changing the temperature at the center of the plate which, in turn, increases the surface temperature gradient. As expected, the free-surface geometry depends strongly on C. The surface temperature gradient induces thermocapillary stresses, which draw liquid away from the center of the plate. As C (*i.e.*, surface temperature gradient) increases, the deformation above the hot spot at $r' = 0$ grows more pronounced until rupture occurs in the range $1.70\times10^{-3} < C < 2.08\times10^{-3}$. In these experiments, rupture is defined to occur when the local thickness of the liquid layer is below the spatial resolution of the needle contact technique, estimated to be ±0.02 mm

(see Appendix A). Note, however, that an extremely thin film remains visible on the surface of the plate at the location of rupture. This very thin layer does not rupture because of its correspondingly small local Bond number prevents the formation of the sharp interfacial structure required to rupture the film, as pointed out by VanHook *et al.* [76].

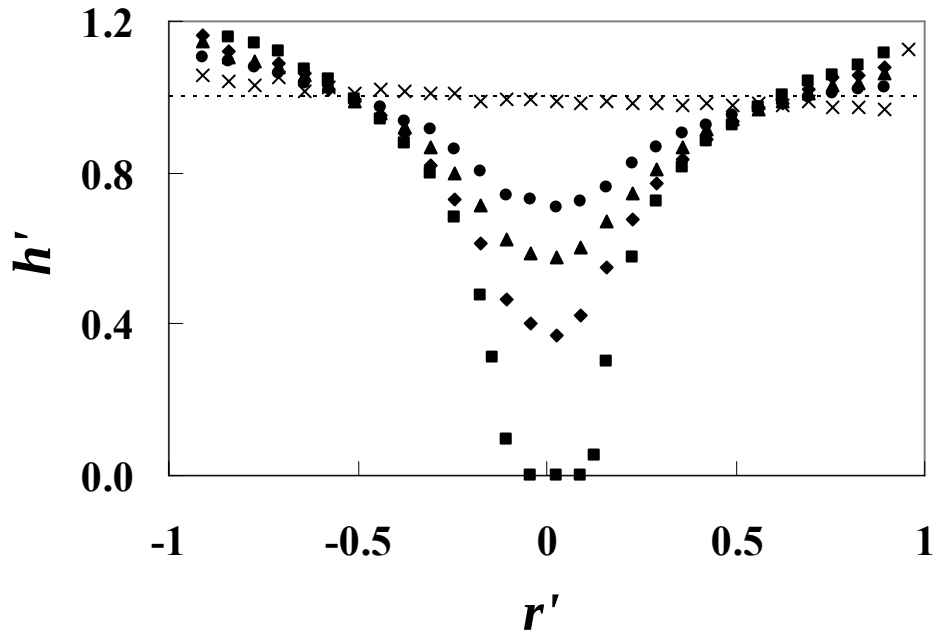

Figure 5.10: Experimental results for a liquid film of $A = 1.17\times10^{-2}$, $Bo = 0.36$, and $C = 0$ (×), 9.34×10^{-4} (●), 1.32×10^{-3} (▲), 1.70×10^{-3} (◆), 2.08×10^{-3} (■). The slight slant in the data for $C = 0$ is due to minor misalignment (< 0.025°) of the stainless steel plate with respect to the true horizontal.

In the case of $C = 0$, a slight tilt (< 0.025°) is apparent in the unheated and thus flat liquid free surface. This is due to minor misalignments between the experimental test section and the horizontal; as discussed in 2.1.2, the test section could only be aligned to within 0.025° of the horizontal. Figure 5.11 shows two radial surface temperature

profiles acquired for a liquid layer of $A = 1.17\times10^{-2}$, $Bo = 0.36$, and $C = 1.70\times10^{-3}$ at θ = 0° (closed symbols) and 180° (open symbols) as recorded by the thermocouples just below the surface of the steel plate, and suggests that the plate is heated in a symmetric fashion.. Although not shown here, similar results were observed for the other experimental cases. Note that temperature measurements above the heater plug ($r' < 0.125$) were inaccessible. The radial near-surface temperature profile monotonically decreases asymptotically to 15.4°C, the cooling channel temperature. The reported dimensionless parameters for all experiments are calculated based upon the temperature difference $\Delta T = T\left(r' = 0.16\right) - 15.4°\text{C}$, since the temperature measurement at $r' = 0.16$ is that closest to the heated copper plug.

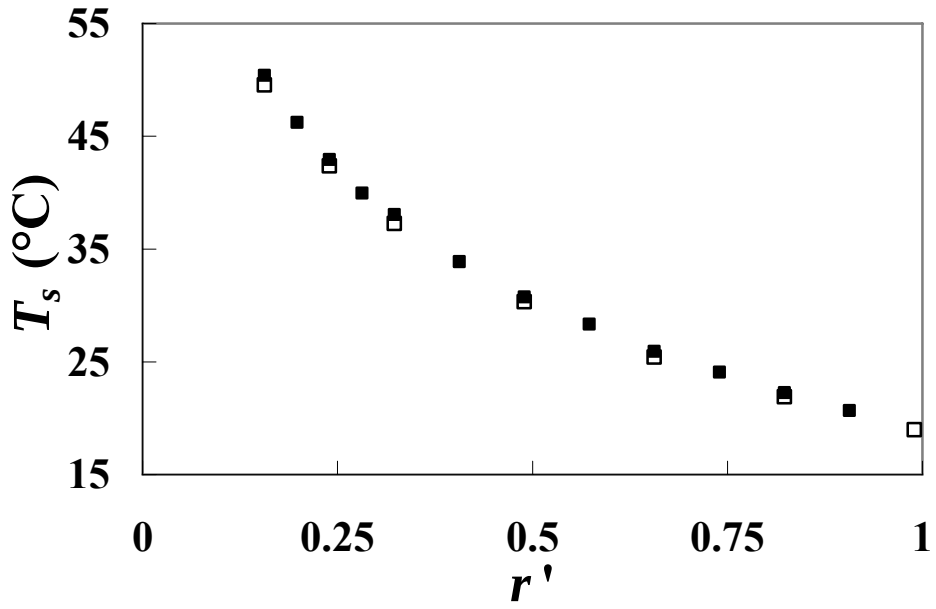

Figure 5.11: Radial thermocouple measurements for θ = 0° (closed symbols) and 180° (open symbols) showing symmetric heating of the test section.

The needle contact method was the primary method used to obtain film heights for thin layers. Figure 5.12 compares results obtained using the needle contact method

(open) and the laser-confocal sensor (closed) at $A = 6.23\times10^{-3}$, $Bo = 0.10$, for $C = 0$ (◆) and 1.42×10^{-4} (■). The laser confocal system gives slightly larger liquid layer height measurements compared with the results from the needle contact method. As discussed in Appendix A, we expect the non-intrusive laser-confocal results to be more accurate than those of the needle contact method. In brief, the intrusive needle contact method requires visual detection of the wetting of the tip of the needle. As it is translated downwards, the needle usually deforms the film before it pierces the liquid-gas interface. The needle contact method therefore typically gives film free-surface heights that are slightly less than the actual film height. Nevertheless, the height measurements of the two methods are still in good agreement for both flat and deformed free surfaces with maximum differences in local film height of 4.6% and 4.7%, respectively.

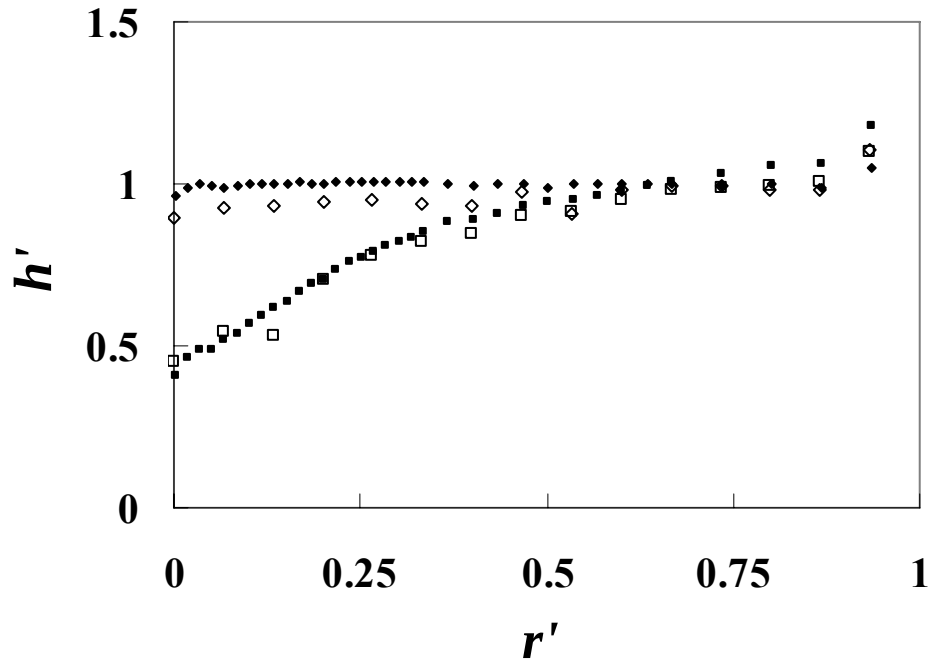

Figure 5.12: Comparison of needle contact (open) and laser-confocal (closed) film height measurements for a layer of $A = 6.23\times10^{-3}$, $Bo = 0.10$, for $C = 0$ (◆) and 1.42×10^{-4} (■).

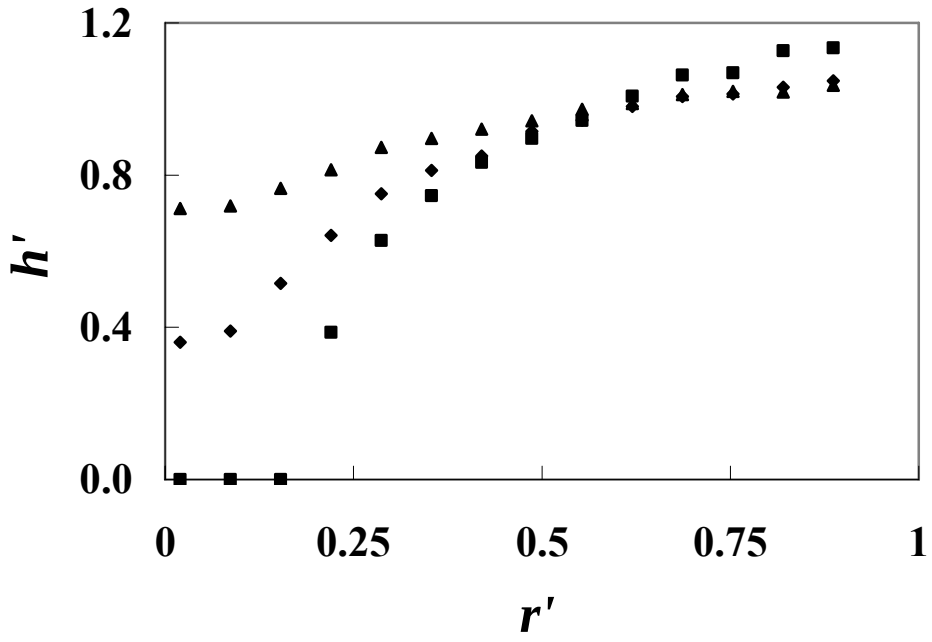

Figure 5.13: Typical experimental results for a thin film of increasing *C*. Data shown for a liquid layer of $A = 9.12 \times 10^{-3}$, $Bo = 0.22$, and $C = 3.86\times10^{-4}$ (▲), 6.49×10^{-4} (◆), 1.01×10^{-3} (■).

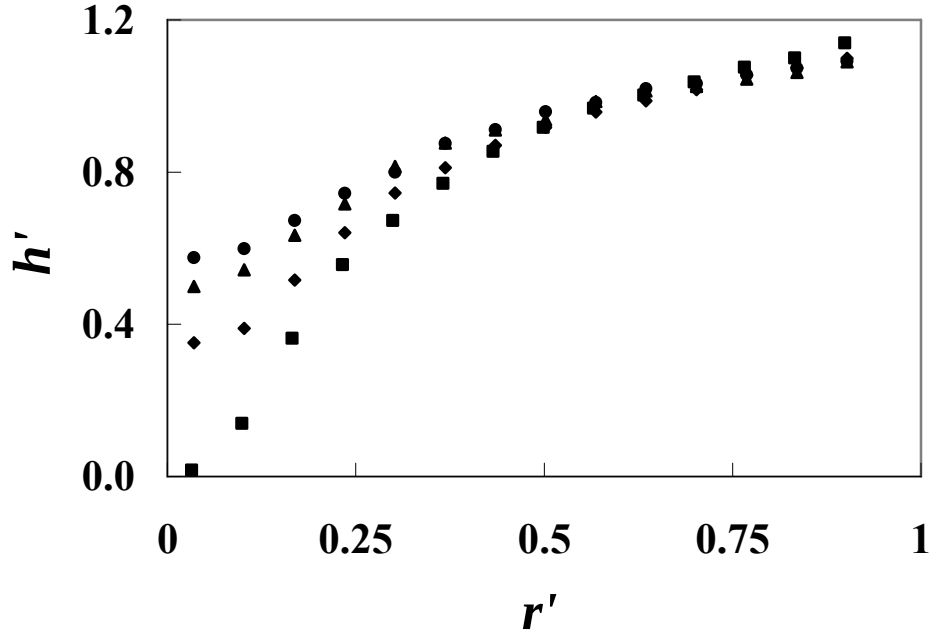

Figure 5.14: Same as Figure 5.13 but for a liquid layer of $A = 1.35 \times 10^{-2}$, $Bo = 0.48$, and $C = 1.70\times10^{-3}$ (●), 2.1×10^{-3} (▲), 2.4×10^{-3} (◆), 2.9×10^{-3} (■).

Based on the shadowgraphy studies, the free-surface deformation in thin films increases with thermocapillary forces and leads to film rupture at the center, or the region of highest temperature. Figure 5.13 and Figure 5.14 show typical thin-film height profiles measured using needle-contact measurements at $A = 9.12\times10^{-3}$, $Bo = 0.22$ and $A = 1.35\times10^{-2}$, $Bo = 0.48$, respectively. The data shown in Figure 5.13 were obtained for $C = 3.86\times10^{-4}$ (▲), 6.49×10^{-4} (◆), 1.01×10^{-3} (■), while Figure 5.14 displays experimental results for $C = 1.70\times10^{-3}$ (●), 2.1×10^{-3} (▲), 2.4×10^{-3} (◆), 2.9×10^{-3} (■). The profiles have the greatest slope near the center of the test section, presumably because the temperature gradients there are the greatest there. As liquid is drawn away from the hotter regions, an increase in height occurs along the cold edge of the liquid layer. The height difference creates a hydrostatic pressure difference between the center and edge of the liquid layer and drives a return flow along the bottom of the test section. Integrating the two height profiles over the entire area of the plate using the trapezoidal rule gives total liquid volume values within 5%. Comparing the parameters of the data shown in these two Figures, smaller thermocapillary stresses are required to rupture films of smaller A and Bo than layers of larger A and Bo since rupture occurs at a lower C when $A = 9.12 \times 10^{-3}$ and $Bo = 0.22$ than when $A = 1.35 \times 10^{-2}$, $Bo = 0.48$.

The effect of liquid material properties on the free-surface behavior of thin films was studied by conducting experiments on silicone oils of different viscosities. Because thermocapillary forces are dominant in thin films, viscosity is not even a parameter in the important nondimensional groups A, Bo, and C for such flows. Figure 5.15 shows radial height profiles for liquid layers of $\mu = 5\times10^{-2}$ N·s/m^2, $A = 1.25\times10^{-2}$, and $Bo = 0.41$ (closed) and 1 N·s/m^2, $A = 1.28\times10^{-2}$, and $Bo = 0.43$ (open symbols) with $C = 1.41\times10^{-3}$

(◆) and 2.49×10^{-3} (■). The free-surface deformation of the lower-viscosity fluid is consistently greater than that of the higher-viscosity silicone oil, most likely due to differences between the two tests near $r' = 0$. Large differences in the local film height occur at small r', especially when film rupture occurs for higher *C*, likely due to disparities in horizontal alignment of the experimental apparatus for the two test cases or differences in contact angles for the liquids on stainless steel. Another source for the discrepancy of the profiles in this Figure may be a small difference in γ_o for the two fluids, a material property assumed to be equivalent for all tested fluids. Differences in γ_o would lead to significantly different behavior for two fluids of similar *A*, *Bo*, and *C*.

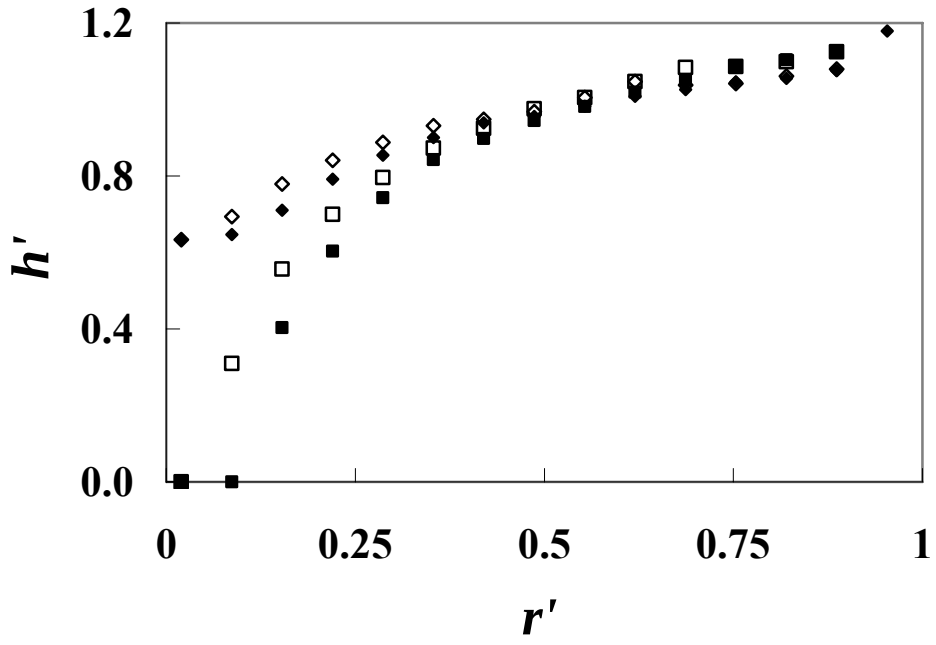

Figure 5.15: Comparison of similar thin films of different viscosities. Results are shown for $C = 1.41\times10^{-3}$ (◆) and 2.49×10^{-3} (■) in liquid layers of $\mu = 5\times10^{-2}$ N·s/m^2, $A = 1.25\times10^{-2}$, and $Bo = 0.41$ (closed symbols) and 1 N·s/m^2, $A = 1.28\times10^{-2}$, and $Bo = 0.43$ (open symbols).

The height of thin films has been shown to be highly dependent upon the capillary number. However, the impact of C on h is also affected by variations in the aspect ratio and Bond number, since thermocapillary forces increase with decreasing A and Bo. This is illustrated in Figure 5.16, where the critical capillary number C_{cr} for thin film rupture, defined as the C where rupture is first experimentally observed, is plotted as a function of A. C_{cr} increases with A, rising very rapidly as the aspect ratio approaches the thin-film limit of $A = 0.016$. Note that these larger values of C_{cr} correspond to maximum surface temperatures near the vaporization limits of the silicone oil. Though not shown here, C_{cr} depends on Bo in a similar fashion, since A and Bo are both proportional to h_o.

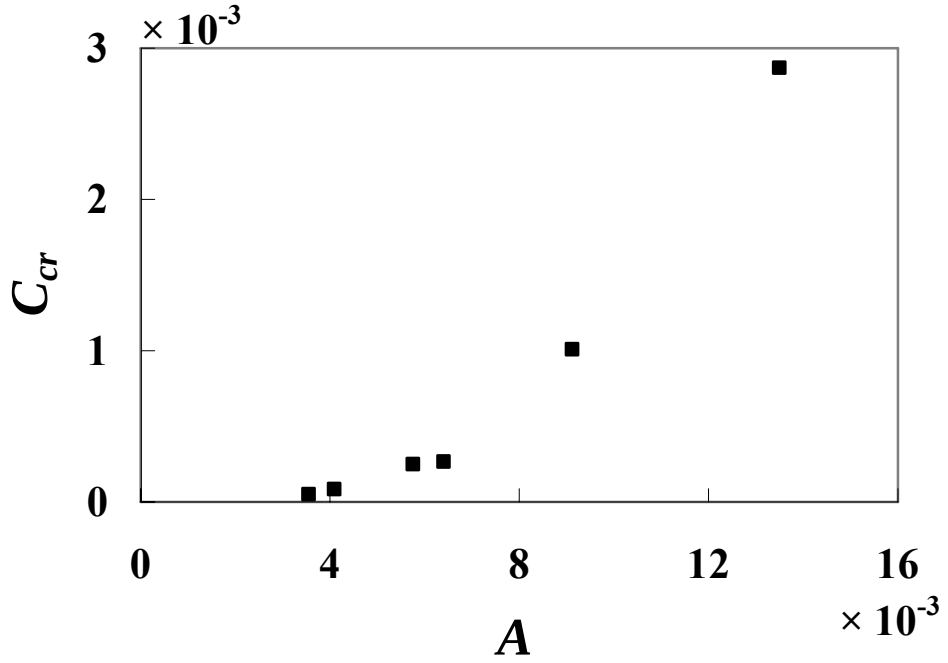

Figure 5.16: Experimental determination of thin film rupture in terms of A and C_{cr} for silicone oil layers of $\mu = 5\times10^{-2}$ N·s/m^2.

5.2.1.2. *Numerical Studies*

The level contour reconstruction method was used to investigate steady axisymmetric thermocapillary flows in thin films in the same parameter range as that for the experiments (A = 0.0035 – 0.016, Bo = 0.03 – 0.65, and $C = 0 - 4.67\times10^{-3}$). The resolution of the stationary grid used in these simulations was typically 15 and 30 cells along the r and z axes, respectively. This rather coarse grid appears to be sufficient based on the grid convergence study results shown in Figure 5.17, which compares numerical height profiles for a liquid layer at $A = 1.33\times10^{-2}$, $Bo = 0.47$, and $C = 1.88\times10^{-3}$ simulated over three grids: 15 × 30 (dotted), 20 × 40 (dashed), and 25 × 50 (solid). The three profiles are essentially identical with a maximum difference of 1% at $r' = 0$. Since increasing the grid size drastically affected computational run times, with solutions converging to their steady-state values in 2, 3, and 4 days using the 15 × 30, 20 × 40, and 25 × 50 grids, respectively, the rest of the results shown here were obtained on a 15 × 30 grid. Given the success of numerical simulations with larger grid size in similar geometries, we suspect that the axisymmetric version of the level contour reconstruction method of Shin and Juric [64] used here may be flawed. Further studies on the grid resolution in level set reconstruction simulations are available in Reference [63]. Clearly using this coarse a grid precludes capturing the thermal boundary layers which must occur next to both the free surface and the solid surfaces. It is likely that the inability of the numerical simulations to capture the thermal boundary layers is responsible for much of the discrepancy between the numerical and experimental results.

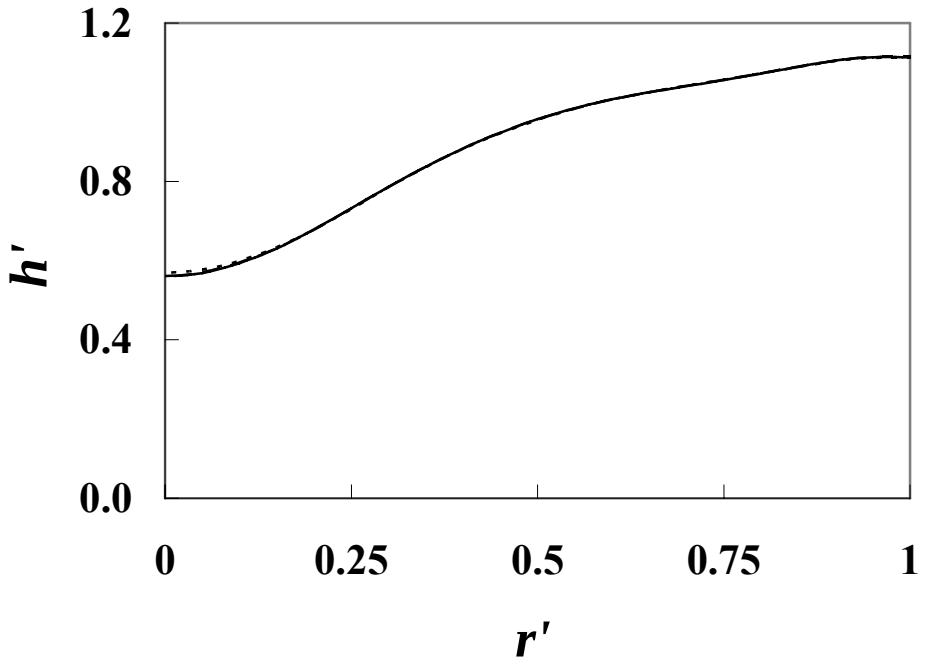

Figure 5.17: Grid convergence study of the numerical method showing converged results for stationary grids of 15 × 30 (dotted), 20 × 40 (dashed), and 25 × 50 (solid) cells for $A = 1.33\times10^{-2}$, $Bo = 0.47$, and $C = 1.88\times10^{-3}$.

Sensitivity studies were performed to evaluate how the numerical predictions varied with changes in liquid material properties. The temperature sensitivity of the surface tension, for instance, drives thermocapillary flows, so the surface tension temperature coefficient γ_o is a critical material property in these studies. However, γ_o is very difficult to measure and may vary slightly from the manufacturer's specified value among different batches of silicone oil. Figure 5.18 shows height profiles obtained with the level reconstruction method for a γ_o value of 6.8×10^{-5} N/(m·°C) (solid) and γ_o ±5% (dashed) for a liquid layer at $A = 1.33\times10^{-2}$, $Bo = 0.47$, and $C = 1.88\times10^{-3}$. The effect of changing γ_o is most noticeable near $r' = 0$ where changes in the free-surface profile due to variations in surface tension are magnified by high surface-temperature gradients. The minimum film height changes by 4.5% when γ_o varies by 5%. It is thus important to note that the numerical simulation is sensitive to material properties; uncertainties in density,

viscosity, thermal conductivity, surface tension, and specific heat may also affect the numerical results even if the uncertainties are rather small (< 1%). Uncertainties in the material properties are evaluated in Appendix A.

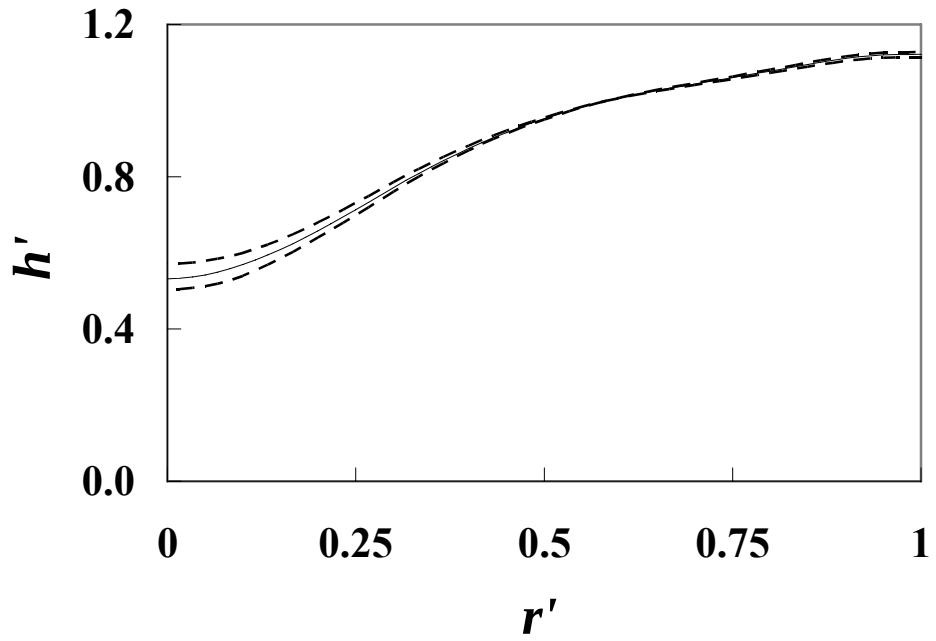

Figure 5.18: Results of numerical sensitivity study of the surface tension temperature coefficient γ_o for a liquid layer of $A = 1.33 \times 10^{-2}$, $Bo = 0.47$, and $C = 1.88 \times 10^{-3}$ for γ_o (solid) and $\gamma_o \pm 5\%$ (dashed) of the manufacturer's specifications.

The sensitivity of the numerical results to other variables, such as the initial height of the liquid layer, was also evaluated to determine how much the numerical predictions would be affected by experimental uncertainties in initial film height measurement. Figure 5.19 shows height profiles for a liquid layer of $A = 1.33\times10^{-2}$, $Bo = 0.47$, and $C = 1.88\times10^{-3}$ for $h_o = 1.00$ mm (solid), $h_o \pm 5\%$ (dashed) and $h_o \pm 10\%$ (dotted curves). Variations in initial film height have a significant impact on the numerical predictions of free-surface profiles, especially when the initial height is underestimated. For an initial film height 10% below the nominal value, the minimum steady-state film height is 21%

lower than that corresponding to the case at the nominal value. The largest differences in film height are again observed near the center (at $r' < 0.35$), with differences exceeding 5% in this region for a 5% variation in initial film height. It is unlikely that experimental uncertainties in h_o affect the validity of the numerical comparisons in these investigations since the uncertainty of h_o is only 0.003 mm or 0.3% for a film of nominal h_o = 1.0 mm as determined in Appendix A.

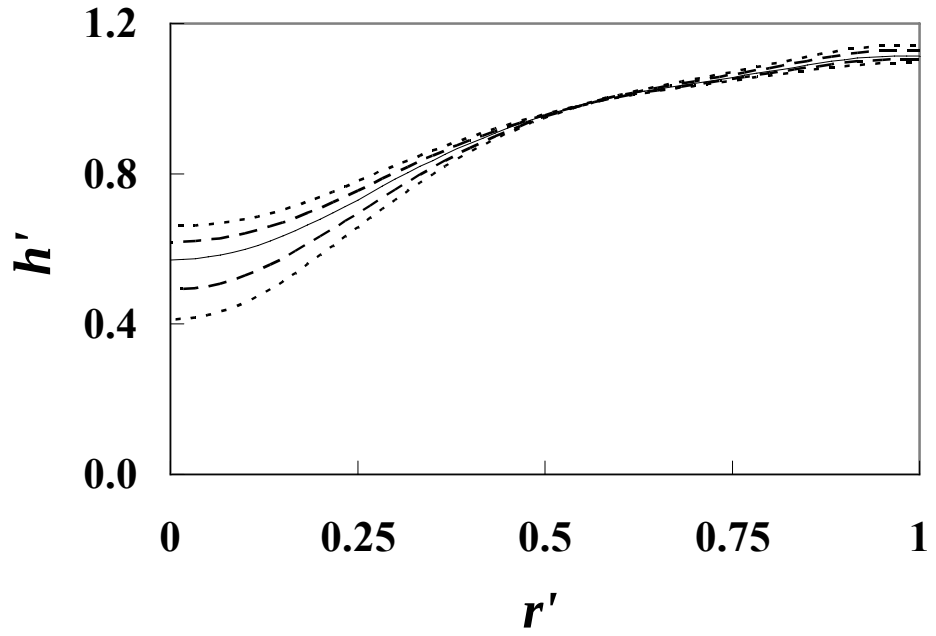

Figure 5.19: Results of numerical sensitivity study of the initial height h_o for a liquid layer of $A = 1.33\times10^{-2}$, $Bo = 0.47$, and $C = 1.88\times10^{-3}$ for h_o (solid), $h_o \pm 5\%$ (dashed), and $h_o \pm 10\%$ (dotted).

Numerical simulations were conducted for axisymmetric, steady-state thin films to study how thermocapillary flows affect the radial height profile. Typical numerical results are shown in Figure 5.20 for a liquid layer of $A = 1.35\times10^{-3}$, $Bo = 0.48$, and $C = 1.70\times10^{-3}$ (dash-dot), 2.1×10^{-3} (dotted), 2.4×10^{-3} (dashed), 2.9×10^{-3} (solid). The steady-state film heights are similar to the experiments in that the liquid layer becomes thinner

near the hot center and thicker at the cold edges. The slope of the free surface is greatest near the center, corresponding to the region of highest temperature gradient. Although the numerical results show that the film ruptures by $C = 2.9\times10^{-3}$, there are minor errors in this particular profile because the simulation does not prevent the free surface from penetrating the solid wall nor is a contact angle considered at $z' = 0$. Thus, the film height is negative for $r' < 0.02$ and mass is not properly conserved.

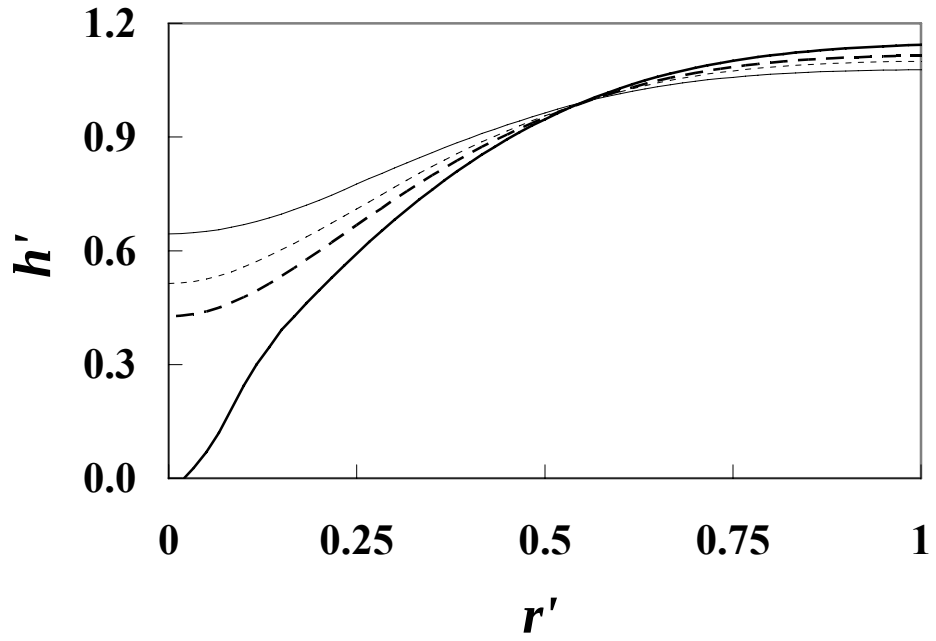

Figure 5.20: Typical numerical results for a thin film of increasing *C*. Data is shown for liquid layer of $A = 1.35 \times 10^{-3}$, $Bo = 0.48$, and $C = 1.70\times10^{-3}$ (dash-dot), 2.1×10^{-3} (dotted), 2.4×10^{-3} (dashed), 2.9×10^{-3} (solid).

It appears that the film height of unicellular, steady thermocapillary flows can be simulated quite well using the level contour reconstruction method, up to the point of rupture. The numerical simulations have the advantage that they solve the full set of governing equations with only a few simplifying assumptions including axisymmetry, constant liquid density, a free surface with zero slope at $r' = 0$ and $r' = 1$, and no

convection in the surrounding gas. These simulations are, however, time-intensive. Steady-state convergence for most cases took 2–7 days on a PC with 1.6 GHz Pentium 4 processors and 512 MB of RAM. The computational time was strongly dependent upon input parameters such as viscosity. A simulation of a 1 $N \cdot s/m^2$ viscosity liquid layer ran for nearly 4 weeks without converging (the simulation was stopped at this point) while that for a 5×10^{-3} $N \cdot s/m^2$ layer converged after 5 days. Films with a larger h_o also required longer computational times. Because the numerical simulation solves transient governing equations, the greater computational burden for films of higher viscosities and larger initial heights is caused by a slower thermal response within the liquid layer to the imposed temperature difference along $z' = 0$. Thus, a greater number of iterations are required to reach steady-state than in a less viscous film of smaller initial height. These unusually long run-times further suggest that the axisymmetric application of the numerical technique may be flawed.

5.2.1.2. *Theoretical Studies*

The asymptotic solution was used as a third method to determine the structure of thin film thermocapillary flows. The asymptotic differential equation Equation 4.89 was solved for h' using a shooting method for thin films within the parameter space explored experimentally (A = 0.0035 – 0.016, Bo = 0.03 – 0.65, and $C = 0 - 4.67 \times 10^{-3}$). In the solutions presented here, 1000 nodes were evenly distributed along r, although the grid convergence study shown in Figure 5.21 suggests that fewer nodes are necessary. The Figure shows height profiles obtained by solving the asymptotic equation for $A = 1.33 \times 10^{-2}$, Bo = 0.47, and $C = 1.88 \times 10^{-3}$ using 10 (dotted), 100 (dashed), and 1000

(solid) nodes along the *r*-axis. The heights are nearly identical for 100 and 1000 nodes, and differ by <0.1% from the 10 node case. The results presented in this thesis were obtained using 1000 nodes to achieve greater spatial in a reasonable computational time. The asymptotic solutions were typically obtained within 20 s for a resolution of 1000 nodes; this computation time was independent of the input parameters.

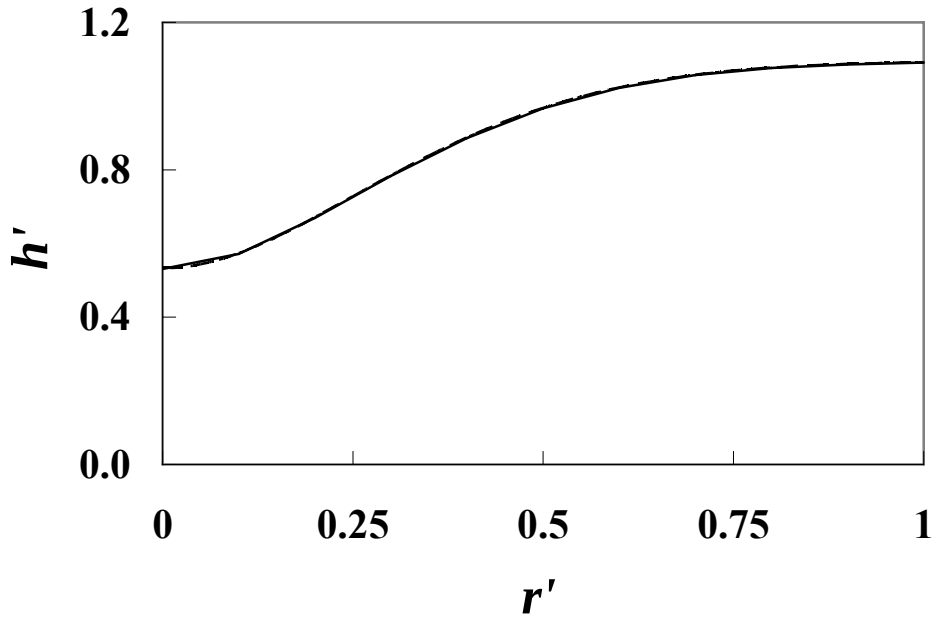

Figure 5.21: Grid convergence study for the shooting method solution to the asymptotic equation showing converged results for 10 nodes (dotted), 100 nodes (dashed), and 1000 nodes (solid) for $A = 1.33\times10^{-2}$, $Bo = 0.47$, and $C = 1.88\times10^{-3}$.

The asymptotic solution for film height in thin films produces results that are very similar to the experimental and numerical studies. The trends in the steady film height profiles are identical; the local film height is smallest at the location of the maximum surface temperature and largest at the location of the minimum surface temperature, and steady-state local film heights equal to zero can occur at $r' = 0$, indicating film rupture. As shown in Figure 5.22 for a liquid layer of $A = 1.35\times10^{-3}$, $Bo = 0.48$, and

$C = 1.70\times10^{-3}$ (dash-dot), 2.1×10^{-3} (dotted), 2.4×10^{-3} (dashed), 2.9×10^{-3} (solid), the deformation of the film grows as C increases until rupture occurs. As in the numerical simulations, the fluid mass is not conserved for solutions where the film ruptures (*i.e.*, $C > C_{cr}$) , and therefore the profile shown for $C = 2.9 \times 10^{-3}$ is not an accurate representation of the film height. The asymptotic equation is nevertheless useful in determining the radial height profiles for thin liquid films because of its computational

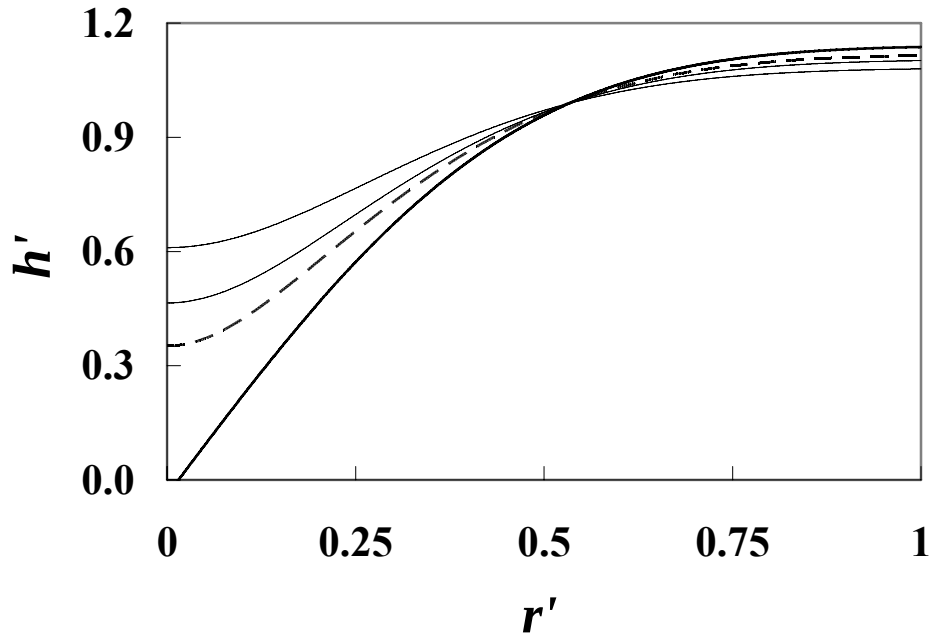

Figure 5.22: Typical asymptotic results for a thin film of increasing C. Data is shown for liquid layer of $A = 1.35\times10^{-3}$, $Bo = 0.48$, and $C = 1.70\times10^{-3}$ (dash-dot), 2.1×10^{-3} (dotted), 2.4×10^{-3} (dashed), 2.9×10^{-3} (solid).

efficiency. This analysis, however, makes more assumptions than the numerical method, namely that the film is asymptotically thin ($A \ll 1$) so that the inertial forces and the temperature gradient along z are negligible, and $A^3 \ll C$ to justify neglecting surface tension terms that improve free-surface smoothness in regions of high curvature,

specifically near $r' = 0$ in this application. The results of Tan, *et al*. [72] suggest that neglecting these terms will result in a more conservative estimate of the film deformation. We note that this assumption held for all thin film cases considered in this thesis.

5.2.1.3. *Comparisons*

The experimental data were used to validate the numerical and asymptotic solutions for thermocapillary flow in thin films. Figure 5.23 compares typical experimental, asymptotic, and numerical nondimensional film height profiles for A = 0.014, Bo = 0.48, and $C = 1.7\times10^{-3}$ (black) and 2.4×10^{-3} (grey). Symbols denote the experimental data, while solid and dotted curves represent the asymptotic solution and numerical predictions, respectively. All three sets of results are in reasonably good agreement, though the numerical profile has smaller free-surface deformations near the center. The asymptotic solution gives a more conservative estimate of film rupture than the numerical prediction since it predicts a slightly greater deformation of the liquid layer at smaller r. Similar results were observed in two-dimensional liquid films [65]. In all cases studied here, the asymptotic solution gives a more conservative estimate of film rupture; additional thin-film ($A < 0.016$ and $Bo < 0.56$) results are tabulated in Appendix C. Given the flaws in the numerical simulations discussed previously, it is unclear if the numerical results are directly applicable to liquid-protected PFCs.

Recall that the experimentally measured radial temperature profiles were curve-fit with a Gaussian function that used ΔT_s to determine the amplitude of the Gaussian distribution. However, ΔT_s underestimates the temperature difference over the solid surface because the temperature difference used to determine the amplitude of the

Gaussian is based upon the highest temperature measured, which occurs at $r' = 0.16$. We expect that the temperature will be higher over the copper heater plug, but were unable to estimate or measure the surface temperature in this region. Furthermore, it is also likely that the temperature over the surface of the heater plug is nearly constant, and the Gaussian profile—which increases monotonically with decreasing r'—probably overestimates the temperature at $r' = 0$. This overestimation should lead to numerical predictions of larger free-surface deformations at the center of the free surface; however, this is not the case, as shown in Figure 5.23. Again, this may be a result of a flaw in the numerical technique as applied for the axisymmetric liquid disc.

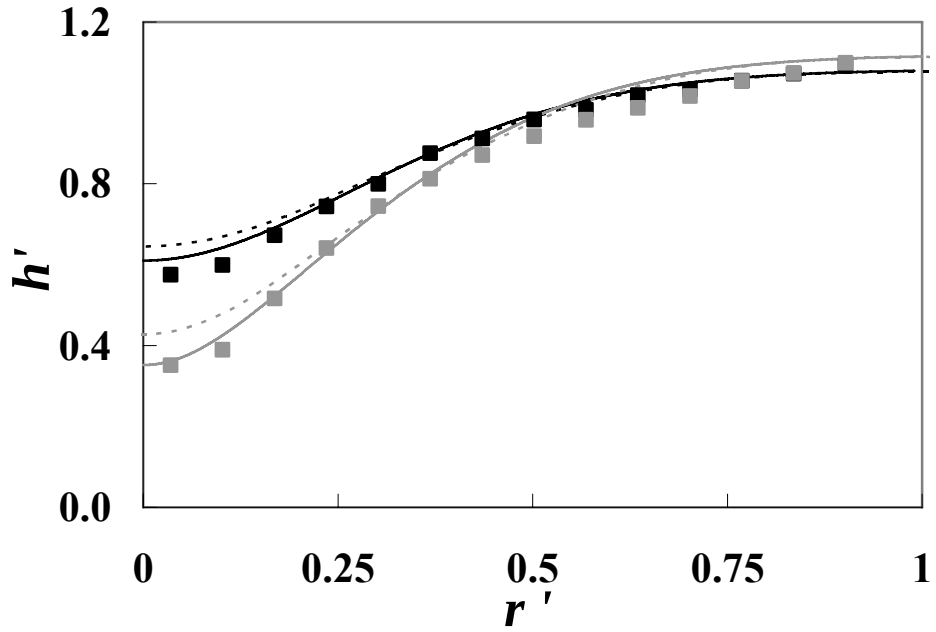

Figure 5.23: Comparison of experimental (symbols), asymptotic (solid), and numerical (dotted) results for a typical thin film of $A = 0.014$, $Bo = 0.48$, and $C = 1.7\times10^{-3}$ (black) and 2.4×10^{-3} (grey).

The (conservative) predictions from the asymptotic analysis were then compared with experimental results for the critical capillary number for thin-film rupture. Figure

5.24 compares experimental data (symbols) with the asymptotic results (lines) for nondimensional minimum film height h_{min}/h_o *vs.* C at $A = 6.6\times10^{-3}$ and $Bo = 0.11$ (dotted, ▲), $A = 9.1\times10^{-3}$ and $Bo = 0.22$ (dashed, ◆), and $A = 1.4\times10^{-2}$ and $Bo = 0.48$ (solid, ■). Again, the asymptotic and experimental results are in reasonably good agreement, with the asymptotic solution predicting rupture at a slightly lower C than the experiments. These and other results for thin films suggest that the asymptotic solution gives a conservative estimate of the maximum allowable temperature difference across the plate, since the capillary number is the non-dimensional radial temperature gradient: $C = (\Delta T / R_o)/(\sigma_o / h_o\gamma_o)$.

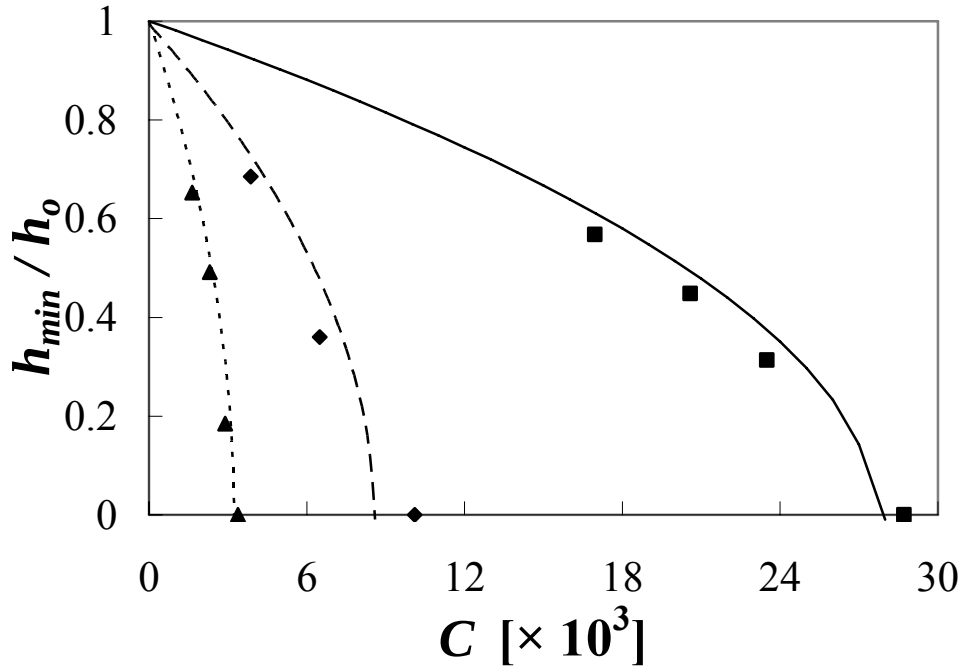

Figure 5.24: Comparisons of experimental (symbols) and asymptotic (lines) predictions of rupture for thin films at $A = 6.6\times10^{-3}$ and $Bo = 0.11$ (dotted, ▲), $A = 9.1\times10^{-3}$ and $Bo = 0.22$ (dashed, ◆), and $A = 1.4\times10^{-2}$ and $Bo = 0.48$ (solid, ■).

5.2.2. Thick Films

In thick (*i.e.*, $A > 0.016$, $Bo > 0.56$ or $Bo_D > 0.19$) films, the shadowgraphs showed flows at higher M that were different from the base flow of steady unicellular thermocapillary flow. In these flows, inertial and buoyancy forces are no longer negligible, as discussed at the beginning of this Chapter. The asymptotic analysis and numerical simulations described in the previous sub-Section for thin films—which neglect such forces by assuming a constant-density fluid—are therefore no longer valid. Figure 5.25 compares results from asymptotic analysis, numerical simulation and experimental measurements for such a film at $A = 0.019$, $Bo = 0.97$ and $C = 7.9\times10^{-3}$. As expected, neither the asymptotic analysis nor the numerical model accurately predicts the actual film height, and therefore cannot accurately predict the characteristics or onset of the experimentally observed multi-cellular and unsteady 3D flow regimes in thick films.

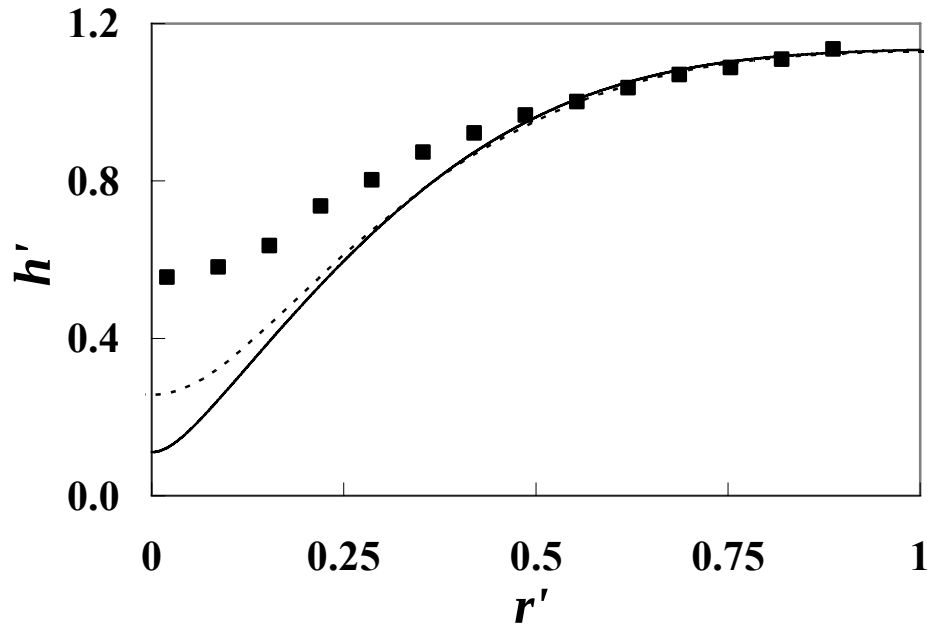

Figure 5.25: Similar to Figure 5.23, but for a thick film of $A = 0.019$, $Bo = 0.97$ and $C = 7.9\times10^{-3}$.

The laser-confocal displacement sensor was used to experimentally determine film radial height profiles for thick films of $0.21 < Bo_D < 1.32$ and $0 < M < 480$, spanning the steady, unicellular and multi-cellular flow regimes. The laser-confocal system was used in lieu of the needle-contact method because it has better accuracy, with an error of ~3 μm (*cf.* Appendix A). Thermal expansion of the liquid layer caused the layer to swell or grow in height even at the lowest input power. The height profiles presented in this section are therefore normalized by the average height h_{avg}, which was determined by dividing the total liquid volume (calculated by integrating the experimentally-measured radial height profile assuming axisymmetry) by the area of the test section. Unlike the initial height h_o, which is evaluated for the liquid at ambient (room) temperature, h_{avg} accounts for thermal expansion of the liquid. Typical height profiles of thick films are shown in Figure 5.26**Error! Reference source not found.**, Figure 5.27, and Figure 5.28 for $Bo_D = 0.21$, 0.48, and 1.31, respectively. The free-surface deformation grows as M (and thermocapillary effects) increases.

Figure 5.26 shows radial height profiles at $Bo_D = 0.21$ for $M = 30$ (×), 60 (●), 80 (▲), 100 (◆), 120 (■). All the flows shown in this plot are in the steady, unicellular regime since the vaporization limit of the silicone oil occurs at $M = 150$. The trends are similar to those observed in thin film flows with the exception that rupture does not occur in these thick films; $h_{\min} / h_{avg} = 0.38$ at $M = 150$. The height profiles in Figure 5.27 for an even thicker film at $Bo_D = 0.48$ and $M = 80$ (×), 130 (●), 180 (▲), 270 (◆), 320 (■) show smaller free-surface deformations than the $Bo_D = 0.21$ case ($h_{\min} / h_{avg} = 0.86$ at $M = 320$), suggesting that the thermocapillary stresses whose magnitude increases with Bo_D (film thickness) are being balanced by inertial effects and capillary pressure. The

shadowgraph results show that the flow at $M = 320$ is in the steady multi-cellular regime. The small free-surface deformations that mark the locations of the co-rotating cells are, however, not detectable in the height profile acquired at $M = 320$. This may be due to slight radial oscillations of the cells due to structural vibrations in either the (mounting of the) laser-confocal displacement sensor or the test section itself.

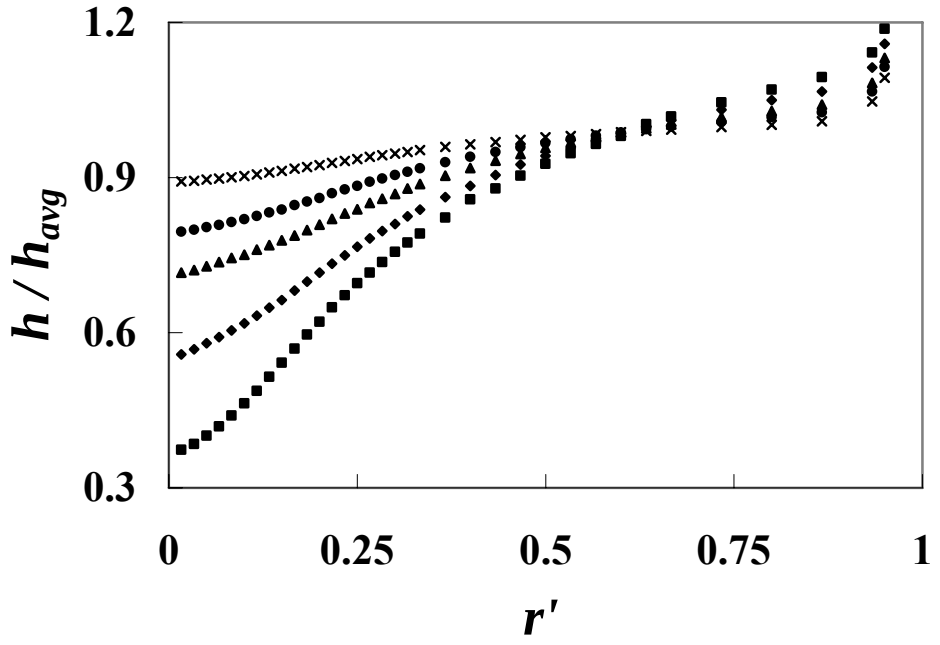

Figure 5.26: Laser-confocal height measurements of a thick film with $Bo_D = 0.21$ and $M = 30$ (×), 60 (●), 80 (▲), 100 (◆), 120 (■).

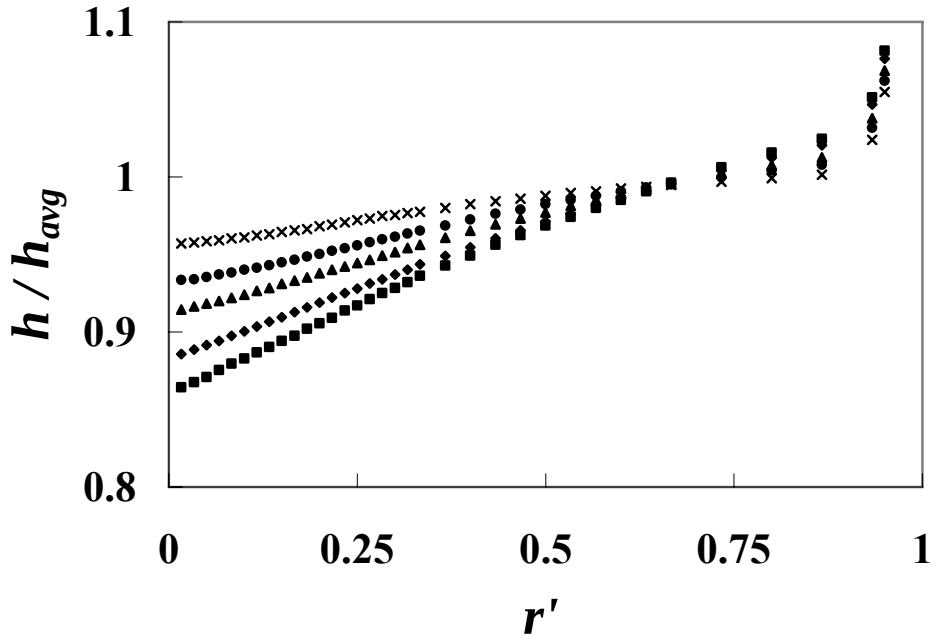

Figure 5.27: Laser-confocal height measurements of a thick film with $Bo_D = 0.48$ and $M = 80$ (×), 130 (●), 180 (▲), 270 (◆), 320 (■).

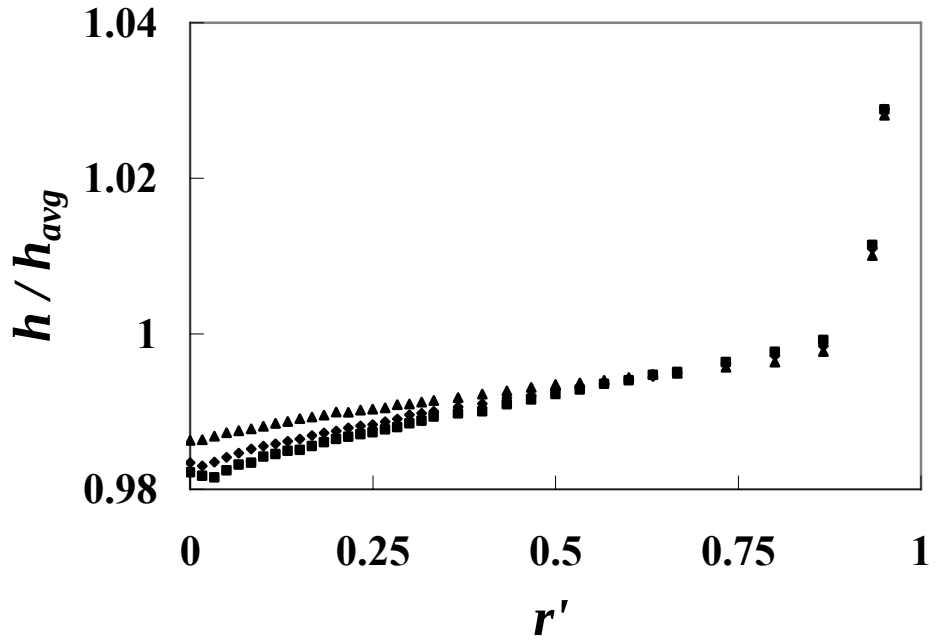

Figure 5.28: Laser-confocal height measurements of a thick film with $Bo_D = 1.31$ and $M = 190$ (▲), 330 (◆), and 450 (■)

Figure 5.28 shows height profiles for the thickest $Bo_D = 1.31$ film at $M = 190$ (▲), 330 (◆), and 450 (■). Here, the maximum free-surface deformation is less than 3% of the average height of the liquid layer. Profiles were acquired in both the steady unicellular ($M < 300$) and multi-cellular ($300 < M < 500$) flow regimes. There is some suggestion of small free-surface perturbations at higher M, which may coincide with the concentric rolls observed in the shadowgraphs. To investigate this, a nondimensional radial intensity I / I_{avg} profile was calculated from a shadowgraph image of a liquid layer at $Bo_D = 1.31$ and $M = 450$. The pixel intensities along a radius were extracted from a single frame of the shadowgraph .avi file and scaled by the average intensity along that radial line to calculate I / I_{avg}.

Figure 5.29 plots this nondimensional radial intensity profile along with the height profile measured with the laser-confocal system for the same test conditions. Although the radial positions of the "bright" and "dark" regions" in the shadowgraph may deviate significantly from their physical locations because of the lensing inherent in these images, the small ripples in the film height do not appear to coincide with the concentric rolls visible in the shadowgraphs. This result suggests that the magnitude of the surface features is below the accuracy of these displacement measurements, about 3 μm.

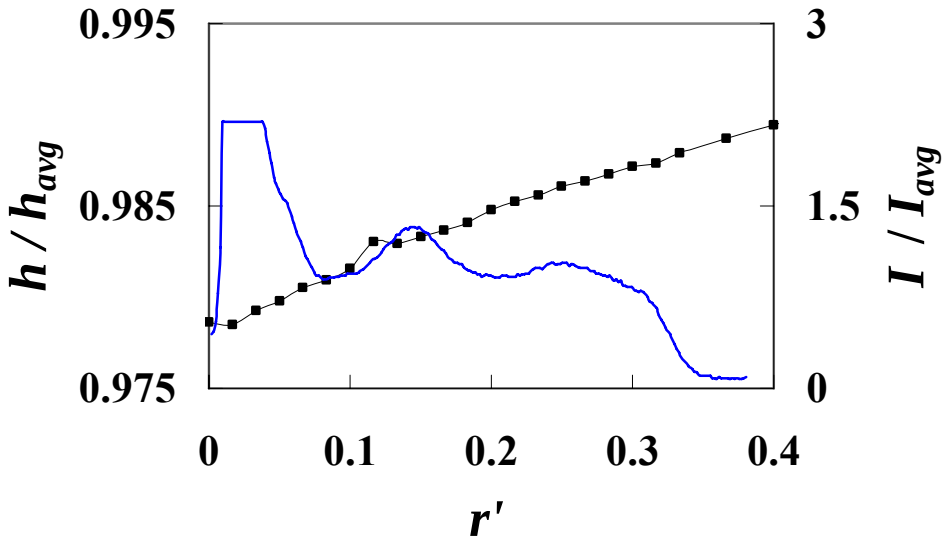

Figure 5.29: Comparison of laser-confocal height measurements (black, left axis) with normalized shadowgraph intensities (blue, right axis) for $Bo_D = 1.31$ and $M = 450$.

CHAPTER 6

CONCLUSIONS AND RECOMMENDATIONS

The purpose of this investigation is to study thermocapillary effects on the free-surface behavior of thin liquid layers. An experimental apparatus was constructed to subject silicone oil layers to radial temperature differences. The resulting thermocapillary flows were qualitatively categorized using a reflectance shadowgraphy method. The steady-state height profile of the liquid layer was quantified using a needle contact method and laser-confocal displacement sensor. In addition, numerical simulations and a theoretical analysis were conducted to study thermocapillary effects in liquid layers of $Bo_D < 0.19$. Data were collected for liquid layers of $0.007 < A < 0.039$, dynamic Bond numbers $0.04 < Bo_D < 1.32$, Bond numbers $0.11 < Bo < 4.10$, Capillary numbers $0 < C < 8.0 \times 10^{-3}$, and Marangoni numbers $0 < M < 990$. This chapter presents the conclusions derived from this investigation, contributions of this work on thermocapillary effects in thin liquid layers, and recommendations for future work

6.1. Conclusions

The conclusions derived from the data collected in this investigation are presented in the following subsections. The conclusions are categorized by the type of study performed, namely, classification of flow regimes, characterization of free surface deformation, and numerical and theoretical modeling of steady-state, axisymmetric thermocapillarity flows in thin liquid layers.

6.1.1. Thermocapillary Flow Regimes

The basic flow state of the open cylindrical geometry is steady, unicellular thermocapillary flow in which surface tension gradients drive flow from the hot spot at the center of the layer to the cooler perimeter. The free surface is deformed by this flow, depressed at the center and elevated at the perimeter. Return flow along the bottom of the liquid layer is hydrostatically driven by the height differences in the liquid free surface. Buoyancy, inertial, and thermocapillary effects are important when $Bo_D > 0.19$, and thus thin films ($Bo_D < 0.19$) behave differently from thick films ($Bo_D > 0.19$). This is consistent with the observations of Riley and Neitzel [48]. In thin liquid layers, steady, unicellular flows can lead to film rupture, while flows in thick layers do not. Instead, the basic thermocapillary flow in thick films becomes unstable at higher M and transitions to other flow regimes

Flow transitions in thick films vary only slightly with the initial height of the liquid layer (*i.e.* Bo_D). The transition from steady, unicellular thermocapillary flow to steady, multi-cellular flow can occur for liquid layers of $M > 280$ and appeared in shadowgraphs as concentric rings that indicate stationary free-surface deformations and thus flows similar to Marangoni convection occur within each of these cells. The appearance of steady, multi-cellular flow structures was observed by previous studies [27, 53] in which end-walls were present.

The onset of unsteady, multi-cellular flows can occur for $M > 480$ and was visualized in the shadowgraphs by the appearance of "spoke"-like cells and surface waves that travel outwards radially. Although the concentric cells remain, the "spokes" indicate the breakdown of axisymmetric flows within the liquid layer, while the surface

waves clearly mark the transition to unsteady flow. Oscillatory and three-dimensional flows with surface waves and "spokes" have been previously observed in annuli [1, 3].

6.1.2. Experimental Investigations of Free Surface Deformation

In silicone oil layers, the radial film height profiles were determined using two experimental techniques; the needle contact method and laser-confocal sensing. The needle contact method consistently measured smaller local film heights when compared to the laser-confocal displacement sensor due to deformation of the free surface by the needle prior to wetting. For thin films, the needle contact method was sufficiently accurate to determine local film heights. The resulting measurements were highly dependent upon the applied radial temperature difference (*i.e. C*). The free surface deforms more for higher *C* and the steepest slopes in the height profiles correspond to the regions of liquid layers subject to the highest temperature gradients. A liquid layer with *C* exceeding a critical value can rupture and expose the hottest portion of the solid surface. The critical value of *C* was found to be dependent upon the aspect ratio and Bond number of the liquid, increasing as *A* and *Bo* increased. The thin film limit (A = 0.016 and Bo = 0.56) was defined as the point at which rupture could not be obtained for liquid temperatures below the vaporization limit of the silicone oil.

Laser-confocal displacement measurements were obtained for thick films to record the surface geometry for steady, unicellular and multi-cellular thermocapillary flows. In unicellular flows, behavior similar to that of thin films was observed, namely, increasing radial temperature differences (*i.e. M*) increased surface deformation. Normalized surface deformation decreased as the initial layer height (*i.e.* Bo_D) was

increased. In multi-cellular flows, radial height profiles gave little evidence to the appearance of surface features indicating multiple concentric cells. It should be noted, however, that the free-surface ripples observed in the shadowgraphs are expected to be smaller ($O(1\ \mu m)$) than the uncertainty of the displacement sensor (~ 3 μm).

6.1.3. Numerical and Theoretical Modeling

An asymptotic analysis and a numerical solution of the full set of governing equations for thin liquid layers subjected to radial temperature gradients were performed. The numerical simulations are very computationally burdensome, requiring multiple days to reach steady-state solutions. Given the success of numerical simulations in similar geometries, we suspect that the adaptation of the level contour reconstruction method of Shin and Juric [64] may be flawed. The simulations in their current form do not provide an accurate representation of the free-surface geometry, since the minimum film height does not agree well with the experiments and asymptotic solution. The asymptotic solution makes many simplifying assumptions regarding the nature of the thermocapillary flow in the liquid layer but is less computationally intensive as a result. Comparisons with experiments showed that the asymptotic provide a good estimate of the shape of the free surface for thin films. The asymptotic solution provides a conservative estimate of rupture (*i.e.*, lower C) compared with the experiments. Thermocapillary forces can cause film rupture and dry out regions of high temperature if these parameters are exceeded. For thick layers at larger A and Bo, however, the asymptotic predictions are in poor agreement with the experimental data, due to the presence of inertia and buoyancy forces, which were not accounted for in the mathematical development.

6.2. Implications for Liquid-Protected Plasma-Facing Components

The work presented in this thesis can be used to develop guidelines for safe implementation of liquid protection schemes of plasma-facing components in magnetic fusion reactors. Hot spots on the free surface of a liquid-protected divertor are likely to occur due to the sharp heat flux gradients typical of a MFE reactor chamber, creating thermocapillary flows in the liquid layer. Understanding the behavior of a liquid layer in these extreme environments is necessary to mitigate film rupture in liquid-protected components. Applying the knowledge and tools developed in this investigation can provide insight to the choice of liquids and operating conditions for liquid-protection schemes.

To show the value of this investigation, design guidelines in terms of the critical Capillary number C_{cr} were determined using the experimentally-validated asymptotic solution for three candidate fusion liquids, namely lithium (Li), Flibe (Li_2BeF_4), and tin-lithium ($Sn_{80}Li_{20}$). The material properties of these liquids were evaluated at their respective maximum operating temperatures, as specified in Reference [49], with a nominal height h_o = 1 mm and an aspect ratio of A = 0.01 (Table 6.1). The Bond number Bo corresponding to this choice of A is also shown for each liquid and it should be noted that all of these example layers are thin films for which the asymptotic solution is applicable. The resulting dimensional maximum surface temperature difference $\Delta T_{s,max}$ is also given. In a fusion reactor, the liquid surface will actually be subject to high heat fluxes, and thus to avoid film rupture, limits must be imposed on the incident heat flux gradient so that temperature variation over the film surface would not exceed $\Delta T_{s,max}$. A good figure of merit (FOM) for comparing different coolants with respect to their

susceptibility to film rupture is the product of $\Delta T_{s,max}$ and the liquid thermal conductivity k. A high FOM indicates that for the same film geometry, a higher surface heat flux gradient can be tolerated prior to film rupture (Table 6.1).

Table 6.1: Critical capillary number of various coolants for h_o = 1 mm and A = 0.01

Coolant	T (K)	Bo	C_{cr}	$\Delta T_{s,max}$ (K)	$\Delta T_{s,max} \cdot k$ (W/m)
Li	653	0.016	6.9×10^{-5}	14	700
Flibe	673	0.12	5.2×10^{-4}	89	89
$Sn_{80}Li_{20}$	863	0.13	5.6×10^{-4}	330	1.4×10^{4}

The results shown in Table 6.1 imply that thermocapillary effects could potentially threaten the integrity of a thin liquid layer. In the case of Li, film rupture will occur if a temperature difference exceeds only 14 K across a radius of 10 mm; a situation that is very likely to occur in fusion reactors, especially at the surface of plasma-facing components. This result suggests that Li might not be the optimal choice for liquid-protection schemes. However, if the FOM ($\Delta T_{s,max} \cdot k$) is considered, Flibe can withstand the smallest heat flux gradient prior to film rupture because of its low thermal conductivity (1 W/m·K).

This investigation concludes that thermocapillary effects must be considered in the design of liquid-protection schemes in fusion reactors, especially when thin layers are employed because film rupture is possible. The asymptotic solution gives a good estimate of thin film behavior and can be used to compare candidate liquids and evaluate

operating conditions. In the case of thick liquid layers, the experiments conducted for this thesis indicate that thermocapillary forces cannot rupture the liquid layer due to increased gravitational effects. Thus, a thick liquid layer would be preferred to a thin film in liquid-protected PFCs because film rupture due to thermocapillary effects is not possible.

In thick layers, however, buoyancy and gravity affect the behavior of the liquid layer, and thus the flow cannot be expected to behave similarly if the liquid film is oriented vertically, at an angle, or facing downward. The experiments discussed in this thesis only considered horizontal liquid films above a solid surface with a temperature gradient imposed at the solid surface. Liquid protection has been proposed for components at other orientations, and thus further work would be necessary to characterize how oblique and even vertical films would be affected by an imposed temperature gradient. Moreover, the liquid surface of PFCs would in reality be heated at the liquid free surface (*i.e.*, from above) rather than from below, as was considered in these investigations. For horizontal liquid layers, the liquid would be naturally stratified with the less dense, directly heated liquid atop the cooler and denser fluid. Buoyancy effects would not contribute to the thermocapillary flow in this case, and thus the critical dynamic Bond number where inertial effects become significant should decrease.

6.3. Contributions

The experimental, numerical, and theoretical work performed in this thesis is the first to characterize thermocapillary-driven rupture of differentially-heated liquid layers in the axisymmetric disc geometry. This work is also the first to characterize free-surface

behavior axisymmetric liquid layers for coupled thermocapillarity and buoyancy. The main contributions of this thesis on the thermocapillary effects in thin liquid layers include the following:

1. Measurement of steady-state radial film height profiles for a wide range of parameters in non-uniformly heated, horizontal liquid layers using two experimental methods.
2. Derivation and solution of an axisymmetric asymptotic equation for thermocapillary flow in a non-uniformly heated cylindrical liquid layer. Parametric limits were set for the application of the asymptotic equation based upon comparisons with experimental data.
3. Characterization of free-surface behavior for liquid layers beyond the regime where numerical and asymptotic analyses were valid. Flow regimes were defined based on the operating parameters of the liquid layer.
4. Establishment of a design database for safe and robust development of thin film liquid-protection of plasma-facing components in fusion reactors.

6.4. Recommendations and Future Work

This thesis is the first work to characterize the influence of thermocapillary effects on the free surface of cylindrical liquid layers. This thesis represents extensive work investigating thin liquid layers and the knowledge gained from this experience can be useful in directing future research of cylindrical thin films, particularly for implementation in fusion reactors. Recommendations for continuing work include the following:

1. Temperature data should be obtained within the liquid layer—especially at the free surface—to estimate the discrepancy between the temperature distribution at the solid surface and that at the film free surface . Vertical temperature profiles (*i.e.*, along z) with appropriate spatial resolution could also provide an estimate of the Rayleigh number and hence an estimate of the relative importance of buoyancy effects.
2. The numerical code should be improved to incorporate more of the phenomena relevant for thick liquid films. Suggested improvements include modifying the code to achieve faster convergence, reducing the grid size and implementing adaptive meshing to capture the very thin thermal boundary layer, using the Boussinesq approximation to incorporate buoyancy effects, and including mass transfer (*i.e.*, evaporation) at the liquid-gas interface. Finally, extending the code to fully three-dimensional behavior would allow validation of the unsteady multicellular flow observed in the shadowgraphy studies.
3. Quantitative methods such as interferometry should be conducted to further characterize surface geometry of thick films ($Bo_D > 0.19$). Transient behavior (*i.e.* wave frequencies) and free-surface displacement measurements of < 1 μm would provide more information about the influence of non-uniform heating on thin liquid layers
4. Design an experimental test section with optical access through the sides and bottom to obtain velocity measurements within the liquid layer to investigate the relationship between flow patterns and free surface geometry.

5. Experimental data for free-surface geometry should be extended to include the behavior of candidate fusion liquids to further validate the applicability of the asymptotic solution.

APPENDIX A

ERROR ANALYSIS

Accurate estimates of experimental errors and uncertainties are critical in properly interpretation these data. This appendix estimates the errors associated with the experimental measurements and through error propagation analysis (EPA) quantifies the uncertainties of the techniques used in this study. The uncertainty analysis is presented with a brief description of each source of error. The Appendix concludes with a brief discussion of the reproducibility of the experimental results.

A.1. Error Propagation Analysis

This section describes the methods used to determine the overall uncertainty in the experimental measurements conducted in this thesis. The standard uncertainty u associated with an indirect measurement y, dependent upon N direct measurements x_i, is analogous to the standard deviation of a statistical series and can be expressed by Equation A.1.

$$u_y^{\,2} = \sum_{i=1}^{N} \left(\frac{\partial y}{\partial x_i} u_{x_i} \right)^2 \tag{A.1}$$

The expanded uncertainty U represents 95% of the possible data and is typically defined by a multiple of the standard uncertainty. For the analysis considered here, the expanded uncertainty is thus twice the standard uncertainty:

$$U_y = 2u_y \tag{A.2}$$

A.1.1. Uncertainty in Initial Film Height

The initial film height h_o was determined from Equation A.3 and depends on the mass m and density ρ of the liquid placed in the experimental apparatus, as well as the diameter D_o of the test section.

$$h_o = \frac{4m}{\pi\rho D_o^{\,2}} \tag{A.3}$$

The uncertainty in h_o was determined using error propagation analysis (EPA) and is given by Equation A.4. The contributions to the uncertainty from the measurements of D_o, m, and ρ are detailed in Table A.1.

$$u_{h_o}^{\,2} = \left(\frac{4}{\pi\rho D_o^{\,2}} u_m\right)^2 + \left(-\frac{8m}{\pi\rho D_o^{\,3}} u_{D_o}\right)^2 + \left(-\frac{4m}{\pi\rho^2 D_o^{\,2}} u_\rho\right)^2 \tag{A.4}$$

Table A.1: Measurement uncertainties and intermediate calculations for h_o.

Measurement, i	Standard Uncertainty, u_i	Influence Coefficient, $\frac{\partial\left(4m/\pi\rho D_o^{\,2}\right)}{\partial i}$	Section Containing Explanation
m	0.05 g	$\frac{4}{\pi\rho D_o^{\,2}}$	A.1.1.1.
D_o	0.013 mm	$-\frac{8m}{\pi\rho D_o^{\,3}}$	A.1.1.2.
ρ	5×10^{-4} g/cm^3	$-\frac{4m}{\pi\rho^2 D_o^{\,2}}$	A.1.1.3.

The overall standard uncertainty in h_o was determined for two masses, m = 4.8 g and 52.8 g, corresponding to $A = 8.9 \times 10^{-4}$ and 9.4×10^{-3}, respectively. These values represent the minimum and maximum aspect ratios considered in this study. The

uncertainty was found to be u_{h_o} = 0.0028 mm and 0.0029 mm for $A = 8.9 \times 10^{-4}$ and 9.4×10^{-3}, respectively. More than 94% of the overall uncertainty was contributed by the error estimate of the mass.

A.1.1.1. *Uncertainty in Liquid Mass m*

The mass of the liquid placed on the experimental section was determined using a digital scale (Ohaus GT8000). The source for the uncertainty in the mass measurements is therefore the resolution of the scale which was capable of measuring within 0.1g. Thus, the standard uncertainty of these measurements is 0.05 g.

A.1.1.2. *Uncertainty in Experimental Test Section Diameter D_o*

The test section was machined in-house such that the acrylic containment ring had an inside diameter D_o of 152.4 mm, with a tolerance of 0.013 mm. Post-machining measurements with a standard caliper verified the diameter within 0.025 mm. Thus, the standard uncertainty in the test section diameter is u_{D_o} = 0.013 mm. Likewise, the radius R_o of the test section was calculated as $D_o/2$ and thus has an uncertainty u_{R_o} = 0.007 mm.

A.1.1.3. *Uncertainty in Material Properties*

Many of the parameters investigated in this Appendix are determined using material properties specified by the manufacturer. The uncertainties in the values of these material properties contribute to the overall uncertainty in the parameters. Table A.2 show the value of the important material properties supplied by the manufacturer for the silicone oil with a viscosity of $\mu = 0.48 \times 10^{-2}$ N·s/m^2. Also shown are the

uncertainties in these values. For simplicity, the uncertainties presented in this Appendix have been determined using the values shown in Table A.2 except where noted otherwise. Thus, the presented uncertainties only pertain to the experiments conducted using the silicone oil with $\mu = 4.8 \times 10^{-3}$ N·s/m^2. The higher viscosity fluids have very similar material properties, except of course for viscosity and thermal diffusivity, and are expected to have similar uncertainties to those that follow. In addition, the overall uncertainties in the calculated parameters are nearly independent of the uncertainties in the material properties, as will be discussed in the following sections.

Table A.2: Manufacturer-specified material properties and associated uncertainties for $\mu = 0.48 \times 10^{-2}$ N·s/m^2

Property, i	Specification for $\mu = 0.48 \times 10^{-2}$ N·s/m^2	u_i
ρ	0.966 g /cm^3	5×10^{-4} g / cm^3
σ	20.8×10^{-4} N / cm	5×10^{-6} N / cm
γ	6.8×10^{-6} N / (cm·°C)	5×10^{-8} N / (cm·°C)
α	1.04×10^{-3} cm^2 / s	5×10^{-6} cm^2 / s
β	1.05×10^{-3} / °C	5×10^{-6} / °C

A.1.2. Uncertainty in Normalized Needle Contact Film Height

This section presents the uncertainty calculations performed for the normalized film height measurements acquired using the needle contact method. The uncertainties discussed here were chosen to be a conservative value and thus represent the maximum uncertainties for the entire data set. The uncertainty in $h' = h/h_o$ is given by Equation A.5 and the values used in this equation are shown in Table A.3.

$$u_{h'}^{\,2} = \left(\frac{1}{h_o} u_h\right)^2 + \left(-\frac{h}{h_o^{\,2}} u_{h_o}\right)^2 \tag{A.5}$$

The largest uncertainties were found for two initial film heights, h_o = 0.271 and 1.200 mm, corresponding to the parameter space for which the needle contact method was applied. The maximum uncertainties (determined for a nominal local film height measurement of 0.05 mm) were determined to be $u_{h'}$ = 7.3 and 1.7% of the initial film height for h_o = 0.271 and 1.200 mm, respectively. Most of the uncertainty in the normalized film height measurements was due to the needle contact film height measurements which contributed more than 99% of the overall uncertainty. Again, these values represent the most conservative uncertainty estimates because local film heights were rarely measured as low as 0.05 mm, except in the cases that experienced film rupture.

Table A.3: Measurement uncertainties and intermediate calculations for h/h_o

Measurement, i	Standard Uncertainty, u_i	Influence Coefficient, $\frac{\partial(h/h_o)}{\partial i}$	Section Containing Explanation
h	0.020 mm	$\frac{1}{h_o}$	A.1.2.1
h_o	0.0029 mm	$\frac{h}{h_o^{\,2}}$	A.1.1.

A.1.2.1. *Uncertainty in Needle Contact Film Height h*

The uncertainty of the needle contact film height measurements is due to the error in the vertical translation stage. Two positions are recorded within 0.001 mm to comprise

each local height measurement, one at the liquid free surface and one at the solid surface. Thus, the stage position z has an uncertainty of u_z = 0.0005 mm and the film height measurement uncertainty is given by $u_h^2 = (2u_z)^2$. The standard uncertainty in h is then 0.0007 for the needle contact method. This value was checked by recording 50 local height measurements at a single location using the needle contact method and calculating the standard deviation of the data. A more conservative estimate of the standard uncertainty was obtained, and therefore the uncertainty in the needle contact measurements of local film height are u_h = 0.02 mm.

A.1.3. Uncertainty in Normalized Laser-Confocal Film Height

The laser-confocal film height measurement uncertainties are discussed in this section. Again, the maximum uncertainties are provided based upon the minimum film height measured with this technique (h = 0.050 mm). Equation A.6 gives the standard uncertainty for the normalized film height and the values of each term are detailed in Table A.4.

$$u_{h'}^2 = \left(\frac{1}{h_o} u_h\right)^2 + \left(-\frac{h}{h_o^2} u_{h_o}\right)^2 \tag{A.6}$$

The maximum uncertainties were calculated for two initial film heights h_o = 0.499 and 2.996 mm, corresponding to the full range of liquid layers investigated using the laser-confocal sensor. The standard uncertainties were found to be $u_{h'}$ = 0.6% and 0.1%, respectively for h_o = 0.499 and 2.996 mm. More than 99% of the overall uncertainty is contributed by uncertainties in the film height measurements. The conservative

uncertainties shown here are significantly less than those associated with the needle contact method for the same initial film heights. In the case of needle contact measurements, the uncertainties for the initial film heights above would be $u_{h'}$ = 4.0% and 0.6%, respectively.

Table A.4: Measurement uncertainties and intermediate calculations for h/h_o.

Measurement, i	Standard Uncertainty, u_i	Influence Coefficient, $\frac{\partial(h/h_o)}{\partial i}$	Section Containing Explanation
h	0.003 mm	$\frac{1}{h_o}$	A.1.3.1.
h_o	0.0029 mm	$\frac{h}{h_o^2}$	A.1.1.

A.1.3.1. *Uncertainty in Laser-Confocal Film Height h*

The laser-confocal sensor was used to measure the local film height of the liquid layer. The z-position of the translation stage was never adjusted during the acquisition of a radial height profile. Therefore, the uncertainty in the measurements was due to the sensor itself. The manufacturer specify a sensitivity of 0.1 μm, however, other sources of error contribute to the uncertainty in the height measurements. These other factors, including building vibrations and aberrant air currents in the laboratory, can significantly affect the local height measurements. The standard error of these measurements was thus determined using a statistical sampling of 100 independent data points at each radial location. The corresponding standard deviation of each set provides an estimate of the

uncertainty in those data. The most conservative such uncertainty was found to be u_h = 0.003 mm.

A.1.4. Uncertainty in Radial Temperature Difference

The radial temperature difference ΔT_s reported in this investigation was determined by the difference between the steady-state temperature (T_m) read at $r' = 0.16$ and the temperature of the cooling channel (T_c). The uncertainty of this calculation is given by Equation A.7 and represents the summation of variances in the two temperature measurements. The values of the two terms on the right hand side of the equation are described in Table A.5.

$$u_{\Delta T_s}{}^2 = \left(u_{T_m}\right)^2 + \left(u_{T_c}\right)^2 \tag{A.7}$$

The overall uncertainty in ΔT_s is independent of the operating temperature profile and was found to be $u_{\Delta T_s}$ = 1.10°C. The largest contributor to this uncertainty is the temperature measurement of the non-calibrated thermocouple measuring the cooling channel temperature.

Table A.5: Measurement uncertainties and intermediate calculations for ΔT.

Measurement, i	Standard Uncertainty, u_i	Influence Coefficient, $\frac{\partial\left(T_c - T_m\right)}{\partial i}$	Section Containing Explanation
T_c	0.48 °C	1	A.1.4.1.
T_m	1.00 °C	−1	A.1.4.1.

A.1.4.1. *Uncertainty in Temperature Measurements T_m and T_c*

The uncertainties of the two temperature measurements used to determine the overall uncertainty in the radial temperature difference are described in more detail in Appendix B. The uncertainties in the measurements stem from a 95% confidence interval that is determined from a linear regression in the analysis of the calibration data for the thermocouples.

A.1.5 Uncertainty in Normalized Radial Position

The uncertainty in the normalized radial position was determined using EPA and is given by Equation A.8. The terms of this equation are developed further in Table A.6.

$$u_{r'}{}^2 = \left(\frac{1}{R_o} u_r \right)^2 + \left(-\frac{r}{R_o{}^2} u_{R_o} \right)^2 \tag{A.8}$$

Table A.6: Measurement uncertainties and intermediate calculations for r/R_o .

Measurement, i	Standard Uncertainty, u_i	Influence Coefficient, $\frac{\partial(r/R_o)}{\partial i}$	Section Containing Explanation
r	0.013 mm	$\frac{1}{R_o}$	A.1.5.1.
R_o	0.013 mm	$-\frac{r}{R_o{}^2}$	A.1.1.1.

The normalized radial position was measured from 0 to 1, and therefore the uncertainty was determined for two radial locations (r = 0 and 76.2 mm). The overall uncertainty was found to be 1.7×10^{-4}% and 2.4×10^{-4}% of R_o. This result indicates that

the normalized radial position is well known, and experimental uncertainties are very small. The uncertainties in both measurements contribute equally to the overall uncertainty.

A.1.5.1. *Uncertainty in Radial Position r*

The radial location of the film height sensor, whether it is the needle or the laser-confocal sensor, is determined by the positioning mechanism on the Velmex Unislide stage. The radial positions were acquired within 0.025 mm and thus the standard uncertainty in r is 0.013 mm.

A.1.6. Uncertainty in Nondimensional Parameters

In this thesis, the non-dimensional parameters for both "thin" and "thick" films were calculated using the experimental variables of initial film height, radial temperature difference, and fluid viscosity. In addition, material properties provided by the manufacturer were used in the determination of the operating parameters. In this section, the uncertainties associated with the governing non-dimensional parameters are discussed.

A.1.6.1. *Uncertainty in Aspect Ratio A*

The aspect ratio was shown in Chapter 4 to be important in the study of "thin" films and is determined for each experimental trial using Equation A.9.

$$A = \frac{h_o}{R_o} \tag{A.9}$$

The corresponding uncertainty of A is found using Equation A.10, derived using EPA. The contributing components are detailed in Table A.7.

$$u_A{}^2 = \left(\frac{1}{R_o} u_{h_o} \right)^2 + \left(-\frac{h_o}{R_o{}^2} u_{R_o} \right)^2 \tag{A.10}$$

The standard uncertainty in A was found for two initial film heights (h_o = 0.272 and 1.200 mm) corresponding to the experimentally-investigated heights of "thin" films. The overall uncertainty was found to be $u_A = 3.8 \times 10^{-5}$ for both initial film heights. In both cases, the error in the initial film height was responsible for over 99% of the overall uncertainty.

Table A.7: Measurement uncertainties and intermediate calculations for A.

Measurement, i	Standard Uncertainty, u_i	Influence Coefficient, $\frac{\partial(h_o/R_o)}{\partial i}$	Section Containing Explanation
h_o	0.003 mm	$\frac{1}{R_o}$	A.1.1.
R_o	0.013 mm	$-\frac{h_o}{R_o{}^2}$	A.1.1.1.

A.1.6.2. *Uncertainty in Bond Number Bo*

The Bond number Bo was determined for each experimental trial of "thin" films using Equation A.11. The uncertainty of Bo thus depends on the errors associated with the quantities shown in Table A.8.

$$Bo = \frac{\rho g h_o{}^2}{\sigma_o} \tag{A.11}$$

Following EPA, the standard uncertainty of Bo is given by Equation A.12.

$$u_{Bo}^{\ 2} = \left(\frac{g h_o^{\ 2}}{\sigma_o} u_\rho \right)^2 + \left(\frac{2\rho g h_o}{\sigma_o} u_{h_o} \right)^2 + \left(-\frac{\rho g h_o^{\ 2}}{\sigma_o^{\ 2}} u_{\sigma_o} \right)^2 \qquad \text{(A.12)}$$

Two initial film heights (h_o = 0.272 mm and 1.200 mm) were used to determine the uncertainty in *Bo* corresponding to the parameter space of "thin" films. The results indicate that the overall uncertainty u_{Bo} ranges from 7×10^{-4} to 3.2×10^{-3}, for a liquid layer of $\mu = 4.8 \times 10^{-3}$ N·s/m^2. For both initial film heights, the major contributor to the overall uncertainty was the estimate of h_o, accounting for more than 99% of the total uncertainty. The material properties combined to contribute only 0.06% of the overall uncertainty in *Bo*.

Table A.8: Measurement uncertainties and intermediate calculations for *Bo*.

Measurement, *i*	Standard Uncertainty, u_i	Influence Coefficient, $\frac{\partial\left(\rho g h_o^{\ 2}/\sigma\right)}{\partial i}$	Section Containing Explanation
ρ	5×10^{-4} g/cm^2	$\frac{g h_o^{\ 2}}{\sigma}$	A.1.1.3.
h_o	0.003 mm	$\frac{2\rho g h_o}{\sigma}$	A.1.1.
σ_o	5×10^{-7} N/cm	$-\frac{\rho g h_o^{\ 2}}{\sigma^2}$	A.1.1.3.

A.1.6.3. *Uncertainty in Capillary Number C*

The Capillary number *C*, a non-dimensional parameter used in the study of "thin" films, was calculated using Equation A.13, which shows that *C* depends on both h_o, and ΔT_s as well as the material properties γ_o and σ_o.

$$C = \frac{\gamma_o \Delta T_s h_o}{\sigma_o R_o} \tag{A.13}$$

The uncertainty in C is determined using Equation A.14 as a result of EPA. The contributing sources to the uncertainty in C are detailed in Table A.9.

$$u_C{}^2 = \left(\frac{\Delta T_s h_o}{\sigma_o R_o} u_{\gamma_o}\right)^2 + \left(\frac{\gamma_o h_o}{\sigma_o R_o} u_{\Delta T_s}\right)^2 + \left(\frac{\gamma_o \Delta T_s}{\sigma_o R_o} u_{h_o}\right)^2 + \left(-\frac{\gamma_o \Delta T_s h_o}{\sigma_o{}^2 R_o} u_{\sigma_o}\right)^2 + \left(-\frac{\gamma_o \Delta T_s h_o}{\sigma_o R_o{}^2} u_{R_o}\right)^2 \tag{A.14}$$

Table A.9: Measurement uncertainties and intermediate calculations for C.

Measurement, i	Standard Uncertainty, u_i	Influence Coefficient, $\frac{\partial(\gamma_o \Delta T_s h_o / \sigma R_o)}{\partial i}$	Section Containing Explanation
γ_o	5×10^{-8} N/(cm·°C)	$\frac{\Delta T_s h_o}{\sigma R_o}$	A.1.1.3.
ΔT_s	1.06 °C	$\frac{\gamma_o h_o}{\sigma R_o}$	A.1.4.
h_o	0.003 mm	$\frac{\gamma_o \Delta T_s}{\sigma R_o}$	A.1.1.
σ_o	5×10^{-7} N/cm	$-\frac{\gamma_o \Delta T_s h_o}{\sigma^2 R_o}$	A.1.1.3.
R_o	0.013 mm	$-\frac{\gamma_o \Delta T_s h_o}{\sigma R_o{}^2}$	A.1.1.2.

In the uncertainty analysis for C, conservative estimates of the uncertainty were determined by considering the largest experimental radial temperature difference (ΔT_s = 65°C). The uncertainties are found for two initial film heights, h_o = 0.272 and 1.200 mm, which defined the "thin" film parameter range. The resulting overall uncertainties in C are 8.1 × 10^{-4} and 8.5 × 10^{-4} for the two initial heights, respectively. The largest

contributing source of error in this calculation is the uncertainty in the initial film height, which accounts for more than 90% of the overall uncertainty in C. Uncertainties in material properties, especially in γ_o, are not negligible in the determination of the standard uncertain for C, however, the total contribution of the uncertainty of the specifications supplied by the manufacturer total less than 9% of the overall uncertainty.

A.1.6.4. *Uncertainty in Dynamic Bond Number Bo_D*

The dynamic Bond number Bo_D is used in this thesis to classify "thick" films using the initial film height as the dependent variable. Equation A.15 was used to calculate Bo_D.

$$Bo_D = \frac{\rho g \beta_o h_o^{\,2}}{\gamma_o} \tag{A.15}$$

Error propagation analysis results in Equation A.16 for the uncertainty in the dynamic Bond number. The standard uncertainty depends on the items listed in Table A.10.

$$u_{Bo_D}^{\,2} = \left(\frac{g \beta_o h_o^{\,2}}{\gamma_o} u_\rho \right)^2 + \left(\frac{\rho g h_o^{\,2}}{\gamma_o} u_{\beta_o} \right)^2 + \left(\frac{2 \rho g \beta_o h_o}{\gamma_o} u_{h_o} \right)^2 + \left(-\frac{\rho g \beta_o h_o^{\,2}}{\gamma_o^{\,2}} u_{\gamma_o} \right)^2 \tag{A.16}$$

The uncertainties in Bo_D were determined for h_o = 0.499 and 2.996 mm, the initial film heights that bound the experimentally investigated parameter space. The respective uncertainties for these film heights were found to be 4.24×10^{-4} and 2.62×10^{-3}. The standard error in initial film height contributed in excess of 99% of the overall uncertainty in Bo_D. Again, the uncertainties for the higher viscosity liquids are expected to differ very slightly from those shown here because the uncertainties in the material properties contribute less than 1% to the total uncertainty.

Table A.10: Measurement uncertainties and intermediate calculations for Bo_D.

Measurement, i	Standard Uncertainty, u_i	Influence Coefficient, $\frac{\partial\left(\rho g\beta_o h_o^2/\gamma_o\right)}{\partial i}$	Section Containing Explanation
ρ	5×10^{-4} g/cm^2	$\frac{g\beta_o h_o^2}{\gamma_o}$	A.1.1.3.
β	5×10^{-6} 1/°C	$\frac{\rho g h_o^2}{\gamma_o}$	A.1.1.3.
h_o	0.003 mm	$\frac{2\rho g\beta_o h_o}{\gamma_o}$	A.1.1.
γ_o	5×10^{-8} N/(cm·°C)	$-\frac{\rho g\beta_o h_o^2}{\gamma_o^2}$	A.1.1.3.

A.1.6.5. *Uncertainty in Marangoni Number M*

The Marangoni number reported for the experimental investigations discussed in this thesis was calculated using Equation A.17 and depends on h_o, ΔT_s, and μ (*i.e.*, α).

$$M = \frac{\gamma_o \Delta T_s h_o^2}{\alpha R_o} \tag{A.17}$$

Error propagation was used to determine the uncertainty in M, as given by Equation A.18, for two initial film heights h_o = 0.499 and 2.996 mm subject to the most severe temperature difference ΔT_s = 65°C.

$$u_M^2 = \left(\frac{2\gamma_o \Delta T_s h_o}{\alpha R_o} u_{h_o}\right)^2 + \left(-\frac{\gamma_o \Delta T_s h_o^2}{\alpha R_o^2} u_{R_o}\right)^2 + \left(\frac{\gamma_o h_o^2}{\alpha R_o} u_{\Delta T_s}\right)^2 + \left(\frac{\Delta T_s h_o^2}{\alpha R_o} u_{\gamma_o}\right)^2 + \left(-\frac{\gamma_o \Delta T_s h_o^2}{\alpha^2 R_o} u_\alpha\right)^2 \tag{A.18}$$

The uncertainties presented here are the conservative values for two viscosity silicone oils ($\mu = 4.8 \times 10^{-3}$ and 9.6 N·s/m^2). The resulting overall uncertainties in M are 0.28 and

8.6 for $\mu = 4.8 \times 10^{-3}$ N·s/m^2 and h_o = 0.499 and 2.996 mm, respectively. For $\mu = 9.6$ N·s/m^2, the overall uncertainties were determined to be 0.001 and 0.04 for h_o = 0.499 and 2.996 mm, respectively. The largest contributor to the uncertainty in M, was the temperature difference in all cases, although the contribution varied from 60% to 90% depending on the initial film heights and viscosities considered.

Table A.11: Measurement uncertainties and intermediate calculations for M.

Measurement, i	Standard Uncertainty, u_i	Influence Coefficient, $\frac{\partial\left(\gamma_o \Delta T_s h_o^2 / \alpha R_o\right)}{\partial i}$	Section Containing Explanation
h_o	0.003 mm	$\frac{2\gamma_o \Delta T_s h_o}{\alpha R_o}$	A.1.1.
R_o	0.013 mm	$-\frac{\gamma_o \Delta T_s h_o^2}{\alpha R_o^2}$	A.1.1.2.
ΔT_s	1.06°C	$\frac{\gamma_o h_o^2}{\alpha R_o}$	A.1.3.
γ_o	5×10^{-8} N/(cm·°C)	$\frac{\Delta T_s h_o^2}{\alpha R_o}$	A.1.1.3.
α	5×10^{-6} cm^2/s	$-\frac{\gamma_o \Delta T_s h_o^2}{\alpha^2 R_o}$	A.1.1.3.

A.2. Experimental Reproducibility

In this section, experimental studies are presented to show the extent of which the experiments can be reproduced. Independent experimental trials are expected to vary slightly for a multitude of reasons such as the horizontal alignment of the apparatus and translational stage, experimental measurement errors as presented in Appendix A.1., air

currents in the laboratory, and building vibrations. It is therefore important to determine whether a particular experiment is repeatable within experimental uncertainty.

A.2.1. Reproducibility of Needle Contact Results

To show the validity of the needle contact height measurements, a study of the repeatability of the measurements was conducted. In this study, film height measurements of two liquid layers with similar initial film heights were compared. The measurements were obtained independently from one another, including the replacement of the first liquid layer with the second layer. Because of this, the initial film heights of the first and second trials were slightly different, $h_o = 0.438$ and 0.489 mm, respectively. These heights correspond to $A = 5.75 \times 10^{-3}$ and 6.41×10^{-3} and $Bo = 8.70 \times 10^{-2}$ and 1.08×10^{-1}. The radial temperature difference ($\Delta T_s = 7.6°C$) was investigated for each h_o, resulting in $C = 1.26 \times 10^{-4}$ and 1.49×10^{-4}, respectively. The comparison of the needle contact film height measurements is shown in Figure A.1. It is obvious here that the initial film height (*i.e.*, A and Bo) is an important factor in the normalized local film height. The resulting profiles are significantly different, with a maximum difference in local film height of 6%. Although the two layers do not lie within the standard error of one another (See Appendix A.1.2.), the difference in the results is not due to the measurement technique. The differences seen in Figure A.1 are a result of applying the same temperature difference across liquid layers of different initial heights. This shows that the needle contact method is capable of accurately detecting significant deformations of the free surface in liquid layers of small aspect ratios ($A \approx 10^{-3}$)

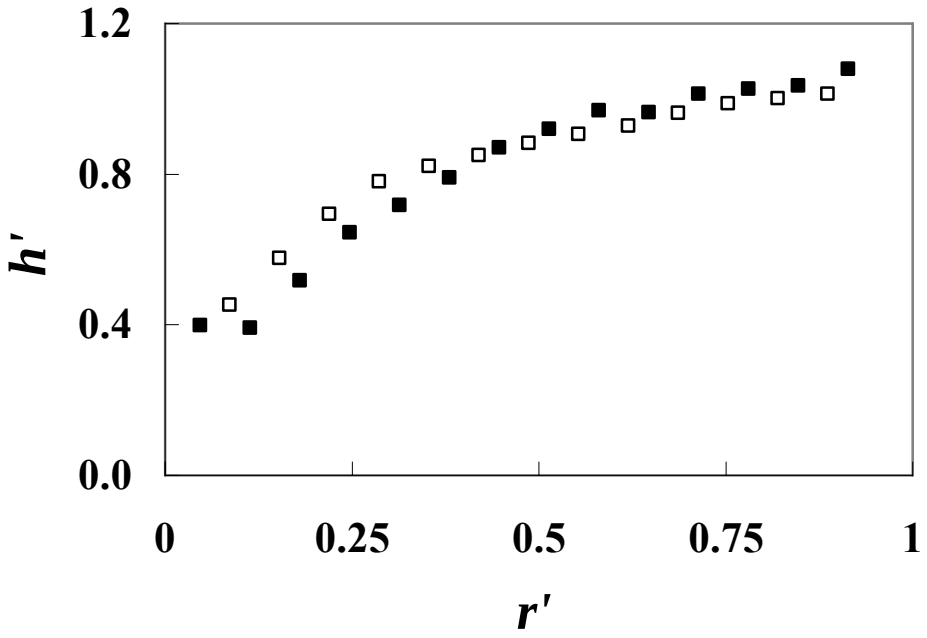

Figure A.1: Needle contact film height measurements of $A = 5.75 \times 10^{-3}$ (solid) and 6.41×10^{-3} (open) and $Bo = 8.70 \times 10^{-2}$ for $C = 1.26 \times 10^{-4}$ and 1.49×10^{-4}, respectively.

A.2.2. Reproducibility of Laser Confocal Displacement Results

The laser-confocal sensor was tested for reproducibility by independently obtaining radial height profiles for two liquid layers of h_o = 2.985 mm (Bo_D = 1.30). Height profiles were acquired for ΔT_s = 0, 11.8, and 28.6°C, corresponding to M = 0, 188, 456, respectively. The resulting profiles are shown in Figure A.2 and are nearly identical, with a maximum difference of only 0.09%, within the standard uncertainty of the measurement technique. Thus, the measurements of the laser-confocal sensor are reproducible for differentially-heated liquid layers.

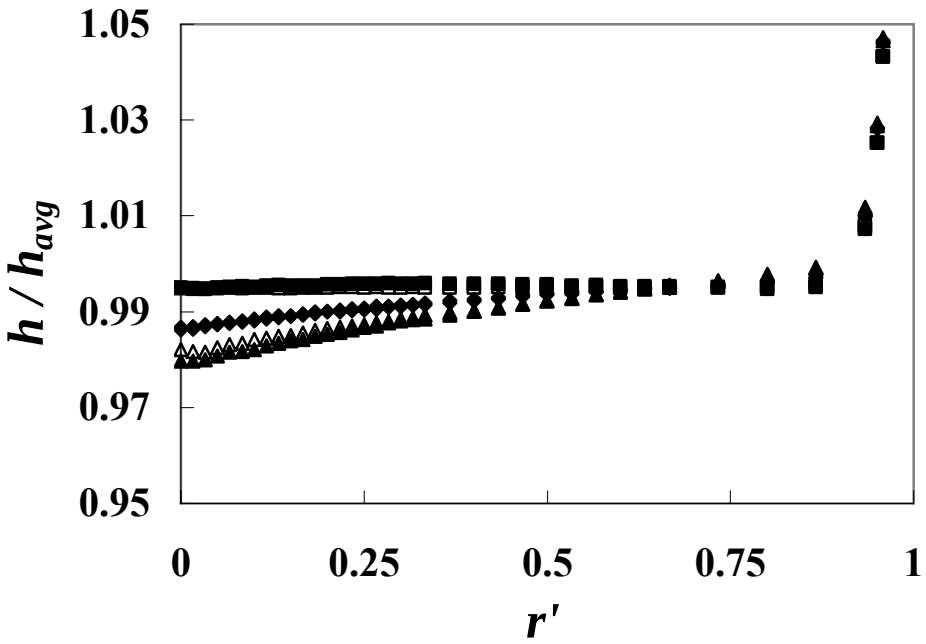

Figure A.2: Laser-confocal film height measurements recorded for two independent trials (solid and open symbols) for $Bo_D = 1.30$ and $M = 0$ (□), 188 (◊), 456 (Δ).

A.2.3. Axisymmetry of Experimental Test Section

The experimental test section was shown in Chapter 5 to be symmetrically heated, however it is also necessary to show that the liquid layer behaved symmetrically. To show this, diametric profiles were acquired at θ = 0° and 90° for a liquid layer of $Bo_D = 0.48$ and $C = 0$ and 168. The comparison of the two profiles is shown in Figure A.3. The symmetry of the profile across θ = 0° is excellent, with a maximum difference between corresponding radial positions of 1.9% and 0.9% for $C = 0$ and 168, respectively. Along θ = 90°, however, a slight asymmetry becomes noticeable for $C = 168$, where the maximum difference between local film heights at corresponding radial locations is 9.9%. Most likely this is due to a small horizontal misalignment of the experimental apparatus which is augmented as the liquid is heated. As the heating increases, liquid will prefer to flow toward the side of lower elevation, causing the film height in that region to increase

more in comparison to the side of higher elevation. The axisymmetry of the test section is also shown in Figure A.3, and shows a good agreement. The largest difference between corresponding local film height measurements is 1.6% and 1.7% for $C = 0$ and 168, respectively. The differences here are greater than the standard error discussed in Appendix A.1.3., but are not excessive, given the difficulties in horizontal alignment of the translation stage and experimental test section.

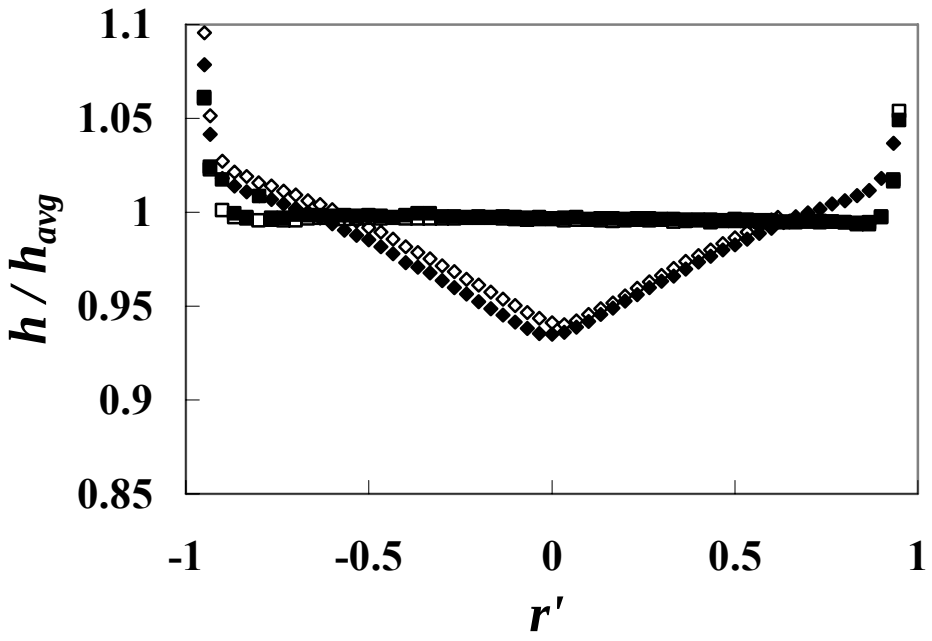

Figure A.3: Comparison of diametric profiles taken at θ = 0° (solid) and 90° (open) for a liquid layer of $Bo_D = 0.48$ and $C = 0$ (□) and 168 (◊).

APPENDIX B

THERMOCOUPLE CALIBRATIONS

This appendix describes the calibrations performed for the thermocouples used to measure the temperature near the surface of the steel plate. The calibration procedure and analysis are presented along with the associated errors of the temperature measurements.

B.1. Calibration Procedure

A constant temperature block calibrator (Techne Laboratory Equipment DB-35L) was used to calibrate the 20 K-type Omega CHAL-010 thermocouples against a platinum resistance temperature detector (RTD, ASL T100-250, SN 440037). The RTD has a manufacturer-specified uncertainty of 0.005°C. The calibrations were performed over a temperature range of -15 to 235°C in 10°C increments. The block calibrator was used to control a small capacity (~10 mL) crucible filled with glycerin. The thermocouples were taped to the RTD and inserted into the crucible. The glycerin reduces temperature variations with the crucible, insuring that the RTD and thermocouples are exposed to the same temperature. For each temperature setting, the block calibrator was allowed 15 minutes to thermally stabilize prior to recording the temperature within the crucible. The thermocouple measurements were recorded in degrees Celsius using an HP Agilent 34970A data acquisition unit. The resistance of the RTD was measured in Ohms using an Agilent 34401A Digital Multimeter. The corresponding temperature of the RTD was calculated using a ninth-order polynomial provided by the manufacturer. The sheathed

K-type thermocouples used to measure the temperature at the inlet and outlet of the water cooling channel were not calibrated using the procedure since the manufacturer provided uncertainty estimates of 1°C for these high-accuracy thermocouples. The calibration measurements for the K-type thermocouples are shown in Table B.1, Table B.2, Table B.3 and Table B.4 Each data point represents the mean temperature of 100 measurements acquired at 0.01 Hz. The RTD measurements are presented in both Ohms and degrees Celsius for each temperature interval.

Table B.1: Calibration data for thermocouples 101 – 105.

RTD (Ω)	**RTD (°C)**	**101 (°C)**	**102 (°C)**	**103 (°C)**	**104 (°C)**	**105 (°C)**
93.953	-15.240	-15.870	-15.757	-15.730	-15.646	-15.505
97.995	-5.140	-5.907	-5.804	-5.783	-5.685	-5.551
102.055	5.035	4.113	4.225	4.259	4.357	4.488
106.045	15.067	14.152	14.269	14.298	14.391	14.519
110.068	25.213	24.327	24.444	24.464	24.550	24.679
114.033	35.243	34.310	34.444	34.479	34.586	34.726
118.023	45.368	44.507	44.637	44.669	44.767	44.880
122.010	55.516	54.675	54.807	54.824	54.923	55.041
125.970	65.628	64.766	64.904	64.925	65.026	65.185
129.940	75.796	75.017	75.159	75.185	75.276	75.483
133.880	85.920	85.157	85.302	85.328	85.418	85.651
137.800	96.023	95.392	95.517	95.557	95.645	95.739
141.650	105.977	105.726	105.836	105.891	105.995	106.088
150.820	129.809	130.141	130.177	130.196	130.228	130.131
156.690	145.158	145.634	145.663	145.687	145.720	145.598
162.540	160.527	161.012	161.036	161.058	161.089	160.958
168.020	174.992	175.202	175.234	175.277	175.315	175.176
173.690	190.027	190.287	190.298	190.335	190.346	190.165
179.380	205.186	205.278	205.270	205.298	205.298	205.101
184.900	219.962	219.858	219.779	219.815	219.785	219.494
190.410	234.779	234.573	234.473	234.492	234.424	234.183

Table B.2: Calibration data for thermocouples 106 – 110.

RTD (Ω)	RTD (°C)	106 (°C)	107 (°C)	108 (°C)	109 (°C)	110 (°C)
93.953	-15.240	-15.384	-15.543	-15.456	-15.423	-15.425
97.995	-5.140	-5.436	-5.595	-5.491	-5.470	-5.462
102.055	5.035	4.621	4.539	4.619	4.646	4.643
106.045	15.067	14.643	14.540	14.590	14.620	14.627
110.068	25.213	24.799	24.710	24.760	24.799	24.803
114.033	35.243	34.858	34.819	34.841	34.894	34.882
118.023	45.368	45.014	44.956	44.967	45.035	45.038
122.010	55.516	55.166	55.123	55.129	55.178	55.184
125.970	65.628	65.284	65.319	65.302	65.360	65.357
129.940	75.796	75.527	75.508	75.518	75.546	75.541
133.880	85.920	85.665	85.617	85.617	85.643	85.636
137.800	96.023	95.880	95.778	95.760	95.799	95.782
141.650	105.977	106.230	106.016	105.979	106.015	106.008
150.820	129.809	130.344	131.190	131.543	130.029	131.081
156.690	145.158	145.812	146.121	146.946	145.285	146.421
162.540	160.527	161.175	160.760	161.009	159.250	160.457
168.020	174.992	175.427	175.472	176.465	174.442	175.868
173.690	190.027	190.415	190.014	191.143	188.788	190.441
179.380	205.186	205.359	205.188	206.042	203.159	204.911
184.900	219.962	219.785	219.900	221.108	218.920	220.229
190.410	234.779	234.494	234.907	235.516	232.959	234.454

Table B.3: Calibration data for thermocouples 111 – 115.

RTD (Ω)	**RTD (°C)**	**111 (°C)**	**112 (°C)**	**113 (°C)**	**114 (°C)**	**115 (°C)**
93.953	-15.240	-15.426	-15.275	-15.343	-15.282	-15.253
97.995	-5.140	-5.473	-5.301	-5.369	-5.306	-5.277
102.055	5.035	4.637	4.813	4.760	4.807	4.826
106.045	15.067	14.627	14.804	14.754	14.779	14.802
110.068	25.213	24.805	24.982	24.953	24.943	24.956
114.033	35.243	34.891	35.065	35.050	35.015	35.034
118.023	45.368	45.037	45.224	45.217	45.165	45.191
122.010	55.516	55.184	55.361	55.368	55.300	55.326
125.970	65.628	65.367	65.548	65.561	65.474	65.496
129.940	75.796	75.541	75.720	75.750	75.643	75.672
133.880	85.920	85.662	85.838	85.890	85.758	85.789
137.800	96.023	95.822	96.008	96.077	95.973	95.999
141.650	105.977	106.073	106.259	106.311	106.232	106.256
150.820	129.809	131.298	130.419	131.437	131.247	147.114
156.690	145.158	146.203	145.551	146.314	146.112	161.878
162.540	160.527	160.854	159.478	160.960	160.752	176.756
168.020	174.992	175.556	174.733	175.679	175.428	191.186
173.690	190.027	190.110	189.307	190.227	189.933	206.346
179.380	205.186	205.299	204.199	205.404	205.061	220.744
184.900	219.962	220.045	221.029	220.096	219.810	236.142
190.410	234.779	235.067	233.710	235.103	234.840	250.749

Table B.4: Calibration data for thermocouples 116 – 120.

RTD (Ω)	RTD (°C)	116 (°C)	117 (°C)	118 (°C)	119 (°C)	120 (°C)
93.953	-15.240	-15.350	-15.375	-15.253	-15.318	-15.499
97.995	-5.140	-5.376	-5.392	-5.332	-5.379	-5.530
102.055	5.035	4.737	4.717	4.728	4.686	4.584
106.045	15.067	14.712	14.690	14.657	14.622	14.556
110.068	25.213	24.884	24.851	24.771	24.761	24.731
114.033	35.243	34.970	34.934	34.812	34.814	34.823
118.023	45.368	45.130	45.093	44.918	44.936	44.988
122.010	55.516	55.266	55.228	55.002	55.041	55.133
125.970	65.628	65.448	65.398	65.128	65.177	65.306
129.940	75.796	75.628	75.569	75.251	75.321	75.490
133.880	85.920	85.752	85.691	85.329	85.413	85.618
137.800	96.023	95.965	95.900	95.483	95.581	95.831
141.650	105.977	106.238	106.159	105.689	105.817	106.091
150.820	129.809	131.702	146.271	146.501	146.138	146.566
156.690	145.158	146.629	161.010	161.209	160.854	161.331
162.540	160.527	161.290	175.758	176.033	175.643	176.182
168.020	174.992	176.001	189.960	190.419	189.976	190.556
173.690	190.027	190.580	205.021	205.548	205.079	205.695
179.380	205.186	205.787	219.337	219.915	219.475	220.091
184.900	219.962	220.555	234.872	235.264	234.938	235.529
190.410	234.779	235.654	249.579	249.853	249.508	250.216

B.2. Calibration Results

A linear regression analysis was conducted to determine the correction factors for each thermocouple. The standard error of the calibration is a 95% confidence interval about the set of data. The resulting slopes, intercepts, and uncertainties used to correct the temperature measurements of each thermocouple are detailed in Table B.5. The other thermocouples used in the experiments are also indicated in this table, with no corrections to the recorded temperatures.

Table B.5: Regression results for the thermocouple calibration.

Thermocouple	Slope	Intercept (°C)	Uncertainty (°C)
101	-0.90018	1.00533	0.68
102	-0.74773	1.00452	0.67
103	-0.72056	1.00454	0.67
104	-0.60401	1.00397	0.68
105	-0.31780	1.00291	0.65
106	-0.31780	1.00291	0.65
107	0.42748	0.99657	0.51
108	0.47683	0.99388	0.72
109	0.01612	1.00681	0.72
110	0.27035	0.99868	0.65
111	0.35535	0.99643	0.51
112	0.01075	1.00293	0.75
113	0.18749	0.99670	0.49
114	0.15728	0.99825	0.48
115	0.15991	0.99613	0.78
116	0.33254	0.99415	0.61
117	0.06875	1.00187	0.72
118	0.27554	0.99947	0.80
119	0.21282	1.00149	0.63
120	0.31201	0.99810	0.68
Other	1	0	1

APPENDIX C

EXPERIMENTAL, NUMERICAL, AND THEORETICAL DATA

The following appendix presents the experimental, numerical, and theoretical data that was collected in this investigation. The results consist of shadowgraph images and film height investigations including needle contact measurements, laser confocal displacement measurements, numerical simulations, and asymptotic solutions. The data is described by three variable quantities; viscosity, initial film height, and radial temperature difference. The viscosity identifies the silicone oil used in the experiment, and the materials properties for the silicone oils investigated are provided in Chapter 3. The initial film heights are calculated from the mass of liquid placed on the test section, and the temperature differences are calculated as described in Chapter 5.

C.1. Shadowgraphs

In this section, instantaneous shadowgraph images for $0.11 < Bo_D < 1.31$ are presented. The images are grouped by viscosity and initial film height and are shown for increasing ΔT_s. The trends observed in each set are consistent with the data shown in Chapter 5.

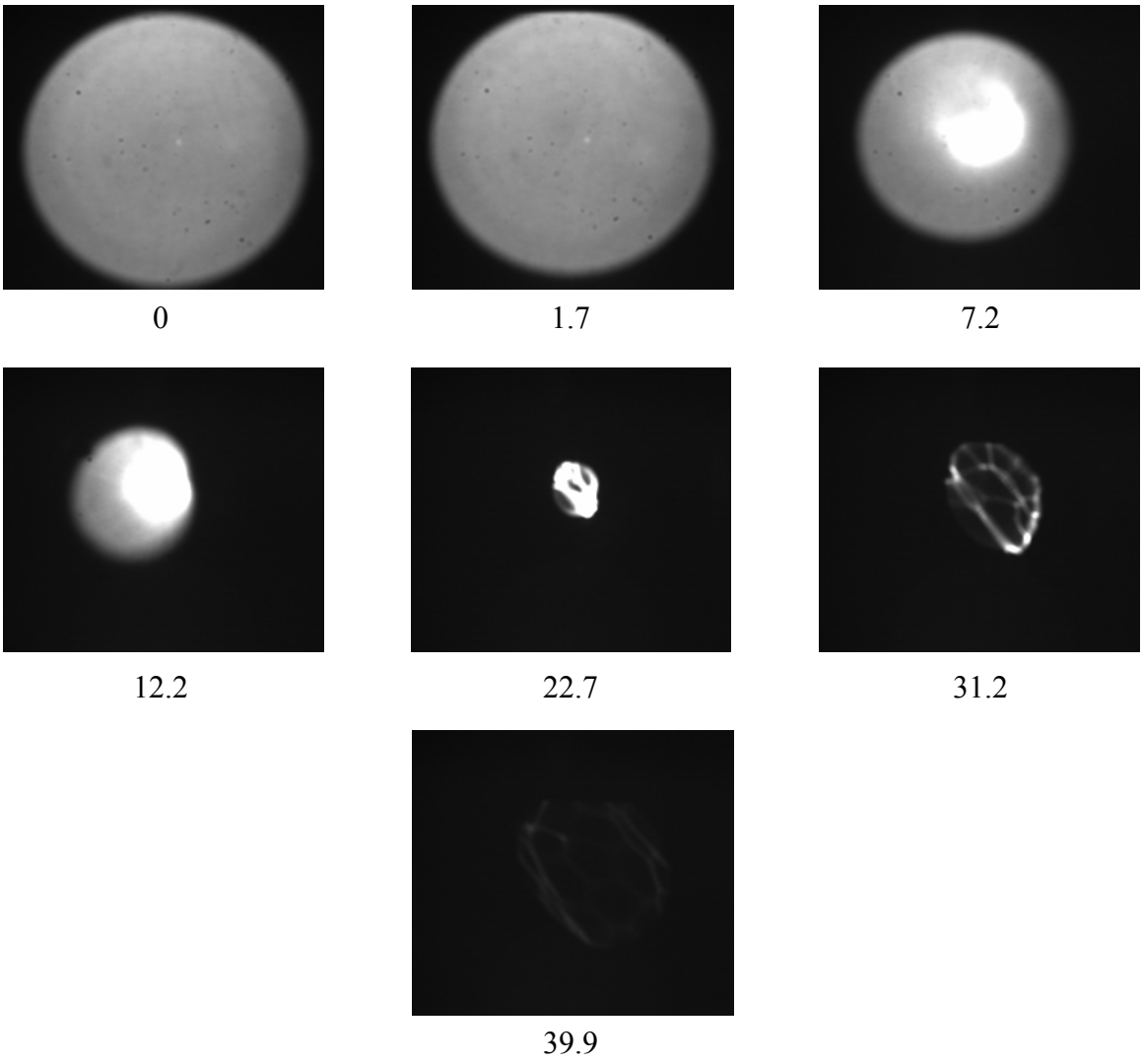

Figure C.1: Shadowgraph images for $\mu = 0.048$ N·s/m^2, $h_o = 1.020$ mm and ΔT_s shown below each image.

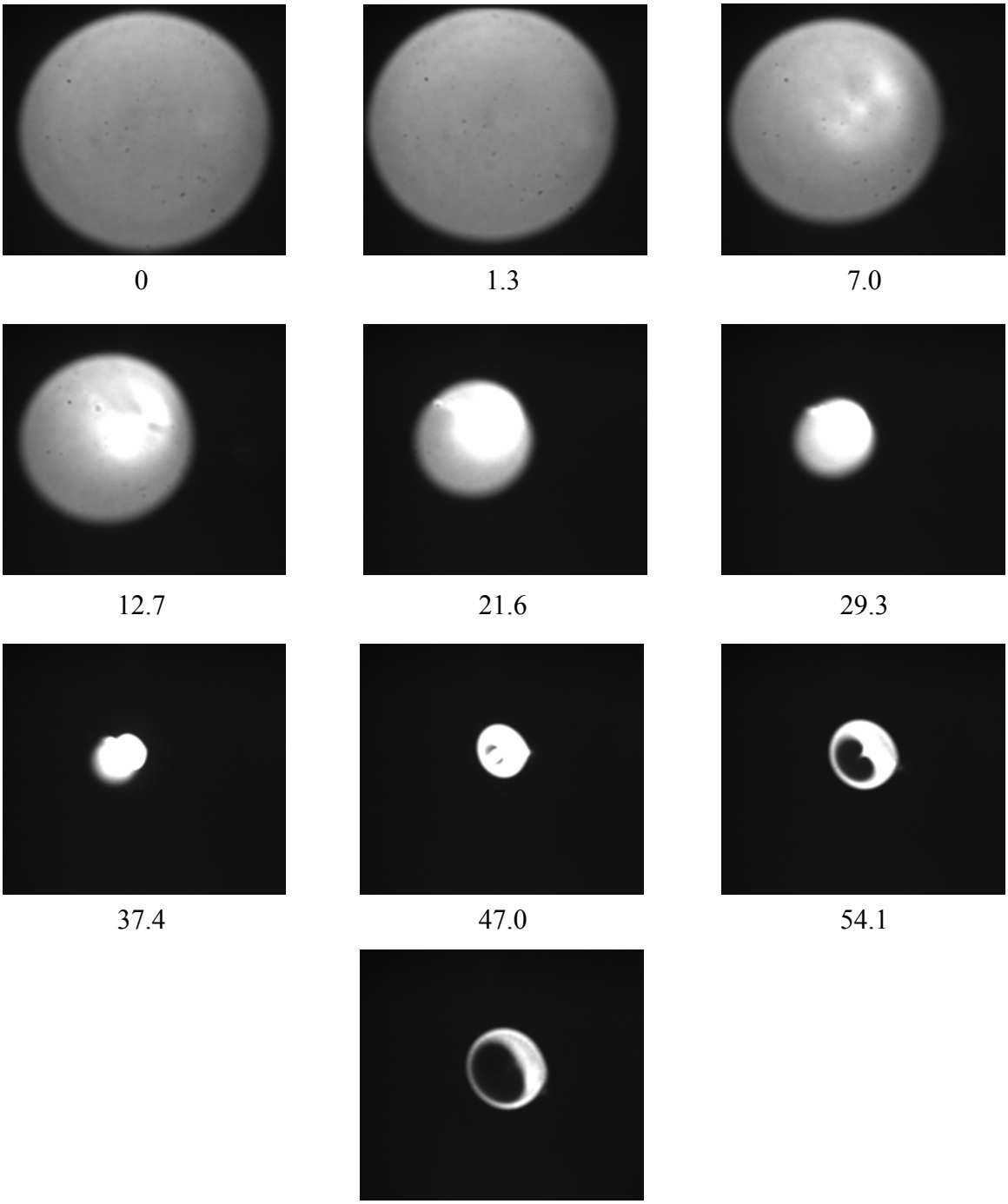

Figure C.2: Shadowgraph images for $\mu = 0.048$ N·s/m^2, $h_o = 1.498$ mm and ΔT_s shown below each image.

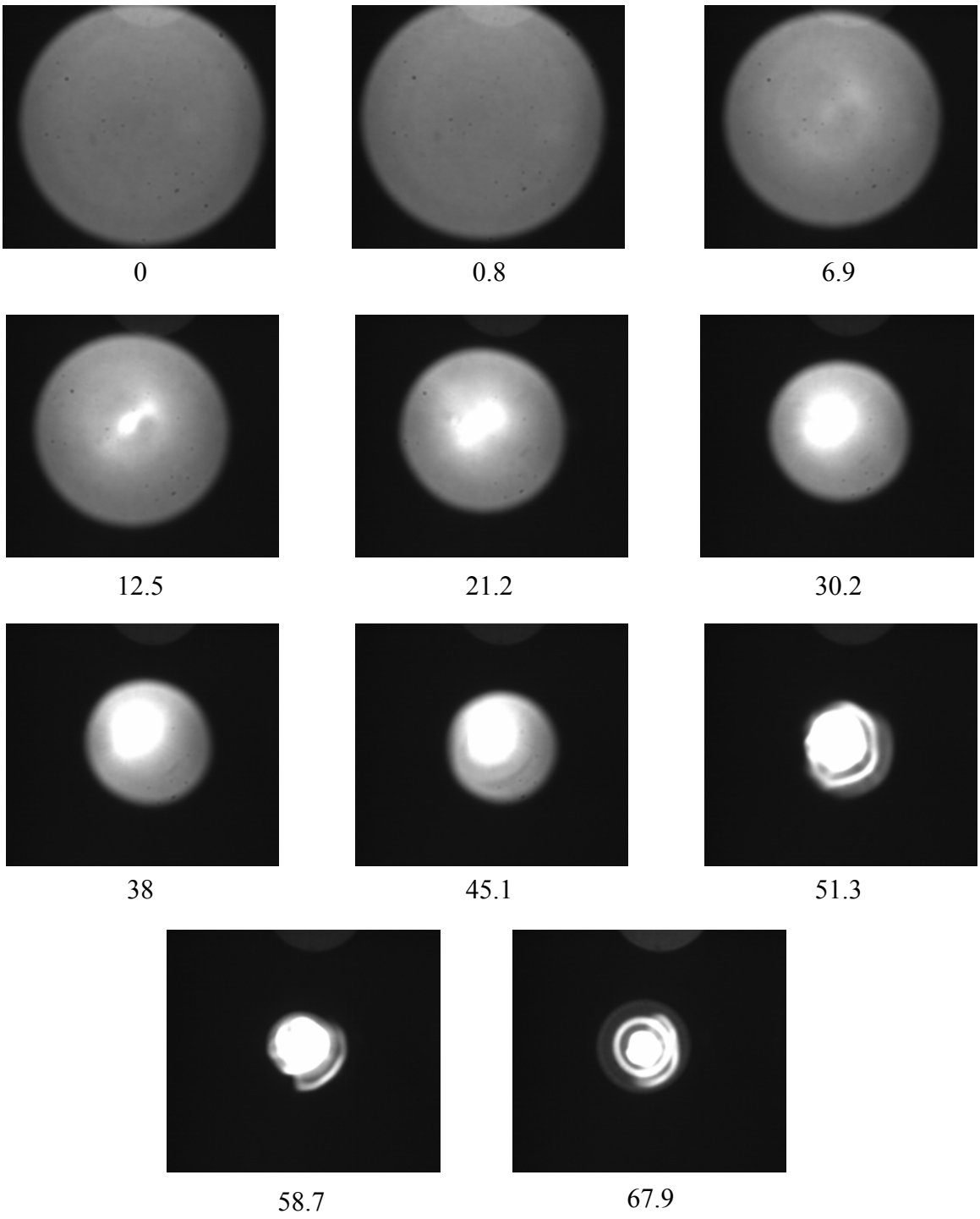

Figure C.3: Shadowgraph images for $\mu = 0.048$ N·s/m^2, $h_o = 1.738$ mm and ΔT_s shown below each image.

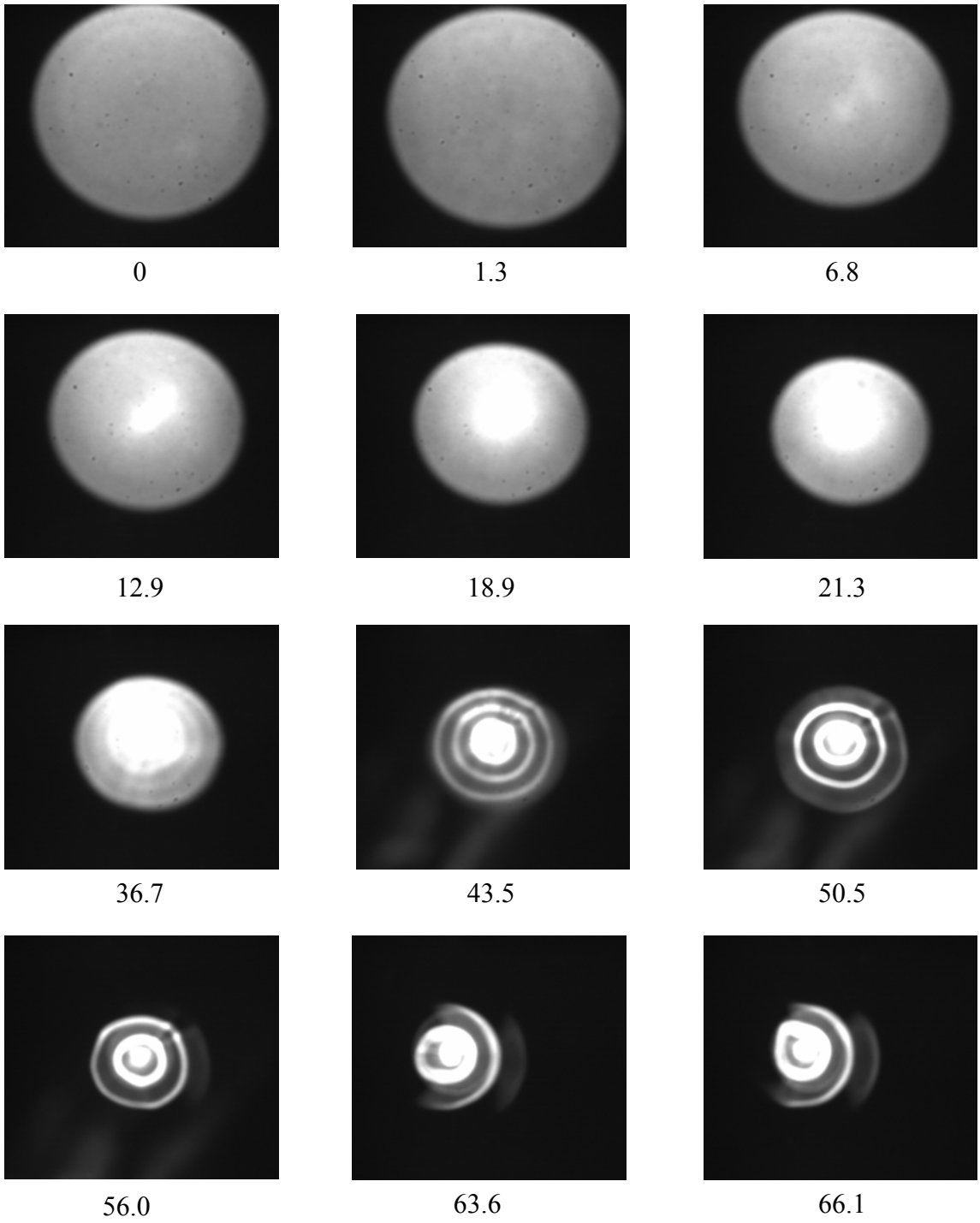

Figure C.4: Shadowgraph images for $\mu = 0.048$ N·s/m^2, $h_o = 1.998$ mm and ΔT_s shown below each image.

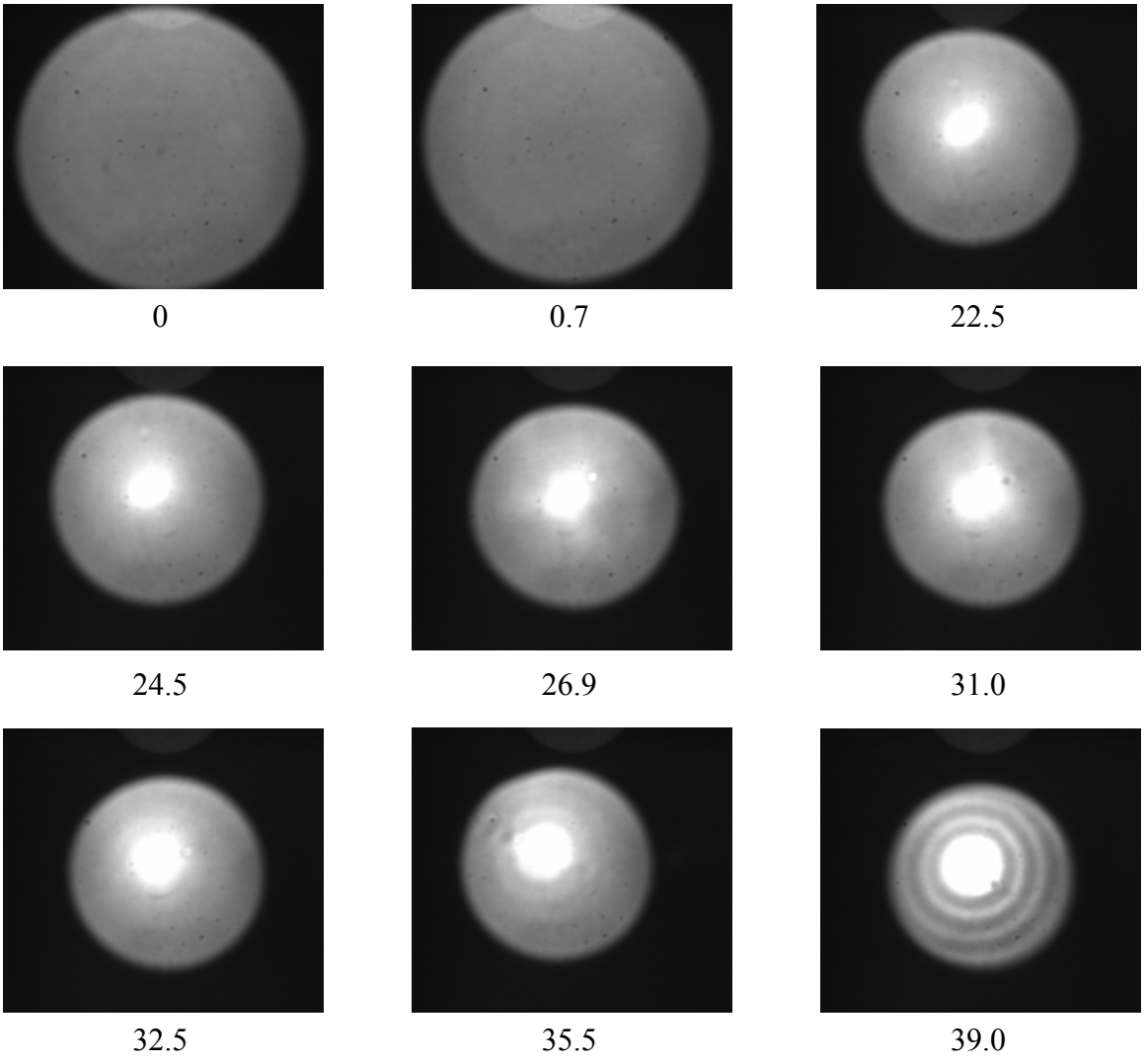

Figure C.5: Shadowgraph images for $\mu = 0.048$ N·s/m^2, $h_o = 1.988$ mm and ΔT_s shown below each image.

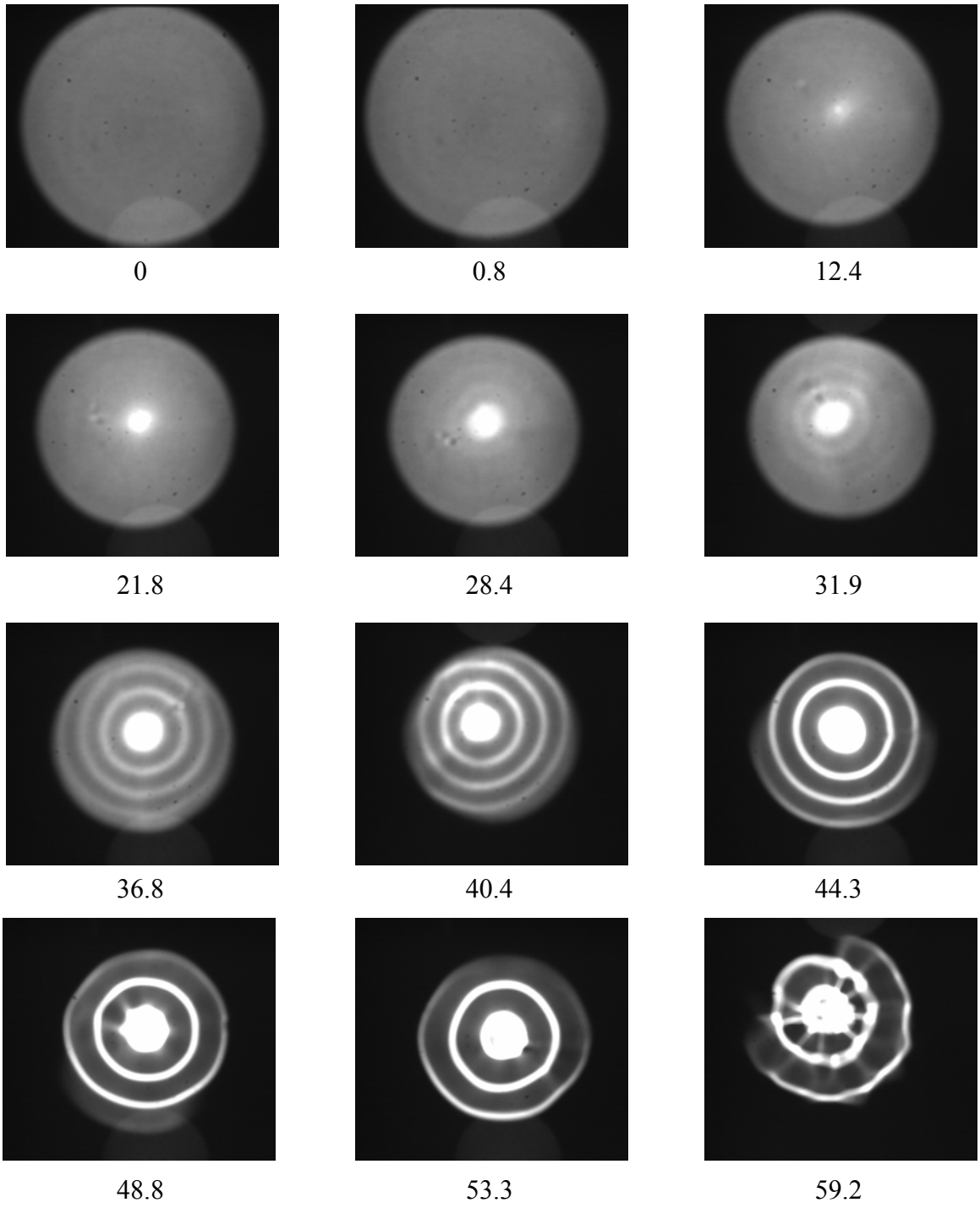

Figure C.6: Shadowgraph images for $\mu = 0.048$ N·s/m^2, $h_o = 2.243$ mm and ΔT_s shown below each image.

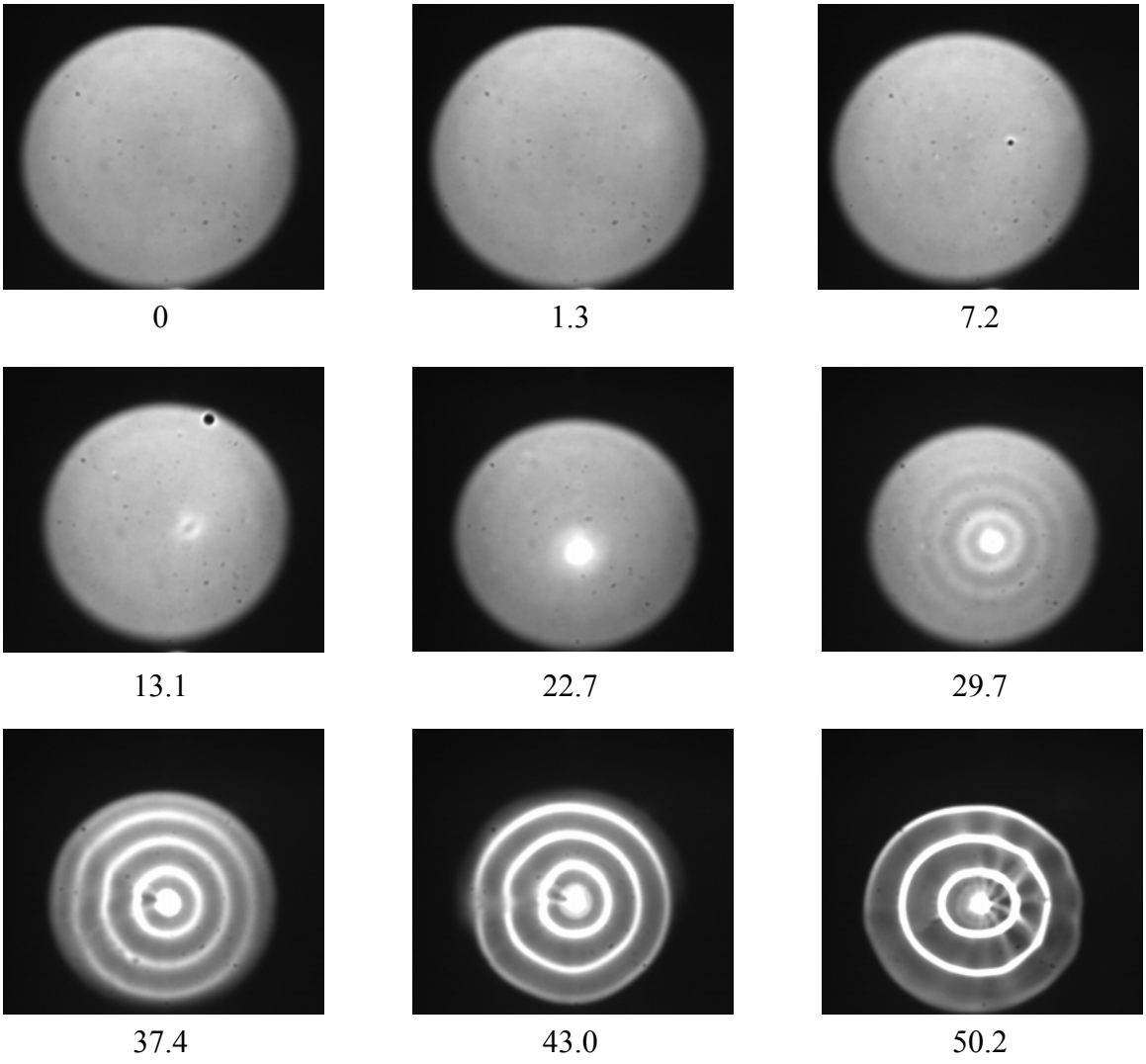

Figure C.7: Shadowgraph images for $\mu = 0.048$ N·s/m^2, $h_o = 2.499$ mm and ΔT_s shown below each image.

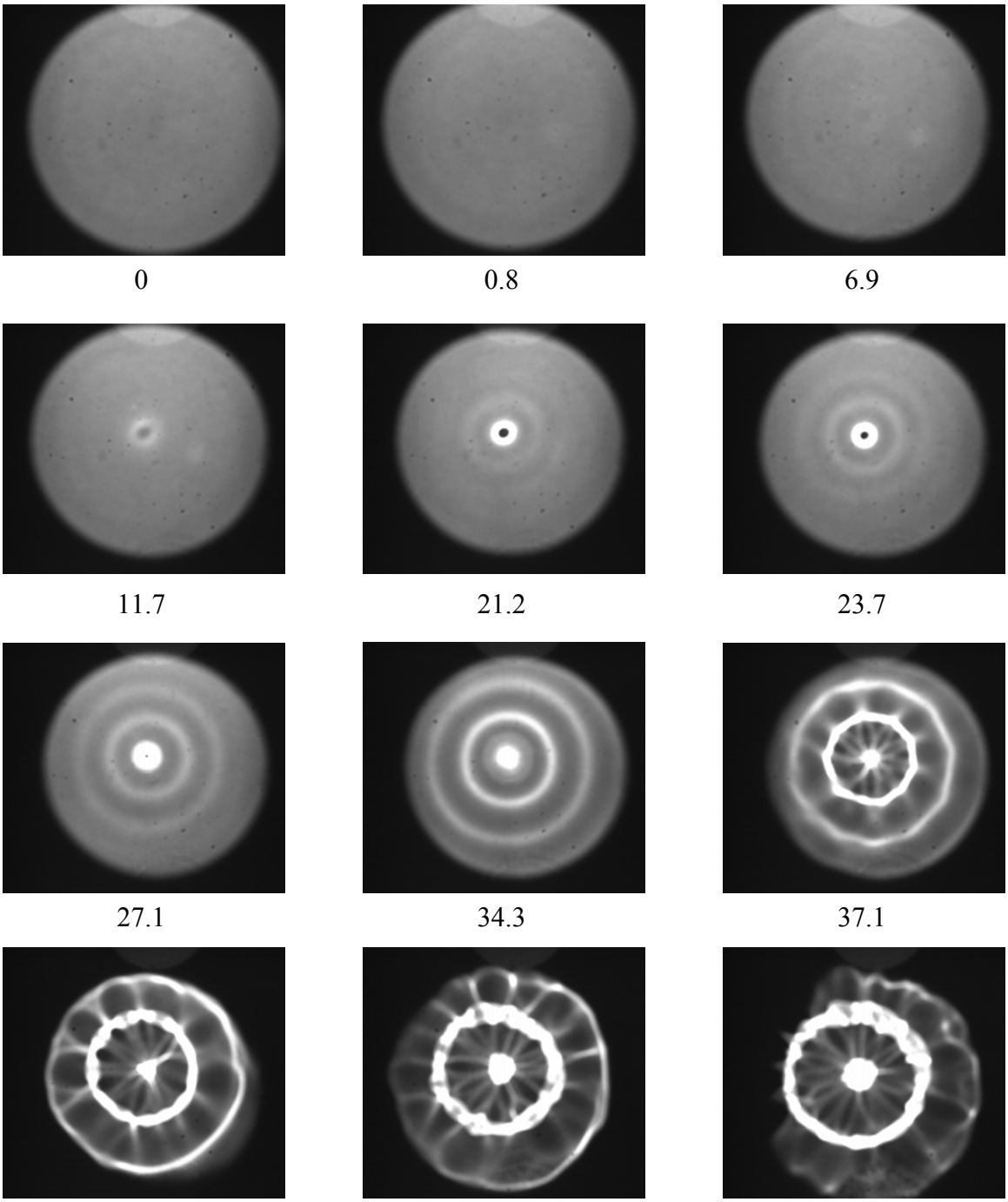

Figure C.8: Shadowgraph images for $\mu = 0.048$ N·s/m^2, $h_o = 2.748$mm and ΔT_s shown below each image.

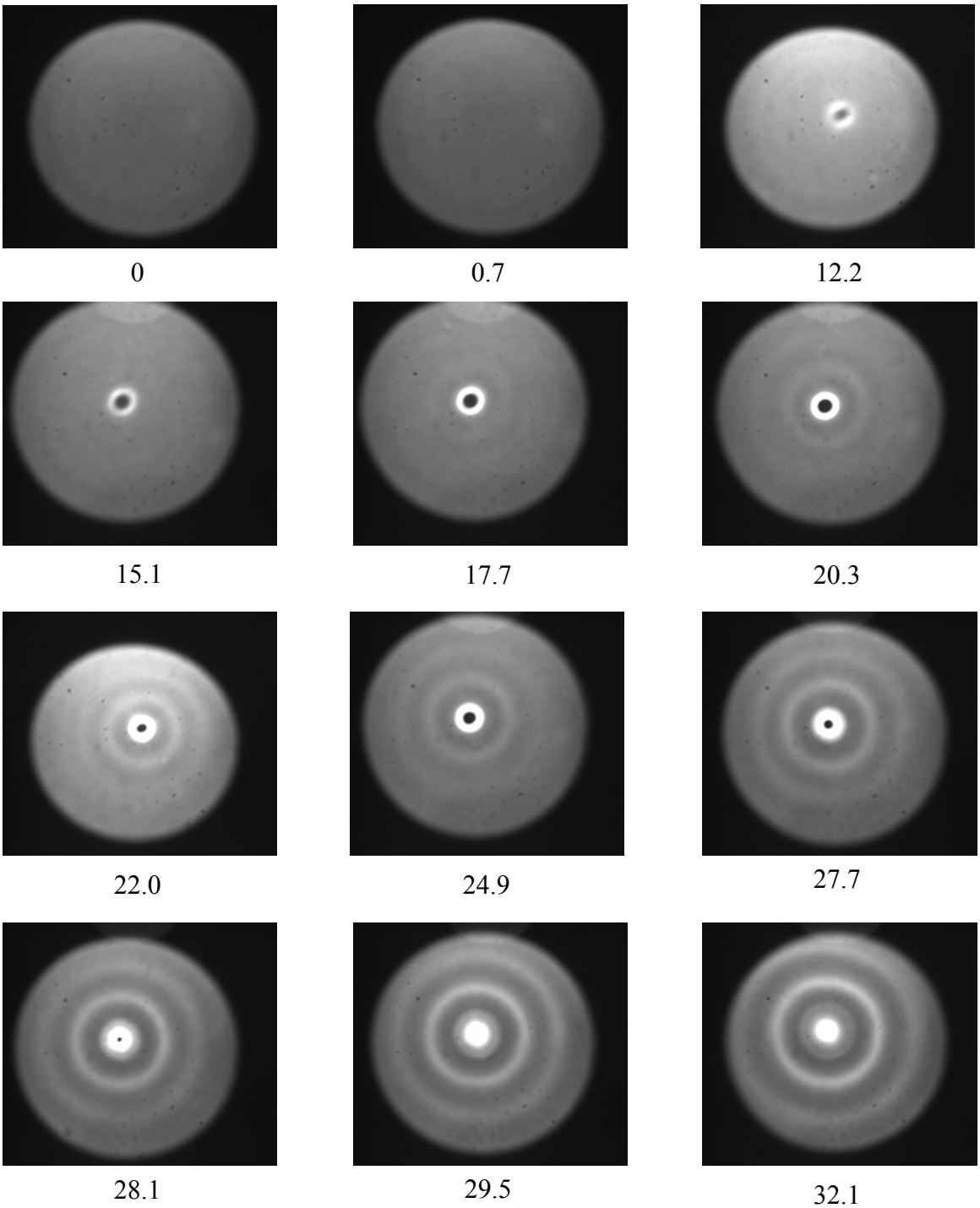

Figure C.9: Shadowgraph images for $\mu = 0.048$ N·s/m^2, $h_o = 2.976$ mm and ΔT_s shown below each image.

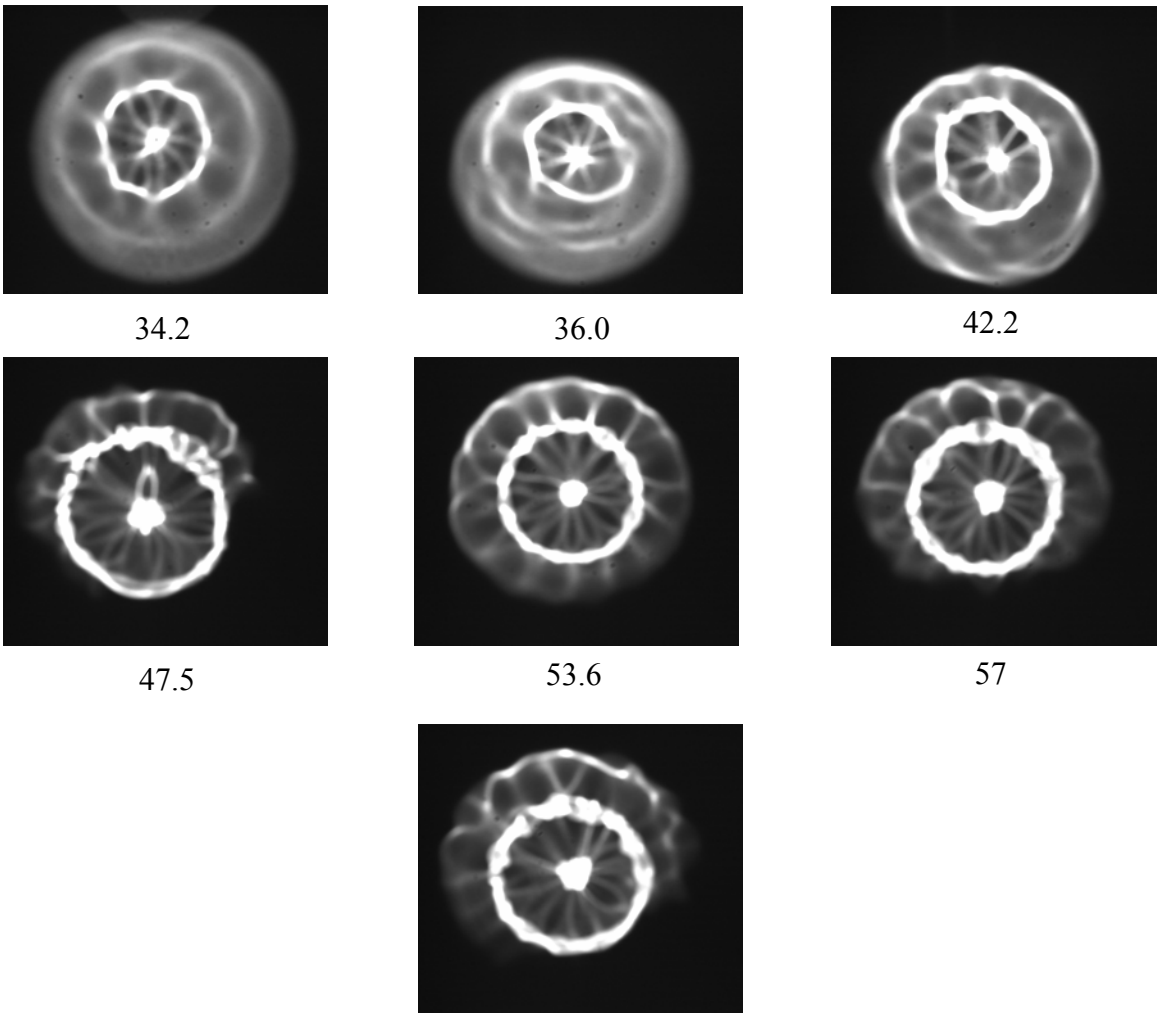

Figure C.10: Shadowgraph images for $\mu = 0.048$ N·s/m^2, $h_o = 2.976$ mm and ΔT_s shown below each image.

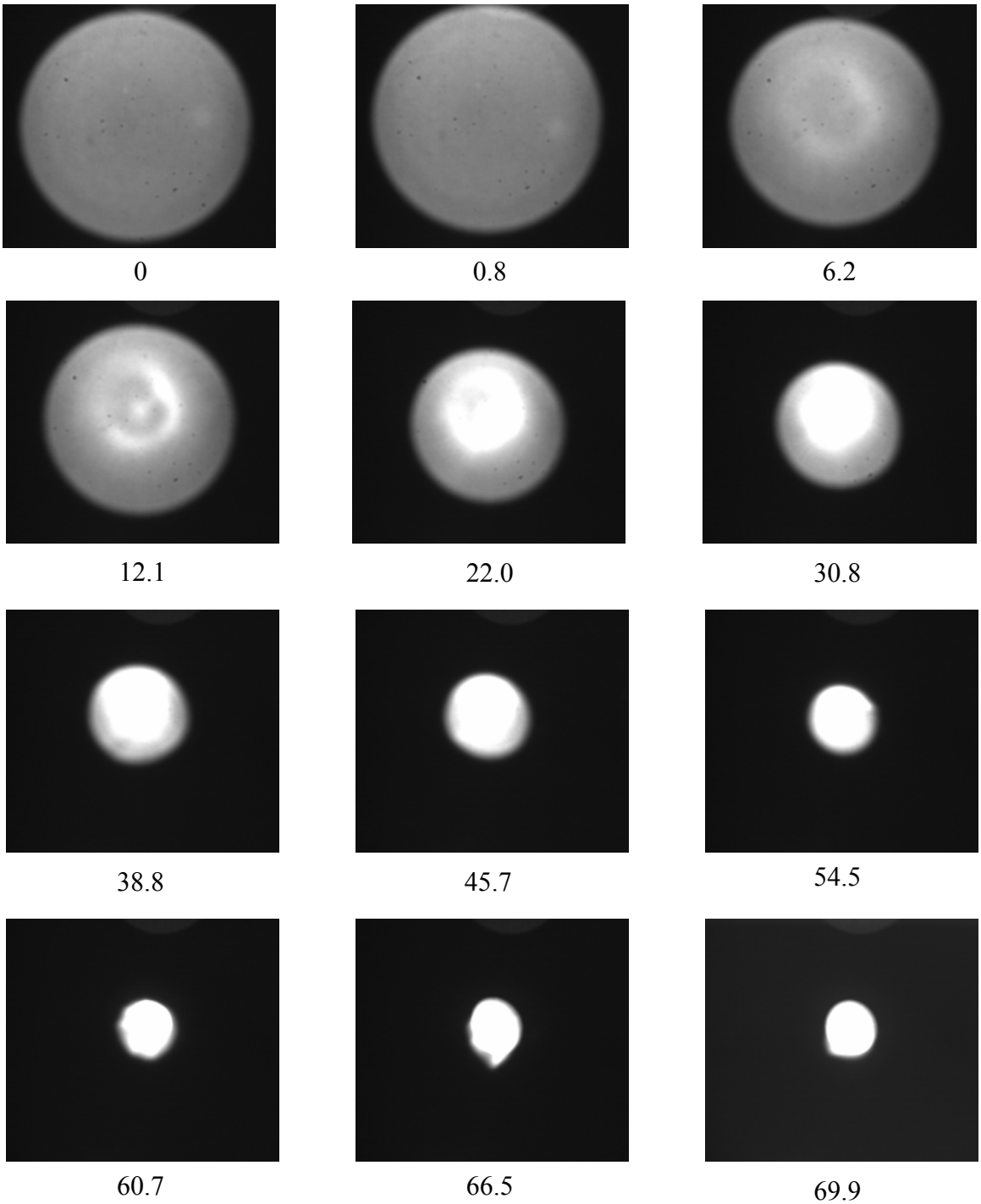

Figure C.11: Shadowgraph images for $\mu = 0.192$ N·s/m^2, $h_o = 1.999$ mm and ΔT_s shown below each image.

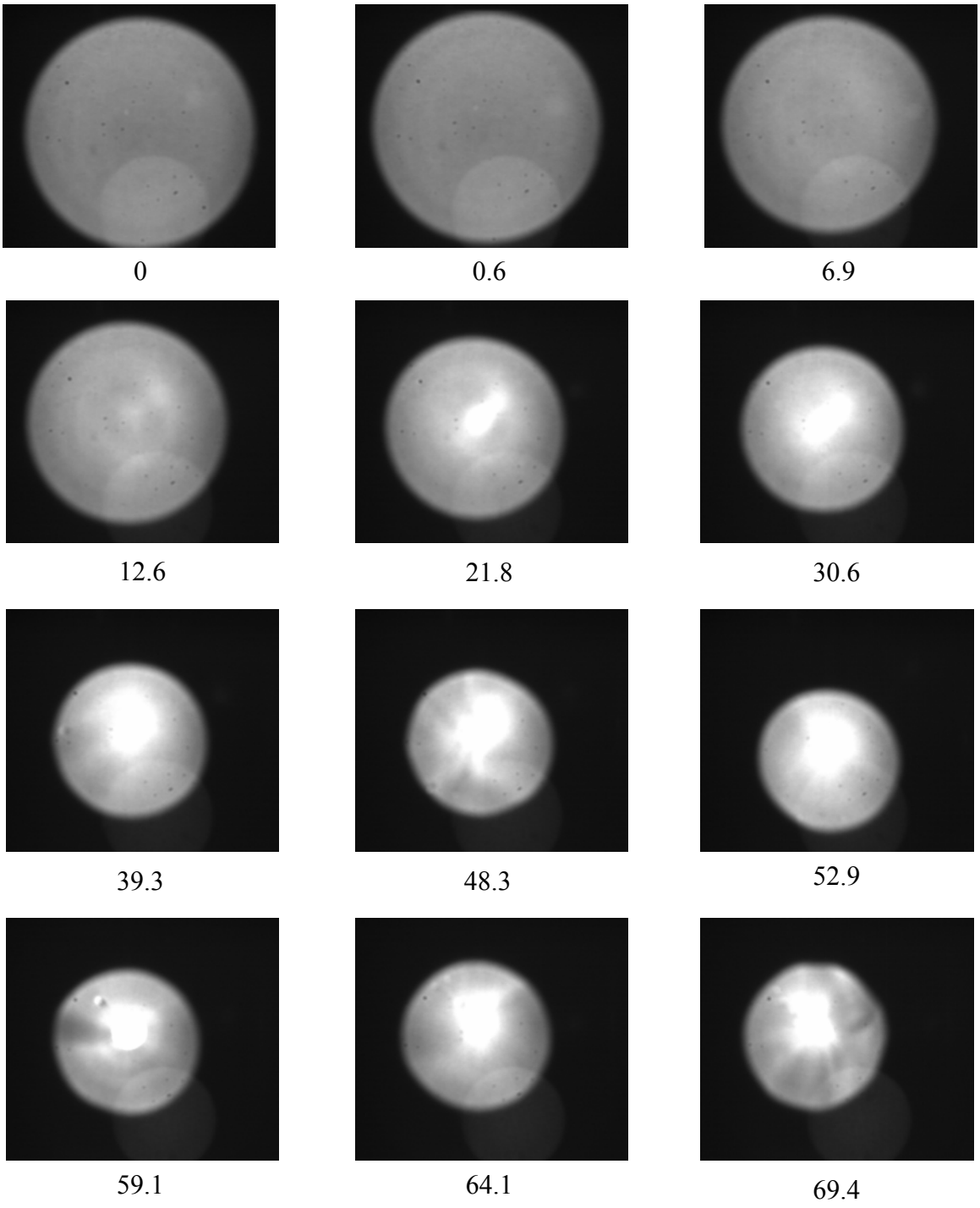

Figure C.12: Shadowgraph images for $\mu = 0.192$ N·s/m^2, $h_o = 2.504$ mm and ΔT_s shown below each image.

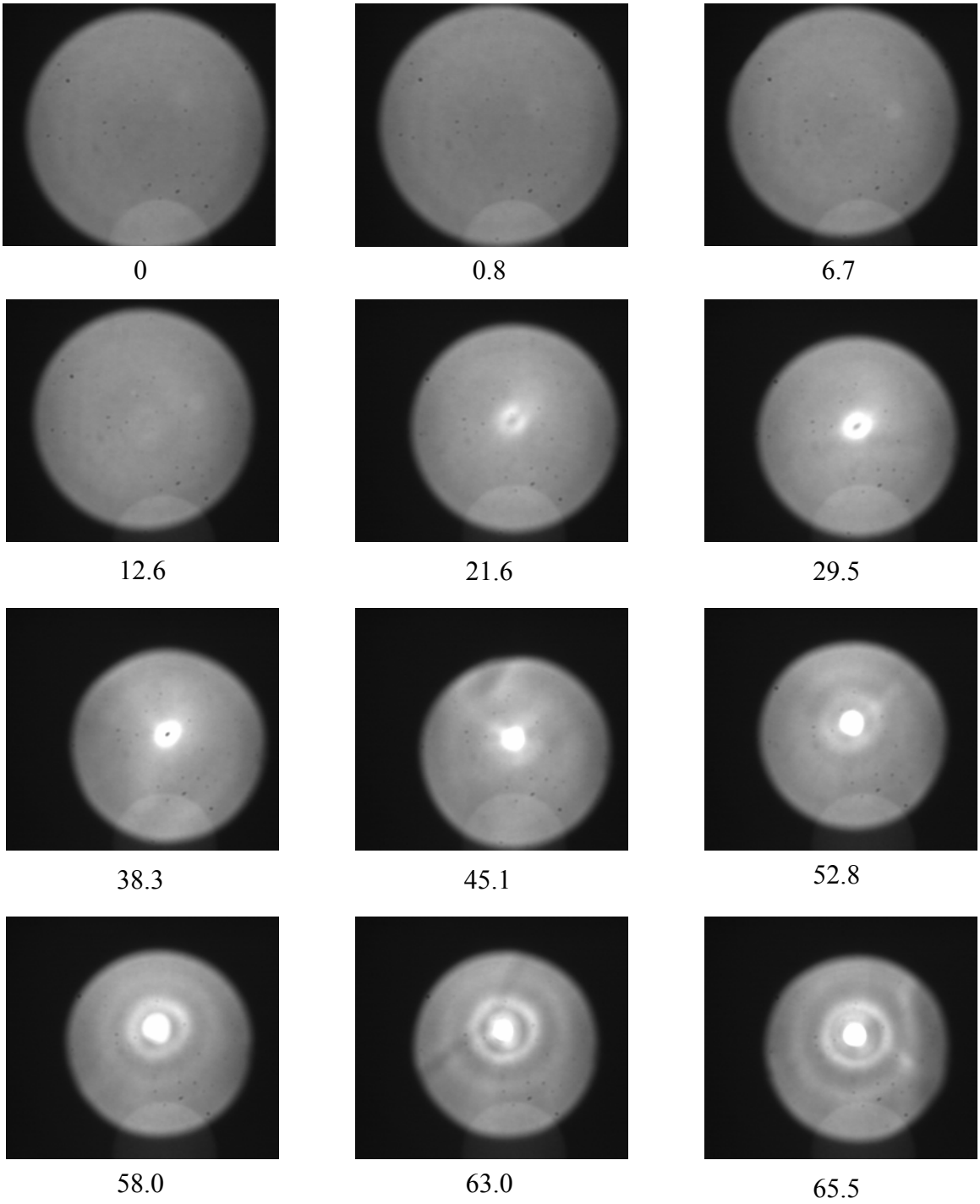

Figure C.13: Shadowgraph images for $\mu = 0.192$ N·s/m^2, $h_o = 2.995$ mm and ΔT_s shown below each image.

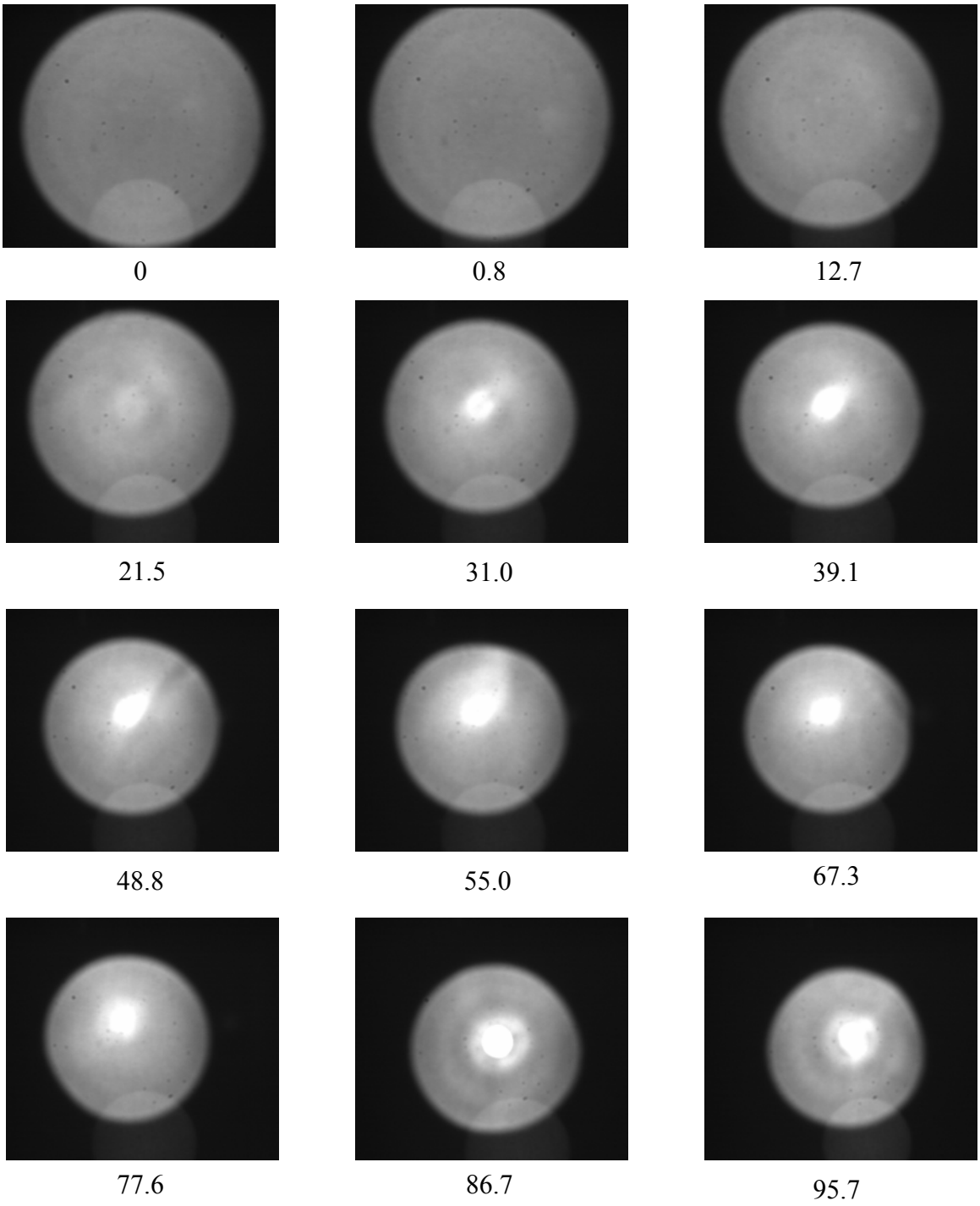

Figure C.14: Shadowgraph images for $\mu = 0.480$ N·s/m^2, $h_o = 2.997$ mm and ΔT_s shown below each image.

C.2. Film Height Studies

In the following subsections, experimental, numerical, and asymptotic results for the steady-state film height of liquid layers are presented in tables. The data provided here represents the results that were discussed in Chapter 5 as well as additional experiments and simulations.

C.2.1. Needle Contact Measurements

The following tables present the experimental data collected using the needle contact method. The local film height measurements are accompanied by the surface temperature measurements for each run. Surface temperatures for initial characterization of the liquid free surface are not provided, since there was no applied temperature difference. The data are organized first by fluid viscosity, then initial film height, and finally, by the imposed temperature difference.

Table C.1: Needle contact data for $\mu = 0.048$ N·s/m^2, $h_o = 0.271$ mm, $\Delta T_s = 0.0$°C.

r'	***h'***	***r'***	***h'***	***r'***	***h'***
-0.95	1.322	-0.19	0.971	0.35	1.045
-0.85	0.927	-0.02	0.938	0.52	1.075
-0.69	0.942	0.00	0.864	0.69	1.090
-0.52	1.005	0.02	0.927	0.85	1.064
-0.35	0.997	0.19	1.019	0.95	1.518

Table C.2: Needle contact data for $\mu = 0.048$ N·s/m^2, $h_o = 0.271$ mm, $\Delta T_s = 3.6$°C.

r'	***h'***	***r'***	***h'***	***r'***	**T (°C)**	***r'***	**T (°C)**
0.00	0.277	0.49	0.957	-0.99	16.1	0.28	18.2
0.02	0.458	0.55	1.008	-0.82	16.5	0.32	18.0
0.09	0.495	0.62	1.019	-0.66	16.9	0.41	17.8
0.15	0.628	0.69	1.078	-0.49	17.3	0.49	17.6
0.22	0.746	0.75	1.090	-0.32	18.1	0.57	17.4
0.29	0.838	0.82	1.097	-0.24	18.4	0.66	17.0
0.35	0.909	0.89	1.104	-0.16	19.0	0.74	16.9
0.42	0.920	0.95	1.559	0.16	19.0	0.82	16.7
				0.20	18.6	0.91	16.5
				0.24	18.4		

Table C.3: Needle contact data for $\mu = 0.048$ N·s/m^2, $h_o = 0.271$ mm, $\Delta T_s = 4.4$°C.

r'	***h'***	***r'***	***h'***	***r'***	**T (°C)**	***r'***	**T (°C)**
0.00	0.000	0.49	0.898	-0.99	16.2	0.28	18.7
0.02	0.000	0.55	0.927	-0.82	16.7	0.32	18.5
0.09	0.000	0.62	0.990	-0.66	17.2	0.41	18.2
0.15	0.336	0.69	1.060	-0.49	17.6	0.49	17.9
0.22	0.617	0.75	1.075	-0.32	18.5	0.57	17.7
0.29	0.776	0.82	1.097	-0.24	19.0	0.66	17.2
0.35	0.813	0.89	1.130	-0.16	19.6	0.74	17.1
0.42	0.879	0.95	1.666	0.16	19.8	0.82	16.9
				0.20	19.3	0.91	16.6
				0.24	19.0		

Table C.4: Needle contact data for $\mu = 0.048$ N·s/m^2, $h_o = 0.271$ mm, $\Delta T_s = 5.0$°C.

r'	***h'***	***r'***	***h'***	***r'***	**T (°C)**	***r'***	**T (°C)**
0.00	0.000	0.49	0.927	-0.99	16.2	0.28	19.1
0.02	0.000	0.55	1.049	-0.82	16.7	0.32	18.9
0.09	0.000	0.62	1.071	-0.66	17.3	0.41	18.5
0.15	0.233	0.69	1.123	-0.49	17.9	0.49	18.1
0.22	0.554	0.75	1.134	-0.32	18.9	0.57	17.9
0.29	0.702	0.82	1.163	-0.24	19.4	0.66	17.4
0.35	0.838	0.89	1.178	-0.16	20.2	0.74	17.2
0.42	0.879	0.95	1.684	0.16	20.4	0.82	17.0
				0.20	19.8	0.91	16.7
				0.24	19.5		

Table C.5: Needle contact data for $\mu = 0.048$ N·s/m^2, $h_o = 0.313$ mm, $\Delta T_s = 0.0$°C.

r'	***h'***	***r'***	***h'***	***r'***	***h'***
-72.64	1.300	-14.22	0.989	26.92	0.992
-65.02	0.960	-1.52	0.957	39.62	0.998
-52.32	1.008	0.00	0.893	52.32	1.120
-39.62	0.982	1.52	0.966	65.02	1.059
-26.92	0.985	14.22	0.985	72.64	1.436

Table C.6: Needle contact data for $\mu = 0.048$ N·s/m^2, $h_o = 0.313$ mm, $\Delta T_s = 3.5$°C.

r'	***h'***	***r'***	***h'***	***r'***	**T (°C)**	***r'***	**T (°C)**
0.00	0.496	0.49	0.963	-0.99	16.1	0.28	18.1
0.02	0.553	0.55	1.005	-0.82	16.5	0.32	17.9
0.09	0.601	0.62	1.033	-0.66	16.9	0.41	17.7
0.15	0.707	0.69	1.065	-0.49	17.3	0.49	17.5
0.22	0.784	0.75	1.065	-0.32	18.0	0.57	17.3
0.29	0.848	0.82	1.091	-0.24	18.3	0.66	16.9
0.35	0.896	0.89	1.097	-0.16	18.8	0.74	16.8
0.42	0.950	0.95	1.574	0.16	18.9	0.82	16.7
				0.20	18.5	0.91	16.5
				0.24	18.3		

Table C.7: Needle contact data for $\mu = 0.048$ N·s/m^2, $h_o = 0.313$ mm, $\Delta T_s = 5.0$°C.

r'	***h'***	***r'***	***h'***	***r'***	**T (°C)**	***r'***	**T (°C)**
0.00	0.000	0.49	0.953	-0.99	16.2	0.28	19.1
0.02	0.144	0.55	0.989	-0.82	16.7	0.32	18.8
0.09	0.307	0.62	1.056	-0.66	17.3	0.41	18.4
0.15	0.493	0.69	1.075	-0.49	17.8	0.49	18.1
0.22	0.662	0.75	1.097	-0.32	18.8	0.57	17.8
0.29	0.793	0.82	1.177	-0.24	19.4	0.66	17.3
0.35	0.857	0.89	1.168	-0.16	20.1	0.74	17.1
0.42	0.918	0.95	1.584	0.16	20.4	0.82	16.9
				0.20	19.8	0.91	16.6
				0.24	19.5		

Table C.8: Needle contact data for $\mu = 0.048$ N·s/m^2, $h_o = 0.313$ mm, $\Delta T_s = 6.2$°C.

r'	***h'***	***r'***	***h'***	***r'***	**T (°C)**	***r'***	**T (°C)**
0.00	0.000	0.49	0.941	-0.99	16.3	0.28	19.9
0.02	0.000	0.55	0.982	-0.82	16.8	0.32	19.6
0.09	0.000	0.62	1.033	-0.66	17.5	0.41	19.0
0.15	0.173	0.69	1.110	-0.49	18.2	0.49	18.5
0.22	0.525	0.75	1.123	-0.32	19.5	0.57	18.2
0.29	0.727	0.82	1.145	-0.24	20.2	0.66	17.6
0.35	0.825	0.89	1.200	-0.16	21.3	0.74	17.4
0.42	0.889	0.95	1.561	0.16	21.6	0.82	17.1
				0.20	20.9	0.91	16.7
				0.24	20.4		

Table C.9: Needle contact data for $\mu = 0.048$ N·s/m^2, $h_o = 0.438$ mm, $\Delta T_s = 0.0$°C.

r'	***h'***	***r'***	***h'***	***r'***	***h'***
0.00	0.915	0.31	1.006	0.65	0.985
0.05	0.999	0.38	1.013	0.71	1.004
0.11	1.006	0.45	0.983	0.78	1.006
0.18	1.004	0.51	0.997	0.85	0.985
0.25	1.017	0.58	0.995	0.91	0.999

Table C.10: Needle contact data for $\mu = 0.048$ N·s/m^2, $h_o = 0.438$ mm, $\Delta T_s = 7.6$°C.

r'	***h'***	***r'***	***h'***	***r'***	**T (°C)**	***r'***	**T (°C)**
0.00	0.276	0.51	0.919	-0.99	16.3	0.28	21.1
0.05	0.399	0.58	0.969	-0.82	17.1	0.32	20.7
0.11	0.392	0.65	0.965	-0.66	18.1	0.41	19.9
0.18	0.518	0.71	1.013	-0.49	19.2	0.49	19.3
0.25	0.646	0.78	1.026	-0.32	20.9	0.57	18.8
0.31	0.719	0.85	1.036	-0.24	22.1	0.66	18.1
0.38	0.792	0.91	1.079	-0.16	23.7	0.74	17.7
0.45	0.871			0.16	23.0	0.82	17.3
				0.20	22.3	0.91	16.9
				0.24	21.6		

Table C.11: Needle contact data for $\mu = 0.048$ N·s/m^2, $h_o = 0.438$ mm, $\Delta T_s = 13.4$°C.

r'	***h'***	***r'***	***h'***	***r'***	**T (°C)**	***r'***	**T (°C)**
0.00	0.000	0.51	0.890	-0.99	17.0	0.28	25.1
0.05	0.000	0.58	0.912	-0.82	18.3	0.32	24.5
0.11	0.000	0.65	1.006	-0.66	19.8	0.41	22.9
0.18	0.000	0.71	1.063	-0.49	21.7	0.49	21.8
0.25	0.347	0.78	1.079	-0.32	24.6	0.57	20.9
0.31	0.591	0.85	1.125	-0.24	26.6	0.66	19.8
0.38	0.762	0.91	1.168	-0.16	29.3	0.74	19.2
0.45	0.833			0.16	28.8	0.82	18.5
				0.20	27.4	0.91	17.8
				0.24	26.2		

Table C.12: Needle contact data for $\mu = 0.048$ N·s/m^2, $h_o = 0.489$ mm, $\Delta T_s = 0.0$°C.

r'	***h'***	***r'***	***h'***	***r'***	***h'***
-0.95	1.295	-0.19	0.994	0.35	1.003
-0.85	1.007	-0.02	0.988	0.52	1.003
-0.69	1.058	0.00	0.923	0.69	0.990
-0.52	1.005	0.02	0.962	0.85	0.994
-0.35	1.013	0.19	0.984	0.95	1.271

Table C.13: Needle contact data for $\mu = 0.048$ N·s/m^2, $h_o = 0.489$ mm, $\Delta T_s = 7.1$°C.

r'	***h'***	***r'***	***h'***	***r'***	**T (°C)**	***r'***	**T (°C)**
0.00	0.156	0.49	0.874	-0.99	16.2	0.28	20.6
0.02	0.213	0.55	0.896	-0.82	16.9	0.32	20.2
0.09	0.403	0.62	0.917	-0.66	17.8	0.41	19.4
0.15	0.577	0.69	0.949	-0.49	18.9	0.49	18.8
0.22	0.692	0.75	0.972	-0.32	20.8	0.57	18.4
0.29	0.778	0.82	0.984	-0.24	22.0	0.66	17.7
0.35	0.868	0.89	0.994	-0.16	24.1	0.74	17.4
0.42	0.843	0.95	1.291	0.16	22.5	0.82	17.1
				0.20	21.7	0.91	16.7
				0.24	21.1		

Table C.14: Needle contact data for $\mu = 0.048$ N·s/m^2, $h_o = 0.489$ mm, $\Delta T_s = 9.8$°C.

r'	***h'***	***r'***	***h'***	***r'***	**T (°C)**	***r'***	**T (°C)**
0.00	0.000	0.49	0.857	-0.99	16.5	0.28	22.5
0.02	0.000	0.55	0.894	-0.82	17.5	0.32	21.9
0.09	0.000	0.62	0.960	-0.66	18.7	0.41	20.8
0.15	0.243	0.69	0.974	-0.49	20.3	0.49	20.0
0.22	0.585	0.75	1.009	-0.32	22.7	0.57	19.4
0.29	0.714	0.82	1.005	-0.24	24.5	0.66	18.6
0.35	0.765	0.89	1.037	-0.16	27.3	0.74	18.1
0.42	0.820	0.95	1.334	0.16	25.2	0.82	17.6
				0.20	24.1	0.91	17.1
				0.24	23.3		

Table C.15: Needle contact data for $\mu = 0.048$ N·s/m^2, $h_o = 0.489$ mm, $\Delta T_s = 12.7$°C.

r'	***h'***	***r'***	***h'***	***r'***	**T (°C)**	***r'***	**T (°C)**
0.00	0.000	0.49	0.925	-0.99	16.8	0.28	24.5
0.02	0.000	0.55	0.956	-0.82	18.0	0.32	23.8
0.09	0.000	0.62	1.015	-0.66	19.5	0.41	22.3
0.15	0.311	0.69	1.062	-0.49	21.5	0.49	21.3
0.22	0.569	0.75	1.076	-0.32	24.5	0.57	20.4
0.29	0.732	0.82	1.093	-0.24	26.7	0.66	19.4
0.35	0.808	0.89	1.107	-0.16	30.2	0.74	18.8
0.42	0.863	0.95	1.393	0.16	28.1	0.82	18.1
				0.20	26.6	0.91	17.5
				0.24	25.5		

Table C.16: Needle contact data for $\mu = 0.048$ N·s/m^2, $h_o = 0.588$ mm, $\Delta T_s = 0.0$°C.

r'	***h'***	***r'***	***h'***	***r'***	***h'***
-0.95	1.239	-0.19	0.979	0.35	1.020
-0.85	0.989	-0.02	0.979	0.52	1.021
-0.69	1.013	0.00	0.923	0.69	1.037
-0.52	0.979	0.02	0.962	0.85	1.032
-0.35	0.993	0.19	0.997	0.95	1.258

Table C.17: Needle contact data for $\mu = 0.048$ N·s/m^2, $h_o = 0.588$ mm, $\Delta T_s = 8.5$°C.

r'	***h'***	***r'***	***h'***	***r'***	**T (°C)**	***r'***	**T (°C)**
0.00	0.697	0.49	0.996	-0.99	16.5	0.28	21.4
0.02	0.710	0.55	1.015	-0.82	17.2	0.32	20.9
0.09	0.758	0.62	1.033	-0.66	18.1	0.41	20.1
0.15	0.800	0.69	1.047	-0.49	19.1	0.49	19.4
0.22	0.882	0.75	1.074	-0.32	20.8	0.57	18.9
0.29	0.914	0.82	1.076	-0.24	21.9	0.66	18.2
0.35	0.947	0.89	1.086	-0.16	23.3	0.74	17.8
0.42	0.977	0.95	1.312	0.16	23.8	0.82	17.4
				0.20	22.8	0.91	17.0
				0.24	22.1		

Table C.18: Needle contact data for $\mu = 0.048$ N·s/m^2, $h_o = 0.588$ mm, $\Delta T_s = 9.8$°C.

r'	***h'***	***r'***	***h'***	***r'***	**T (°C)**	***r'***	**T (°C)**
0.00	0.644	0.49	0.993	-0.99	16.6	0.28	22.4
0.02	0.673	0.55	1.004	-0.82	17.5	0.32	21.8
0.09	0.702	0.62	1.021	-0.66	18.5	0.41	20.8
0.15	0.809	0.69	1.045	-0.49	19.7	0.49	20.0
0.22	0.846	0.75	1.054	-0.32	21.6	0.57	19.4
0.29	0.889	0.82	1.081	-0.24	22.8	0.66	18.6
0.35	0.931	0.89	1.069	-0.16	24.5	0.74	18.2
0.42	0.964	0.95	1.276	0.16	25.2	0.82	17.7
				0.20	24.0	0.91	17.2
				0.24	23.1		

Table C.19: Needle contact data for $\mu = 0.048$ N·s/m^2, $h_o = 0.695$ mm, $\Delta T_s = 0.0$°C.

r'	***h'***	***r'***	***h'***	***r'***	***h'***	***r'***	***h'***
-0.95	1.214	-0.02	1.006	0.29	1.007	0.69	0.993
-0.85	1.034	0.00	0.973	0.35	1.016	0.75	0.996
-0.69	1.055	0.02	0.998	0.42	0.997	0.82	0.981
-0.52	1.045	0.09	1.057	0.49	0.991	0.89	0.983
-0.35	1.023	0.15	1.006	0.55	0.977	0.95	1.152
-0.19	1.023	0.22	1.009	0.62	1.017		

Table C.20: Needle contact data for $\mu = 0.048$ N·s/m^2, $h_o = 0.695$ mm, $\Delta T_s = 13.0$°C.

r'	***h'***	***r'***	***h'***	***r'***	**T (°C)**	***r'***	**T (°C)**
0.00	0.685	0.49	0.942	-0.99	16.9	0.28	24.9
0.02	0.712	0.55	0.973	-0.82	18.1	0.32	24.2
0.09	0.719	0.62	0.988	-0.66	19.6	0.41	22.7
0.15	0.765	0.69	1.011	-0.49	21.5	0.49	21.6
0.22	0.814	0.75	1.020	-0.32	24.3	0.57	20.8
0.29	0.873	0.82	1.019	-0.24	26.4	0.66	19.7
0.35	0.897	0.89	1.036	-0.16	29.1	0.74	19.0
0.42	0.921	0.95	1.253	0.16	28.4	0.82	18.4
				0.20	27.0	0.91	17.7
				0.24	25.9		

Table C.21: Needle contact data for $\mu = 0.048$ N·s/m^2, $h_o = 0.695$ mm, $\Delta T_s = 21.7$°C.

r'	***h'***	***r'***	***h'***	***r'***	**T (°C)**	***r'***	**T (°C)**
0.00	0.324	0.49	0.915	-0.99	17.9	0.28	31.1
0.02	0.360	0.55	0.945	-0.82	19.9	0.32	29.9
0.09	0.391	0.62	0.981	-0.66	22.3	0.41	27.3
0.15	0.515	0.69	1.006	-0.49	25.4	0.49	25.4
0.22	0.642	0.75	1.014	-0.32	30.0	0.57	23.9
0.29	0.751	0.82	1.031	-0.24	33.5	0.66	22.3
0.35	0.813	0.89	1.048	-0.16	38.0	0.74	21.2
0.42	0.850	0.95	1.235	0.16	37.1	0.82	20.0
				0.20	34.8	0.91	19.0
				0.24	32.8		

Table C.22: Needle contact data for $\mu = 0.048$ N·s/m^2, $h_o = 0.695$ mm, $\Delta T_s = 34.4$°C.

r'	***h'***	***r'***	***h'***	***r'***	**T (°C)**	***r'***	**T (°C)**
0.00	0.000	0.49	0.896	-0.99	19.3	0.28	40.1
0.02	0.000	0.55	0.943	-0.82	22.4	0.32	38.3
0.09	0.000	0.62	1.007	-0.66	26.0	0.41	34.1
0.15	0.000	0.69	1.063	-0.49	31.1	0.49	31.0
0.22	0.387	0.75	1.069	-0.32	38.3	0.57	28.6
0.29	0.628	0.82	1.127	-0.24	43.6	0.66	26.2
0.35	0.746	0.89	1.134	-0.16	50.7	0.74	24.3
0.42	0.834	0.95	1.348	0.16	49.8	0.82	22.5
				0.20	46.1	0.91	20.8
				0.24	42.9		

Table C.23: Needle contact data for $\mu = 0.048$ N·s/m^2, $h_o = 1.026$ mm, $\Delta T_s = 0.0$°C.

r'	***h'***	***r'***	***h'***	***r'***	***h'***
-0.96	1.197	-0.20	1.000	0.64	1.002
-0.86	1.006	0.00	0.973	0.80	0.997
-0.70	1.012	0.14	1.004	0.97	1.278
-0.53	0.997	0.30	1.000		
-0.36	1.009	0.47	0.998		

Table C.24: Needle contact data for $\mu = 0.048$ N·s/m^2, $h_o = 1.026$ mm, $\Delta T_s = 38.5$°C.

r'	***h'***	***r'***	***h'***	***r'***	**T (°C)**	***r'***	**T (°C)**
0.00	0.568	0.50	0.959	-0.99	19.6	0.28	42.8
0.04	0.575	0.57	0.983	-0.82	23.1	0.32	40.7
0.10	0.599	0.64	1.019	-0.66	27.2	0.41	35.9
0.17	0.673	0.70	1.033	-0.49	33.0	0.49	32.4
0.24	0.744	0.77	1.055	-0.32	41.1	0.57	29.7
0.30	0.800	0.84	1.073	-0.24	47.2	0.66	27.0
0.37	0.876	0.90	1.091	-0.16	55.2	0.74	24.9
0.44	0.912	0.97	1.387	0.16	53.9	0.82	22.9
				0.20	49.7	0.91	21.2
				0.24	46.0		

Table C.25: Needle contact data for $\mu = 0.048$ N·s/m^2, $h_o = 1.026$ mm, $\Delta T_s = 47.3$°C.

r'	***h'***	***r'***	***h'***	***r'***	**T (°C)**	***r'***	**T (°C)**
0.00	0.448	0.50	0.937	-0.99	20.6	0.28	49.0
0.04	0.500	0.57	0.986	-0.82	24.8	0.32	46.5
0.10	0.543	0.64	1.013	-0.66	29.8	0.41	40.6
0.17	0.634	0.70	1.025	-0.49	36.9	0.49	36.3
0.24	0.717	0.77	1.045	-0.32	46.7	0.57	33.0
0.30	0.815	0.84	1.062	-0.24	54.1	0.66	29.7
0.37	0.876	0.90	1.090	-0.16	64.0	0.74	27.1
0.44	0.911	0.97	1.420	0.16	62.7	0.82	24.7
				0.20	57.4		
				0.24	53.0		

Table C.26: Needle contact data for $\mu = 0.048$ N·s/m^2, $h_o = 1.026$ mm, $\Delta T_s = 53.8$°C.

r'	***h'***	***r'***	***h'***	***r'***	**T (°C)**	***r'***	**T (°C)**
0.00	0.313	0.50	0.918	-0.99	21.5	0.28	53.6
0.04	0.351	0.57	0.958	-0.82	26.3	0.32	50.7
0.10	0.390	0.64	0.988	-0.66	32.0	0.41	44.1
0.17	0.516	0.70	1.017	-0.49	40.1	0.49	39.2
0.24	0.641	0.77	1.054	-0.32	51.2	0.57	35.4
0.30	0.745	0.84	1.074	-0.24	59.6	0.66	31.7
0.37	0.812	0.90	1.099	-0.16	70.7	0.74	28.7
0.44	0.871	0.97	1.378	0.16	69.2	0.82	25.9
				0.20	63.2	0.91	23.4
				0.24	58.2		

Table C.27: Needle contact data for $\mu = 0.048$ N·s/m^2, $h_o = 1.026$ mm, $\Delta T_s = 57.9$°C.

r'	***h'***	***r'***	***h'***	***r'***	**T (°C)**	***r'***	**T (°C)**
0.00	0.000	0.50	0.918	-0.99	23.3	0.28	62.7
0.03	0.017	0.57	0.968	-0.82	29.2	0.32	59.1
0.10	0.140	0.63	1.002	-0.66	36.2	0.41	51.1
0.17	0.363	0.70	1.037	-0.49	46.0	0.49	45.2
0.23	0.556	0.77	1.075	-0.32	59.3	0.57	40.6
0.30	0.672	0.83	1.100	-0.24	69.3	0.66	36.2
0.37	0.770	0.90	1.139	-0.16	82.6	0.74	32.5
0.43	0.855	0.97	1.416	0.16	81.3	0.82	28.9
				0.20	74.1	0.91	25.8
				0.24	68.1		

Table C.28: Needle contact data for $\mu = 0.048$ N·s/m^2, $h_o = 1.026$ mm, $\Delta T_s = 68.6$°C.

r'	***h'***	***r'***	***h'***	***r'***	**T (°C)**	***r'***	**T (°C)**
0.00	0.000	0.53	0.965	-0.99	23.5	0.28	64.6
0.06	0.000	0.59	1.022	-0.82	29.7	0.32	60.9
0.13	0.086	0.66	1.065	-0.66	37.1	0.41	52.6
0.19	0.470	0.73	1.097	-0.49	47.3	0.49	46.4
0.26	0.646	0.79	1.126	-0.32	61.1	0.57	41.6
0.33	0.760	0.86	1.155	-0.24	71.5	0.66	37.0
0.39	0.841	0.93	1.215	-0.16	85.3	0.74	33.2
0.46	0.909	0.97	1.519	0.16	84.0	0.82	29.5
				0.20	76.5	0.91	26.2
				0.24	70.3		

Table C.29: Needle contact data for $\mu = 0.048$ N·s/m^2, $h_o = 1.134$ mm, $\Delta T_s = 0.0$°C.

r'	***h'***	***r'***	***h'***	***r'***	***h'***
-0.95	1.242	-0.19	1.031	0.35	1.009
-0.85	1.081	-0.02	1.030	0.52	0.988
-0.69	1.087	0.00	1.002	0.69	0.994
-0.52	1.069	0.02	1.016	0.85	0.975
-0.35	1.054	0.19	1.016	0.95	1.077

Table C.30: Needle contact data for $\mu = 0.048$ N·s/m^2, $h_o = 1.134$ mm, $\Delta T_s = 32.6$°C.

r'	***h'***	***r'***	***h'***	***r'***	**T (°C)**	***r'***	**T (°C)**
0.00	0.744	0.49	0.949	-0.99	18.9	0.28	38.7
0.02	0.767	0.55	0.975	-0.82	21.7	0.32	36.9
0.09	0.790	0.62	0.999	-0.66	25.2	0.41	33.0
0.15	0.806	0.69	1.011	-0.49	30.0	0.49	30.0
0.22	0.845	0.75	1.013	-0.32	36.9	0.57	27.8
0.29	0.876	0.82	1.016	-0.24	42.1	0.66	25.4
0.35	0.917	0.89	1.032	-0.16	49.1	0.74	23.7
0.42	0.934	0.95	1.128	0.16	48.0	0.82	22.0
				0.20	44.4	0.91	20.5
				0.24	41.4		

Table C.31: Needle contact data for $\mu = 0.048$ N·s/m^2, $h_o = 1.134$ mm, $\Delta T_s = 59.9$°C.

r'	***h'***	***r'***	***h'***	***r'***	**T (°C)**	***r'***	**T (°C)**
0.00	0.501	0.49	0.922	-0.99	21.9	0.28	58.1
0.02	0.481	0.55	0.962	-0.82	27.1	0.32	54.8
0.09	0.508	0.62	1.000	-0.66	33.3	0.41	47.5
0.15	0.603	0.69	1.012	-0.49	42.2	0.49	42.0
0.22	0.698	0.75	1.041	-0.32	54.5	0.57	37.8
0.29	0.770	0.82	1.073	-0.24	64.0	0.66	33.7
0.35	0.831	0.89	1.078	-0.16	76.6	0.74	30.4
0.42	0.880	0.95	1.125	0.16	75.3	0.82	27.2
				0.20	68.7	0.91	24.4
				0.24	63.1		

Table C.32: Needle contact data for $\mu = 0.480$ N·s/m^2, $h_o = 0.467$ mm, $\Delta T_s = 0.0$°C.

r'	***h'***	***r'***	***h'***	***r'***	***h'***
-0.95	1.446	-0.19	1.013	0.35	0.996
-0.85	1.017	-0.02	0.981	0.52	0.989
-0.69	1.041	0.00	0.949	0.69	0.992
-0.52	1.034	0.02	0.968	0.85	0.987
-0.35	1.039	0.19	0.994	0.95	1.206

Table C.33: Needle contact data for $\mu = 0.480$ N·s/m^2, $h_o = 0.467$ mm, $\Delta T_s = 8.5$°C.

r'	***h'***	***r'***	***h'***	***r'***	**T (°C)**	***r'***	**T (°C)**
0.00	0.497	0.49	0.929	-0.99	16.4	0.28	21.7
0.02	0.512	0.55	0.968	-0.82	17.2	0.32	21.2
0.09	0.576	0.62	0.998	-0.66	18.1	0.41	20.3
0.15	0.660	0.69	1.019	-0.49	19.2	0.49	19.6
0.22	0.747	0.75	1.034	-0.32	20.9	0.57	19.1
0.29	0.820	0.82	1.037	-0.24	22.0	0.66	18.4
0.35	0.855	0.89	1.039	-0.16	23.7	0.74	18.0
0.42	0.897	0.95	1.283	0.16	23.9	0.82	17.5
				0.20	23.0	0.91	17.1
				0.24	22.3		

Table C.34: Needle contact data for $\mu = 0.480$ N·s/m^2, $h_o = 0.467$ mm, $\Delta T_s = 11.4$°C.

r'	***h'***	***r'***	***h'***	***r'***	**T (°C)**	***r'***	**T (°C)**
0.00	0.118	0.49	0.876	-0.99	16.6	0.28	23.6
0.02	0.169	0.55	0.932	-0.82	17.6	0.32	23.0
0.09	0.261	0.62	0.966	-0.66	18.8	0.41	21.7
0.15	0.480	0.69	1.024	-0.49	20.3	0.49	20.8
0.22	0.636	0.75	1.019	-0.32	22.6	0.57	20.1
0.29	0.745	0.82	1.043	-0.24	24.1	0.66	19.1
0.35	0.803	0.89	1.079	-0.16	26.4	0.74	18.6
0.42	0.852	0.95	1.319	0.16	26.8	0.82	18.0
				0.20	25.5	0.91	17.4
				0.24	24.5		

Table C.35: Needle contact data for $\mu = 0.480$ N·s/m^2, $h_o = 0.467$ mm, $\Delta T_s = 14.0$°C.

r'	***h'***	***r'***	***h'***	***r'***	**T (°C)**	***r'***	**T (°C)**
0.00	0.000	0.49	0.925	-0.99	16.9	0.28	25.4
0.02	0.000	0.55	0.942	-0.82	18.2	0.32	24.7
0.09	0.000	0.62	0.989	-0.66	19.7	0.41	23.1
0.15	0.000	0.69	1.032	-0.49	21.5	0.49	21.9
0.22	0.505	0.75	1.034	-0.32	24.3	0.57	21.0
0.29	0.690	0.82	1.077	-0.24	26.2	0.66	19.9
0.35	0.784	0.89	1.103	-0.16	29.0	0.74	19.2
0.42	0.857	0.95	1.345	0.16	29.4	0.82	18.5
				0.20	27.7	0.91	17.8
				0.24	26.5		

Table C.36: Needle contact data for $\mu = 0.480$ N·s/m^2, $h_o = 0.956$ mm, $\Delta T_s = 0.0$°C.

r'	***h'***	***r'***	***h'***	***r'***	***h'***
-0.95	1.202	-0.19	1.007	0.35	1.012
-0.85	1.000	-0.02	0.985	0.52	1.006
-0.69	1.010	0.00	0.974	0.69	1.010
-0.52	0.998	0.02	0.981	0.85	1.002
-0.35	1.009	0.19	1.004	0.95	1.099

Table C.37: Needle contact data for $\mu = 0.480$ N·s/m^2, $h_o = 0.956$ mm, $\Delta T_s = 35.0$°C.

r'	***h'***	***r'***	***h'***	***r'***	**T (°C)**	***r'***	**T (°C)**
0.00	0.606	0.49	0.956	-0.99	19.0	0.28	40.0
0.02	0.634	0.55	0.982	-0.82	21.9	0.32	38.0
0.09	0.646	0.62	1.008	-0.66	25.4	0.41	33.9
0.15	0.710	0.69	1.026	-0.49	30.3	0.49	30.8
0.22	0.792	0.75	1.046	-0.32	37.2	0.57	28.3
0.29	0.855	0.82	1.055	-0.24	42.4	0.66	25.9
0.35	0.901	0.89	1.075	-0.16	49.6	0.74	24.1
0.42	0.939	0.95	1.179	0.16	50.4	0.82	22.3
				0.20	46.2	0.91	20.7
				0.24	42.9		

Table C.38: Needle contact data for $\mu = 0.480$ N·s/m^2, $h_o = 0.956$ mm, $\Delta T_s = 44.3$°C.

r'	***h'***	***r'***	***h'***	***r'***	**T (°C)**	***r'***	**T (°C)**
0.00	0.498	0.49	0.953	-0.99	19.8	0.28	46.4
0.02	0.519	0.55	0.980	-0.82	23.5	0.32	44.0
0.09	0.527	0.62	1.009	-0.66	27.9	0.41	38.6
0.15	0.618	0.69	1.041	-0.49	34.1	0.49	34.7
0.22	0.733	0.75	1.054	-0.32	42.8	0.57	31.6
0.29	0.814	0.82	1.070	-0.24	49.2	0.66	28.6
0.35	0.874	0.89	1.096	-0.16	58.4	0.74	26.2
0.42	0.917	0.95	1.208	0.16	59.7	0.82	23.9
				0.20	54.4	0.91	21.9
				0.24	50.2		

Table C.39: Needle contact data for $\mu = 0.480$ N·s/m^2, $h_o = 0.956$ mm, $\Delta T_s = 54.1$°C.

r'	***h'***	***r'***	***h'***	***r'***	**T (°C)**	***r'***	**T (°C)**
0.00	0.353	0.49	0.949	-0.99	21.1	0.28	53.4
0.02	0.386	0.55	0.981	-0.82	25.7	0.32	50.4
0.09	0.369	0.62	1.014	-0.66	31.1	0.41	43.9
0.15	0.518	0.69	1.038	-0.49	38.8	0.49	39.1
0.22	0.657	0.75	1.069	-0.32	49.4	0.57	35.3
0.29	0.772	0.82	1.089	-0.24	57.3	0.66	31.7
0.35	0.848	0.89	1.100	-0.16	68.3	0.74	28.8
0.42	0.904	0.95	1.217	0.16	69.5	0.82	25.9
				0.20	63.1	0.91	23.5
				0.24	58.0		

Table C.40: Needle contact data for $\mu = 0.480$ N·s/m^2, $h_o = 0.956$ mm, $\Delta T_s = 62.6$°C.

r'	***h'***	***r'***	***h'***	***r'***	**T (°C)**	***r'***	**T (°C)**
0.00	0.000	0.49	0.945	-0.99	22.0	0.28	59.4
0.02	0.000	0.55	0.981	-0.82	27.3	0.32	56.0
0.09	0.000	0.62	1.019	-0.66	33.7	0.41	48.4
0.15	0.404	0.69	1.050	-0.49	42.6	0.49	42.8
0.22	0.604	0.75	1.084	-0.32	54.8	0.57	38.4
0.29	0.743	0.82	1.104	-0.24	64.0	0.66	34.3
0.35	0.843	0.89	1.124	-0.16	76.7	0.74	30.8
0.42	0.897	0.95	1.229	0.16	78.0	0.82	27.6
				0.20	70.6	0.91	24.7
				0.24	64.8		

Table C.41: Needle contact data for $\mu = 0.480$ N·s/m^2, $h_o = 1.461$ mm, $\Delta T_s = 0.0$°C.

r'	***h'***	***r'***	***h'***	***r'***	***h'***
-0.95	1.123	-0.19	1.002	0.35	1.002
-0.85	1.010	-0.02	0.995	0.52	0.997
-0.69	1.015	0.00	0.977	0.69	1.004
-0.52	1.004	0.02	0.987	0.85	0.995
-0.35	1.010	0.19	1.000	0.95	1.066

Table C.42: Needle contact data for $\mu = 0.480$ N·s/m^2, $h_o = 1.461$ mm, $\Delta T_s = 44.9$°C.

r'	***h'***	***r'***	***h'***	***r'***	**T (°C)**	***r'***	**T (°C)**
0.00	0.821	0.49	0.986	-0.99	20.2	0.28	47.0
0.02	0.832	0.55	1.002	-0.82	24.0	0.32	44.5
0.09	0.849	0.62	1.013	-0.66	28.5	0.41	39.1
0.15	0.873	0.69	1.028	-0.49	34.9	0.49	35.2
0.22	0.904	0.75	1.035	-0.32	43.8	0.57	32.1
0.29	0.931	0.82	1.040	-0.24	50.4	0.66	29.0
0.35	0.954	0.89	1.041	-0.16	59.5	0.74	26.6
0.42	0.977	0.95	1.119	0.16	60.3	0.82	24.2
				0.20	55.0	0.91	22.2
				0.24	50.8		

Table C.43: Needle contact data for $\mu = 0.480$ N·s/m^2, $h_o = 1.461$ mm, $\Delta T_s = 63.7$°C.

r'	***h'***	***r'***	***h'***	***r'***	**T (°C)**	***r'***	**T (°C)**
0.00	0.754	0.49	0.980	-0.99	22.3	0.28	60.2
0.02	0.763	0.55	1.002	-0.82	27.7	0.32	56.8
0.09	0.784	0.62	1.023	-0.66	34.2	0.41	49.1
0.15	0.819	0.69	1.036	-0.49	43.3	0.49	43.4
0.22	0.861	0.75	1.047	-0.32	55.8	0.57	38.9
0.29	0.907	0.82	1.050	-0.24	65.1	0.66	34.7
0.35	0.934	0.89	1.061	-0.16	78.0	0.74	31.2
0.42	0.960	0.95	1.137	0.16	79.1	0.82	27.9
				0.20	71.6	0.91	25.0
				0.24	65.7		

Table C.44: Needle contact data for $\mu = 0.480$ N·s/m^2, $h_o = 1.461$ mm, $\Delta T_s = 89.7$°C.

r'	***h'***	***r'***	***h'***	***r'***	**T (°C)**	***r'***	**T (°C)**
0.00	0.663	0.49	0.979	-0.99	25.1	0.28	78.6
0.02	0.678	0.55	1.004	-0.82	32.8	0.32	73.8
0.09	0.705	0.62	1.034	-0.66	42.0	0.41	62.9
0.15	0.750	0.69	1.051	-0.49	55.0	0.49	54.8
0.22	0.805	0.75	1.065	-0.32	72.6	0.57	48.6
0.29	0.869	0.82	1.082	-0.24	85.9	0.66	42.7
0.35	0.911	0.89	1.091	-0.16	104.3	0.74	37.7
0.42	0.946	0.95	1.174	0.16	105.1	0.82	32.9
				0.20	94.6	0.91	28.8
				0.24	86.3		

Table C.45: Needle contact data for $\mu = 0.480$ N·s/m^2, $h_o = 1.461$ mm, $\Delta T_s = 125.4$°C.

r'	***h'***	***r'***	***h'***	***r'***	**T (°C)**	***r'***	**T (°C)**
0.00	0.541	0.49	0.967	-0.99	29.4	0.28	104.2
0.02	0.555	0.55	1.002	-0.82	40.3	0.32	97.3
0.09	0.581	0.62	1.037	-0.66	53.2	0.41	82.0
0.15	0.635	0.69	1.071	-0.49	71.6	0.49	70.7
0.22	0.736	0.75	1.088	-0.32	96.4	0.57	61.9
0.29	0.803	0.82	1.109	-0.24	115.1	0.66	53.7
0.35	0.874	0.89	1.135	-0.16	140.9	0.74	46.6
0.42	0.922	0.95	1.201	0.16	140.8	0.82	39.9
				0.20	126.5	0.91	34.2
				0.24	114.9		

Table C.46: Needle contact data for $\mu = 0.480$ N·s/m^2, $h_o = 1.461$ mm, $\Delta T_s = 152.8$°C.

r'	***h'***	***r'***	***h'***	***r'***	**T (°C)**	***r'***	**T (°C)**
0.00	0.444	0.49	0.960	-0.99	32.6	0.28	123.4
0.02	0.459	0.55	1.006	-0.82	46.1	0.32	115.0
0.09	0.492	0.62	1.048	-0.66	62.1	0.41	96.4
0.15	0.567	0.69	1.081	-0.49	84.7	0.49	82.7
0.22	0.679	0.75	1.110	-0.32	115.1	0.57	72.0
0.29	0.771	0.82	1.136	-0.24	138.0	0.66	62.1
0.35	0.853	0.89	1.160	-0.16	168.8	0.74	53.5
0.42	0.910	0.95	1.233	0.16	167.2	0.82	45.3
				0.20	150.2	0.91	38.3
				0.24	136.3		

Table C.47: Needle contact data for $\mu = 0.480$ N·s/m^2, $h_o = 1.461$ mm, $\Delta T_s = 175.0$°C.

r'	***h'***	***r'***	***h'***	***r'***	**T (°C)**	***r'***	**T (°C)**
0.00	0.368	0.49	0.989	-0.99	35.4	0.28	140.4
0.02	0.380	0.55	1.008	-0.82	50.8	0.32	130.8
0.09	0.412	0.62	1.055	-0.66	69.4	0.41	109.3
0.15	0.509	0.69	1.089	-0.49	95.7	0.49	93.4
0.22	0.641	0.75	1.123	-0.32	131.3	0.57	81.0
0.29	0.739	0.82	1.149	-0.24	158.0	0.66	69.6
0.35	0.829	0.89	1.177	-0.16	192.5	0.74	59.6
0.42	0.898	0.95	1.277	0.16	190.4	0.82	50.1
				0.20	171.0	0.91	41.9
				0.24	155.1		

Table C.48: Needle contact data for $\mu = 0.480$ N·s/m^2, $h_o = 1.461$ mm, $\Delta T_s = 203$°C.

r'	***h'***	***r'***	***h'***	***r'***	**T (°C)**	***r'***	**T (°C)**
0.00	0.231	0.49	0.951	-0.99	39.3	0.28	161.0
0.02	0.246	0.55	1.008	-0.82	57.6	0.32	150.1
0.09	0.298	0.62	1.053	-0.66	79.4	0.41	125.1
0.15	0.450	0.69	1.101	-0.49	110.2	0.49	106.8
0.22	0.595	0.75	1.136	-0.32	151.2	0.57	92.4
0.29	0.719	0.82	1.173	-0.24	181.6	0.66	79.1
0.35	0.814	0.89	1.208	-0.16	221.3	0.74	67.4
0.42	0.882	0.95	1.303	0.16	218.4	0.82	56.3
				0.20	196.2	0.91	46.8
				0.24	178.1		

Table C.49: Needle contact data for $\mu = 0.480$ N·s/m^2, $h_o = 1.461$ mm, $\Delta T_s = 233.6$°C.

r'	***h'***	***r'***	***h'***	***r'***	**T (°C)**	***r'***	**T (°C)**
0.00	0.000	0.49	0.953	-0.99	43.1	0.28	183.2
0.02	0.000	0.55	1.012	-0.82	64.5	0.32	170.5
0.09	0.000	0.62	1.065	-0.66	89.5	0.41	142.3
0.15	0.331	0.69	1.114	-0.49	124.7	0.49	121.4
0.22	0.565	0.75	1.156	-0.32	171.1	0.57	104.9
0.29	0.695	0.82	1.197	-0.24	205.9	0.66	89.5
0.35	0.802	0.89	1.228	-0.16	250.8	0.74	76.0
0.42	0.874	0.95	1.320	0.16	249.0	0.82	63.2
				0.20	223.5	0.91	52.1
				0.24	203.0		

Table C.50: Needle contact data for $\mu = 9.6$ N·s/m^2, $h_o = 0.502$ mm, $\Delta T_s = 0.0$°C.

r'	***h'***	***r'***	***h'***	***r'***	***h'***
-0.95	1.232	-0.19	1.011	0.35	1.047
-0.85	0.945	-0.02	1.001	0.52	1.021
-0.69	0.945	0.00	0.975	0.69	1.007
-0.52	0.977	0.02	1.025	0.85	1.003
-0.35	1.015	0.19	1.027	0.95	1.300

Table C.51: Needle contact data for $\mu = 9.6$ N·s/m^2, $h_o = 0.502$ mm, $\Delta T_s = 7.6$°C.

r'	***h'***	***r'***	***h'***	***r'***	**T (°C)**	***r'***	**T (°C)**
0.00	0.571	0.49	0.985	-0.99	16.1	0.28	21.0
0.02	0.653	0.55	0.997	-0.82	16.9	0.32	20.6
0.09	0.804	0.62	1.029	-0.66	17.9	0.41	19.7
0.15	0.802	0.69	1.053	-0.49	19.0	0.49	19.2
0.22	0.874	0.75	1.043	-0.32	20.8	0.57	18.7
0.29	0.912	0.82	1.067	-0.24	22.0	0.66	18.0
0.35	0.927	0.89	1.077	-0.16	23.6	0.74	17.6
0.42	0.977	0.95	1.345	0.16	23.0	0.82	17.2
				0.20	22.1	0.91	16.8
				0.24	21.5		

Table C.52: Needle contact data for $\mu = 9.6$ N·s/m^2, $h_o = 0.502$ mm, $\Delta T_s = 10.7$°C.

r'	***h'***	***r'***	***h'***	***r'***	**T (°C)**	***r'***	**T (°C)**
0.00	0.360	0.49	0.995	-0.99	16.6	0.28	23.2
0.02	0.492	0.55	1.033	-0.82	17.7	0.32	22.6
0.09	0.541	0.62	1.063	-0.66	18.9	0.41	21.4
0.15	0.695	0.69	1.071	-0.49	20.5	0.49	20.6
0.22	0.812	0.75	1.079	-0.32	22.8	0.57	19.9
0.29	0.888	0.82	1.089	-0.24	24.4	0.66	19.0
0.35	0.923	0.89	1.122	-0.16	26.6	0.74	18.5
0.42	0.973	0.95	1.363	0.16	26.1	0.82	17.9
				0.20	24.9	0.91	17.4
				0.24	24.0		

Table C.53: Needle contact data for $\mu = 9.6$ N·s/m^2, $h_o = 0.502$ mm, $\Delta T_s = 13.4$°C.

r'	***h'***	***r'***	***h'***	***r'***	**T (°C)**	***r'***	**T (°C)**
0.00	0.048	0.49	1.007	-0.99	16.9	0.28	25.1
0.02	0.185	0.55	1.033	-0.82	18.2	0.32	24.4
0.09	0.356	0.62	1.047	-0.66	19.7	0.41	22.9
0.15	0.565	0.69	1.073	-0.49	21.6	0.49	21.8
0.22	0.728	0.75	1.087	-0.32	24.5	0.57	20.9
0.29	0.846	0.82	1.089	-0.24	26.5	0.66	19.8
0.35	0.906	0.89	1.126	-0.16	29.3	0.74	19.2
0.42	0.935	0.95	1.377	0.16	28.8	0.82	18.5
				0.20	27.3	0.91	17.8
				0.24	26.1		

Table C.54: Needle contact data for $\mu = 9.6$ N·s/m^2, $h_o = 0.502$ mm, $\Delta T_s = 13.4$°C.

r'	***h'***	***r'***	***h'***	***r'***	**T (°C)**	***r'***	**T (°C)**
0.00	0.000	0.49	1.057	-0.99	17.1	0.28	26.6
0.02	0.000	0.55	1.021	-0.82	18.5	0.32	25.8
0.09	0.161	0.62	1.134	-0.66	20.3	0.41	24.0
0.15	0.476	0.69	1.168	-0.49	22.6	0.49	22.7
0.22	0.714	0.75	1.158	-0.32	26.0	0.57	21.6
0.29	0.860	0.82	1.115	-0.24	28.3	0.66	20.4
0.35	0.912	0.89	1.168	-0.16	31.7	0.74	19.6
0.42	0.921	0.95	1.298	0.16	31.1	0.82	18.8
				0.20	29.3	0.91	18.0
				0.24	27.9		

Table C.55: Needle contact data for $\mu = 9.6$ N·s/m^2, $h_o = 0.975$ mm, $\Delta T_s = 0.0$°C.

r'	***h'***	***r'***	***h'***	***r'***	***h'***
-0.95	1.145	-0.19	0.997	0.35	1.008
-0.85	1.010	-0.02	0.991	0.52	1.004
-0.69	1.007	0.00	0.965	0.69	1.010
-0.52	1.002	0.02	0.996	0.85	1.000
-0.35	1.008	0.19	1.004	0.95	1.128

Table C.56: Needle contact data for $\mu = 9.6$ N·s/m^2, $h_o = 0.975$ mm, $\Delta T_s = 33.6$°C.

r'	***h'***	***r'***	***h'***	***r'***	**T (°C)**	***r'***	**T (°C)**
0.00	0.601	0.49	0.968	-0.99	19.2	0.28	39.2
0.02	0.634	0.55	1.005	-0.82	22.3	0.32	37.3
0.09	0.694	0.62	1.047	-0.66	26.0	0.41	33.4
0.15	0.779	0.69	1.038	-0.49	31.1	0.49	30.5
0.22	0.841	0.75	1.042	-0.32	38.4	0.57	28.2
0.29	0.888	0.82	1.061	-0.24	43.8	0.66	25.8
0.35	0.931	0.89	1.080	-0.16	51.2	0.74	24.0
0.42	0.948	0.95	1.209	0.16	49.0	0.82	22.2
				0.20	45.0	0.91	20.6
				0.24	42.0		

Table C.57: Needle contact data for $\mu = 9.6$ N·s/m^2, $h_o = 0.975$ mm, $\Delta T_s = 43.3$°C.

r'	***h'***	***r'***	***h'***	***r'***	**T (°C)**	***r'***	**T (°C)**
0.00	0.482	0.49	0.988	-0.99	20.2	0.28	45.8
0.02	0.516	0.55	0.998	-0.82	24.1	0.32	43.5
0.09	0.584	0.62	1.023	-0.66	28.7	0.41	38.4
0.15	0.713	0.69	1.051	-0.49	35.2	0.49	34.6
0.22	0.805	0.75	1.058	-0.32	44.2	0.57	31.6
0.29	0.862	0.82	1.090	-0.24	50.8	0.66	28.6
0.35	0.897	0.89	1.095	-0.16	60.0	0.74	26.3
0.42	0.916	0.95	1.239	0.16	58.7	0.82	24.0
				0.20	53.5	0.91	22.0
				0.24	49.5		

Table C.58: Needle contact data for $\mu = 9.6$ N·s/m^2, $h_o = 0.975$ mm, $\Delta T_s = 53.5$°C.

r'	***h'***	***r'***	***h'***	***r'***	**T (°C)**	***r'***	**T (°C)**
0.00	0.286	0.49	0.961	-0.99	21.2	0.28	53.0
0.02	0.357	0.55	0.996	-0.82	25.9	0.32	50.1
0.09	0.451	0.62	1.026	-0.66	31.6	0.41	43.7
0.15	0.629	0.69	1.050	-0.49	39.6	0.49	39.0
0.22	0.755	0.75	1.064	-0.32	50.8	0.57	35.3
0.29	0.832	0.82	1.088	-0.24	59.1	0.66	31.6
0.35	0.899	0.89	1.107	-0.16	70.5	0.74	28.7
0.42	0.931	0.95	1.247	0.16	68.9	0.82	25.9
				0.20	62.5	0.91	23.4
				0.24	57.6		

Table C.59: Needle contact data for $\mu = 9.6$ N·s/m^2, $h_o = 0.975$ mm, $\Delta T_s = 59.4$°C.

r'	***h'***	***r'***	***h'***	***r'***	**T (°C)**	***r'***	**T (°C)**
0.00	0.000	0.49	0.976	-0.99	22.2	0.28	57.2
0.02	0.000	0.55	1.005	-0.82	27.6	0.32	54.0
0.09	0.310	0.62	1.047	-0.66	34.0	0.41	47.0
0.15	0.557	0.69	1.084	-0.49	43.0	0.49	41.7
0.22	0.699	0.75	1.086	-0.32	55.5	0.57	37.6
0.29	0.796	0.82	1.099	-0.24	64.9	0.66	33.6
0.35	0.873	0.89	1.125	-0.16	77.7	0.74	30.3
0.42	0.925	0.95	1.258	0.16	74.8	0.82	27.2
				0.20	67.7	0.91	24.4
				0.24	62.3		

Table C.60: Needle contact data for $\mu = 0.048$ N·s/m^2, $h_o = 1.487$ mm, $\Delta T_s = 0.0$°C.

r'	***h'***	***r'***	***h'***	***r'***	***h'***
-0.95	1.095	-0.19	0.990	0.35	1.000
-0.85	1.018	-0.02	0.988	0.52	0.996
-0.69	1.018	0.00	0.967	0.69	0.997
-0.52	1.000	0.02	0.993	0.85	0.991
-0.35	1.007	0.19	1.002	0.95	1.090

Table C.61: Needle contact data for $\mu = 0.048$ N·s/m^2, $h_o = 1.487$ mm, $\Delta T_s = 79.3$°C.

r'	***h'***	***r'***	***h'***	***r'***	**T (°C)**	***r'***	**T (°C)**
0.00	0.669	0.49	0.961	-0.99	25.6	0.28	70.8
0.02	0.696	0.55	0.996	-0.82	32.9	0.32	66.5
0.09	0.735	0.62	1.017	-0.66	41.6	0.41	57.1
0.15	0.770	0.69	1.034	-0.49	53.9	0.49	50.2
0.22	0.816	0.75	1.052	-0.32	71.3	0.57	44.8
0.29	0.860	0.82	1.062	-0.24	84.8	0.66	39.7
0.35	0.899	0.89	1.087	-0.16	104.5	0.74	35.4
0.42	0.942	0.95	1.203	0.16	94.7	0.82	31.3
				0.20	85.1	0.91	27.7
				0.24	77.8		

Table C.62: Needle contact data for $\mu = 0.048$ N·s/m^2, $h_o = 1.487$ mm, $\Delta T_s = 114.9$°C.

r'	***h'***	***r'***	***h'***	***r'***	**T (°C)**	***r'***	**T (°C)**
0.00	0.337	0.49	0.863	-0.99	29.9	0.28	94.7
0.02	0.361	0.55	0.907	-0.82	40.2	0.32	88.5
0.09	0.408	0.62	0.950	-0.66	52.3	0.41	74.7
0.15	0.517	0.69	0.979	-0.49	69.8	0.49	64.7
0.22	0.624	0.75	1.004	-0.32	94.3	0.57	57.0
0.29	0.710	0.82	1.028	-0.24	113.4	0.66	49.8
0.35	0.776	0.89	1.047	-0.16	139.6	0.74	43.6
0.42	0.817	0.95	1.136	0.16	130.3	0.82	37.9
				0.20	115.6	0.91	32.9
				0.24	105.0		

Table C.63: Needle contact data for $\mu = 0.048$ N·s/m^2, $h_o = 1.487$ mm, $\Delta T_s = 136.4$°C.

r'	***h'***	***r'***	***h'***	***r'***	**T (°C)**	***r'***	**T (°C)**
0.00	0.461	0.49	0.927	-0.99	33.2	0.28	110.0
0.02	0.486	0.55	0.960	-0.82	45.3	0.32	102.6
0.09	0.565	0.62	1.004	-0.66	59.5	0.41	86.1
0.15	0.610	0.69	1.036	-0.49	79.7	0.49	74.2
0.22	0.688	0.75	1.063	-0.32	108.1	0.57	65.2
0.29	0.773	0.82	1.088	-0.24	130.2	0.66	56.8
0.35	0.831	0.89	1.109	-0.16	159.6	0.74	49.5
0.42	0.895	0.95	1.191	0.16	151.8	0.82	42.8
				0.20	135.2	0.91	36.9
				0.24	122.3		

Table C.64: Needle contact data for $\mu = 9.600$ N·s/m^2, $h_o = 1.562$ mm, $\Delta T_s = 0.0$°C.

r'	***h'***	***r'***	***h'***	***r'***	***h'***
-0.95	1.112	-0.19	1.010	0.35	0.989
-0.85	1.008	-0.02	0.996	0.52	0.984
-0.69	1.005	0.00	0.984	0.69	0.988
-0.52	1.025	0.02	0.996	0.85	0.978
-0.35	1.019	0.19	1.003	0.95	1.061

Table C.65: Needle contact data for $\mu = 9.600$ N·s/m^2, $h_o = 1.562$ mm, $\Delta T_s = 90.7$°C.

r'	***h'***	***r'***	***h'***	***r'***	**T (°C)**	***r'***	**T (°C)**
0.00	0.741	0.49	0.975	-0.99	25.8	0.28	79.3
0.02	0.750	0.55	0.991	-0.82	33.6	0.32	74.4
0.09	0.770	0.62	1.010	-0.66	42.8	0.41	63.6
0.15	0.809	0.69	1.024	-0.49	55.7	0.49	55.5
0.22	0.863	0.75	1.030	-0.32	73.4	0.57	49.3
0.29	0.903	0.82	1.038	-0.24	86.6	0.66	43.3
0.35	0.932	0.89	1.046	-0.16	103.9	0.74	38.3
0.42	0.958	0.95	1.146	0.16	106.1	0.82	33.6
				0.20	95.5	0.91	29.4
				0.24	87.2		

Table C.66: Needle contact data for $\mu = 9.600$ N·s/m^2, $h_o = 1.562$ mm, $\Delta T_s = 90.7$°C.

r'	***h'***	***r'***	***h'***	***r'***	**T (°C)**	***r'***	**T (°C)**
0.00	0.578	0.49	0.971	-0.99	33.4	0.28	125.5
0.02	0.588	0.55	1.003	-0.82	47.1	0.32	117.0
0.09	0.606	0.62	1.029	-0.66	63.3	0.41	98.3
0.15	0.664	0.69	1.051	-0.49	86.1	0.49	84.3
0.22	0.756	0.75	1.071	-0.32	117.0	0.57	73.4
0.29	0.833	0.82	1.085	-0.24	140.0	0.66	63.3
0.35	0.891	0.89	1.098	-0.16	168.9	0.74	54.5
0.42	0.933	0.95	1.179	0.16	168.9	0.82	46.2
				0.20	152.4	0.91	39.0
				0.24	138.9		

Table C.67: Needle contact data for $\mu = 0.192$ N·s/m^2, $h_o = 0.537$ mm, $\Delta T_s = 0.0$°C.

r'	***h'***	***r'***	***h'***	***r'***	***h'***
-0.95	1.203	-0.19	0.985	0.35	1.013
-0.85	0.996	-0.02	0.981	0.52	1.011
-0.69	0.998	0.00	0.944	0.69	1.024
-0.52	1.000	0.02	0.976	0.85	1.015
-0.35	0.987	0.19	1.013	0.95	1.259

Table C.68: Needle contact data for $\mu = 0.192$ N·s/m^2, $h_o = 0.537$ mm, $\Delta T_s = 6.1$°C.

r'	***h'***	***r'***	***h'***	***r'***	**T (°C)**	***r'***	**T (°C)**
0.00	0.730	0.49	0.989	-0.99	16.4	0.28	19.9
0.02	0.782	0.55	0.989	-0.82	16.9	0.32	19.6
0.09	0.790	0.62	1.006	-0.66	17.6	0.41	19.0
0.15	0.829	0.69	1.032	-0.49	18.3	0.49	18.6
0.22	0.892	0.75	1.032	-0.32	19.5	0.57	18.2
0.29	0.916	0.82	1.052	-0.24	20.2	0.66	17.7
0.35	0.939	0.89	1.041	-0.16	21.2	0.74	17.4
0.42	0.961	0.95	1.276	0.16	21.5	0.82	17.2
				0.20	20.8	0.91	16.8
				0.24	20.3		

Table C.69: Needle contact data for $\mu = 0.192$ N·s/m^2, $h_o = 0.537$ mm, $\Delta T_s = 8.8$°C.

r'	***h'***	***r'***	***h'***	***r'***	**T (°C)**	***r'***	**T (°C)**
0.00	0.607	0.49	0.985	-0.99	16.7	0.28	21.8
0.02	0.641	0.55	1.004	-0.82	17.5	0.32	21.3
0.09	0.682	0.62	1.017	-0.66	18.4	0.41	20.4
0.15	0.756	0.69	1.041	-0.49	19.4	0.49	19.7
0.22	0.808	0.75	1.052	-0.32	21.1	0.57	19.2
0.29	0.868	0.82	1.069	-0.24	22.2	0.66	18.5
0.35	0.912	0.89	1.067	-0.16	23.7	0.74	18.1
0.42	0.920	0.95	1.315	0.16	24.2	0.82	17.7
				0.20	23.2	0.91	17.3
				0.24	22.4		

Table C.70: Needle contact data for $\mu = 0.192$ N·s/m^2, $h_o = 0.537$ mm, $\Delta T_s = 11.1$°C.

r'	***h'***	***r'***	***h'***	***r'***	**T (°C)**	***r'***	**T (°C)**
0.00	0.425	0.49	0.959	-0.99	16.8	0.28	23.3
0.02	0.480	0.55	0.976	-0.82	17.7	0.32	22.6
0.09	0.536	0.62	1.002	-0.66	18.9	0.41	21.5
0.15	0.624	0.69	1.011	-0.49	20.2	0.49	20.6
0.22	0.741	0.75	1.032	-0.32	22.4	0.57	19.9
0.29	0.819	0.82	1.045	-0.24	23.8	0.66	19.0
0.35	0.855	0.89	1.056	-0.16	25.6	0.74	18.5
0.42	0.901	0.95	1.302	0.16	26.5	0.82	18.0
				0.20	25.1	0.91	17.5
				0.24	24.1		

Table C.71: Needle contact data for $\mu = 0.192$ N·s/m^2, $h_o = 0.537$ mm, $\Delta T_s = 13.2$°C.

r'	***h'***	***r'***	***h'***	***r'***	**T (°C)**	***r'***	**T (°C)**
0.00	0.242	0.49	0.959	-0.99	17.1	0.28	24.7
0.02	0.296	0.55	0.974	-0.82	18.2	0.32	24.0
0.09	0.384	0.62	1.019	-0.66	19.5	0.41	22.6
0.15	0.525	0.69	1.026	-0.49	21.2	0.49	21.5
0.22	0.691	0.75	1.045	-0.32	23.7	0.57	20.7
0.29	0.793	0.82	1.050	-0.24	25.4	0.66	19.6
0.35	0.847	0.89	1.076	-0.16	27.7	0.74	19.0
0.42	0.957	0.95	1.330	0.16	28.6	0.82	18.4
				0.20	27.0	0.91	17.8
				0.24	25.8		

Table C.72: Needle contact data for $\mu = 0.192$ N·s/m^2, $h_o = 0.537$ mm, $\Delta T_s = 14.3$°C.

r'	***h'***	***r'***	***h'***	***r'***	**T (°C)**	***r'***	**T (°C)**
0.00	0.007	0.49	0.914	-0.99	17.2	0.28	25.5
0.02	0.089	0.55	0.980	-0.82	18.3	0.32	24.6
0.09	0.285	0.62	1.000	-0.66	19.8	0.41	23.1
0.15	0.488	0.69	1.035	-0.49	21.6	0.49	21.9
0.22	0.655	0.75	1.047	-0.32	24.3	0.57	21.0
0.29	0.788	0.82	1.073	-0.24	26.1	0.66	19.9
0.35	0.847	0.89	1.095	-0.16	28.6	0.74	19.3
0.42	0.896	0.95	1.352	0.16	29.7	0.82	18.6
				0.20	27.9	0.91	17.9
				0.24	26.6		

Table C.73: Needle contact data for $\mu = 0.192$ N·s/m^2, $h_o = 0.537$ mm, $\Delta T_s = 15.7$°C.

r'	***h'***	***r'***	***h'***	***r'***	**T (°C)**	***r'***	**T (°C)**
0.00	0.000	0.49	0.911	-0.99	17.3	0.28	26.5
0.02	0.000	0.55	0.948	-0.82	18.6	0.32	25.6
0.09	0.000	0.62	0.970	-0.66	20.2	0.41	23.8
0.15	0.337	0.69	1.041	-0.49	22.2	0.49	22.6
0.22	0.665	0.75	1.048	-0.32	25.1	0.57	21.6
0.29	0.784	0.82	1.073	-0.24	27.2	0.66	20.4
0.35	0.816	0.89	1.104	-0.16	30.0	0.74	19.6
0.42	0.879	0.95	1.348	0.16	31.1	0.82	18.9
				0.20	29.2	0.91	18.1
				0.24	27.7		

C.2.2. Laser-Confocal Displacement Measurements

The tables presented in this section provide the film height measurements acquired using the Keyence laser-confocal displacement sensor. The non-dimensional local film heights are provided, as before, with the corresponding surface temperature measurements for each experimental run. The organization of the data is such that the runs are presented first by viscosity, then by initial film height, and finally by surface temperature difference. As discussed in Chapter 5, the dimensionless film heights are scaled by the average height (shown at the bottom of each table) for each experimental run instead of the initial film height to account for the volumetric expansion of the liquid layer.

Table C.74: Experimental data for $\mu = 0.048$ N·s/m^2, $h_o = 0.499$ mm, $\Delta T_s = 0.1$°C.

r'	h / h_{avg}	r'	h / h_{avg}	r'	h / h_{avg}	r'	T_s (°C)
0.00	1.020	0.20	0.979	0.47	0.985	0.16	22.2
0.02	0.999	0.22	0.973	0.50	0.992	0.20	22.2
0.04	0.985	0.24	0.972	0.54	0.990	0.24	22.2
0.05	0.988	0.25	0.975	0.57	0.988	0.28	22.2
0.07	0.994	0.27	0.975	0.60	0.985	0.32	22.2
0.09	0.989	0.29	0.975	0.64	0.980	0.41	22.2
0.10	0.984	0.30	0.974	0.67	0.984	0.49	22.3
0.12	0.983	0.32	0.976	0.74	0.991	0.57	22.4
0.14	0.983	0.34	0.976	0.80	0.986	0.66	22.2
0.15	0.980	0.37	0.981	0.87	1.000	0.74	22.3
0.17	0.975	0.40	0.984	0.94	1.033	0.82	22.3
0.19	0.980	0.44	0.982	0.95	1.072	0.91	22.3
						0.99	22.1
h_{avg} (μm) =		508				1.00	22.1

Table C.75: Experimental data for $\mu = 0.048$ N·s/m^2, $h_o = 0.499$ mm, $\Delta T_s = 7.0$°C.

r'	h / h_{avg}	r'	h / h_{avg}	r'	h / h_{avg}	r'	T_s (°C)
0.00	0.826	0.20	0.857	0.47	0.919	0.16	23.5
0.02	0.808	0.22	0.858	0.50	0.922	0.20	22.6
0.04	0.805	0.24	0.859	0.54	0.935	0.24	22.0
0.05	0.820	0.25	0.869	0.57	0.932	0.28	21.3
0.07	0.824	0.27	0.871	0.60	0.932	0.32	20.8
0.09	0.826	0.29	0.874	0.64	0.935	0.41	20.0
0.10	0.825	0.30	0.882	0.67	0.941	0.49	19.4
0.12	0.827	0.32	0.887	0.74	0.953	0.57	18.9
0.14	0.832	0.34	0.890	0.80	0.958	0.66	18.1
0.15	0.840	0.37	0.895	0.87	0.971	0.74	17.8
0.17	0.840	0.40	0.906	0.94	1.005	0.82	17.4
0.19	0.845	0.44	0.917	0.95	1.043	0.91	16.9
						0.99	16.5
h_{avg} (μm) =		483				1.00	16.5

Table C.76: Experimental data for $\mu = 0.048$ N·s/m^2, $h_o = 0.499$ mm, $\Delta T_s = 9.5$°C.

r'	h / h_{avg}	r'	h / h_{avg}	r'	h / h_{avg}	r'	T_s (°C)
0.00	0.480	0.22	0.576	0.50	0.676	0.16	26.3
0.02	0.458	0.24	0.584	0.54	0.685	0.20	25.1
0.04	0.440	0.25	0.597	0.57	0.691	0.24	24.2
0.05	0.465	0.27	0.601	0.60	0.687	0.28	23.3
0.07	0.500	0.29	0.612	0.64	0.696	0.32	22.7
0.09	0.503	0.30	0.621	0.67	0.698	0.41	21.5
0.10	0.505	0.32	0.623	0.74	0.706	0.49	20.6
0.12	0.513	0.34	0.631	0.80	0.718	0.57	19.9
0.14	0.530	0.37	0.638	0.87	0.725	0.66	19.0
0.15	0.537	0.40	0.648	0.94	0.761	0.74	18.5
0.19	0.559	0.44	0.664	0.95	0.805	0.82	17.9
0.20	0.558	0.47	0.665			0.91	17.4
						0.99	16.8
h_{avg} (μm) =		356				1.00	16.8

Table C.77: Experimental data for $\mu = 0.048$ N·s/m^2, $h_o = 0.999$ mm, $\Delta T_s = 0.2$°C.

r'	h / h_{avg}	r'	h / h_{avg}	r'	h / h_{avg}	r'	T_s (°C)
0.00	1.012	0.22	0.989	0.50	0.995	0.16	21.6
0.02	1.003	0.24	0.986	0.54	0.996	0.20	21.5
0.04	0.994	0.25	0.989	0.57	0.993	0.24	21.5
0.05	0.997	0.27	0.985	0.60	0.991	0.28	21.6
0.07	0.996	0.29	0.990	0.64	0.992	0.32	21.5
0.09	0.996	0.30	0.987	0.67	0.994	0.41	21.6
0.10	0.993	0.32	0.988	0.74	0.996	0.49	21.7
0.14	0.989	0.34	0.988	0.80	0.993	0.57	21.7
0.15	0.993	0.37	0.992	0.87	1.000	0.66	21.6
0.17	0.988	0.40	0.991	0.94	1.015	0.74	21.7
0.19	0.989	0.44	0.991	0.95	1.038	0.82	21.7
0.20	0.990	0.47	0.991			0.91	21.6
						0.99	21.3
h_{avg} (μm) =		1007				1.00	21.3

Table C.78: Experimental data for $\mu = 0.048$ N·s/m^2, $h_o = 0.999$ mm, $\Delta T_s = 6.9$°C.

r'	h / h_{avg}	r'	h / h_{avg}	r'	h / h_{avg}	r'	T_s (°C)
0.00	0.938	0.20	0.955	0.47	0.981	0.16	23.4
0.02	0.939	0.22	0.958	0.50	0.983	0.20	22.6
0.04	0.940	0.24	0.959	0.54	0.985	0.24	21.9
0.05	0.941	0.25	0.961	0.57	0.986	0.28	21.3
0.07	0.942	0.27	0.963	0.60	0.988	0.32	20.9
0.09	0.943	0.29	0.965	0.64	0.990	0.41	20.0
0.10	0.945	0.30	0.967	0.67	0.991	0.49	19.4
0.12	0.946	0.32	0.968	0.74	0.994	0.57	18.9
0.14	0.948	0.34	0.970	0.80	0.996	0.66	18.1
0.15	0.949	0.37	0.972	0.87	0.999	0.74	17.8
0.17	0.952	0.40	0.977	0.94	1.025	0.82	17.4
0.19	0.954	0.10	0.971	0.95	1.059	0.91	16.9
						0.99	16.5
h_{avg} (μm) =		1699				1.00	16.5

Table C.79: Experimental data for $\mu = 0.048$ N·s/m^2, $h_o = 0.999$ mm, $\Delta T_s = 12.8$°C.

r'	h / h_{avg}	r'	h / h_{avg}	r'	h / h_{avg}	r'	T_s (°C)
0.00	0.899	0.20	0.932	0.47	0.977	0.16	29.9
0.02	0.899	0.22	0.935	0.50	0.981	0.20	28.4
0.03	0.901	0.23	0.940	0.53	0.984	0.24	27.1
0.05	0.903	0.25	0.943	0.57	0.988	0.28	25.9
0.07	0.906	0.27	0.946	0.60	0.990	0.32	25.1
0.08	0.908	0.28	0.949	0.63	0.993	0.41	23.4
0.10	0.911	0.30	0.953	0.67	0.996	0.49	22.2
0.12	0.914	0.32	0.956	0.73	1.001	0.57	21.2
0.13	0.917	0.33	0.959	0.80	1.006	0.66	20.0
0.15	0.920	0.37	0.964	0.87	1.010	0.74	19.3
0.17	0.924	0.40	0.968	0.93	1.038	0.82	18.6
0.18	0.928	0.43	0.973	0.95	1.073	0.91	17.8
						0.99	17.2
h_{avg} (μm) =		1690				1.00	17.2

Table C.80: Experimental data for $\mu = 0.048$ N·s/m^2, $h_o = 0.999$ mm, $\Delta T_s = 22.4$

r'	h / h_{avg}	r'	h / h_{avg}	r'	h / h_{avg}	r'	T_s (°C)
0.00	0.817	0.20	0.882	0.47	0.966	0.16	40.8
0.02	0.820	0.22	0.890	0.50	0.973	0.20	38.1
0.03	0.824	0.23	0.896	0.53	0.979	0.24	35.9
0.05	0.829	0.25	0.903	0.57	0.985	0.28	33.7
0.07	0.833	0.27	0.909	0.60	0.991	0.32	32.3
0.08	0.838	0.28	0.916	0.63	0.995	0.41	29.3
0.10	0.844	0.30	0.921	0.67	1.000	0.49	27.1
0.12	0.849	0.32	0.926	0.73	1.008	0.57	25.4
0.13	0.855	0.33	0.932	0.80	1.016	0.66	23.5
0.15	0.861	0.37	0.942	0.87	1.023	0.74	22.1
0.17	0.868	0.40	0.951	0.93	1.054	0.82	20.7
0.18	0.875	0.43	0.959	0.95	1.088	0.91	19.5
						0.99	18.4
h_{avg} (μm) =		1697				1.00	18.4

Table C.81: Experimental data for $\mu = 0.048$ N·s/m^2, $h_o = 0.999$ mm, $\Delta T_s = 30$°C.

r'	h / h_{avg}	r'	h / h_{avg}	r'	h / h_{avg}	r'	T_s (°C)
0.00	0.737	0.20	0.836	0.47	0.957	0.16	50.5
0.02	0.741	0.22	0.847	0.50	0.966	0.20	46.8
0.03	0.746	0.23	0.857	0.53	0.974	0.24	43.7
0.05	0.753	0.25	0.866	0.57	0.983	0.28	40.7
0.07	0.760	0.27	0.876	0.60	0.991	0.32	38.8
0.08	0.768	0.28	0.885	0.63	0.997	0.41	34.6
0.10	0.776	0.30	0.893	0.67	1.004	0.49	31.5
0.12	0.785	0.32	0.901	0.73	1.015	0.57	29.0
0.13	0.794	0.33	0.909	0.80	1.026	0.66	26.5
0.15	0.804	0.37	0.922	0.87	1.037	0.74	24.6
0.17	0.814	0.40	0.935	0.93	1.067	0.82	22.7
0.18	0.824	0.43	0.947	0.95	1.102	0.91	21.0
						0.99	19.6
h_{avg} (μm) =		1703				1.00	19.6

Table C.82: Experimental data for $\mu = 0.048$ N·s/m^2, $h_o = 0.999$ mm, $\Delta T_s = 39.5$

r'	h / h_{avg}	r'	h / h_{avg}	r'	h / h_{avg}	r'	T_s (°C)
0.00	0.633	0.20	0.786	0.47	0.948	0.16	60.2
0.02	0.638	0.22	0.802	0.50	0.961	0.20	55.5
0.03	0.648	0.23	0.816	0.53	0.972	0.24	51.6
0.05	0.659	0.25	0.829	0.57	0.983	0.28	47.7
0.07	0.670	0.27	0.842	0.60	0.992	0.32	45.2
0.08	0.683	0.28	0.854	0.63	1.000	0.41	39.8
0.10	0.697	0.30	0.866	0.67	1.008	0.49	35.8
0.12	0.710	0.32	0.876	0.73	1.022	0.57	32.7
0.13	0.725	0.33	0.886	0.80	1.036	0.66	29.5
0.15	0.740	0.37	0.905	0.87	1.048	0.74	27.0
0.17	0.756	0.40	0.921	0.93	1.081	0.82	24.5
0.18	0.771	0.43	0.937	0.95	1.115	0.91	22.4
						0.99	20.7
h_{avg} (μm) =		1708				1.00	20.7

Table C.83: Experimental data for $\mu = 0.048$ N·s/m^2, $h_o = 0.999$ mm, $\Delta T_s = 46.9$°C.

r'	h / h_{avg}	r'	h / h_{avg}	r'	h / h_{avg}	r'	T_s (°C)
0.00	0.501	0.20	0.745	0.47	0.943	0.16	68.5
0.02	0.530	0.22	0.764	0.50	0.957	0.20	63.0
0.03	0.504	0.23	0.783	0.53	0.971	0.24	58.4
0.05	0.517	0.25	0.801	0.57	0.982	0.28	53.7
0.07	0.542	0.27	0.814	0.60	0.992	0.32	50.8
0.08	0.568	0.28	0.830	0.63	1.003	0.41	44.4
0.10	0.600	0.30	0.844	0.67	1.013	0.49	39.7
0.12	0.627	0.32	0.856	0.73	1.029	0.57	35.9
0.13	0.651	0.33	0.868	0.80	1.044	0.66	32.2
0.15	0.677	0.37	0.890	0.87	1.058	0.74	29.2
0.17	0.700	0.40	0.910	0.93	1.094	0.82	26.3
0.18	0.723	0.43	0.927	0.95	1.128	0.91	23.7
						0.99	21.7
h_{avg} (μm) =		1715				1.00	21.7

Table C.84: Experimental data for $\mu = 0.048$ N·s/m^2, $h_o = 0.999$ mm, $\Delta T_s = 53.5$°C.

r'	h / h_{avg}	r'	h / h_{avg}	r'	h / h_{avg}	r'	T_s (°C)
0.00	0.759	0.20	0.852	0.47	0.967	0.16	76.1
0.02	0.745	0.22	0.863	0.50	0.978	0.20	69.8
0.03	0.736	0.23	0.875	0.53	0.986	0.24	64.5
0.05	0.742	0.25	0.887	0.57	0.989	0.28	59.2
0.07	0.740	0.27	0.894	0.60	0.993	0.32	55.8
0.08	0.738	0.28	0.903	0.63	0.997	0.41	48.5
0.10	0.736	0.30	0.906	0.67	1.003	0.49	43.0
0.12	0.750	0.32	0.918	0.73	1.017	0.57	38.7
0.13	0.771	0.33	0.924	0.80	1.023	0.66	34.5
0.15	0.801	0.37	0.937	0.87	1.037	0.74	31.1
0.17	0.820	0.40	0.948	0.93	1.055	0.82	27.7
0.18	0.835	0.43	0.957	0.95	1.081	0.91	24.9
						0.99	22.6
h_{avg} (μm) =		1008				1.00	22.6

Table C.85: Experimental data for $\mu = 0.048$ N·s/m^2, $h_o = 1.189$ mm, $\Delta T_s = 0.1$°C.

r'	h / h_{avg}	r'	h / h_{avg}	r'	h / h_{avg}	r'	T_s (°C)
0.00	0.993	0.20	0.989	0.47	0.990	0.16	21.5
0.02	0.993	0.22	0.989	0.50	0.991	0.20	21.5
0.03	0.993	0.23	0.989	0.53	0.990	0.24	21.5
0.05	0.994	0.25	0.990	0.57	0.990	0.28	21.5
0.07	0.989	0.27	0.990	0.60	0.990	0.32	21.5
0.08	0.988	0.28	0.990	0.63	0.990	0.41	21.5
0.10	0.988	0.30	0.990	0.67	0.989	0.49	21.6
0.12	0.989	0.32	0.990	0.73	0.989	0.57	21.6
0.13	0.989	0.33	0.989	0.80	0.990	0.66	21.5
0.15	0.989	0.37	0.989	0.87	0.990	0.74	21.6
0.17	0.988	0.40	0.990	0.93	1.023	0.82	21.6
0.18	0.989	0.43	0.989	0.95	1.069	0.91	21.6
						0.99	21.4
h_{avg} (μm) =		1198				1.00	21.4

Table C.86: Experimental data for $\mu = 0.048$ N·s/m^2, $h_o = 1.189$ mm, $\Delta T_s = 12.3$°C.

r'	h / h_{avg}	r'	h / h_{avg}	r'	h / h_{avg}	r'	T_s (°C)
0.00	0.892	0.20	0.924	0.47	0.973	0.16	29.4
0.02	0.893	0.22	0.929	0.50	0.978	0.20	27.9
0.03	0.894	0.23	0.932	0.53	0.980	0.24	26.7
0.05	0.896	0.25	0.936	0.57	0.984	0.28	25.5
0.07	0.898	0.27	0.940	0.60	0.988	0.32	24.8
0.08	0.901	0.28	0.943	0.63	0.990	0.41	23.2
0.10	0.903	0.30	0.946	0.67	0.993	0.49	22.0
0.12	0.906	0.32	0.950	0.73	0.998	0.57	21.0
0.13	0.910	0.33	0.953	0.80	1.002	0.66	19.9
0.15	0.913	0.37	0.960	0.87	1.009	0.74	19.2
0.17	0.917	0.40	0.964	0.93	1.047	0.82	18.4
0.18	0.920	0.43	0.968	0.95	1.093	0.91	17.8
						0.99	17.1
h_{avg} (μm) =		1183				1.00	17.1

Table C.87: Experimental data for $\mu = 0.048$ N·s/m^2, $h_o = 1.189$ mm, $\Delta T_s = 22.6$°C.

r'	h / h_{avg}	r'	h / h_{avg}	r'	h / h_{avg}	r'	T_s (°C)
0.00	0.791	0.20	0.860	0.47	0.958	0.16	41.1
0.02	0.796	0.22	0.870	0.50	0.967	0.20	38.3
0.03	0.799	0.23	0.877	0.53	0.974	0.24	36.1
0.05	0.804	0.25	0.884	0.57	0.981	0.28	33.9
0.07	0.809	0.27	0.892	0.60	0.987	0.32	32.5
0.08	0.814	0.28	0.898	0.63	0.993	0.41	29.4
0.10	0.819	0.30	0.905	0.67	0.999	0.49	27.2
0.12	0.826	0.32	0.911	0.73	1.008	0.57	25.4
0.13	0.832	0.33	0.918	0.80	1.017	0.66	23.5
0.15	0.838	0.37	0.930	0.87	1.026	0.74	22.2
0.17	0.847	0.40	0.940	0.93	1.066	0.82	20.8
0.18	0.854	0.43	0.950	0.95	1.114	0.91	19.5
						0.99	18.4
h_{avg} (μm) =		1187				1.00	18.4

Table C.88: Experimental data for $\mu = 0.048$ N·s/m^2, $h_o = 1.189$ mm, $\Delta T_s = 30.8$°C.

r'	h / h_{avg}	r'	h / h_{avg}	r'	h / h_{avg}	r'	T_s (°C)
0.00	0.710	0.20	0.809	0.47	0.946	0.16	50.3
0.02	0.716	0.22	0.820	0.50	0.957	0.20	46.5
0.03	0.721	0.23	0.831	0.53	0.968	0.24	43.5
0.05	0.729	0.25	0.839	0.57	0.978	0.28	40.5
0.07	0.737	0.27	0.851	0.60	0.987	0.32	38.5
0.08	0.745	0.28	0.859	0.63	0.996	0.41	34.4
0.10	0.751	0.30	0.869	0.67	1.003	0.49	31.3
0.12	0.761	0.32	0.879	0.73	1.017	0.57	28.8
0.13	0.769	0.33	0.888	0.80	1.029	0.66	26.3
0.15	0.779	0.37	0.903	0.87	1.041	0.74	24.4
0.17	0.788	0.40	0.919	0.93	1.083	0.82	22.5
0.18	0.799	0.43	0.933	0.95	1.131	0.91	20.9
						0.99	19.5
h_{avg} (μm) =		1194				1.00	19.5

Table C.89: Experimental data for $\mu = 0.048$ N·s/m^2, $h_o = 1.189$ mm, $\Delta T_s = 39.4$°C.

r'	h / h_{avg}	r'	h / h_{avg}	r'	h / h_{avg}	r'	T_s (°C)
0.00	0.623	0.20	0.758	0.47	0.932	0.16	60.0
0.02	0.630	0.22	0.771	0.50	0.948	0.20	55.3
0.03	0.637	0.23	0.785	0.53	0.961	0.24	51.4
0.05	0.647	0.25	0.799	0.57	0.974	0.28	47.5
0.07	0.658	0.27	0.812	0.60	0.985	0.32	45.0
0.08	0.668	0.28	0.824	0.63	0.997	0.41	39.7
0.10	0.678	0.30	0.837	0.67	1.006	0.49	35.7
0.12	0.690	0.32	0.848	0.73	1.025	0.57	32.5
0.13	0.702	0.33	0.857	0.80	1.042	0.66	29.3
0.15	0.714	0.37	0.880	0.87	1.056	0.74	26.9
0.17	0.728	0.40	0.899	0.93	1.100	0.82	24.4
0.18	0.744	0.43	0.916	0.95	1.146	0.91	22.4
						0.99	20.6
h_{avg} (μm) =		1198				1.00	20.6

Table C.90: Experimental data for $\mu = 0.048$ N·s/m^2, $h_o = 1.189$ mm, $\Delta T_s = 45.8$°C.

r'	h / h_{avg}	r'	h / h_{avg}	r'	h / h_{avg}	r'	T_s (°C)
0.00	0.553	0.20	0.716	0.47	0.925	0.16	67.4
0.02	0.558	0.22	0.734	0.50	0.942	0.20	61.9
0.03	0.568	0.23	0.750	0.53	0.958	0.24	57.3
0.05	0.579	0.25	0.767	0.57	0.973	0.28	52.8
0.07	0.592	0.27	0.782	0.60	0.985	0.32	49.9
0.08	0.604	0.28	0.797	0.63	0.999	0.41	43.7
0.10	0.618	0.30	0.811	0.67	1.011	0.49	39.0
0.12	0.633	0.32	0.825	0.73	1.031	0.57	35.4
0.13	0.648	0.33	0.838	0.80	1.050	0.66	31.7
0.15	0.663	0.37	0.862	0.87	1.066	0.74	28.8
0.17	0.682	0.40	0.884	0.93	1.113	0.82	26.0
0.18	0.699	0.43	0.905	0.95	1.159	0.91	23.5
						0.99	21.6
h_{avg} (μm) =		1202				1.00	21.6

Table C.91: Experimental data for $\mu = 0.048$ N·s/m^2, $h_o = 1.189$ mm, $\Delta T_s = 54.4$°C.

r'	h / h_{avg}	r'	h / h_{avg}	r'	h / h_{avg}	r'	T_s (°C)
0.00	0.475	0.20	0.667	0.47	0.914	0.16	77.2
0.02	0.463	0.22	0.688	0.50	0.934	0.20	70.7
0.03	0.471	0.23	0.708	0.53	0.952	0.24	65.3
0.05	0.483	0.25	0.727	0.57	0.970	0.28	59.9
0.07	0.499	0.27	0.746	0.60	0.986	0.32	56.5
0.08	0.516	0.28	0.764	0.63	1.001	0.41	49.1
0.10	0.536	0.30	0.781	0.67	1.014	0.49	43.6
0.12	0.555	0.32	0.797	0.73	1.039	0.57	39.2
0.13	0.577	0.33	0.811	0.80	1.061	0.66	34.9
0.15	0.599	0.37	0.841	0.87	1.080	0.74	31.4
0.17	0.622	0.40	0.868	0.93	1.129	0.82	28.0
0.18	0.645	0.43	0.891	0.95	1.173	0.91	25.1
						0.99	22.8
h_{avg} (μm) =		1209				1.00	22.8

Table C.92: Experimental data for $\mu = 0.048$ N·s/m^2, $h_o = 1.189$ mm, $\Delta T_s = 59.5$°C.

r'	h / h_{avg}	r'	h / h_{avg}	r'	h / h_{avg}	r'	T_s (°C)
0.00	0.381	0.20	0.621	0.47	0.904	0.16	83.0
0.02	0.374	0.22	0.649	0.50	0.927	0.20	75.9
0.03	0.385	0.23	0.673	0.53	0.947	0.24	70.0
0.05	0.401	0.25	0.696	0.57	0.965	0.28	64.1
0.07	0.419	0.27	0.717	0.60	0.981	0.32	60.4
0.08	0.440	0.28	0.737	0.63	1.003	0.41	52.3
0.10	0.463	0.30	0.757	0.67	1.018	0.49	46.2
0.12	0.488	0.32	0.775	0.73	1.046	0.57	41.4
0.13	0.515	0.33	0.792	0.80	1.070	0.66	36.8
0.15	0.542	0.37	0.823	0.87	1.094	0.74	32.9
0.17	0.569	0.40	0.858	0.93	1.142	0.82	29.2
0.18	0.596	0.43	0.879	0.95	1.187	0.91	26.1
						0.99	23.5
h_{avg} (μm) =		1216				1.00	23.5

Table C.93: Experimental data for $\mu = 0.048$ N·s/m^2, $h_o = 1.458$ mm, $\Delta T_s = 0.1$°C.

r'	h / h_{avg}	r'	h / h_{avg}	r'	h / h_{avg}	r'	T_s (°C)
0.00	0.991	0.20	0.990	0.47	0.990	0.16	21.2
0.02	0.990	0.22	0.990	0.50	0.990	0.20	21.2
0.03	0.990	0.23	0.990	0.53	0.989	0.24	21.2
0.05	0.990	0.25	0.990	0.57	0.990	0.28	21.3
0.07	0.990	0.27	0.990	0.60	0.989	0.32	21.2
0.08	0.990	0.28	0.990	0.63	0.990	0.41	21.3
0.10	0.990	0.30	0.990	0.67	0.989	0.49	21.4
0.12	0.991	0.32	0.990	0.73	0.990	0.57	21.4
0.13	0.990	0.33	0.990	0.80	0.990	0.66	21.3
0.15	0.991	0.37	0.990	0.87	0.990	0.74	21.3
0.17	0.991	0.40	0.990	0.93	1.016	0.82	21.3
0.18	0.990	0.43	0.991	0.95	1.055	0.91	21.3
				0.96	1.092	0.99	21.1
h_{avg} (μm) =		1473				1.00	21.1

Table C.94: Experimental data for $\mu = 0.048$ N·s/m^2, $h_o = 1.458$ mm, $\Delta T_s = 6.8$°C.

r'	h / h_{avg}	r'	h / h_{avg}	r'	h / h_{avg}	r'	T_s (°C)
0.00	0.952	0.20	0.966	0.47	0.983	0.16	23.2
0.02	0.954	0.22	0.967	0.50	0.985	0.20	22.4
0.03	0.955	0.23	0.968	0.53	0.985	0.24	21.7
0.05	0.956	0.25	0.970	0.57	0.987	0.28	21.1
0.07	0.956	0.27	0.971	0.60	0.988	0.32	20.7
0.08	0.957	0.28	0.972	0.63	0.989	0.41	19.8
0.10	0.959	0.30	0.973	0.67	0.990	0.49	19.2
0.12	0.959	0.32	0.974	0.73	0.992	0.57	18.7
0.13	0.961	0.33	0.976	0.80	0.994	0.66	18.0
0.15	0.961	0.37	0.978	0.87	0.997	0.74	17.6
0.17	0.963	0.40	0.980	0.93	1.026	0.82	17.3
0.18	0.964	0.43	0.982	0.95	1.066	0.91	16.9
				0.96	1.104	0.99	16.4
h_{avg} (μm) =		1452				1.00	16.4

Table C.95: Experimental data for $\mu = 0.048$ N·s/m^2, $h_o = 1.458$ mm, $\Delta T_s = 12.8$°C.

r'	h / h_{avg}	r'	h / h_{avg}	r'	h / h_{avg}	r'	T_s (°C)
0.00	0.919	0.20	0.944	0.47	0.978	0.16	30.0
0.02	0.921	0.22	0.946	0.50	0.980	0.20	28.4
0.03	0.922	0.23	0.949	0.53	0.983	0.24	27.2
0.05	0.924	0.25	0.952	0.57	0.986	0.28	26.0
0.07	0.926	0.27	0.954	0.60	0.987	0.32	25.1
0.08	0.928	0.28	0.956	0.63	0.990	0.41	23.5
0.10	0.930	0.30	0.959	0.67	0.993	0.49	22.3
0.12	0.932	0.32	0.961	0.73	0.996	0.57	21.3
0.13	0.934	0.33	0.963	0.80	0.999	0.66	20.1
0.15	0.936	0.37	0.967	0.87	1.003	0.74	19.4
0.17	0.939	0.40	0.971	0.93	1.033	0.82	18.6
0.18	0.941	0.43	0.974	0.95	1.073	0.91	17.9
				0.96	1.110	0.99	17.2
h_{avg} (μm) =		1455				1.00	17.2

Table C.96: Experimental data for $\mu = 0.048$ N·s/m^2, $h_o = 1.458$ mm, $\Delta T_s = 22.2$°C.

r'	h / h_{avg}	r'	h / h_{avg}	r'	h / h_{avg}	r'	T_s (°C)
0.00	0.868	0.20	0.907	0.47	0.966	0.16	40.5
0.02	0.870	0.22	0.911	0.50	0.971	0.20	37.9
0.03	0.873	0.23	0.916	0.53	0.976	0.24	35.6
0.05	0.876	0.25	0.920	0.57	0.982	0.28	33.5
0.07	0.878	0.27	0.924	0.60	0.985	0.32	32.0
0.08	0.881	0.28	0.928	0.63	0.990	0.41	29.1
0.10	0.884	0.30	0.932	0.67	0.994	0.49	26.9
0.12	0.888	0.32	0.936	0.73	1.001	0.57	25.1
0.13	0.891	0.33	0.940	0.80	1.008	0.66	23.3
0.15	0.895	0.37	0.947	0.87	1.014	0.74	21.9
0.17	0.900	0.40	0.954	0.93	1.046	0.82	20.6
0.18	0.903	0.43	0.960	0.95	1.087	0.91	19.4
				0.96	1.123	0.99	18.4
h_{avg} (μm) =		1463				1.00	18.4

Table C.97: Experimental data for $\mu = 0.048$ N·s/m^2, $h_o = 1.458$ mm, $\Delta T_s = 30.3$°C.

r'	h / h_{avg}	r'	h / h_{avg}	r'	h / h_{avg}	r'	T_s (°C)
0.00	0.828	0.20	0.879	0.47	0.957	0.16	49.8
0.02	0.830	0.22	0.884	0.50	0.965	0.20	46.1
0.03	0.835	0.23	0.890	0.53	0.971	0.24	43.1
0.05	0.837	0.25	0.895	0.57	0.978	0.28	40.1
0.07	0.841	0.27	0.901	0.60	0.985	0.32	38.1
0.08	0.845	0.28	0.907	0.63	0.991	0.41	34.1
0.10	0.849	0.30	0.912	0.67	0.996	0.49	31.0
0.12	0.854	0.32	0.916	0.73	1.006	0.57	28.6
0.13	0.858	0.33	0.921	0.80	1.015	0.66	26.1
0.15	0.863	0.37	0.931	0.87	1.023	0.74	24.3
0.17	0.869	0.40	0.940	0.93	1.056	0.82	22.4
0.18	0.873	0.43	0.948	0.95	1.096	0.91	20.8
				0.96	1.132	0.99	19.5
h_{avg} (μm) =		1471				1.00	19.5

Table C.98: Experimental data for $\mu = 0.048$ N·s/m^2, $h_o = 1.458$ mm, $\Delta T_s = 38.2$°C.

r'	h / h_{avg}	r'	h / h_{avg}	r'	h / h_{avg}	r'	T_s (°C)
0.00	0.788	0.20	0.853	0.47	0.948	0.16	58.9
0.02	0.792	0.22	0.859	0.50	0.957	0.20	54.3
0.03	0.796	0.23	0.866	0.53	0.966	0.24	50.5
0.05	0.800	0.25	0.872	0.57	0.975	0.28	46.7
0.07	0.806	0.27	0.879	0.60	0.983	0.32	44.3
0.08	0.810	0.28	0.885	0.63	0.990	0.41	39.1
0.10	0.816	0.30	0.892	0.67	0.997	0.49	35.3
0.12	0.821	0.32	0.898	0.73	1.011	0.57	32.2
0.13	0.827	0.33	0.905	0.80	1.022	0.66	29.2
0.15	0.833	0.37	0.916	0.87	1.031	0.74	26.7
0.17	0.839	0.40	0.927	0.93	1.066	0.82	24.4
0.18	0.846	0.43	0.938	0.95	1.106	0.91	22.3
				0.96	1.142	0.99	20.7
h_{avg} (μm) =		1480				1.00	20.7

Table C.99: Experimental data for $\mu = 0.048$ N·s/m^2, $h_o = 1.458$ mm, $\Delta T_s = 45.3$°C.

r'	h / h_{avg}	r'	h / h_{avg}	r'	h / h_{avg}	r'	T_s (°C)
0.00	0.756	0.20	0.831	0.47	0.940	0.16	67.0
0.02	0.761	0.22	0.839	0.50	0.951	0.20	61.4
0.03	0.764	0.23	0.847	0.53	0.961	0.24	56.9
0.05	0.768	0.25	0.854	0.57	0.971	0.28	52.4
0.07	0.776	0.27	0.862	0.60	0.980	0.32	49.6
0.08	0.781	0.28	0.870	0.63	0.989	0.41	43.5
0.10	0.788	0.30	0.876	0.67	0.998	0.49	38.9
0.12	0.795	0.32	0.883	0.73	1.013	0.57	35.3
0.13	0.802	0.33	0.890	0.80	1.026	0.66	31.7
0.15	0.808	0.37	0.904	0.87	1.040	0.74	28.8
0.17	0.816	0.40	0.916	0.93	1.076	0.82	26.0
0.18	0.824	0.43	0.928	0.95	1.114	0.91	23.6
				0.96	1.150	0.99	21.6
h_{avg} (mm) =		1486				1.00	21.6

Table C.100: Experimental data for $\mu = 0.048$ N·s/m^2, $h_o = 1.458$ mm, $\Delta T_s = 56.9$°C.

r'	h / h_{avg}	r'	h / h_{avg}	r'	h / h_{avg}	r'	T_s (°C)
0.00	0.702	0.20	0.798	0.47	0.931	0.16	80.1
0.02	0.705	0.22	0.807	0.50	0.945	0.20	73.2
0.03	0.711	0.23	0.818	0.53	0.957	0.24	67.5
0.05	0.719	0.25	0.827	0.57	0.970	0.28	61.9
0.07	0.726	0.27	0.836	0.60	0.981	0.32	58.3
0.08	0.734	0.28	0.845	0.63	0.992	0.41	50.6
0.10	0.742	0.30	0.853	0.67	1.001	0.49	44.9
0.12	0.751	0.32	0.862	0.73	1.021	0.57	40.4
0.13	0.760	0.33	0.870	0.80	1.038	0.66	36.0
0.15	0.769	0.37	0.886	0.87	1.054	0.74	32.3
0.17	0.779	0.40	0.902	0.93	1.093	0.82	28.8
0.18	0.788	0.43	0.917	0.95	1.132	0.91	25.8
						0.99	23.3
h_{avg} (μm) =		1487				1.00	23.3

Table C.101: Experimental data for $\mu = 0.048$ N·s/m^2, $h_o = 1.606$ mm, $\Delta T_s = 0.2$°C.

r'	h / h_{avg}	r'	h / h_{avg}	r'	h / h_{avg}	r'	T_s (°C)
0.00	0.991	0.20	0.991	0.47	0.992	0.16	20.1
0.02	0.990	0.22	0.991	0.50	0.991	0.20	20.1
0.03	0.991	0.23	0.991	0.53	0.991	0.24	20.1
0.05	0.990	0.25	0.991	0.57	0.991	0.28	20.1
0.07	0.991	0.27	0.991	0.60	0.991	0.32	20.1
0.08	0.990	0.28	0.991	0.63	0.991	0.41	20.2
0.10	0.990	0.30	0.991	0.67	0.991	0.49	20.2
0.12	0.990	0.32	0.992	0.73	0.991	0.57	20.3
0.13	0.991	0.33	0.992	0.80	0.991	0.66	20.1
0.15	0.991	0.37	0.992	0.87	0.991	0.74	20.2
0.17	0.991	0.40	0.991	0.93	1.014	0.82	20.2
0.18	0.991	0.43	0.991	0.95	1.048	0.91	20.2
				0.96	1.081	0.99	19.9
h_{avg} (μm) =		1621				1.00	19.9

Table C.102: Experimental data for $\mu = 0.048$ N·s/m^2, $h_o = 1.606$ mm, $\Delta T_s = 12.5$°C.

r'	h / h_{avg}	r'	h / h_{avg}	r'	h / h_{avg}	r'	T_s (°C)
0.00	0.942	0.20	0.958	0.47	0.982	0.16	29.7
0.02	0.942	0.22	0.959	0.50	0.983	0.20	28.2
0.03	0.944	0.23	0.961	0.53	0.985	0.24	27.0
0.05	0.945	0.25	0.963	0.57	0.988	0.28	25.8
0.07	0.946	0.27	0.965	0.60	0.989	0.32	25.0
0.08	0.947	0.28	0.966	0.63	0.991	0.41	23.4
0.10	0.948	0.30	0.968	0.67	0.993	0.49	22.2
0.12	0.950	0.32	0.969	0.73	0.996	0.57	21.2
0.13	0.951	0.33	0.971	0.80	0.998	0.66	20.1
0.15	0.953	0.37	0.973	0.87	1.001	0.74	19.3
0.17	0.954	0.40	0.976	0.93	1.026	0.82	18.6
0.18	0.956	0.43	0.979	0.95	1.061	0.91	17.9
				0.96	1.093	0.99	17.2
h_{avg} (μm) =		1605				1.00	17.2

Table C.103: Experimental data for $\mu = 0.048$ N·s/m^2, $h_o = 1.606$ mm, $\Delta T_s = 22.4$°C.

r'	h / h_{avg}	r'	h / h_{avg}	r'	h / h_{avg}	r'	T_s (°C)
0.00	0.909	0.20	0.934	0.47	0.973	0.16	40.9
0.02	0.910	0.22	0.936	0.50	0.977	0.20	38.2
0.03	0.912	0.23	0.939	0.53	0.981	0.24	36.0
0.05	0.913	0.25	0.942	0.57	0.984	0.28	33.8
0.07	0.915	0.27	0.945	0.60	0.988	0.32	32.3
0.08	0.917	0.28	0.947	0.63	0.991	0.41	29.4
0.10	0.919	0.30	0.950	0.67	0.994	0.49	27.1
0.12	0.921	0.32	0.952	0.73	1.000	0.57	25.4
0.13	0.924	0.33	0.954	0.80	1.004	0.66	23.5
0.15	0.926	0.37	0.960	0.87	1.009	0.74	22.1
0.17	0.928	0.40	0.965	0.93	1.036	0.82	20.8
0.18	0.931	0.43	0.969	0.95	1.069	0.91	19.6
				0.96	1.101	0.99	18.5
h_{avg} (μm) =		1619				1.00	18.5

Table C.104: Experimental data for $\mu = 0.048$ N·s/m^2, $h_o = 1.606$ mm, $\Delta T_s = 30.0$°C.

r'	h / h_{avg}	r'	h / h_{avg}	r'	h / h_{avg}	r'	T_s (°C)
0.00	0.879	0.20	0.914	0.47	0.965	0.16	49.6
0.02	0.881	0.22	0.918	0.50	0.971	0.20	45.8
0.03	0.883	0.23	0.922	0.53	0.976	0.24	42.8
0.05	0.886	0.25	0.925	0.57	0.981	0.28	39.8
0.07	0.889	0.27	0.928	0.60	0.986	0.32	37.9
0.08	0.892	0.28	0.932	0.63	0.991	0.41	33.9
0.10	0.895	0.30	0.935	0.67	0.994	0.49	30.9
0.12	0.898	0.32	0.938	0.73	1.002	0.57	28.5
0.13	0.901	0.33	0.942	0.80	1.009	0.66	26.1
0.15	0.904	0.37	0.948	0.87	1.016	0.74	24.2
0.17	0.907	0.40	0.953	0.93	1.044	0.82	22.4
0.18	0.911	0.43	0.960	0.95	1.078	0.91	20.8
				0.96	1.109	0.99	19.5
h_{avg} (μm) =		1621				1.00	19.5

Table C.105: Experimental data for $\mu = 0.048$ N·s/m^2, $h_o = 1.606$ mm, $\Delta T_s = 38.4$°C.

r'	h / h_{avg}	r'	h / h_{avg}	r'	h / h_{avg}	r'	T_s (°C)
0.00	0.855	0.20	0.897	0.47	0.958	0.16	59.4
0.02	0.857	0.22	0.901	0.50	0.965	0.20	54.7
0.03	0.860	0.23	0.906	0.53	0.971	0.24	50.8
0.05	0.863	0.25	0.909	0.57	0.978	0.28	47.0
0.07	0.866	0.27	0.913	0.60	0.983	0.32	44.6
0.08	0.870	0.28	0.917	0.63	0.989	0.41	39.4
0.10	0.874	0.30	0.922	0.67	0.994	0.49	35.6
0.12	0.878	0.32	0.926	0.73	1.004	0.57	32.6
0.13	0.881	0.33	0.929	0.80	1.013	0.66	29.5
0.15	0.885	0.37	0.937	0.87	1.022	0.74	27.1
0.17	0.889	0.40	0.944	0.93	1.053	0.82	24.7
0.18	0.893	0.43	0.951	0.95	1.086	0.91	22.6
				0.96	1.116	0.99	21.0
h_{avg} (μm) =		1631				1.00	21.0

Table C.106: Experimental data for $\mu = 0.048$ N·s/m^2, $h_o = 1.606$ mm, $\Delta T_s = 44.9$°C.

r'	h / h_{avg}	r'	h / h_{avg}	r'	h / h_{avg}	r'	T_s (°C)
0.00	0.839	0.20	0.886	0.47	0.954	0.16	66.8
0.02	0.841	0.22	0.891	0.50	0.962	0.20	61.3
0.03	0.844	0.23	0.895	0.53	0.969	0.24	56.7
0.05	0.848	0.25	0.900	0.57	0.976	0.28	52.3
0.07	0.852	0.27	0.904	0.60	0.982	0.32	49.4
0.08	0.856	0.28	0.909	0.63	0.988	0.41	43.4
0.10	0.860	0.30	0.914	0.67	0.994	0.49	38.9
0.12	0.864	0.32	0.918	0.73	1.005	0.57	35.4
0.13	0.869	0.33	0.922	0.80	1.016	0.66	31.8
0.15	0.873	0.37	0.930	0.87	1.026	0.74	29.0
0.17	0.878	0.40	0.939	0.93	1.057	0.82	26.2
0.18	0.882	0.43	0.946	0.95	1.090	0.91	23.8
				0.96	1.122	0.99	21.9
h_{avg} (μm) =		1629				1.00	21.9

Table C.107: Experimental data for $\mu = 0.048$ N·s/m^2, $h_o = 1.606$ mm, $\Delta T_s = 50.5$°C.

r'	h / h_{avg}	r'	h / h_{avg}	r'	h / h_{avg}	r'	T_s (°C)
0.00	0.817	0.20	0.874	0.47	0.950	0.16	73.1
0.02	0.822	0.22	0.880	0.50	0.958	0.20	66.8
0.03	0.826	0.23	0.885	0.53	0.967	0.24	61.6
0.05	0.831	0.25	0.890	0.57	0.973	0.28	56.6
0.07	0.834	0.27	0.895	0.60	0.981	0.32	53.3
0.08	0.839	0.28	0.900	0.63	0.987	0.41	46.5
0.10	0.844	0.30	0.904	0.67	0.994	0.49	41.4
0.12	0.849	0.32	0.909	0.73	1.008	0.57	37.4
0.13	0.854	0.33	0.914	0.80	1.019	0.66	33.5
0.15	0.859	0.37	0.924	0.87	1.030	0.74	30.3
0.17	0.864	0.40	0.933	0.93	1.062	0.82	27.3
0.18	0.869	0.43	0.941	0.95	1.095	0.91	24.6
				0.96	1.127	0.99	22.6
h_{avg} (μm) =		1621				1.00	22.6

Table C.108: Experimental data for $\mu = 0.048$ N·s/m^2, $h_o = 1.606$ mm, $\Delta T_s = 56.8$°C.

r'	h / h_{avg}	r'	h / h_{avg}	r'	h / h_{avg}	r'	T_s (°C)
0.00	0.800	0.20	0.863	0.47	0.946	0.16	80.6
0.02	0.804	0.22	0.870	0.50	0.955	0.20	73.5
0.03	0.808	0.23	0.875	0.53	0.964	0.24	67.7
0.05	0.813	0.25	0.881	0.57	0.972	0.28	62.0
0.07	0.819	0.27	0.887	0.60	0.980	0.32	58.3
0.08	0.824	0.28	0.892	0.63	0.988	0.41	50.7
0.10	0.830	0.30	0.897	0.67	0.995	0.49	45.0
0.12	0.836	0.32	0.902	0.73	1.009	0.57	40.5
0.13	0.841	0.33	0.907	0.80	1.022	0.66	36.2
0.15	0.846	0.37	0.918	0.87	1.034	0.74	32.6
0.17	0.852	0.40	0.928	0.93	1.066	0.82	29.1
0.18	0.858	0.43	0.938	0.95	1.099	0.91	26.1
				0.96	1.131	0.99	23.7
h_{avg} (μm) =		1617				1.00	23.7

Table C.109: Experimental data for $\mu = 0.048$ N·s/m^2, $h_o = 1.810$ mm, $\Delta T_s = 0.1$°C.

r'	h / h_{avg}	r'	h / h_{avg}	r'	h / h_{avg}	r'	T_s (°C)
0.00	0.994	0.20	0.994	0.47	0.994	0.16	24.9
0.02	0.995	0.22	0.994	0.50	0.994	0.20	24.8
0.03	0.993	0.23	0.994	0.53	0.994	0.24	24.8
0.05	0.994	0.25	0.994	0.57	0.994	0.28	24.8
0.07	0.994	0.27	0.994	0.60	0.994	0.32	24.8
0.08	0.994	0.28	0.994	0.63	0.993	0.41	24.8
0.10	0.994	0.30	0.994	0.67	0.994	0.49	24.9
0.12	0.993	0.32	0.994	0.73	0.994	0.57	24.9
0.13	0.994	0.33	0.994	0.80	0.994	0.66	24.8
0.15	0.994	0.37	0.994	0.87	0.994	0.74	24.8
0.17	0.994	0.40	0.994	0.93	1.014	0.82	24.9
0.18	0.994	0.43	0.994	0.95	1.043	0.91	24.9
						0.99	24.8
h_{avg} (μm) =		1822				1.00	24.8

Table C.110: Experimental data for $\mu = 0.048$ N·s/m^2, $h_o = 1.810$ mm, $\Delta T_s = 12.7$°C.

r'	h / h_{avg}	r'	h / h_{avg}	r'	h / h_{avg}	r'	T_s (°C)
0.00	0.957	0.20	0.968	0.47	0.986	0.16	30.1
0.02	0.957	0.22	0.969	0.50	0.988	0.20	28.5
0.03	0.958	0.23	0.971	0.53	0.990	0.24	27.3
0.05	0.958	0.25	0.972	0.57	0.991	0.28	26.1
0.07	0.959	0.27	0.973	0.60	0.993	0.32	25.3
0.08	0.960	0.28	0.975	0.63	0.994	0.41	23.7
0.10	0.961	0.30	0.976	0.67	0.995	0.49	22.5
0.12	0.962	0.32	0.977	0.73	0.997	0.57	21.5
0.13	0.963	0.33	0.978	0.80	0.999	0.66	20.3
0.15	0.964	0.37	0.980	0.87	1.001	0.74	19.6
0.17	0.965	0.40	0.982	0.93	1.024	0.82	18.8
0.18	0.966	0.43	0.984	0.95	1.055	0.91	18.0
						0.99	17.3
h_{avg} (μm) =		1784				1.00	17.3

Table C.111: Experimental data for $\mu = 0.048$ N·s/m^2, $h_o = 1.810$ mm, $\Delta T_s = 22.6$°C.

r'	h / h_{avg}	r'	h / h_{avg}	r'	h / h_{avg}	r'	T_s (°C)
0.00	0.932	0.20	0.950	0.47	0.979	0.16	41.3
0.02	0.934	0.22	0.952	0.50	0.982	0.20	38.6
0.03	0.934	0.23	0.954	0.53	0.985	0.24	36.4
0.05	0.935	0.25	0.956	0.57	0.988	0.28	34.1
0.07	0.937	0.27	0.958	0.60	0.991	0.32	32.7
0.08	0.938	0.28	0.960	0.63	0.993	0.41	29.7
0.10	0.940	0.30	0.962	0.67	0.996	0.49	27.5
0.12	0.941	0.32	0.964	0.73	1.000	0.57	25.7
0.13	0.943	0.33	0.965	0.80	1.004	0.66	23.8
0.15	0.945	0.37	0.969	0.87	1.008	0.74	22.5
0.17	0.947	0.40	0.972	0.93	1.032	0.82	21.1
0.18	0.949	0.43	0.976	0.95	1.062	0.91	19.8
						0.99	18.7
h_{avg} (μm) =		1796				1.00	18.7

Table C.112: Experimental data for $\mu = 0.048$ N·s/m^2, $h_o = 1.810$ mm, $\Delta T_s = 30.3$°C.

r'	h / h_{avg}	r'	h / h_{avg}	r'	h / h_{avg}	r'	T_s (°C)
0.00	0.913	0.20	0.938	0.47	0.973	0.16	50.0
0.02	0.915	0.22	0.940	0.50	0.977	0.20	46.2
0.03	0.916	0.23	0.942	0.53	0.981	0.24	43.2
0.05	0.918	0.25	0.945	0.57	0.985	0.28	40.2
0.07	0.920	0.27	0.947	0.60	0.989	0.32	38.3
0.08	0.922	0.28	0.949	0.63	0.992	0.41	34.2
0.10	0.924	0.30	0.952	0.67	0.995	0.49	31.2
0.12	0.927	0.32	0.954	0.73	1.002	0.57	28.8
0.13	0.929	0.33	0.956	0.80	1.008	0.66	26.4
0.15	0.931	0.37	0.961	0.87	1.013	0.74	24.5
0.17	0.933	0.40	0.965	0.93	1.038	0.82	22.7
0.18	0.935	0.43	0.969	0.95	1.069	0.91	21.1
						0.99	19.6
h_{avg} (μm) =		1791				1.00	19.6

Table C.113: Experimental data for $\mu = 0.048$ N·s/m^2, $h_o = 1.810$ mm, $\Delta T_s = 37.7$°C.

r'	h / h_{avg}	r'	h / h_{avg}	r'	h / h_{avg}	r'	T_s (°C)
0.00	0.899	0.20	0.928	0.47	0.969	0.16	58.3
0.02	0.901	0.22	0.930	0.50	0.974	0.20	53.6
0.03	0.902	0.23	0.933	0.53	0.978	0.24	49.8
0.05	0.905	0.25	0.936	0.57	0.983	0.28	46.0
0.07	0.907	0.27	0.939	0.60	0.987	0.32	43.6
0.08	0.909	0.28	0.942	0.63	0.991	0.41	38.6
0.10	0.912	0.30	0.944	0.67	0.995	0.49	34.8
0.12	0.915	0.32	0.947	0.73	1.003	0.57	31.9
0.13	0.917	0.33	0.949	0.80	1.010	0.66	28.9
0.15	0.919	0.37	0.955	0.87	1.017	0.74	26.6
0.17	0.923	0.40	0.960	0.93	1.043	0.82	24.3
0.18	0.925	0.43	0.964	0.95	1.074	0.91	22.3
						0.99	20.6
h_{avg} (μm) =		1799				1.00	20.6

Table C.114: Experimental data for $\mu = 0.048$ N·s/m^2, $h_o = 1.810$ mm, $\Delta T_s = 46.0$°C.

r'	h / h_{avg}	r'	h / h_{avg}	r'	h / h_{avg}	r'	T_s (°C)
0.00	0.884	0.20	0.919	0.47	0.966	0.16	68.1
0.02	0.886	0.22	0.922	0.50	0.971	0.20	62.3
0.03	0.889	0.23	0.925	0.53	0.976	0.24	57.6
0.05	0.891	0.25	0.928	0.57	0.982	0.28	53.0
0.07	0.894	0.27	0.931	0.60	0.987	0.32	50.1
0.08	0.898	0.28	0.934	0.63	0.991	0.41	43.9
0.10	0.900	0.30	0.937	0.67	0.996	0.49	39.3
0.12	0.904	0.32	0.940	0.73	1.004	0.57	35.7
0.13	0.907	0.33	0.944	0.80	1.012	0.66	32.2
0.15	0.909	0.37	0.949	0.87	1.020	0.74	29.3
0.17	0.913	0.40	0.955	0.93	1.047	0.82	26.5
0.18	0.916	0.43	0.960	0.95	1.076	0.91	24.1
						0.99	22.1
h_{avg} (μm) =		1804				1.00	22.1

Table C.115: Experimental data for $\mu = 0.048$ N·s/m^2, $h_o = 1.810$ mm, $\Delta T_s = 51.4$°C.

r'	h / h_{avg}	r'	h / h_{avg}	r'	h / h_{avg}	r'	T_s (°C)
0.00	0.869	0.20	0.911	0.47	0.964	0.16	74.3
0.02	0.872	0.22	0.915	0.50	0.969	0.20	67.9
0.03	0.876	0.23	0.918	0.53	0.975	0.24	62.6
0.05	0.879	0.25	0.921	0.57	0.981	0.28	57.4
0.07	0.883	0.27	0.925	0.60	0.986	0.32	54.1
0.08	0.886	0.28	0.929	0.63	0.991	0.41	47.1
0.10	0.890	0.30	0.932	0.67	0.996	0.49	42.0
0.12	0.893	0.32	0.936	0.73	1.006	0.57	38.0
0.13	0.897	0.33	0.939	0.80	1.014	0.66	34.1
0.15	0.901	0.37	0.946	0.87	1.023	0.74	30.9
0.17	0.904	0.40	0.952	0.93	1.049	0.82	27.8
0.18	0.908	0.43	0.958	0.95	1.080	0.91	25.1
						0.99	22.9
h_{avg} (μm) =		1803				1.00	22.9

Table C.116: Experimental data for $\mu = 0.048$ N·s/m^2, $h_o = 1.810$ mm, $\Delta T_s = 54.3$°C.

r'	h / h_{avg}	r'	h / h_{avg}	r'	h / h_{avg}	r'	T_s (°C)
0.00	0.862	0.20	0.906	0.47	0.962	0.16	78.0
0.02	0.864	0.22	0.909	0.50	0.969	0.20	71.1
0.03	0.868	0.23	0.914	0.53	0.974	0.24	65.5
0.05	0.871	0.25	0.917	0.57	0.980	0.28	60.0
0.07	0.875	0.27	0.921	0.60	0.985	0.32	56.4
0.08	0.879	0.28	0.925	0.63	0.991	0.41	49.0
0.10	0.883	0.30	0.928	0.67	0.996	0.49	43.6
0.12	0.887	0.32	0.932	0.73	1.006	0.57	39.4
0.13	0.890	0.33	0.936	0.80	1.016	0.66	35.2
0.15	0.894	0.37	0.943	0.87	1.025	0.74	31.8
0.17	0.898	0.40	0.949	0.93	1.051	0.82	28.6
0.18	0.902	0.43	0.956	0.95	1.081	0.91	25.7
						0.99	23.7
h_{avg} (μm) =		1809				1.00	23.7

Table C.117: Experimental data for $\mu = 0.048$ N·s/m^2, $h_o = 2.122$ mm, $\Delta T_s = 0.1$°C.

r'	h / h_{avg}	r'	h / h_{avg}	r'	h / h_{avg}	r'	T_s (°C)
0.00	0.995	0.18	0.995	0.43	0.995	0.16	26.3
0.02	0.995	0.20	0.995	0.47	0.995	0.20	26.2
0.03	0.996	0.22	0.995	0.50	0.995	0.24	26.2
0.05	0.996	0.23	0.995	0.53	0.995	0.28	26.2
0.04	0.995	0.25	0.995	0.57	0.995	0.32	26.2
0.07	0.996	0.27	0.995	0.60	0.995	0.41	26.2
0.08	0.996	0.28	0.995	0.63	0.995	0.49	26.3
0.10	0.995	0.30	0.995	0.67	0.995	0.57	26.3
0.12	0.995	0.32	0.995	0.73	0.995	0.66	26.2
0.13	0.995	0.33	0.995	0.80	0.995	0.74	26.2
0.15	0.995	0.37	0.995	0.87	0.995	0.82	26.2
0.17	0.995	0.40	0.995	0.93	1.011	0.91	26.2
				0.95	1.035	0.99	26.2
h_{avg} (μm) =		2133				1.00	26.2

Table C.118: Experimental data for $\mu = 0.048$ N·s/m^2, $h_o = 2.122$ mm, $\Delta T_s = 12.6$°C.

r'	h / h_{avg}	r'	h / h_{avg}	r'	h / h_{avg}	r'	T_s (°C)
0.00	0.970	0.20	0.978	0.47	0.990	0.16	30.0
0.02	0.971	0.22	0.979	0.50	0.991	0.20	28.5
0.03	0.971	0.23	0.980	0.53	0.992	0.24	27.3
0.05	0.972	0.25	0.981	0.57	0.992	0.28	26.1
0.07	0.973	0.27	0.981	0.60	0.994	0.32	25.3
0.08	0.973	0.28	0.982	0.63	0.995	0.41	23.7
0.10	0.974	0.30	0.983	0.67	0.995	0.49	22.5
0.12	0.974	0.32	0.984	0.73	0.997	0.57	21.5
0.13	0.975	0.33	0.984	0.80	0.998	0.66	20.4
0.15	0.976	0.37	0.986	0.87	1.000	0.74	19.6
0.17	0.977	0.40	0.987	0.93	1.019	0.82	18.8
0.18	0.978	0.43	0.988	0.95	1.044	0.91	18.0
						0.99	17.4
h_{avg} (μm) =		2078				1.00	17.4

Table C.119: Experimental data for $\mu = 0.048$ N·s/m^2, $h_o = 2.122$ mm, $\Delta T_s = 21.8$°C.

r'	h / h_{avg}	r'	h / h_{avg}	r'	h / h_{avg}	r'	T_s (°C)
0.00	0.956	0.20	0.967	0.47	0.985	0.16	40.4
0.02	0.956	0.22	0.969	0.50	0.987	0.20	37.8
0.03	0.957	0.23	0.970	0.53	0.989	0.24	35.6
0.05	0.958	0.25	0.971	0.57	0.991	0.28	33.5
0.07	0.959	0.27	0.973	0.60	0.992	0.32	32.1
0.08	0.960	0.28	0.973	0.63	0.994	0.41	29.2
0.10	0.961	0.30	0.974	0.67	0.996	0.49	27.0
0.12	0.962	0.32	0.976	0.73	0.999	0.57	25.4
0.13	0.963	0.33	0.977	0.80	1.001	0.66	23.5
0.15	0.964	0.37	0.979	0.87	1.004	0.74	22.2
0.17	0.965	0.40	0.981	0.93	1.023	0.82	20.8
0.18	0.967	0.43	0.983	0.95	1.048	0.91	19.6
						0.99	18.6
h_{avg} (μm) =		2091				1.00	18.6

Table C.120: Experimental data for $\mu = 0.048$ N·s/m^2, $h_o = 2.122$ mm, $\Delta T_s = 30.0$°C.

r'	h / h_{avg}	r'	h / h_{avg}	r'	h / h_{avg}	r'	T_s (°C)
0.00	0.944	0.20	0.960	0.47	0.982	0.16	49.7
0.02	0.945	0.22	0.962	0.50	0.985	0.20	46.0
0.03	0.946	0.23	0.963	0.53	0.987	0.24	43.0
0.05	0.948	0.25	0.965	0.57	0.989	0.28	40.0
0.07	0.949	0.27	0.966	0.60	0.991	0.32	38.1
0.08	0.951	0.28	0.968	0.63	0.993	0.41	34.1
0.10	0.952	0.30	0.969	0.67	0.996	0.49	31.1
0.12	0.953	0.32	0.970	0.73	1.000	0.57	28.8
0.13	0.955	0.33	0.972	0.80	1.003	0.66	26.4
0.15	0.956	0.37	0.974	0.87	1.007	0.74	24.5
0.17	0.958	0.40	0.977	0.93	1.027	0.82	22.7
0.18	0.959	0.43	0.980	0.95	1.052	0.91	21.1
						0.99	19.7
h_{avg} (μm) =		2100				1.00	19.7

Table C.121: Experimental data for $\mu = 0.048$ N·s/m^2, $h_o = 2.122$ mm, $\Delta T_s = 35.4$°C.

r'	h / h_{avg}	r'	h / h_{avg}	r'	h / h_{avg}	r'	T_s (°C)
0.00	0.938	0.20	0.957	0.47	0.980	0.16	55.7
0.02	0.940	0.22	0.959	0.50	0.983	0.20	51.2
0.03	0.941	0.23	0.960	0.53	0.986	0.24	47.6
0.05	0.943	0.25	0.962	0.57	0.989	0.28	44.0
0.07	0.944	0.27	0.963	0.60	0.991	0.32	41.7
0.08	0.946	0.28	0.965	0.63	0.993	0.41	37.0
0.10	0.948	0.30	0.966	0.67	0.996	0.49	33.5
0.12	0.949	0.32	0.967	0.73	1.000	0.57	30.7
0.13	0.951	0.33	0.970	0.80	1.004	0.66	27.9
0.15	0.952	0.37	0.972	0.87	1.008	0.74	25.7
0.17	0.954	0.40	0.975	0.93	1.028	0.82	23.7
0.18	0.955	0.43	0.978	0.95	1.053	0.91	21.9
						0.99	20.3
h_{avg} (μm) =		2099				1.00	20.3

Table C.122: Experimental data for $\mu = 0.048$ N·s/m^2, $h_o = 2.122$ mm, $\Delta T_s = 44.7$°C.

r'	h / h_{avg}	r'	h / h_{avg}	r'	h / h_{avg}	r'	T_s (°C)
0.00	0.927	0.20	0.950	0.47	0.978	0.16	66.8
0.02	0.929	0.22	0.952	0.50	0.981	0.20	61.1
0.03	0.930	0.23	0.954	0.53	0.983	0.24	56.5
0.05	0.933	0.25	0.956	0.57	0.987	0.28	52.0
0.07	0.935	0.27	0.957	0.60	0.991	0.32	49.1
0.08	0.937	0.28	0.960	0.63	0.994	0.41	43.0
0.10	0.939	0.30	0.961	0.67	0.996	0.49	38.6
0.12	0.941	0.32	0.963	0.73	1.001	0.57	35.2
0.13	0.943	0.33	0.965	0.80	1.006	0.66	31.8
0.15	0.944	0.37	0.968	0.87	1.011	0.74	29.0
0.17	0.947	0.40	0.971	0.93	1.032	0.82	26.4
0.18	0.949	0.43	0.974	0.95	1.055	0.91	24.0
						0.99	22.1
h_{avg} (μm) =		2115				1.00	22.1

Table C.123: Experimental data for $\mu = 0.048$ N·s/m^2, $h_o = 2.122$ mm, $\Delta T_s = 49.7$°C.

r'	h / h_{avg}	r'	h / h_{avg}	r'	h / h_{avg}	r'	T_s (°C)
0.00	0.926	0.20	0.949	0.47	0.977	0.16	72.2
0.02	0.926	0.22	0.950	0.50	0.981	0.20	65.9
0.03	0.928	0.23	0.952	0.53	0.984	0.24	60.7
0.05	0.931	0.25	0.954	0.57	0.987	0.28	55.6
0.07	0.933	0.27	0.957	0.60	0.989	0.32	52.4
0.08	0.935	0.28	0.958	0.63	0.992	0.41	45.6
0.10	0.937	0.30	0.959	0.67	0.995	0.49	40.7
0.12	0.939	0.32	0.962	0.73	1.001	0.57	36.8
0.13	0.941	0.33	0.963	0.80	1.007	0.66	33.1
0.15	0.943	0.37	0.967	0.87	1.012	0.74	30.0
0.17	0.944	0.40	0.970	0.93	1.032	0.82	27.1
0.18	0.946	0.43	0.974	0.95	1.056	0.91	24.7
						0.99	22.5
h_{avg} (μm) =		2121				1.00	22.5

Table C.124: Experimental data for $\mu = 0.048$ N·s/m^2, $h_o = 2.122$ mm, $\Delta T_s = 54.5$°C.

r'	h / h_{avg}	r'	h / h_{avg}	r'	h / h_{avg}	r'	T_s (°C)
0.00	0.920	0.20	0.945	0.47	0.977	0.16	78.1
0.02	0.920	0.22	0.948	0.50	0.981	0.20	71.2
0.03	0.923	0.23	0.949	0.53	0.984	0.24	65.5
0.05	0.925	0.25	0.951	0.57	0.987	0.28	59.9
0.07	0.927	0.27	0.954	0.60	0.990	0.32	56.4
0.08	0.930	0.28	0.956	0.63	0.993	0.41	49.0
0.10	0.932	0.30	0.958	0.67	0.996	0.49	43.6
0.12	0.934	0.32	0.960	0.73	1.002	0.57	39.4
0.13	0.937	0.33	0.962	0.80	1.007	0.66	35.3
0.15	0.939	0.37	0.966	0.87	1.012	0.74	32.0
0.17	0.941	0.40	0.970	0.93	1.033	0.82	28.8
0.18	0.943	0.43	0.974	0.95	1.057	0.91	26.0
						0.99	23.6
h_{avg} (μm) =		2111				1.00	23.6

Table C.125: Experimental data for $\mu = 0.048$ N·s/m^2, $h_o = 2.383$ mm, $\Delta T_s = 0.2$°C.

r'	h / h_{avg}	r'	h / h_{avg}	r'	h / h_{avg}	r'	T_s (°C)
0.00	0.994	0.20	0.994	0.47	0.994	0.16	21.8
0.02	0.994	0.22	0.994	0.50	0.994	0.20	21.7
0.03	0.994	0.23	0.994	0.53	0.994	0.24	21.7
0.05	0.994	0.25	0.994	0.57	0.994	0.28	21.7
0.07	0.994	0.27	0.994	0.60	0.994	0.32	21.7
0.08	0.994	0.28	0.994	0.63	0.994	0.41	21.8
0.10	0.994	0.30	0.994	0.67	0.994	0.49	21.8
0.12	0.994	0.32	0.994	0.73	0.994	0.57	21.9
0.13	0.994	0.33	0.994	0.80	0.994	0.66	21.7
0.15	0.994	0.37	0.994	0.87	0.994	0.74	21.8
0.17	0.994	0.40	0.994	0.93	1.009	0.82	21.8
0.18	0.994	0.43	0.994	0.95	1.032	0.91	21.8
				0.96	1.056	0.99	21.6
h_{avg} (μm) =		2398				1.00	21.6

Table C.126: Experimental data for $\mu = 0.048$ N·s/m^2, $h_o = 2.383$ mm, $\Delta T_s = 12.4$°C.

r'	h / h_{avg}	r'	h / h_{avg}	r'	h / h_{avg}	r'	T_s (°C)
0.00	0.975	0.20	0.983	0.47	0.990	0.16	29.5
0.02	0.975	0.22	0.983	0.50	0.991	0.20	28.0
0.03	0.976	0.23	0.983	0.53	0.991	0.24	26.8
0.05	0.976	0.25	0.984	0.57	0.992	0.28	25.7
0.07	0.977	0.27	0.984	0.60	0.993	0.32	24.9
0.08	0.977	0.28	0.985	0.63	0.994	0.41	23.3
0.10	0.978	0.30	0.985	0.67	0.994	0.49	22.1
0.12	0.978	0.32	0.986	0.73	0.995	0.57	21.2
0.13	0.979	0.33	0.986	0.80	0.996	0.66	20.0
0.15	0.979	0.37	0.987	0.87	0.998	0.74	19.3
0.17	0.981	0.40	0.988	0.93	1.015	0.82	18.6
0.18	0.982	0.43	0.989	0.95	1.038	0.91	17.9
				0.96	1.062	0.99	17.2
h_{avg} (μm) =		2377				1.00	17.2

Table C.127: Experimental data for $\mu = 0.048$ N·s/m^2, $h_o = 2.383$ mm, $\Delta T_s = 22.2$°C.

r'	h / h_{avg}	r'	h / h_{avg}	r'	h / h_{avg}	r'	T_s (°C)
0.00	0.965	0.20	0.975	0.47	0.987	0.16	40.7
0.02	0.966	0.22	0.976	0.50	0.988	0.20	38.0
0.03	0.967	0.23	0.977	0.53	0.989	0.24	35.7
0.05	0.968	0.25	0.977	0.57	0.991	0.28	33.5
0.07	0.968	0.27	0.978	0.60	0.992	0.32	32.1
0.08	0.969	0.28	0.979	0.63	0.993	0.41	29.2
0.10	0.970	0.30	0.979	0.67	0.994	0.49	27.0
0.12	0.971	0.32	0.980	0.73	0.996	0.57	25.3
0.13	0.972	0.33	0.981	0.80	0.999	0.66	23.5
0.15	0.972	0.37	0.982	0.87	1.001	0.74	22.2
0.17	0.973	0.40	0.984	0.93	1.018	0.82	20.9
0.18	0.974	0.43	0.985	0.95	1.041	0.91	19.6
				0.96	1.065	0.99	18.5
h_{avg} (μm) =		2381				1.00	18.5

Table C.128: Experimental data for $\mu = 0.048$ N·s/m^2, $h_o = 2.383$ mm, $\Delta T_s = 28.3$°C.

r'	h / h_{avg}	r'	h / h_{avg}	r'	h / h_{avg}	r'	T_s (°C)
0.00	0.960	0.20	0.971	0.47	0.985	0.16	47.9
0.02	0.961	0.22	0.972	0.50	0.987	0.20	44.3
0.03	0.962	0.23	0.973	0.53	0.988	0.24	41.4
0.05	0.963	0.25	0.974	0.57	0.990	0.28	38.6
0.07	0.964	0.27	0.975	0.60	0.991	0.32	36.7
0.08	0.965	0.28	0.976	0.63	0.993	0.41	32.9
0.10	0.966	0.30	0.977	0.67	0.994	0.49	30.2
0.12	0.967	0.32	0.977	0.73	0.997	0.57	28.0
0.13	0.968	0.33	0.978	0.80	0.999	0.66	25.8
0.15	0.969	0.37	0.980	0.87	1.003	0.74	24.1
0.17	0.969	0.40	0.982	0.93	1.019	0.82	22.4
0.18	0.970	0.43	0.983	0.95	1.043	0.91	20.9
				0.96	1.066	0.99	19.6
h_{avg} (μm) =		2395				1.00	19.6

Table C.129: Experimental data for $\mu = 0.048$ N·s/m^2, $h_o = 2.383$ mm, $\Delta T_s = 36.6$°C.

r'	h / h_{avg}	r'	h / h_{avg}	r'	h / h_{avg}	r'	T_s (°C)
0.00	0.955	0.20	0.968	0.47	0.984	0.16	57.5
0.02	0.955	0.22	0.969	0.50	0.985	0.20	52.8
0.03	0.956	0.23	0.970	0.53	0.987	0.24	49.0
0.05	0.957	0.25	0.971	0.57	0.989	0.28	45.3
0.07	0.959	0.27	0.972	0.60	0.991	0.32	42.9
0.08	0.960	0.28	0.973	0.63	0.993	0.41	38.0
0.10	0.961	0.30	0.974	0.67	0.994	0.49	34.4
0.12	0.962	0.32	0.975	0.73	0.997	0.57	31.6
0.13	0.963	0.33	0.976	0.80	1.000	0.66	28.8
0.15	0.964	0.37	0.978	0.87	1.004	0.74	26.6
0.17	0.965	0.40	0.980	0.93	1.021	0.82	24.5
0.18	0.967	0.43	0.982	0.95	1.044	0.91	22.5
				0.96	1.067	0.99	20.9
h_{avg} (μm) =		2404				1.00	20.9

Table C.130: Experimental data for $\mu = 0.048$ N·s/m^2, $h_o = 2.383$ mm, $\Delta T_s = 42.1$°C.

r'	h / h_{avg}	r'	h / h_{avg}	r'	h / h_{avg}	r'	T_s (°C)
0.00	0.950	0.20	0.966	0.47	0.983	0.16	63.7
0.02	0.951	0.22	0.967	0.50	0.985	0.20	58.3
0.03	0.952	0.23	0.968	0.53	0.987	0.24	53.9
0.05	0.954	0.25	0.970	0.57	0.989	0.28	49.6
0.07	0.955	0.27	0.971	0.60	0.991	0.32	46.9
0.08	0.957	0.28	0.972	0.63	0.993	0.41	41.2
0.10	0.958	0.30	0.973	0.67	0.994	0.49	37.1
0.12	0.960	0.32	0.974	0.73	0.998	0.57	33.9
0.13	0.961	0.33	0.975	0.80	1.001	0.66	30.7
0.15	0.963	0.37	0.977	0.87	1.004	0.74	28.2
0.17	0.964	0.40	0.979	0.93	1.021	0.82	25.7
0.18	0.965	0.43	0.981	0.95	1.044	0.91	23.5
				0.96	1.067	0.99	21.6
h_{avg} (μm) =		2406				1.00	21.6

Table C.131: Experimental data for $\mu = 0.048$ N·s/m^2, $h_o = 2.383$ mm, $\Delta T_s = 49.7$°C.

r'	h / h_{avg}	r'	h / h_{avg}	r'	h / h_{avg}	r'	T_s (°C)
0.00	0.952	0.20	0.964	0.47	0.982	0.16	72.5
0.02	0.951	0.22	0.964	0.50	0.985	0.20	66.0
0.03	0.952	0.23	0.966	0.53	0.987	0.24	60.8
0.05	0.953	0.25	0.967	0.57	0.989	0.28	55.7
0.07	0.955	0.27	0.969	0.60	0.991	0.32	52.5
0.08	0.956	0.28	0.970	0.63	0.993	0.41	45.8
0.10	0.956	0.30	0.971	0.67	0.995	0.49	40.9
0.12	0.957	0.32	0.972	0.73	0.998	0.57	37.1
0.13	0.958	0.33	0.974	0.80	1.001	0.66	33.5
0.15	0.960	0.37	0.976	0.87	1.005	0.74	30.5
0.17	0.961	0.40	0.978	0.93	1.022	0.82	27.6
0.18	0.963	0.43	0.980	0.95	1.045	0.91	25.1
				0.96	1.067	0.99	22.8
h_{avg} (μm) =		2415				1.00	22.8

Table C.132: Experimental data for $\mu = 0.048$ N·s/m^2, $h_o = 2.383$ mm, $\Delta T_s = 54.2$°C.

r'	h / h_{avg}	r'	h / h_{avg}	r'	h / h_{avg}	r'	T_s (°C)
0.00	0.948	0.20	0.962	0.47	0.982	0.16	77.8
0.02	0.948	0.22	0.963	0.50	0.984	0.20	70.8
0.03	0.948	0.23	0.964	0.53	0.986	0.24	65.1
0.05	0.950	0.25	0.965	0.57	0.989	0.28	59.5
0.07	0.952	0.27	0.967	0.60	0.990	0.32	56.0
0.08	0.954	0.28	0.969	0.63	0.993	0.41	48.6
0.10	0.954	0.30	0.970	0.67	0.995	0.49	43.3
0.12	0.955	0.32	0.971	0.73	0.998	0.57	39.2
0.13	0.956	0.33	0.972	0.80	1.002	0.66	35.2
0.15	0.957	0.37	0.975	0.87	1.006	0.74	32.0
0.17	0.959	0.40	0.978	0.93	1.023	0.82	28.9
0.18	0.961	0.43	0.979	0.95	1.045	0.91	26.1
				0.96	1.068	0.99	23.6
h_{avg} (μm) =		2406				1.00	23.6

Table C.133: Experimental data for $\mu = 0.048$ N·s/m^2, $h_o = 2.383$ mm, $\Delta T_s = 0.1$°C.

r'	h / h_{avg}	r'	h / h_{avg}	r'	h / h_{avg}	r'	T_s (°C)
0.00	0.996	0.20	0.996	0.47	0.995	0.16	22.2
0.02	0.996	0.22	0.995	0.50	0.995	0.20	22.1
0.03	0.996	0.23	0.996	0.53	0.996	0.24	22.2
0.05	0.996	0.25	0.996	0.57	0.995	0.28	22.2
0.07	0.996	0.27	0.995	0.60	0.995	0.32	22.2
0.08	0.996	0.28	0.995	0.63	0.995	0.41	22.3
0.10	0.996	0.30	0.996	0.67	0.995	0.49	22.3
0.12	0.996	0.32	0.996	0.73	0.995	0.57	22.4
0.13	0.996	0.33	0.996	0.80	0.995	0.66	22.2
0.15	0.996	0.37	0.995	0.87	0.995	0.74	22.3
0.17	0.996	0.40	0.995	0.93	1.011	0.82	22.3
0.18	0.996	0.43	0.995	0.95	1.034	0.91	22.3
						0.99	22.0
h_{avg} (μm) =		2354				1.00	22.0

Table C.134: Experimental data for $\mu = 0.048$ N·s/m^2, $h_o = 2.622$ mm, $\Delta T_s = 0.1$°C.

r'	h / h_{avg}	r'	h / h_{avg}	r'	h / h_{avg}	r'	T_s (°C)
0.00	0.994	0.20	0.995	0.47	0.995	0.16	23.0
0.02	0.994	0.22	0.995	0.50	0.995	0.20	23.0
0.03	0.994	0.23	0.995	0.53	0.995	0.24	23.0
0.05	0.994	0.25	0.995	0.57	0.994	0.28	23.0
0.07	0.995	0.27	0.995	0.60	0.995	0.32	23.0
0.08	0.995	0.28	0.995	0.63	0.995	0.41	23.0
0.10	0.994	0.30	0.995	0.67	0.995	0.49	23.1
0.12	0.994	0.32	0.995	0.73	0.995	0.57	23.1
0.13	0.994	0.33	0.995	0.80	0.994	0.66	23.0
0.15	0.995	0.37	0.995	0.87	0.995	0.74	23.1
0.17	0.995	0.40	0.995	0.93	1.008	0.82	23.1
0.18	0.995	0.43	0.994	0.95	1.029	0.91	23.1
				0.96	1.050	0.99	22.9
h_{avg} (μm) =		2636				1.00	22.9

Table C.135: Experimental data for $\mu = 0.048$ N·s/m^2, $h_o = 2.622$ mm, $\Delta T_s = 12.1$°C.

r'	h / h_{avg}	r'	h / h_{avg}	r'	h / h_{avg}	r'	T_s (°C)
0.00	0.981	0.20	0.986	0.47	0.991	0.16	29.3
0.02	0.981	0.22	0.986	0.50	0.992	0.20	27.8
0.03	0.982	0.23	0.986	0.53	0.992	0.24	26.7
0.05	0.982	0.25	0.987	0.57	0.993	0.28	25.5
0.07	0.983	0.27	0.987	0.60	0.993	0.32	24.7
0.08	0.983	0.28	0.988	0.63	0.994	0.41	23.2
0.10	0.983	0.30	0.988	0.67	0.995	0.49	22.1
0.12	0.984	0.32	0.988	0.73	0.996	0.57	21.2
0.13	0.984	0.33	0.988	0.80	0.996	0.66	20.0
0.15	0.985	0.37	0.989	0.87	0.998	0.74	19.4
0.17	0.985	0.40	0.990	0.93	1.012	0.82	18.6
0.18	0.985	0.43	0.991	0.95	1.034	0.91	17.9
				0.96	1.056	0.99	17.3
h_{avg} (μm) =		2608				1.00	17.3

Table C.136: Experimental data for $\mu = 0.048$ N·s/m^2, $h_o = 2.622$ mm, $\Delta T_s = 21.6$°C.

r'	h / h_{avg}	r'	h / h_{avg}	r'	h / h_{avg}	r'	T_s (°C)
0.00	0.974	0.20	0.981	0.47	0.989	0.16	40.0
0.02	0.974	0.22	0.981	0.50	0.990	0.20	37.3
0.03	0.974	0.23	0.982	0.53	0.991	0.24	35.1
0.05	0.975	0.25	0.982	0.57	0.992	0.28	33.0
0.07	0.976	0.27	0.983	0.60	0.993	0.32	31.6
0.08	0.977	0.28	0.984	0.63	0.994	0.41	28.7
0.10	0.977	0.30	0.984	0.67	0.995	0.49	26.6
0.12	0.978	0.32	0.985	0.73	0.996	0.57	25.0
0.13	0.979	0.33	0.985	0.80	0.998	0.66	23.2
0.15	0.979	0.37	0.986	0.87	0.999	0.74	22.0
0.17	0.979	0.40	0.987	0.93	1.014	0.82	20.7
0.18	0.980	0.43	0.988	0.95	1.035	0.91	19.5
				0.96	1.057	0.99	18.4
h_{avg} (μm) =		2624				1.00	18.4

Table C.137: Experimental data for $\mu = 0.048$ N·s/m^2, $h_o = 2.622$ mm, $\Delta T_s = 28.9$°C.

r'	h / h_{avg}	r'	h / h_{avg}	r'	h / h_{avg}	r'	T_s (°C)
0.00	0.970	0.20	0.979	0.47	0.988	0.16	48.6
0.02	0.970	0.22	0.979	0.50	0.990	0.20	44.9
0.03	0.971	0.23	0.980	0.53	0.991	0.24	41.9
0.05	0.972	0.25	0.981	0.57	0.992	0.28	39.0
0.07	0.973	0.27	0.981	0.60	0.993	0.32	37.2
0.08	0.974	0.28	0.982	0.63	0.994	0.41	33.3
0.10	0.974	0.30	0.982	0.67	0.995	0.49	30.4
0.12	0.975	0.32	0.983	0.73	0.997	0.57	28.2
0.13	0.976	0.33	0.984	0.80	0.998	0.66	26.0
0.15	0.977	0.37	0.985	0.87	1.001	0.74	24.3
0.17	0.977	0.40	0.986	0.93	1.015	0.82	22.6
0.18	0.978	0.43	0.987	0.95	1.036	0.91	21.0
				0.96	1.058	0.99	19.7
h_{avg} (μm) =		2632				1.00	19.7

Table C.138: Experimental data for $\mu = 0.048$ N·s/m^2, $h_o = 2.622$ mm, $\Delta T_s = 36.3$°C.

r'	h / h_{avg}	r'	h / h_{avg}	r'	h / h_{avg}	r'	T_s (°C)
0.00	0.966	0.20	0.977	0.47	0.987	0.16	57.2
0.02	0.966	0.22	0.978	0.50	0.989	0.20	52.5
0.03	0.967	0.23	0.978	0.53	0.990	0.24	48.7
0.05	0.969	0.25	0.979	0.57	0.991	0.28	45.1
0.07	0.970	0.27	0.980	0.60	0.993	0.32	42.7
0.08	0.971	0.28	0.980	0.63	0.994	0.41	37.8
0.10	0.972	0.30	0.981	0.67	0.995	0.49	34.3
0.12	0.973	0.32	0.982	0.73	0.997	0.57	31.5
0.13	0.974	0.33	0.982	0.80	0.999	0.66	28.7
0.15	0.974	0.37	0.984	0.87	1.001	0.74	26.6
0.17	0.975	0.40	0.985	0.93	1.016	0.82	24.5
0.18	0.976	0.43	0.987	0.95	1.037	0.91	22.6
				0.96	1.058	0.99	20.9
h_{avg} (μm) =		2645				1.00	20.9

Table C.139: Experimental data for $\mu = 0.048$ N·s/m^2, $h_o = 2.622$ mm, $\Delta T_s = 42.3$°C.

r'	h / h_{avg}	r'	h / h_{avg}	r'	h / h_{avg}	r'	T_s (°C)
0.00	0.966	0.20	0.975	0.47	0.987	0.16	64.1
0.02	0.966	0.22	0.975	0.50	0.988	0.20	58.7
0.03	0.966	0.23	0.976	0.53	0.990	0.24	54.2
0.05	0.967	0.25	0.977	0.57	0.991	0.28	49.9
0.07	0.968	0.27	0.978	0.60	0.993	0.32	47.2
0.08	0.969	0.28	0.979	0.63	0.994	0.41	41.4
0.10	0.969	0.30	0.979	0.67	0.995	0.49	37.3
0.12	0.970	0.32	0.980	0.73	0.997	0.57	34.1
0.13	0.971	0.33	0.981	0.80	1.000	0.66	30.9
0.15	0.972	0.37	0.983	0.87	1.002	0.74	28.4
0.17	0.973	0.40	0.984	0.93	1.017	0.82	26.0
0.18	0.974	0.43	0.985	0.95	1.037	0.91	23.8
				0.96	1.058	0.99	21.9
h_{avg} (μm) =		2660				1.00	21.9

Table C.140: Experimental data for $\mu = 0.048$ N·s/m^2, $h_o = 2.991$ mm, $\Delta T_s = 0.2$°C.

r'	h / h_{avg}	r'	h / h_{avg}	r'	h / h_{avg}	r'	T_s (°C)
0.00	0.992	0.20	0.996	0.47	0.996	0.00	23.2
0.02	0.992	0.22	0.995	0.50	0.995	0.16	23.2
0.03	0.995	0.23	0.995	0.53	0.995	0.20	23.2
0.05	0.995	0.25	0.996	0.57	0.995	0.24	23.3
0.07	0.995	0.27	0.995	0.60	0.995	0.28	23.3
0.08	0.995	0.28	0.995	0.63	0.995	0.32	23.4
0.10	0.995	0.30	0.995	0.67	0.996	0.41	23.5
0.12	0.995	0.32	0.995	0.73	0.995	0.49	23.5
0.13	0.995	0.33	0.995	0.80	0.995	0.57	23.5
0.15	0.996	0.37	0.996	0.87	0.995	0.66	23.4
0.17	0.996	0.40	0.996	0.93	1.007	0.74	23.4
0.18	0.995	0.43	0.996	0.95	1.025	0.82	23.4
				0.96	1.043	0.91	23.5
h_{avg} (μm) =		3005				1.00	23.5

Table C.141: Experimental data for $\mu = 0.048$ N·s/m^2, $h_o = 2.991$ mm, $\Delta T_s = 12.3$°C.

r'	h / h_{avg}	r'	h / h_{avg}	r'	h / h_{avg}	r'	T_s (°C)
0.00	0.984	0.20	0.988	0.47	0.993	0.16	29.6
0.02	0.984	0.22	0.988	0.50	0.993	0.20	28.1
0.03	0.984	0.23	0.988	0.53	0.994	0.24	26.9
0.05	0.985	0.25	0.989	0.57	0.994	0.28	25.7
0.07	0.985	0.27	0.989	0.60	0.994	0.32	24.9
0.08	0.985	0.28	0.989	0.63	0.995	0.41	23.4
0.10	0.986	0.30	0.990	0.67	0.995	0.49	22.2
0.12	0.986	0.32	0.990	0.73	0.996	0.57	21.3
0.13	0.986	0.33	0.990	0.80	0.997	0.66	20.1
0.15	0.987	0.37	0.991	0.87	0.997	0.74	19.4
0.17	0.987	0.40	0.991	0.93	1.011	0.82	18.7
0.18	0.987	0.43	0.992	0.95	1.029	0.91	17.9
				0.96	1.049	0.99	17.2
h_{avg} (μm) =		2945				1.00	17.2

Table C.142: Experimental data for $\mu = 0.048$ N·s/m^2, $h_o = 2.991$ mm, $\Delta T_s = 21.7$°C.

r'	h / h_{avg}	r'	h / h_{avg}	r'	h / h_{avg}	r'	T_s (°C)
0.00	0.982	0.20	0.988	0.47	0.995	0.16	40.2
0.02	0.982	0.22	0.988	0.50	0.996	0.20	37.5
0.03	0.982	0.23	0.989	0.53	0.996	0.24	35.3
0.05	0.983	0.25	0.989	0.57	0.997	0.28	33.2
0.07	0.983	0.27	0.990	0.60	0.998	0.32	31.8
0.08	0.984	0.28	0.990	0.63	0.999	0.41	28.9
0.10	0.985	0.30	0.990	0.67	1.000	0.49	26.8
0.12	0.985	0.32	0.991	0.73	1.001	0.57	25.1
0.13	0.986	0.33	0.991	0.80	1.002	0.66	23.4
0.15	0.986	0.37	0.992	0.87	1.003	0.74	22.1
0.17	0.986	0.40	0.993	0.93	1.006	0.82	20.8
0.18	0.987	0.43	0.994	0.95	1.009	0.91	19.6
				0.96	1.012	0.99	18.5
h_{avg} (μm) =		2944				1.00	18.5

Table C.143: Experimental data for $\mu = 0.048$ N·s/m^2, $h_o = 2.991$ mm, $\Delta T_s = 28.5$°C.

r'	h / h_{avg}	r'	h / h_{avg}	r'	h / h_{avg}	r'	T_s (°C)
0.00	0.974	0.20	0.981	0.47	0.990	0.16	48.0
0.02	0.974	0.22	0.982	0.50	0.991	0.20	44.4
0.03	0.975	0.23	0.982	0.53	0.992	0.24	41.4
0.05	0.975	0.25	0.983	0.57	0.993	0.28	38.6
0.07	0.976	0.27	0.984	0.60	0.994	0.32	36.8
0.08	0.977	0.28	0.984	0.63	0.994	0.41	33.0
0.10	0.978	0.30	0.985	0.67	0.995	0.49	30.2
0.12	0.978	0.32	0.985	0.73	0.997	0.57	28.0
0.13	0.979	0.33	0.986	0.80	0.998	0.66	25.8
0.15	0.979	0.37	0.987	0.87	1.000	0.74	24.1
0.17	0.980	0.40	0.988	0.93	1.014	0.82	22.4
0.18	0.981	0.43	0.989	0.95	1.032	0.91	20.9
				0.96	1.051	0.99	19.5
h_{avg} (μm) =		2964				1.00	19.5

Table C.144: Experimental data for $\mu = 0.048$ N·s/m^2, $h_o = 2.991$ mm, $\Delta T_s = 35.4$°C.

r'	h / h_{avg}	r'	h / h_{avg}	r'	h / h_{avg}	r'	T_s (°C)
0.00	0.972	0.20	0.980	0.47	0.989	0.16	55.9
0.02	0.972	0.22	0.980	0.50	0.990	0.20	51.4
0.03	0.972	0.23	0.981	0.53	0.992	0.24	47.7
0.05	0.973	0.25	0.982	0.57	0.993	0.28	44.1
0.07	0.974	0.27	0.982	0.60	0.994	0.32	41.8
0.08	0.975	0.28	0.983	0.63	0.994	0.41	37.1
0.10	0.976	0.30	0.984	0.67	0.995	0.49	33.6
0.12	0.976	0.32	0.984	0.73	0.997	0.57	30.9
0.13	0.977	0.33	0.985	0.80	0.999	0.66	28.2
0.15	0.978	0.37	0.986	0.87	1.001	0.74	26.1
0.17	0.978	0.40	0.987	0.93	1.014	0.82	24.1
0.18	0.979	0.43	0.988	0.95	1.033	0.91	22.3
				0.96	1.052	0.99	20.6
h_{avg} (μm) =		2969				1.00	20.6

Table C.145: Experimental data for $\mu = 0.048$ N·s/m^2, $h_o = 2.991$ mm, $\Delta T_s = 42.0$°C.

r'	h / h_{avg}	r'	h / h_{avg}	r'	h / h_{avg}	r'	T_s (°C)
0.00	0.970	0.20	0.978	0.47	0.988	0.16	64.0
0.02	0.970	0.22	0.979	0.50	0.990	0.20	58.6
0.03	0.970	0.23	0.979	0.53	0.991	0.24	54.1
0.05	0.972	0.25	0.980	0.57	0.992	0.28	49.8
0.07	0.972	0.27	0.981	0.60	0.993	0.32	47.1
0.08	0.973	0.28	0.982	0.63	0.994	0.41	41.4
0.10	0.974	0.30	0.982	0.67	0.995	0.49	37.2
0.12	0.974	0.32	0.983	0.73	0.997	0.57	34.1
0.13	0.975	0.33	0.984	0.80	0.999	0.66	30.9
0.15	0.975	0.37	0.985	0.87	1.002	0.74	28.4
0.17	0.976	0.40	0.986	0.93	1.015	0.82	26.0
0.18	0.978	0.43	0.987	0.95	1.033	0.91	23.8
				0.96	1.052	0.99	21.9
h_{avg} (μm) =		2981				1.00	21.9

Table C.146: Experimental data for $\mu = 0.048$ N·s/m^2, $h_o = 2.991$ mm, $\Delta T_s = 48.5$°C.

r'	h / h_{avg}	r'	h / h_{avg}	r'	h / h_{avg}	r'	T_s (°C)
0.00	0.967	0.20	0.977	0.47	0.988	0.16	71.3
0.02	0.967	0.22	0.977	0.50	0.990	0.20	65.1
0.03	0.968	0.23	0.978	0.53	0.991	0.24	59.9
0.05	0.969	0.25	0.979	0.57	0.992	0.28	55.0
0.07	0.971	0.27	0.979	0.60	0.993	0.32	51.8
0.08	0.972	0.28	0.980	0.63	0.994	0.41	45.2
0.10	0.972	0.30	0.981	0.67	0.995	0.49	40.4
0.12	0.973	0.32	0.982	0.73	0.998	0.57	36.8
0.13	0.973	0.33	0.983	0.80	1.000	0.66	33.2
0.15	0.973	0.37	0.984	0.87	1.002	0.74	30.4
0.17	0.975	0.40	0.986	0.93	1.015	0.82	27.6
0.18	0.976	0.43	0.987	0.95	1.033	0.91	25.0
				0.96	1.052	0.99	22.8
h_{avg} (μm) =		2991				1.00	22.8

Table C.147: Experimental data for $\mu = 0.048$ N·s/m^2, $h_o = 2.991$ mm, $\Delta T_s = 0.1$°C.

r'	h / h_{avg}	r'	h / h_{avg}	r'	h / h_{avg}	r'	T_s (°C)
0.00	0.994	0.20	0.995	0.47	0.995	0.16	21.7
0.02	0.994	0.22	0.995	0.50	0.995	0.20	21.7
0.03	0.994	0.23	0.995	0.53	0.995	0.24	21.7
0.05	0.995	0.25	0.995	0.57	0.995	0.28	21.8
0.07	0.995	0.27	0.995	0.60	0.995	0.32	21.7
0.08	0.995	0.28	0.996	0.63	0.995	0.41	21.8
0.10	0.995	0.30	0.996	0.67	0.995	0.49	21.9
0.12	0.995	0.32	0.995	0.73	0.995	0.57	21.9
0.13	0.995	0.33	0.996	0.80	0.995	0.66	21.7
0.15	0.995	0.37	0.996	0.87	0.995	0.74	21.8
0.17	0.995	0.40	0.995	0.93	1.008	0.82	21.8
0.18	0.995	0.43	0.995	0.95	1.025	0.91	21.9
				0.96	1.044	0.99	21.7
h_{avg} (μm) =		3005				1.00	21.7

Table C.148: Experimental data for $\mu = 0.048$ N·s/m^2, $h_o = 2.991$ mm, $\Delta T_s = 11.7$°C.

r'	h / h_{avg}	r'	h / h_{avg}	r'	h / h_{avg}	r'	T_s (°C)
0.00	0.985	0.20	0.988	0.47	0.993	0.16	28.8
0.02	0.985	0.22	0.989	0.50	0.993	0.20	27.4
0.03	0.986	0.23	0.989	0.53	0.994	0.24	26.2
0.05	0.986	0.25	0.989	0.57	0.994	0.28	25.1
0.07	0.986	0.27	0.990	0.60	0.994	0.32	24.4
0.08	0.986	0.28	0.990	0.63	0.995	0.41	22.9
0.10	0.987	0.30	0.990	0.67	0.996	0.49	21.8
0.12	0.987	0.32	0.991	0.73	0.996	0.57	20.9
0.13	0.987	0.33	0.991	0.80	0.997	0.66	19.8
0.15	0.988	0.37	0.991	0.87	0.997	0.74	19.2
0.17	0.988	0.40	0.992	0.93	1.010	0.82	18.5
0.18	0.988	0.43	0.992	0.95	1.029	0.91	17.8
				0.96	1.048	0.99	17.1
h_{avg} (μm) =		2983				1.00	17.1

Table C.149: Experimental data for $\mu = 0.048$ N·s/m^2, $h_o = 2.991$ mm, $\Delta T_s = 21.3$°C.

r'	h / h_{avg}	r'	h / h_{avg}	r'	h / h_{avg}	r'	T_s (°C)
0.00	0.982	0.20	0.985	0.47	0.992	0.16	39.8
0.02	0.981	0.22	0.986	0.50	0.992	0.20	37.1
0.03	0.982	0.23	0.986	0.53	0.993	0.24	34.9
0.05	0.982	0.25	0.987	0.57	0.993	0.28	32.8
0.07	0.982	0.27	0.987	0.60	0.994	0.32	31.4
0.08	0.983	0.28	0.987	0.63	0.995	0.41	28.6
0.10	0.983	0.30	0.988	0.67	0.995	0.49	26.5
0.12	0.983	0.32	0.988	0.73	0.996	0.57	24.9
0.13	0.984	0.33	0.988	0.80	0.998	0.66	23.2
0.15	0.984	0.37	0.989	0.87	0.999	0.74	22.0
0.17	0.985	0.40	0.990	0.93	1.012	0.82	20.7
0.18	0.985	0.43	0.991	0.95	1.030	0.91	19.5
				0.96	1.048	0.99	18.4
h_{avg} (μm) =		3003				1.00	18.4

Table C.150: Experimental data for $\mu = 0.048$ N·s/m^2, $h_o = 2.991$ mm, $\Delta T_s = 28.7$°C.

r'	h / h_{avg}	r'	h / h_{avg}	r'	h / h_{avg}	r'	T_s (°C)
0.00	0.978	0.20	0.984	0.47	0.991	0.16	48.3
0.02	0.978	0.22	0.984	0.50	0.991	0.20	44.6
0.03	0.978	0.23	0.985	0.53	0.992	0.24	41.6
0.05	0.979	0.25	0.985	0.57	0.993	0.28	38.8
0.07	0.980	0.27	0.985	0.60	0.994	0.32	36.9
0.08	0.980	0.28	0.986	0.63	0.995	0.41	33.0
0.10	0.981	0.30	0.986	0.67	0.995	0.49	30.2
0.12	0.981	0.32	0.987	0.73	0.997	0.57	28.1
0.13	0.982	0.33	0.987	0.80	0.998	0.66	25.8
0.15	0.982	0.37	0.988	0.87	1.000	0.74	24.2
0.17	0.983	0.40	0.989	0.93	1.012	0.82	22.5
0.18	0.983	0.43	0.990	0.95	1.031	0.91	21.0
				0.96	1.049	0.99	19.6
h_{avg} (μm) =		3016				1.00	19.6

Table C.151: Experimental data for $\mu = 0.048$ N·s/m^2, $h_o = 2.991$ mm, $\Delta T_s = 35.8$°C.

r'	h / h_{avg}	r'	h / h_{avg}	r'	h / h_{avg}	r'	T_s (°C)
0.00	0.973	0.20	0.981	0.47	0.990	0.16	56.3
0.02	0.973	0.22	0.982	0.50	0.991	0.20	51.7
0.03	0.974	0.23	0.982	0.53	0.992	0.24	48.0
0.05	0.975	0.25	0.983	0.57	0.993	0.28	44.3
0.07	0.976	0.27	0.984	0.60	0.994	0.32	42.0
0.08	0.977	0.28	0.984	0.63	0.995	0.41	37.2
0.10	0.977	0.30	0.985	0.67	0.995	0.49	33.7
0.12	0.978	0.32	0.985	0.73	0.997	0.57	31.0
0.13	0.979	0.33	0.986	0.80	0.999	0.66	28.3
0.15	0.979	0.37	0.987	0.87	1.001	0.74	26.2
0.17	0.980	0.40	0.988	0.93	1.013	0.82	24.1
0.18	0.981	0.43	0.989	0.95	1.031	0.91	22.3
				0.96	1.049	0.99	20.6
h_{avg} (μm) =		3017				1.00	20.6

Table C.152: Experimental data for $\mu = 0.048$ N·s/m^2, $h_o = 2.985$ mm, $\Delta T_s = 0.1$°C.

r'	h / h_{avg}	r'	h / h_{avg}	r'	h / h_{avg}	r'	T_s (°C)
0.00	0.995	0.20	0.996	0.47	0.996	0.16	21.4
0.02	0.995	0.22	0.996	0.50	0.996	0.20	21.4
0.03	0.995	0.23	0.996	0.53	0.995	0.24	21.4
0.05	0.995	0.25	0.996	0.57	0.996	0.28	21.4
0.07	0.995	0.27	0.996	0.60	0.995	0.32	21.4
0.08	0.995	0.28	0.996	0.63	0.995	0.41	21.4
0.10	0.995	0.30	0.996	0.67	0.995	0.49	21.5
0.12	0.995	0.32	0.996	0.73	0.995	0.57	21.5
0.13	0.996	0.33	0.996	0.80	0.995	0.66	21.4
0.15	0.995	0.37	0.996	0.87	0.995	0.74	21.5
0.17	0.995	0.40	0.996	0.93	1.007	0.82	21.5
0.18	0.995	0.43	0.996	0.95	1.025	0.91	21.5
				0.96	1.043	0.99	21.3
h_{avg} (μm) =		2999				1.00	21.3

Table C.153: Experimental data for $\mu = 0.048$ N·s/m^2, $h_o = 2.985$ mm, $\Delta T_s = 11.8$°C.

r'	h / h_{avg}	r'	h / h_{avg}	r'	h / h_{avg}	r'	T_s (°C)
0.00	0.987	0.20	0.990	0.47	0.994	0.16	29.0
0.02	0.987	0.22	0.990	0.50	0.994	0.20	27.5
0.03	0.987	0.23	0.991	0.53	0.994	0.24	26.3
0.05	0.988	0.25	0.991	0.57	0.994	0.28	25.2
0.07	0.988	0.27	0.991	0.60	0.995	0.32	24.4
0.08	0.988	0.28	0.991	0.63	0.995	0.41	22.9
0.10	0.988	0.30	0.991	0.67	0.995	0.49	21.8
0.12	0.989	0.32	0.992	0.73	0.996	0.57	20.9
0.13	0.989	0.33	0.992	0.80	0.996	0.66	19.9
0.15	0.989	0.37	0.992	0.87	0.997	0.74	19.2
0.17	0.990	0.40	0.993	0.93	1.010	0.82	18.5
0.18	0.990	0.43	0.993	0.95	1.028	0.91	17.8
				0.96	1.046	0.99	17.1
h_{avg} (μm) =		2979				1.00	17.1

Table C.154: Experimental data for $\mu = 0.048$ N·s/m^2, $h_o = 2.985$ mm, $\Delta T_s = 15.2$°C.

r'	h / h_{avg}	r'	h / h_{avg}	r'	h / h_{avg}	r'	T_s (°C)
0.00	0.985	0.20	0.988	0.47	0.993	0.16	32.7
0.02	0.985	0.22	0.989	0.50	0.993	0.20	30.8
0.03	0.985	0.23	0.989	0.53	0.993	0.24	29.2
0.05	0.986	0.25	0.989	0.57	0.994	0.28	27.7
0.07	0.986	0.27	0.990	0.60	0.994	0.32	26.8
0.08	0.987	0.28	0.990	0.63	0.995	0.41	24.8
0.10	0.987	0.30	0.990	0.67	0.995	0.49	23.3
0.12	0.987	0.32	0.990	0.73	0.996	0.57	22.2
0.13	0.987	0.33	0.991	0.80	0.997	0.66	20.9
0.15	0.987	0.37	0.991	0.87	0.998	0.74	20.0
0.17	0.988	0.40	0.992	0.93	1.010	0.82	19.2
0.18	0.988	0.43	0.992	0.95	1.029	0.91	18.3
				0.96	1.047	0.99	17.5
h_{avg} (μm) =		2986				1.00	17.5

Table C.155: Experimental data for $\mu = 0.048$ N·s/m^2, $h_o = 2.985$ mm, $\Delta T_s = 21.4$°C.

r'	h / h_{avg}	r'	h / h_{avg}	r'	h / h_{avg}	r'	T_s (°C)
0.00	0.982	0.20	0.987	0.47	0.992	0.16	39.8
0.02	0.982	0.22	0.987	0.50	0.992	0.20	37.2
0.03	0.982	0.23	0.988	0.53	0.993	0.24	35.0
0.05	0.983	0.25	0.988	0.57	0.993	0.28	32.8
0.07	0.983	0.27	0.988	0.60	0.994	0.32	31.4
0.08	0.984	0.28	0.988	0.63	0.994	0.41	28.6
0.10	0.984	0.30	0.989	0.67	0.995	0.49	26.5
0.12	0.985	0.32	0.989	0.73	0.996	0.57	24.9
0.13	0.985	0.33	0.989	0.80	0.997	0.66	23.2
0.15	0.986	0.37	0.990	0.87	0.999	0.74	21.9
0.17	0.986	0.40	0.991	0.93	1.012	0.82	20.7
0.18	0.986	0.43	0.991	0.95	1.030	0.91	19.6
				0.96	1.048	0.99	18.4
h_{avg} (μm) =		2996				1.00	18.4

Table C.156: Experimental data for $\mu = 0.048$ N·s/m^2, $h_o = 2.985$ mm, $\Delta T_s = 24.7$°C.

r'	h / h_{avg}	r'	h / h_{avg}	r'	h / h_{avg}	r'	T_s (°C)
0.00	0.980	0.20	0.986	0.47	0.991	0.16	43.6
0.02	0.980	0.22	0.986	0.50	0.992	0.20	40.5
0.03	0.981	0.23	0.987	0.53	0.993	0.24	37.9
0.05	0.981	0.25	0.987	0.57	0.993	0.28	35.4
0.07	0.982	0.27	0.987	0.60	0.994	0.32	33.8
0.08	0.983	0.28	0.988	0.63	0.994	0.41	30.5
0.10	0.983	0.30	0.988	0.67	0.995	0.49	28.1
0.12	0.984	0.32	0.989	0.73	0.996	0.57	26.2
0.13	0.984	0.33	0.989	0.80	0.998	0.66	24.3
0.15	0.985	0.37	0.990	0.87	0.999	0.74	22.9
0.17	0.985	0.40	0.990	0.93	1.012	0.82	21.5
0.18	0.985	0.43	0.991	0.95	1.030	0.91	20.2
				0.96	1.048	0.99	19.0
h_{avg} (μm) =		3003				1.00	19.0

Table C.157: Experimental data for $\mu = 0.048$ N·s/m^2, $h_o = 2.985$ mm, $\Delta T_s = 28.6$°C.

r'	h / h_{avg}	r'	h / h_{avg}	r'	h / h_{avg}	r'	T_s (°C)
0.00	0.987	0.20	0.992	0.47	0.999	0.16	48.2
0.02	0.987	0.22	0.993	0.50	0.999	0.20	44.5
0.03	0.987	0.23	0.993	0.53	1.000	0.24	41.5
0.05	0.988	0.25	0.994	0.57	1.001	0.28	38.6
0.07	0.989	0.27	0.994	0.60	1.001	0.32	36.7
0.08	0.989	0.28	0.995	0.63	1.002	0.41	32.9
0.10	0.989	0.30	0.995	0.67	1.003	0.49	30.1
0.12	0.990	0.32	0.996	0.73	1.004	0.57	28.0
0.13	0.991	0.33	0.996	0.80	1.005	0.66	25.7
0.15	0.991	0.37	0.996	0.87	1.006	0.74	24.1
0.17	0.991	0.40	0.997	0.93	1.019	0.82	22.4
0.18	0.992	0.43	0.998	0.95	1.037	0.91	20.9
				0.96	1.055	0.99	19.6
h_{avg} (μm) =		3007				1.00	19.6

Table C.158: Experimental data for $\mu = 0.048$ N·s/m^2, $h_o = 2.985$ mm, $\Delta T_s = 31.4$°C.

r'	h / h_{avg}	r'	h / h_{avg}	r'	h / h_{avg}	r'	T_s (°C)
0.00	0.978	0.20	0.985	0.47	0.992	0.16	51.3
0.02	0.979	0.22	0.986	0.50	0.992	0.20	47.2
0.03	0.979	0.23	0.986	0.53	0.993	0.24	43.8
0.05	0.979	0.25	0.986	0.57	0.993	0.28	40.6
0.07	0.980	0.27	0.987	0.60	0.994	0.32	38.5
0.08	0.981	0.28	0.987	0.63	0.995	0.41	34.3
0.10	0.982	0.30	0.988	0.67	0.996	0.49	31.2
0.12	0.983	0.32	0.988	0.73	0.997	0.57	28.8
0.13	0.983	0.33	0.989	0.80	0.998	0.66	26.4
0.15	0.983	0.37	0.989	0.87	0.999	0.74	24.6
0.17	0.984	0.40	0.990	0.93	1.012	0.82	22.9
0.18	0.985	0.43	0.991	0.95	1.029	0.91	21.3
				0.96	1.047	0.99	19.8
h_{avg} (μm) =		3010				1.00	19.8

Table C.159: Experimental data for $\mu = 0.048$ N·s/m^2, $h_o = 2.985$ mm, $\Delta T_s = 35.2$°C.

r'	h / h_{avg}	r'	h / h_{avg}	r'	h / h_{avg}	r'	T_s (°C)
0.00	0.980	0.20	0.984	0.47	0.991	0.16	56.0
0.02	0.979	0.22	0.984	0.50	0.992	0.20	51.4
0.03	0.979	0.23	0.985	0.53	0.992	0.24	47.7
0.05	0.980	0.25	0.985	0.57	0.993	0.28	44.1
0.07	0.981	0.27	0.986	0.60	0.994	0.32	41.8
0.08	0.981	0.28	0.986	0.63	0.995	0.41	37.0
0.10	0.981	0.30	0.987	0.67	0.996	0.49	33.6
0.12	0.982	0.32	0.987	0.73	0.997	0.57	30.9
0.13	0.982	0.33	0.987	0.80	0.998	0.66	28.2
0.15	0.982	0.37	0.988	0.87	1.000	0.74	26.2
0.17	0.983	0.40	0.989	0.93	1.012	0.82	24.2
0.18	0.983	0.43	0.990	0.95	1.030	0.91	22.3
				0.96	1.048	0.99	20.7
h_{avg} (μm) =		3018				1.00	20.7

Table C.160: Experimental data for $\mu = 0.048$ N·s/m^2, $h_o = 2.985$ mm, $\Delta T_s = 0.1$°C.

r'	h / h_{avg}	r'	h / h_{avg}	r'	h / h_{avg}	r'	T_s (°C)
0.00	0.997	0.22	0.997	0.50	0.996	0.16	21.4
0.02	0.997	0.23	0.997	0.53	0.996	0.20	21.4
0.03	0.997	0.25	0.997	0.57	0.995	0.24	21.4
0.05	0.997	0.27	0.997	0.60	0.996	0.28	21.4
0.07	0.997	0.28	0.997	0.63	0.995	0.32	21.4
0.10	0.998	0.30	0.996	0.67	0.995	0.41	21.4
0.12	0.998	0.32	0.997	0.73	0.995	0.49	21.5
0.13	0.998	0.33	0.996	0.80	0.995	0.57	21.5
0.15	0.997	0.37	0.997	0.87	0.995	0.66	21.4
0.17	0.997	0.40	0.996	0.93	1.007	0.74	21.5
0.18	0.997	0.43	0.996	0.95	1.025	0.82	21.5
0.20	0.997	0.47	0.996	0.96	1.043	0.91	21.5
						0.99	21.3
h_{avg} (μm) =		2990				1.00	21.3

Table C.161: Experimental data for $\mu = 0.048$ N·s/m^2, $h_o = 2.991$ mm, $\Delta T_s = 0.1$°C.

r'	h / h_{avg}	r'	h / h_{avg}	r'	h / h_{avg}	r'	T_s (°C)
0.00	0.995	0.20	0.995	0.47	0.995	0.16	21.0
0.02	0.995	0.22	0.995	0.50	0.995	0.20	20.9
0.03	0.995	0.23	0.995	0.53	0.995	0.24	20.9
0.05	0.995	0.25	0.995	0.57	0.995	0.28	21.0
0.07	0.995	0.27	0.995	0.60	0.995	0.32	20.9
0.08	0.995	0.28	0.995	0.63	0.995	0.41	21.0
0.10	0.995	0.30	0.995	0.67	0.995	0.49	21.1
0.12	0.995	0.32	0.995	0.73	0.995	0.57	21.1
0.13	0.995	0.33	0.995	0.80	0.995	0.66	21.0
0.15	0.995	0.37	0.995	0.87	0.996	0.74	21.0
0.17	0.995	0.40	0.995	0.93	1.008	0.82	21.1
0.18	0.995	0.43	0.995	0.95	1.025	0.91	21.0
				0.96	1.043	0.99	20.8
h_{avg} (μm) =		3006				1.00	20.8

Table C.162: Experimental data for $\mu = 0.048$ N·s/m^2, $h_o = 2.985$ mm, $\Delta T_s = 11.9$°C.

r'	h / h_{avg}	r'	h / h_{avg}	r'	h / h_{avg}	r'	T_s (°C)
0.00	0.986	0.20	0.990	0.47	0.993	0.16	29.0
0.02	0.986	0.22	0.990	0.50	0.993	0.20	27.5
0.03	0.987	0.23	0.990	0.53	0.994	0.24	26.3
0.05	0.987	0.25	0.990	0.57	0.994	0.28	25.2
0.07	0.988	0.27	0.991	0.60	0.994	0.32	24.4
0.08	0.988	0.28	0.991	0.63	0.995	0.41	22.9
0.10	0.988	0.30	0.991	0.67	0.995	0.49	21.7
0.12	0.988	0.32	0.991	0.73	0.996	0.57	20.8
0.13	0.989	0.33	0.991	0.80	0.996	0.66	19.7
0.15	0.989	0.37	0.992	0.87	0.998	0.74	19.1
0.17	0.989	0.40	0.992	0.93	1.010	0.82	18.4
0.18	0.990	0.43	0.993	0.95	1.028	0.91	17.7
				0.96	1.046	0.99	17.1
h_{avg} (μm) =		2982				1.00	17.1

Table C.163: Experimental data for $\mu = 0.048$ N·s/m^2, $h_o = 2.985$ mm, $\Delta T_s = 20.8$°C.

r'	h / h_{avg}	r'	h / h_{avg}	r'	h / h_{avg}	r'	T_s (°C)
0.00	0.983	0.20	0.988	0.47	0.992	0.16	39.1
0.02	0.983	0.22	0.988	0.50	0.993	0.20	36.4
0.03	0.983	0.23	0.988	0.53	0.993	0.24	34.3
0.05	0.984	0.25	0.988	0.57	0.994	0.28	32.2
0.07	0.985	0.27	0.989	0.60	0.994	0.32	30.9
0.08	0.985	0.28	0.989	0.63	0.995	0.41	28.1
0.10	0.986	0.30	0.990	0.67	0.995	0.49	26.1
0.12	0.986	0.32	0.990	0.73	0.996	0.57	24.6
0.13	0.986	0.33	0.990	0.80	0.997	0.66	22.9
0.15	0.986	0.37	0.991	0.87	0.998	0.74	21.7
0.17	0.987	0.40	0.991	0.93	1.011	0.82	20.5
0.18	0.987	0.43	0.992	0.95	1.029	0.91	19.4
				0.96	1.047	0.99	18.3
h_{avg} (μm) =		2991				1.00	18.3

Table C.164: Experimental data for $\mu = 0.048$ N·s/m^2, $h_o = 2.985$ mm, $\Delta T_s = 28.1$°C.

r'	h / h_{avg}	r'	h / h_{avg}	r'	h / h_{avg}	r'	T_s (°C)
0.00	0.982	0.20	0.986	0.47	0.992	0.16	47.6
0.02	0.982	0.22	0.987	0.50	0.992	0.20	43.9
0.03	0.982	0.23	0.987	0.53	0.993	0.24	41.0
0.05	0.982	0.25	0.987	0.57	0.994	0.28	38.2
0.07	0.983	0.27	0.988	0.60	0.994	0.32	36.4
0.08	0.983	0.28	0.988	0.63	0.995	0.41	32.6
0.10	0.984	0.30	0.988	0.67	0.995	0.49	29.8
0.12	0.985	0.32	0.989	0.73	0.996	0.57	27.7
0.13	0.985	0.33	0.989	0.80	0.998	0.66	25.5
0.15	0.985	0.37	0.990	0.87	0.999	0.74	23.9
0.17	0.986	0.40	0.990	0.93	1.011	0.82	22.3
0.18	0.986	0.43	0.991	0.95	1.029	0.91	20.8
				0.96	1.047	0.99	19.5
h_{avg} (μm) =		3009				1.00	19.5

Table C.165: Experimental data for $\mu = 0.048$ N·s/m^2, $h_o = 2.985$ mm, $\Delta T_s = 34.5$°C.

r'	h / h_{avg}	r'	h / h_{avg}	r'	h / h_{avg}	r'	T_s (°C)
0.00	0.979	0.20	0.985	0.47	0.991	0.16	55.0
0.02	0.978	0.22	0.985	0.50	0.992	0.20	50.6
0.03	0.979	0.23	0.986	0.53	0.992	0.24	46.9
0.05	0.980	0.25	0.986	0.57	0.993	0.28	43.4
0.07	0.981	0.27	0.986	0.60	0.994	0.32	41.2
0.08	0.981	0.28	0.987	0.63	0.995	0.41	36.5
0.10	0.982	0.30	0.987	0.67	0.995	0.49	33.1
0.12	0.983	0.32	0.987	0.73	0.996	0.57	30.5
0.13	0.983	0.33	0.988	0.80	0.998	0.66	27.9
0.15	0.983	0.37	0.989	0.87	1.000	0.74	25.9
0.17	0.984	0.40	0.989	0.93	1.012	0.82	24.0
0.18	0.984	0.43	0.990	0.95	1.029	0.91	22.2
				0.96	1.047	0.99	20.5
h_{avg} (μm) =		3009				1.00	20.5

Table C.166: Experimental data for $\mu = 0.048$ N·s/m^2, $h_o = 2.985$ mm, $\Delta T_s = 40.9$°C.

r'	h / h_{avg}	r'	h / h_{avg}	r'	h / h_{avg}	r'	T_s (°C)
0.00	0.979	0.20	0.983	0.47	0.990	0.16	62.3
0.02	0.978	0.22	0.983	0.50	0.991	0.20	57.0
0.03	0.978	0.23	0.984	0.53	0.992	0.24	52.6
0.05	0.979	0.25	0.985	0.57	0.993	0.28	48.4
0.07	0.980	0.27	0.985	0.60	0.994	0.32	45.8
0.08	0.981	0.28	0.986	0.63	0.994	0.41	40.2
0.10	0.982	0.30	0.986	0.67	0.996	0.49	36.2
0.12	0.982	0.32	0.987	0.73	0.997	0.57	33.1
0.13	0.982	0.33	0.987	0.80	0.998	0.66	30.1
0.15	0.982	0.37	0.988	0.87	1.000	0.74	27.7
0.17	0.982	0.40	0.989	0.93	1.013	0.82	25.4
0.18	0.982	0.43	0.990	0.95	1.030	0.91	23.4
				0.96	1.047	0.99	21.4
h_{avg} (μm) =		3016				1.00	21.4

Table C.167: Experimental data for $\mu = 0.048$ N·s/m^2, $h_o = 2.985$ mm, $\Delta T_s = 46.4$°C.

r'	h / h_{avg}	r'	h / h_{avg}	r'	h / h_{avg}	r'	T_s (°C)
0.00	0.977	0.20	0.982	0.47	0.991	0.16	68.9
0.02	0.977	0.22	0.983	0.50	0.991	0.20	62.9
0.03	0.976	0.23	0.983	0.53	0.992	0.24	57.9
0.05	0.977	0.25	0.984	0.57	0.993	0.28	53.2
0.07	0.979	0.27	0.985	0.60	0.994	0.32	50.1
0.08	0.980	0.28	0.985	0.63	0.995	0.41	43.8
0.10	0.980	0.30	0.985	0.67	0.995	0.49	39.3
0.12	0.981	0.32	0.986	0.73	0.997	0.57	35.8
0.13	0.982	0.33	0.986	0.80	0.999	0.66	32.5
0.15	0.981	0.37	0.987	0.87	1.000	0.74	29.7
0.17	0.981	0.40	0.988	0.93	1.013	0.82	27.1
0.18	0.982	0.43	0.990	0.95	1.029	0.91	24.7
				0.96	1.046	0.99	22.5
h_{avg} (μm) =		3019				1.00	22.5

Table C.168: Experimental data for $\mu = 0.192$ N·s/m^2, $h_o = 0.505$ mm, $\Delta T_s = 0.1$°C.

r'	h / h_{avg}	r'	h / h_{avg}	r'	h / h_{avg}	r'	T_s (°C)
0.00	0.965	0.20	0.965	0.47	0.966	0.16	22.8
0.02	0.965	0.22	0.965	0.50	0.966	0.20	22.7
0.03	0.965	0.23	0.966	0.53	0.966	0.24	22.7
0.05	0.966	0.25	0.966	0.57	0.965	0.28	22.7
0.07	0.965	0.27	0.965	0.60	0.965	0.32	22.7
0.08	0.966	0.28	0.966	0.63	0.966	0.41	22.7
0.10	0.966	0.30	0.965	0.67	0.966	0.49	22.8
0.12	0.966	0.32	0.966	0.73	0.965	0.57	22.8
0.13	0.966	0.33	0.966	0.80	0.965	0.66	22.7
0.15	0.965	0.37	0.966	0.87	0.968	0.74	22.8
0.17	0.965	0.40	0.965	0.93	1.053	0.82	22.8
0.18	0.965	0.43	0.966	0.95	1.185	0.91	22.8
				0.96	1.314	0.99	22.7
h_{avg} (μm) =		523				1.00	22.7

Table C.169: Experimental data for $\mu = 0.192$ N·s/m^2, $h_o = 0.505$ mm, $\Delta T_s = 6.9$°C.

r'	h / h_{avg}	r'	h / h_{avg}	r'	h / h_{avg}	r'	T_s (°C)
0.00	0.531	0.20	0.712	0.47	0.896	0.16	23.4
0.02	0.540	0.22	0.728	0.50	0.910	0.20	22.6
0.03	0.550	0.23	0.745	0.53	0.940	0.24	21.9
0.05	0.563	0.25	0.762	0.57	0.951	0.28	21.3
0.07	0.575	0.27	0.776	0.60	0.960	0.32	20.9
0.08	0.590	0.28	0.789	0.63	0.973	0.41	20.0
0.10	0.605	0.30	0.801	0.67	0.982	0.49	19.4
0.12	0.622	0.32	0.813	0.73	0.998	0.57	18.9
0.13	0.640	0.33	0.824	0.80	1.014	0.66	18.2
0.15	0.655	0.37	0.845	0.87	1.028	0.74	17.8
0.17	0.677	0.40	0.862	0.93	1.132	0.82	17.4
0.18	0.694	0.43	0.880	0.95	1.275	0.91	16.9
				0.96	1.440	0.99	16.5
h_{avg} (μm) =		500				1.00	16.5

Table C.170: Experimental data for $\mu = 0.192$ N·s/m^2, $h_o = 0.505$ mm, $\Delta T_s = 9.6$°C.

r'	h / h_{avg}	r'	h / h_{avg}	r'	h / h_{avg}	r'	T_s (°C)
0.00	0.137	0.20	0.584	0.47	0.885	0.16	26.4
0.02	0.123	0.22	0.616	0.50	0.906	0.20	25.3
0.03	0.130	0.23	0.645	0.53	0.924	0.24	24.3
0.05	0.169	0.25	0.671	0.57	0.942	0.28	23.4
0.07	0.455	0.27	0.696	0.60	0.958	0.32	22.8
0.08	0.320	0.28	0.719	0.63	0.973	0.41	21.6
0.10	0.364	0.30	0.739	0.67	0.986	0.49	20.7
0.12	0.405	0.32	0.759	0.73	1.010	0.57	20.0
0.13	0.442	0.33	0.778	0.80	1.034	0.66	19.1
0.15	0.480	0.37	0.809	0.87	1.059	0.74	18.5
0.17	0.517	0.40	0.837	0.93	1.167	0.82	18.0
0.18	0.552	0.43	0.862	0.95	1.313	0.91	17.4
				0.96	1.482	0.99	16.8
h_{avg} (μm) =		500				1.00	16.8

Table C.171: Experimental data for $\mu = 0.192$ N·s/m^2, $h_o = 0.732$ mm, $\Delta T_s = 0.1$°C.

r'	h / h_{avg}	r'	h / h_{avg}	r'	h / h_{avg}	r'	T_s (°C)
0.00	0.978	0.20	0.977	0.47	0.976	0.16	22.3
0.02	0.977	0.22	0.977	0.50	0.976	0.20	22.2
0.03	0.978	0.23	0.978	0.53	0.978	0.24	22.3
0.05	0.977	0.25	0.977	0.57	0.977	0.28	22.3
0.07	0.977	0.27	0.977	0.60	0.978	0.32	22.2
0.08	0.977	0.28	0.977	0.63	0.978	0.41	22.3
0.10	0.977	0.30	0.978	0.67	0.977	0.49	22.4
0.12	0.978	0.32	0.976	0.73	0.977	0.57	22.4
0.13	0.977	0.33	0.977	0.80	0.976	0.66	22.3
0.15	0.977	0.37	0.977	0.87	0.977	0.74	22.3
0.17	0.977	0.40	0.977	0.93	1.037	0.82	22.4
0.18	0.978	0.43	0.977	0.95	1.124	0.91	22.3
				0.96	1.209	0.99	22.2
h_{avg} (μm) =		749				1.00	22.2

Table C.172: Experimental data for $\mu = 0.192$ N·s/m^2, $h_o = 0.732$ mm, $\Delta T_s = 6.9$°C.

r'	h / h_{avg}	r'	h / h_{avg}	r'	h / h_{avg}	r'	T_s (°C)
0.00	0.812	0.20	0.877	0.47	0.951	0.16	23.3
0.02	0.815	0.22	0.882	0.50	0.957	0.20	22.5
0.03	0.819	0.23	0.889	0.53	0.963	0.24	21.9
0.05	0.824	0.25	0.893	0.57	0.968	0.28	21.2
0.07	0.829	0.27	0.900	0.60	0.973	0.32	20.8
0.08	0.834	0.28	0.906	0.63	0.978	0.41	20.0
0.10	0.838	0.30	0.911	0.67	0.981	0.49	19.3
0.12	0.843	0.32	0.915	0.73	0.987	0.57	18.8
0.13	0.849	0.33	0.921	0.80	0.994	0.66	18.1
0.15	0.856	0.37	0.930	0.87	1.003	0.74	17.8
0.17	0.863	0.40	0.937	0.93	1.074	0.82	17.3
0.18	0.869	0.43	0.944	0.95	1.167	0.91	16.9
				0.96	1.254	0.99	16.4
h_{avg} (μm) =		720				1.00	16.4

Table C.173: Experimental data for $\mu = 0.192$ N·s/m^2, $h_o = 0.732$ mm, $\Delta T_s = 10.1$°C.

r'	h / h_{avg}	r'	h / h_{avg}	r'	h / h_{avg}	r'	T_s (°C)
0.00	0.732	0.20	0.826	0.47	0.940	0.16	26.8
0.02	0.737	0.22	0.836	0.50	0.948	0.20	25.7
0.03	0.742	0.23	0.846	0.53	0.955	0.24	24.7
0.05	0.748	0.25	0.856	0.57	0.964	0.28	23.8
0.07	0.754	0.27	0.864	0.60	0.971	0.32	23.1
0.08	0.763	0.28	0.871	0.63	0.978	0.41	21.9
0.10	0.770	0.30	0.880	0.67	0.984	0.49	20.9
0.12	0.778	0.32	0.887	0.73	0.996	0.57	20.1
0.13	0.787	0.33	0.894	0.80	1.006	0.66	19.2
0.15	0.798	0.37	0.907	0.87	1.018	0.74	18.6
0.17	0.808	0.40	0.918	0.93	1.087	0.82	18.0
0.18	0.816	0.43	0.929	0.95	1.182	0.91	17.4
				0.96	1.270	0.99	16.8
h_{avg} (μm) =		723				1.00	16.8

Table C.174: Experimental data for $\mu = 0.192$ N·s/m^2, $h_o = 0.732$ mm, $\Delta T_s = 12.8$°C.

r'	h / h_{avg}	r'	h / h_{avg}	r'	h / h_{avg}	r'	T_s (°C)
0.00	0.652	0.20	0.778	0.47	0.929	0.16	30.0
0.02	0.656	0.22	0.792	0.50	0.940	0.20	28.5
0.03	0.664	0.23	0.805	0.53	0.951	0.24	27.2
0.05	0.672	0.25	0.818	0.57	0.961	0.28	26.0
0.07	0.680	0.27	0.829	0.60	0.970	0.32	25.2
0.08	0.689	0.28	0.840	0.63	0.979	0.41	23.5
0.10	0.700	0.30	0.850	0.67	0.987	0.49	22.3
0.12	0.712	0.32	0.860	0.73	1.002	0.57	21.3
0.13	0.725	0.33	0.870	0.80	1.016	0.66	20.1
0.15	0.736	0.37	0.886	0.87	1.031	0.74	19.4
0.17	0.750	0.40	0.903	0.93	1.103	0.82	18.6
0.18	0.764	0.43	0.916	0.95	1.195	0.91	17.9
				0.96	1.284	0.99	17.2
h_{avg} (μm) =		727				1.00	17.2

Table C.175: Experimental data for $\mu = 0.192$ N·s/m^2, $h_o = 0.732$ mm, $\Delta T_s = 17.5$°C.

r'	h / h_{avg}	r'	h / h_{avg}	r'	h / h_{avg}	r'	T_s (°C)
0.00	0.487	0.20	0.697	0.47	0.915	0.16	35.3
0.02	0.495	0.22	0.719	0.50	0.931	0.20	33.2
0.03	0.508	0.23	0.737	0.53	0.945	0.24	31.4
0.05	0.522	0.25	0.756	0.57	0.959	0.28	29.8
0.07	0.538	0.27	0.774	0.60	0.971	0.32	28.6
0.08	0.554	0.28	0.789	0.63	0.984	0.41	26.3
0.10	0.572	0.30	0.803	0.67	0.994	0.49	24.6
0.12	0.590	0.32	0.819	0.73	1.014	0.57	23.3
0.13	0.611	0.33	0.832	0.80	1.031	0.66	21.7
0.15	0.632	0.37	0.856	0.87	1.051	0.74	20.7
0.17	0.654	0.40	0.877	0.93	1.125	0.82	19.6
0.18	0.675	0.43	0.897	0.95	1.217	0.91	18.7
				0.96	1.304	0.99	17.7
h_{avg} (μm) =		732				1.00	17.7

Table C.176: Experimental data for $\mu = 0.192$ N·s/m^2, $h_o = 0.732$ mm, $\Delta T_s = 22.9$°C.

r'	h / h_{avg}	r'	h / h_{avg}	r'	h / h_{avg}	r'	T_s (°C)
0.00	0.104	0.20	0.594	0.47	0.901	0.16	41.3
0.02	0.092	0.22	0.625	0.50	0.923	0.20	38.6
0.03	0.102	0.23	0.656	0.53	0.942	0.24	36.4
0.05	0.209	0.25	0.682	0.57	0.959	0.28	34.1
0.07	0.268	0.27	0.708	0.60	0.975	0.32	32.7
0.08	0.317	0.28	0.731	0.63	0.990	0.41	29.6
0.10	0.363	0.30	0.752	0.67	1.004	0.49	27.3
0.12	0.405	0.32	0.772	0.73	1.028	0.57	25.5
0.13	0.442	0.33	0.791	0.80	1.052	0.66	23.6
0.15	0.482	0.37	0.824	0.87	1.074	0.74	22.2
0.17	0.520	0.40	0.852	0.93	1.152	0.82	20.8
0.18	0.559	0.43	0.879	0.95	1.244	0.91	19.6
				0.96	1.330	0.99	18.4
h_{avg} (μm) =		737				1.00	18.4

Table C.177: Experimental data for $\mu = 0.192$ N·s/m^2, $h_o = 0.732$ mm, $\Delta T_s = 0.1$°C.

r'	h / h_{avg}	r'	h / h_{avg}	r'	h / h_{avg}	r'	T_s (°C)
0.00	0.971	0.20	0.977	0.47	0.978	0.16	21.3
0.02	0.974	0.22	0.976	0.50	0.978	0.20	21.2
0.03	0.973	0.23	0.977	0.53	0.978	0.24	21.3
0.05	0.974	0.25	0.977	0.57	0.979	0.28	21.3
0.07	0.975	0.27	0.977	0.60	0.978	0.32	21.3
0.08	0.975	0.28	0.977	0.63	0.978	0.41	21.3
0.10	0.975	0.30	0.976	0.67	0.976	0.49	21.4
0.12	0.975	0.32	0.976	0.73	0.975	0.57	21.4
0.13	0.975	0.33	0.977	0.80	0.974	0.66	21.3
0.15	0.976	0.37	0.977	0.87	0.977	0.74	21.3
0.17	0.975	0.40	0.978	0.93	1.037	0.82	21.4
0.18	0.976	0.43	0.979	0.95	1.127	0.91	21.3
				0.96	1.212	0.99	21.2
h_{avg} (μm) =		740				1.00	21.2

Table C.178: Experimental data for $\mu = 0.192$ N·s/m^2, $h_o = 0.999$ mm, $\Delta T_s = 0.2$°C.

r'	h / h_{avg}	r'	h / h_{avg}	r'	h / h_{avg}	r'	T_s (°C)
0.00	0.983	0.20	0.983	0.47	0.983	0.16	21.6
0.02	0.984	0.22	0.983	0.50	0.983	0.20	21.5
0.03	0.983	0.23	0.983	0.53	0.983	0.24	21.5
0.05	0.984	0.25	0.983	0.57	0.983	0.28	21.5
0.07	0.983	0.27	0.984	0.60	0.983	0.32	21.5
0.08	0.983	0.28	0.983	0.63	0.984	0.41	21.6
0.10	0.983	0.30	0.983	0.67	0.983	0.49	21.6
0.12	0.983	0.32	0.983	0.73	0.983	0.57	21.7
0.13	0.983	0.33	0.983	0.80	0.984	0.66	21.5
0.15	0.983	0.37	0.983	0.87	0.985	0.74	21.6
0.17	0.984	0.40	0.983	0.93	1.027	0.82	21.6
0.18	0.984	0.43	0.983	0.95	1.087	0.91	21.6
				0.96	1.144	0.99	21.4
h_{avg} (μm) =		1016				1.00	21.4

Table C.179: Experimental data for $\mu = 0.192$ N·s/m^2, $h_o = 0.999$ mm, $\Delta T_s = 7.0$°C.

r'	h / h_{avg}	r'	h / h_{avg}	r'	h / h_{avg}	r'	T_s (°C)
0.00	0.898	0.20	0.929	0.47	0.966	0.16	23.6
0.02	0.899	0.22	0.933	0.50	0.970	0.20	22.8
0.03	0.901	0.23	0.935	0.53	0.973	0.24	22.1
0.05	0.904	0.25	0.938	0.57	0.976	0.28	21.5
0.07	0.906	0.27	0.941	0.60	0.979	0.32	21.0
0.08	0.909	0.28	0.944	0.63	0.981	0.41	20.2
0.10	0.911	0.30	0.947	0.67	0.984	0.49	19.5
0.12	0.914	0.32	0.949	0.73	0.989	0.57	19.0
0.13	0.917	0.33	0.951	0.80	0.992	0.66	18.2
0.15	0.920	0.37	0.956	0.87	0.997	0.74	17.9
0.17	0.922	0.40	0.960	0.93	1.054	0.82	17.5
0.18	0.926	0.43	0.964	0.95	1.107	0.91	17.0
				0.96	1.167	0.99	16.5
h_{avg} (μm) =		991				1.00	16.5

Table C.180: Experimental data for $\mu = 0.192$ N·s/m^2, $h_o = 0.999$ mm, $\Delta T_s = 13.0$°C.

r'	h / h_{avg}	r'	h / h_{avg}	r'	h / h_{avg}	r'	T_s (°C)
0.00	0.829	0.20	0.884	0.47	0.958	0.16	30.3
0.02	0.832	0.22	0.891	0.50	0.964	0.20	28.7
0.03	0.835	0.23	0.897	0.53	0.969	0.24	27.5
0.05	0.839	0.25	0.903	0.57	0.975	0.28	26.2
0.07	0.843	0.27	0.908	0.60	0.979	0.32	25.4
0.08	0.847	0.28	0.912	0.63	0.984	0.41	23.7
0.10	0.852	0.30	0.918	0.67	0.989	0.49	22.5
0.12	0.856	0.32	0.923	0.73	0.997	0.57	21.5
0.13	0.861	0.33	0.928	0.80	1.003	0.66	20.3
0.15	0.866	0.37	0.935	0.87	1.012	0.74	19.6
0.17	0.873	0.40	0.944	0.93	1.061	0.82	18.8
0.18	0.878	0.43	0.951	0.95	1.123	0.91	18.0
				0.96	1.182	0.99	17.3
h_{avg} (μm) =		997				1.00	17.3

Table C.181: Experimental data for $\mu = 0.192$ N·s/m^2, $h_o = 0.999$ mm, $\Delta T_s = 23.2$°C.

r'	h / h_{avg}	r'	h / h_{avg}	r'	h / h_{avg}	r'	T_s (°C)
0.00	0.703	0.20	0.807	0.47	0.941	0.16	41.7
0.02	0.709	0.22	0.819	0.50	0.951	0.20	38.9
0.03	0.715	0.23	0.830	0.53	0.960	0.24	36.6
0.05	0.721	0.25	0.841	0.57	0.969	0.28	34.4
0.07	0.728	0.27	0.851	0.60	0.977	0.32	32.9
0.08	0.736	0.28	0.861	0.63	0.985	0.41	29.8
0.10	0.743	0.30	0.871	0.67	0.993	0.49	27.5
0.12	0.752	0.32	0.879	0.73	1.008	0.57	25.7
0.13	0.762	0.33	0.888	0.80	1.020	0.66	23.8
0.15	0.773	0.37	0.902	0.87	1.032	0.74	22.4
0.17	0.783	0.40	0.917	0.93	1.085	0.82	20.9
0.18	0.796	0.43	0.929	0.95	1.148	0.91	19.7
				0.96	1.203	0.99	18.5
h_{avg} (μm) =		1005				1.00	18.5

Table C.182: Experimental data for $\mu = 0.192$ N·s/m^2, $h_o = 0.999$ mm, $\Delta T_s = 32.0$°C.

r'	h / h_{avg}	r'	h / h_{avg}	r'	h / h_{avg}	r'	T_s (°C)
0.00	0.573	0.20	0.734	0.47	0.926	0.16	51.7
0.02	0.580	0.22	0.752	0.50	0.940	0.20	47.9
0.03	0.589	0.23	0.768	0.53	0.954	0.24	44.7
0.05	0.596	0.25	0.783	0.57	0.966	0.28	41.5
0.07	0.609	0.27	0.799	0.60	0.977	0.32	39.5
0.08	0.623	0.28	0.812	0.63	0.988	0.41	35.2
0.10	0.634	0.30	0.825	0.67	0.999	0.49	32.0
0.12	0.648	0.32	0.839	0.73	1.017	0.57	29.4
0.13	0.662	0.33	0.851	0.80	1.033	0.66	26.8
0.15	0.679	0.37	0.874	0.87	1.048	0.74	24.8
0.17	0.697	0.40	0.893	0.93	1.103	0.82	22.9
0.18	0.714	0.43	0.910	0.95	1.190	0.91	21.2
				0.96	1.240	0.99	19.6
h_{avg} (μm) =		1016				1.00	19.6

Table C.183: Experimental data for $\mu = 0.192$ N·s/m^2, $h_o = 0.999$ mm, $\Delta T_s = 40.3$°C.

r'	h / h_{avg}	r'	h / h_{avg}	r'	h / h_{avg}	r'	T_s (°C)
0.00	0.415	0.20	0.663	0.47	0.916	0.16	61.0
0.02	0.427	0.22	0.686	0.50	0.933	0.20	56.2
0.03	0.442	0.23	0.710	0.53	0.950	0.24	52.2
0.05	0.460	0.25	0.731	0.57	0.965	0.28	48.3
0.07	0.477	0.27	0.751	0.60	0.980	0.32	45.7
0.08	0.497	0.28	0.771	0.63	0.993	0.41	40.2
0.10	0.519	0.30	0.788	0.67	1.005	0.49	36.2
0.12	0.538	0.32	0.805	0.73	1.028	0.57	32.9
0.13	0.562	0.33	0.821	0.80	1.048	0.66	29.7
0.15	0.588	0.37	0.848	0.87	1.067	0.74	27.2
0.17	0.612	0.40	0.873	0.93	1.123	0.82	24.7
0.18	0.637	0.43	0.895	0.95	1.185	0.91	22.5
				0.96	1.254	0.99	20.7
h_{avg} (μm) =		1024				1.00	20.7

Table C.184: Experimental data for $\mu = 0.192$ N·s/m^2, $h_o = 0.999$ mm, $\Delta T_s = 46.6$°C.

r'	h / h_{avg}	r'	h / h_{avg}	r'	h / h_{avg}	r'	T_s (°C)
0.00	0.212	0.20	0.599	0.47	0.908	0.16	68.1
0.02	0.224	0.22	0.633	0.50	0.929	0.20	62.6
0.03	0.253	0.23	0.661	0.53	0.948	0.24	57.9
0.05	0.289	0.25	0.687	0.57	0.966	0.28	53.3
0.07	0.322	0.27	0.710	0.60	0.982	0.32	50.3
0.08	0.356	0.28	0.735	0.63	0.996	0.41	44.0
0.10	0.392	0.30	0.756	0.67	1.010	0.49	39.2
0.12	0.429	0.32	0.777	0.73	1.036	0.57	35.5
0.13	0.463	0.33	0.795	0.80	1.059	0.66	31.7
0.15	0.500	0.37	0.828	0.87	1.080	0.74	28.8
0.17	0.531	0.40	0.858	0.93	1.139	0.82	25.9
0.18	0.566	0.43	0.884	0.95	1.222	0.91	23.5
				0.96	1.254	0.99	21.5
h_{avg} (μm) =		1030				1.00	21.5

Table C.185: Experimental data for $\mu = 0.192$ N·s/m^2, $h_o = 0.999$ mm, $\Delta T_s = 54.0$°C.

r'	h / h_{avg}	r'	h / h_{avg}	r'	h / h_{avg}	r'	T_s (°C)
0.00	0.083	0.20	0.536	0.47	0.903	0.16	76.6
0.02	0.069	0.22	0.577	0.50	0.928	0.20	70.3
0.03	0.065	0.23	0.611	0.53	0.948	0.24	64.9
0.05	0.064	0.25	0.647	0.57	0.968	0.28	59.6
0.07	0.066	0.27	0.676	0.60	0.986	0.32	56.1
0.08	0.063	0.28	0.703	0.63	1.004	0.41	48.8
0.10	0.072	0.30	0.729	0.67	1.018	0.49	43.3
0.12	0.210	0.32	0.753	0.73	1.046	0.57	38.9
0.13	0.301	0.33	0.774	0.80	1.072	0.66	34.7
0.15	0.372	0.37	0.811	0.87	1.096	0.74	31.2
0.17	0.434	0.40	0.848	0.93	1.157	0.82	27.9
0.18	0.488	0.43	0.878	0.95	1.238	0.91	25.0
				0.96	1.270	0.99	22.6
h_{avg} (μm) =		1035				1.00	22.6

Table C.186: Experimental data for $\mu = 0.192$ N·s/m^2, $h_o = 0.999$ mm, $\Delta T_s = 0.2$°C.

r'	h / h_{avg}	r'	h / h_{avg}	r'	h / h_{avg}	r'	T_s (°C)
0.00	0.978	0.20	0.982	0.47	0.987	0.16	21.3
0.02	0.985	0.22	0.983	0.50	0.987	0.20	21.3
0.03	0.980	0.23	0.984	0.53	0.985	0.24	21.3
0.05	0.980	0.25	0.984	0.57	0.986	0.28	21.3
0.07	0.980	0.27	0.984	0.60	0.987	0.32	21.3
0.08	0.981	0.28	0.985	0.63	0.987	0.41	21.3
0.10	0.981	0.30	0.983	0.67	0.987	0.49	21.4
0.12	0.982	0.32	0.986	0.73	0.987	0.57	21.4
0.13	0.981	0.33	0.986	0.80	0.987	0.66	21.3
0.15	0.982	0.37	0.986	0.87	0.988	0.74	21.3
0.17	0.981	0.40	0.987	0.93	1.031	0.82	21.4
0.18	0.983	0.43	0.987	0.95	1.091	0.91	21.3
						0.99	21.1
h_{avg} (μm) =		1006				1.00	21.1

Table C.187: Experimental data for $\mu = 0.192$ N·s/m^2, $h_o = 1.498$ mm, $\Delta T_s = 0.2$°C.

r'	h / h_{avg}	r'	h / h_{avg}	r'	h / h_{avg}	r'	T_s (°C)
0.00	0.989	0.20	0.991	0.47	0.990	0.16	21.2
0.02	0.990	0.22	0.991	0.50	0.990	0.20	21.2
0.03	0.990	0.23	0.991	0.53	0.990	0.24	21.2
0.05	0.990	0.25	0.991	0.57	0.990	0.28	21.2
0.07	0.990	0.27	0.991	0.60	0.990	0.32	21.2
0.08	0.990	0.28	0.991	0.63	0.989	0.41	21.2
0.10	0.991	0.30	0.990	0.67	0.989	0.49	21.3
0.12	0.990	0.32	0.991	0.73	0.990	0.57	21.3
0.13	0.990	0.33	0.991	0.80	0.989	0.66	21.2
0.15	0.991	0.37	0.990	0.87	0.989	0.74	21.2
0.17	0.990	0.40	0.991	0.93	1.017	0.82	21.2
0.18	0.991	0.43	0.990	0.95	1.054	0.91	21.2
				0.96	1.091	0.99	21.0
h_{avg} (μm) =		1513				1.00	21.0

Table C.188: Experimental data for $\mu = 0.192$ N·s/m^2, $h_o = 1.498$ mm, $\Delta T_s = 12.8$°C.

r'	h / h_{avg}	r'	h / h_{avg}	r'	h / h_{avg}	r'	T_s (°C)
0.00	0.937	0.20	0.954	0.47	0.981	0.16	30.0
0.02	0.938	0.22	0.956	0.50	0.982	0.20	28.5
0.03	0.938	0.23	0.958	0.53	0.984	0.24	27.2
0.05	0.939	0.25	0.960	0.57	0.986	0.28	26.0
0.07	0.940	0.27	0.963	0.60	0.988	0.32	25.2
0.08	0.941	0.28	0.964	0.63	0.990	0.41	23.6
0.10	0.943	0.30	0.966	0.67	0.992	0.49	22.3
0.12	0.944	0.32	0.968	0.73	0.994	0.57	21.3
0.13	0.946	0.33	0.970	0.80	0.997	0.66	20.2
0.15	0.948	0.37	0.972	0.87	1.001	0.74	19.4
0.17	0.949	0.40	0.976	0.93	1.029	0.82	18.7
0.18	0.952	0.43	0.978	0.95	1.069	0.91	17.9
				0.96	1.106	0.99	17.2
h_{avg} (μm) =		1497				1.00	17.2

Table C.189: Experimental data for $\mu = 0.192$ N·s/m^2, $h_o = 1.498$ mm, $\Delta T_s = 22.7$°C.

r'	h / h_{avg}	r'	h / h_{avg}	r'	h / h_{avg}	r'	T_s (°C)
0.00	0.892	0.20	0.924	0.47	0.973	0.16	41.1
0.02	0.894	0.22	0.928	0.50	0.977	0.20	38.4
0.03	0.896	0.23	0.932	0.53	0.981	0.24	36.1
0.05	0.898	0.25	0.935	0.57	0.984	0.28	33.9
0.07	0.900	0.27	0.939	0.60	0.987	0.32	32.5
0.08	0.902	0.28	0.943	0.63	0.990	0.41	29.4
0.10	0.904	0.30	0.946	0.67	0.993	0.49	27.2
0.12	0.907	0.32	0.949	0.73	0.998	0.57	25.4
0.13	0.910	0.33	0.952	0.80	1.003	0.66	23.5
0.15	0.913	0.37	0.958	0.87	1.008	0.74	22.1
0.17	0.916	0.40	0.964	0.93	1.039	0.82	20.8
0.18	0.920	0.43	0.968	0.95	1.078	0.91	19.5
				0.96	1.115	0.99	18.4
h_{avg} (μm) =		1505				1.00	18.4

Table C.190: Experimental data for $\mu = 0.192$ N·s/m^2, $h_o = 1.498$ mm, $\Delta T_s = 31.2$°C.

r'	h / h_{avg}	r'	h / h_{avg}	r'	h / h_{avg}	r'	T_s (°C)
0.00	0.854	0.20	0.897	0.47	0.967	0.16	50.7
0.02	0.855	0.22	0.902	0.50	0.972	0.20	47.0
0.03	0.858	0.23	0.908	0.53	0.978	0.24	43.9
0.05	0.860	0.25	0.913	0.57	0.983	0.28	40.8
0.07	0.863	0.27	0.918	0.60	0.987	0.32	38.8
0.08	0.866	0.28	0.923	0.63	0.991	0.41	34.7
0.10	0.870	0.30	0.928	0.67	0.995	0.49	31.5
0.12	0.874	0.32	0.932	0.73	1.002	0.57	29.0
0.13	0.878	0.33	0.937	0.80	1.008	0.66	26.5
0.15	0.882	0.37	0.946	0.87	1.016	0.74	24.5
0.17	0.887	0.40	0.953	0.93	1.047	0.82	22.6
0.18	0.892	0.43	0.960	0.95	1.087	0.91	21.0
				0.96	1.123	0.99	19.5
h_{avg} (μm) =		1514				1.00	19.5

Table C.191: Experimental data for $\mu = 0.192$ N·s/m^2, $h_o = 1.498$ mm, $\Delta T_s = 40.0$°C.

r'	h / h_{avg}	r'	h / h_{avg}	r'	h / h_{avg}	r'	T_s (°C)
0.00	0.813	0.20	0.871	0.47	0.960	0.16	60.6
0.02	0.815	0.22	0.877	0.50	0.968	0.20	55.8
0.03	0.819	0.23	0.883	0.53	0.974	0.24	51.8
0.05	0.823	0.25	0.890	0.57	0.981	0.28	47.9
0.07	0.826	0.27	0.896	0.60	0.988	0.32	45.3
0.08	0.831	0.28	0.903	0.63	0.993	0.41	39.9
0.10	0.835	0.30	0.911	0.67	0.997	0.49	35.8
0.12	0.840	0.32	0.916	0.73	1.007	0.57	32.6
0.13	0.845	0.33	0.921	0.80	1.015	0.66	29.4
0.15	0.851	0.37	0.933	0.87	1.023	0.74	26.9
0.17	0.857	0.40	0.943	0.93	1.056	0.82	24.5
0.18	0.864	0.43	0.952	0.95	1.094	0.91	22.4
				0.96	1.130	0.99	20.6
h_{avg} (μm) =		1522				1.00	20.6

Table C.192: Experimental data for $\mu = 0.192$ N·s/m^2, $h_o = 1.498$ mm, $\Delta T_s = 48.0$°C.

r'	h / h_{avg}	r'	h / h_{avg}	r'	h / h_{avg}	r'	T_s (°C)
0.00	0.777	0.20	0.846	0.47	0.952	0.16	69.8
0.02	0.780	0.22	0.854	0.50	0.962	0.20	64.1
0.03	0.784	0.23	0.861	0.53	0.971	0.24	59.3
0.05	0.790	0.25	0.869	0.57	0.979	0.28	54.5
0.07	0.795	0.27	0.877	0.60	0.986	0.32	51.4
0.08	0.801	0.28	0.885	0.63	0.993	0.41	44.9
0.10	0.805	0.30	0.892	0.67	0.999	0.49	40.0
0.12	0.810	0.32	0.899	0.73	1.010	0.57	36.1
0.13	0.816	0.33	0.906	0.80	1.020	0.66	32.3
0.15	0.823	0.37	0.919	0.87	1.031	0.74	29.3
0.17	0.831	0.40	0.931	0.93	1.064	0.82	26.3
0.18	0.838	0.43	0.943	0.95	1.103	0.91	23.8
				0.96	1.139	0.99	21.7
h_{avg} (μm) =		1529				1.00	21.7

Table C.193: Experimental data for $\mu = 0.192$ N·s/m^2, $h_o = 1.498$ mm, $\Delta T_s = 55.9$°C.

r'	h / h_{avg}	r'	h / h_{avg}	r'	h / h_{avg}	r'	T_s (°C)
0.00	0.752	0.20	0.826	0.47	0.947	0.16	78.8
0.02	0.754	0.22	0.836	0.50	0.958	0.20	72.2
0.03	0.758	0.23	0.844	0.53	0.968	0.24	66.7
0.05	0.763	0.25	0.853	0.57	0.977	0.28	61.2
0.07	0.770	0.27	0.862	0.60	0.985	0.32	57.6
0.08	0.776	0.28	0.870	0.63	0.993	0.41	50.1
0.10	0.781	0.30	0.878	0.67	1.001	0.49	44.4
0.12	0.787	0.32	0.887	0.73	1.013	0.57	39.9
0.13	0.793	0.33	0.894	0.80	1.024	0.66	35.5
0.15	0.801	0.37	0.909	0.87	1.035	0.74	31.9
0.17	0.809	0.40	0.923	0.93	1.072	0.82	28.4
0.18	0.817	0.43	0.935	0.95	1.109	0.91	25.4
				0.96	1.143	0.99	22.9
h_{avg} (μm) =		1542				1.00	22.9

Table C.194: Experimental data for $\mu = 0.192$ N·s/m^2, $h_o = 1.498$ mm, $\Delta T_s = 62.2$°C.

r'	h / h_{avg}	r'	h / h_{avg}	r'	h / h_{avg}	r'	T_s (°C)
0.00	0.719	0.20	0.804	0.47	0.942	0.16	85.9
0.02	0.723	0.22	0.816	0.50	0.954	0.20	78.5
0.03	0.728	0.23	0.824	0.53	0.965	0.24	72.3
0.05	0.734	0.25	0.835	0.57	0.976	0.28	66.2
0.07	0.740	0.27	0.845	0.60	0.986	0.32	62.3
0.08	0.746	0.28	0.854	0.63	0.994	0.41	53.8
0.10	0.752	0.30	0.864	0.67	1.003	0.49	47.5
0.12	0.759	0.32	0.872	0.73	1.018	0.57	42.5
0.13	0.766	0.33	0.881	0.80	1.030	0.66	37.6
0.15	0.775	0.37	0.898	0.87	1.041	0.74	33.6
0.17	0.783	0.40	0.914	0.93	1.078	0.82	29.7
0.18	0.794	0.43	0.928	0.95	1.115	0.91	26.4
				0.96	1.150	0.99	23.7
h_{avg} (μm) =		1545				1.00	23.7

Table C.195: Experimental data for $\mu = 0.192$ N·s/m^2, $h_o = 1.498$ mm, $\Delta T_s = 0.1$°C.

r'	h / h_{avg}	r'	h / h_{avg}	r'	h / h_{avg}	r'	T_s (°C)
0.00	0.992	0.20	0.994	0.47	0.992	0.16	21.0
0.02	0.993	0.22	0.994	0.50	0.992	0.20	21.0
0.03	0.993	0.23	0.994	0.53	0.992	0.24	21.0
0.05	0.992	0.25	0.994	0.57	0.992	0.28	21.0
0.07	0.993	0.27	0.994	0.60	0.992	0.32	21.0
0.08	0.993	0.28	0.994	0.63	0.992	0.41	21.1
0.10	0.994	0.30	0.993	0.67	0.992	0.49	21.1
0.12	0.994	0.32	0.993	0.73	0.991	0.57	21.2
0.13	0.994	0.33	0.993	0.80	0.990	0.66	21.0
0.15	0.994	0.37	0.993	0.87	0.991	0.74	21.1
0.17	0.993	0.40	0.993	0.93	1.018	0.82	21.1
0.18	0.993	0.43	0.993	0.95	1.056	0.91	21.1
						0.99	20.9
h_{avg} (μm) =		1507				1.00	20.9

Table C.196: Experimental data for $\mu = 0.192$ N·s/m^2, $h_o = 1.969$ mm, $\Delta T_s = 0.0$°C.

r'	h / h_{avg}	r'	h / h_{avg}	r'	h / h_{avg}	r'	T_s (°C)
0.00	0.993	0.20	0.992	0.47	0.992	0.16	21.1
0.02	0.993	0.22	0.992	0.50	0.992	0.20	21.1
0.03	0.993	0.23	0.993	0.53	0.992	0.24	21.1
0.05	0.992	0.25	0.993	0.57	0.992	0.28	21.1
0.07	0.992	0.27	0.992	0.60	0.993	0.32	21.1
0.08	0.992	0.28	0.992	0.63	0.993	0.41	21.2
0.10	0.992	0.30	0.992	0.67	0.993	0.49	21.2
0.12	0.992	0.32	0.992	0.73	0.992	0.57	21.3
0.13	0.992	0.33	0.992	0.80	0.992	0.66	21.1
0.15	0.992	0.37	0.992	0.87	0.993	0.74	21.2
0.17	0.992	0.40	0.992	0.93	1.013	0.82	21.2
0.18	0.992	0.43	0.992	0.95	1.040	0.91	21.2
				0.96	1.066	0.99	21.1
h_{avg} (μm) =		1984				1.00	21.1

Table C.197: Experimental data for $\mu = 0.192$ N·s/m^2, $h_o = 1.969$ mm, $\Delta T_s = 12.1$°C.

r'	h / h_{avg}	r'	h / h_{avg}	r'	h / h_{avg}	r'	T_s (°C)
0.00	0.965	0.20	0.973	0.47	0.987	0.16	29.2
0.02	0.965	0.22	0.974	0.50	0.988	0.20	27.7
0.03	0.966	0.23	0.976	0.53	0.989	0.24	26.5
0.05	0.966	0.25	0.976	0.57	0.990	0.28	25.4
0.07	0.967	0.27	0.978	0.60	0.991	0.32	24.6
0.08	0.967	0.28	0.979	0.63	0.992	0.41	23.1
0.10	0.968	0.30	0.980	0.67	0.993	0.49	21.9
0.12	0.968	0.32	0.980	0.73	0.995	0.57	21.0
0.13	0.969	0.33	0.981	0.80	0.996	0.66	19.9
0.15	0.970	0.37	0.983	0.87	0.998	0.74	19.2
0.17	0.971	0.40	0.984	0.93	1.020	0.82	18.5
0.18	0.973	0.43	0.986	0.95	1.048	0.91	17.8
				0.96	1.074	0.99	17.0
h_{avg} (μm) =		1966				1.00	17.0

Table C.198: Experimental data for $\mu = 0.192$ N·s/m^2, $h_o = 1.969$ mm, $\Delta T_s = 22.6$°C.

r'	h / h_{avg}	r'	h / h_{avg}	r'	h / h_{avg}	r'	T_s (°C)
0.00	0.940	0.20	0.957	0.47	0.983	0.16	41.0
0.02	0.942	0.22	0.959	0.50	0.986	0.20	38.3
0.03	0.942	0.23	0.961	0.53	0.987	0.24	36.0
0.05	0.944	0.25	0.963	0.57	0.989	0.28	33.8
0.07	0.945	0.27	0.964	0.60	0.991	0.32	32.3
0.08	0.946	0.28	0.967	0.63	0.993	0.41	29.3
0.10	0.947	0.30	0.968	0.67	0.994	0.49	27.0
0.12	0.949	0.32	0.970	0.73	0.997	0.57	25.3
0.13	0.950	0.33	0.972	0.80	1.000	0.66	23.4
0.15	0.952	0.37	0.974	0.87	1.002	0.74	22.0
0.17	0.954	0.40	0.978	0.93	1.025	0.82	20.7
0.18	0.955	0.43	0.980	0.95	1.054	0.91	19.5
				0.96	1.080	0.99	18.4
h_{avg} (μm) =		1974				1.00	18.4

Table C.199: Experimental data for $\mu = 0.192$ N·s/m^2, $h_o = 1.969$ mm, $\Delta T_s = 31.1$°C.

r'	h / h_{avg}	r'	h / h_{avg}	r'	h / h_{avg}	r'	T_s (°C)
0.00	0.921	0.20	0.943	0.47	0.978	0.16	50.5
0.02	0.925	0.22	0.946	0.50	0.982	0.20	46.8
0.03	0.923	0.23	0.948	0.53	0.985	0.24	43.6
0.05	0.925	0.25	0.951	0.57	0.988	0.28	40.6
0.07	0.927	0.27	0.952	0.60	0.991	0.32	38.6
0.08	0.928	0.28	0.955	0.63	0.994	0.41	34.4
0.10	0.930	0.30	0.958	0.67	0.995	0.49	31.3
0.12	0.932	0.32	0.960	0.73	1.000	0.57	28.8
0.13	0.935	0.33	0.962	0.80	1.003	0.66	26.3
0.15	0.937	0.37	0.966	0.87	1.008	0.74	24.4
0.17	0.939	0.40	0.971	0.93	1.029	0.82	22.5
0.18	0.941	0.43	0.975	0.95	1.057	0.91	20.9
				0.96	1.084	0.99	19.4
h_{avg} (μm) =		1982				1.00	19.4

Table C.200: Experimental data for $\mu = 0.192$ N·s/m^2, $h_o = 1.969$ mm, $\Delta T_s = 39.4$°C

r'	h / h_{avg}	r'	h / h_{avg}	r'	h / h_{avg}	r'	T_s (°C)
0.00	0.904	0.20	0.931	0.47	0.973	0.16	60.0
0.02	0.908	0.22	0.934	0.50	0.978	0.20	55.3
0.03	0.908	0.23	0.937	0.53	0.982	0.24	51.3
0.05	0.909	0.25	0.940	0.57	0.986	0.28	47.4
0.07	0.911	0.27	0.943	0.60	0.989	0.32	44.9
0.08	0.914	0.28	0.946	0.63	0.993	0.41	39.6
0.10	0.916	0.30	0.948	0.67	0.996	0.49	35.6
0.12	0.918	0.32	0.951	0.73	1.002	0.57	32.4
0.13	0.921	0.33	0.954	0.80	1.007	0.66	29.2
0.15	0.923	0.37	0.959	0.87	1.011	0.74	26.8
0.17	0.925	0.40	0.965	0.93	1.034	0.82	24.4
0.18	0.929	0.43	0.969	0.95	1.063	0.91	22.3
				0.96	1.089	0.99	20.5
h_{avg} (μm) =		1991				1.00	20.5

Table C.201: Experimental data for $\mu = 0.192$ N·s/m^2, $h_o = 1.969$ mm, $\Delta T_s = 46.2$°C.

r'	h / h_{avg}	r'	h / h_{avg}	r'	h / h_{avg}	r'	T_s (°C)
0.00	0.892	0.20	0.921	0.47	0.970	0.16	67.7
0.02	0.894	0.22	0.924	0.50	0.975	0.20	62.2
0.03	0.895	0.23	0.928	0.53	0.980	0.24	57.6
0.05	0.897	0.25	0.932	0.57	0.984	0.28	53.0
0.07	0.900	0.27	0.934	0.60	0.989	0.32	50.1
0.08	0.902	0.28	0.938	0.63	0.993	0.41	43.8
0.10	0.904	0.30	0.941	0.67	0.997	0.49	39.1
0.12	0.907	0.32	0.944	0.73	1.003	0.57	35.5
0.13	0.909	0.33	0.947	0.80	1.009	0.66	31.8
0.15	0.912	0.37	0.953	0.87	1.015	0.74	28.8
0.17	0.915	0.40	0.959	0.93	1.038	0.82	26.0
0.18	0.918	0.43	0.965	0.95	1.066	0.91	23.5
				0.96	1.092	0.99	21.5
h_{avg} (μm) =		2001				1.00	21.5

Table C.202: Experimental data for $\mu = 0.192$ N·s/m^2, $h_o = 1.969$ mm, $\Delta T_s = 54.4$°C.

r'	h / h_{avg}	r'	h / h_{avg}	r'	h / h_{avg}	r'	T_s (°C)
0.00	0.868	0.20	0.906	0.47	0.961	0.16	77.1
0.02	0.870	0.22	0.909	0.50	0.968	0.20	70.5
0.03	0.872	0.23	0.912	0.53	0.974	0.24	65.1
0.05	0.875	0.25	0.917	0.57	0.980	0.28	59.7
0.07	0.878	0.27	0.920	0.60	0.985	0.32	56.2
0.08	0.881	0.28	0.923	0.63	0.991	0.41	48.9
0.10	0.885	0.30	0.928	0.67	0.995	0.49	43.3
0.12	0.888	0.32	0.932	0.73	1.006	0.57	39.0
0.13	0.891	0.33	0.935	0.80	1.014	0.66	34.7
0.15	0.894	0.37	0.942	0.87	1.019	0.74	31.2
0.17	0.898	0.40	0.949	0.93	1.047	0.82	27.8
0.18	0.902	0.43	0.955	0.95	1.074	0.91	25.0
				0.96	1.097	0.99	22.6
h_{avg} (μm) =		2023				1.00	22.6

Table C.203: Experimental data for $\mu = 0.192$ N·s/m^2, $h_o = 2.486$ mm, $\Delta T_s = 0.1$°C.

r'	h / h_{avg}	r'	h / h_{avg}	r'	h / h_{avg}	r'	T_s (°C)
0.00	0.994	0.20	0.994	0.47	0.994	0.16	21.9
0.02	0.994	0.22	0.994	0.50	0.994	0.20	21.9
0.03	0.994	0.23	0.994	0.53	0.994	0.24	21.9
0.05	0.994	0.25	0.995	0.57	0.994	0.28	22.0
0.07	0.994	0.27	0.995	0.60	0.994	0.32	21.9
0.08	0.994	0.28	0.995	0.63	0.994	0.41	22.0
0.10	0.994	0.30	0.995	0.67	0.994	0.49	22.1
0.12	0.994	0.32	0.994	0.73	0.994	0.57	22.1
0.13	0.995	0.33	0.994	0.80	0.994	0.66	22.0
0.15	0.994	0.37	0.994	0.87	0.994	0.74	22.0
0.17	0.994	0.40	0.994	0.93	1.009	0.82	22.1
0.18	0.994	0.43	0.994	0.95	1.032	0.91	22.1
				0.96	1.055	0.99	21.8
h_{avg} (μm) =		2500				1.00	21.8

Table C.204: Experimental data for $\mu = 0.192$ N·s/m^2, $h_o = 2.486$ mm, $\Delta T_s = 12.5$°C.

r'	h / h_{avg}	r'	h / h_{avg}	r'	h / h_{avg}	r'	T_s (°C)
0.00	0.978	0.20	0.982	0.47	0.991	0.16	29.6
0.02	0.978	0.22	0.983	0.50	0.991	0.20	28.1
0.03	0.978	0.23	0.984	0.53	0.992	0.24	26.9
0.05	0.978	0.25	0.984	0.57	0.992	0.28	25.7
0.07	0.978	0.27	0.985	0.60	0.993	0.32	24.9
0.08	0.979	0.28	0.985	0.63	0.994	0.41	23.3
0.10	0.979	0.30	0.986	0.67	0.994	0.49	22.1
0.12	0.980	0.32	0.986	0.73	0.995	0.57	21.2
0.13	0.980	0.33	0.987	0.80	0.996	0.66	20.0
0.15	0.981	0.37	0.988	0.87	0.998	0.74	19.3
0.17	0.981	0.40	0.989	0.93	1.014	0.82	18.6
0.18	0.982	0.43	0.990	0.95	1.037	0.91	17.8
				0.96	1.061	0.99	17.1
h_{avg} (μm) =		2475				1.00	17.1

Table C.205: Experimental data for $\mu = 0.192$ N·s/m^2, $h_o = 2.486$ mm, $\Delta T_s = 22.6$°C.

r'	h / h_{avg}	r'	h / h_{avg}	r'	h / h_{avg}	r'	T_s (°C)
0.00	0.962	0.20	0.973	0.47	0.987	0.16	41.0
0.02	0.963	0.22	0.974	0.50	0.989	0.20	38.3
0.03	0.964	0.23	0.975	0.53	0.990	0.24	36.1
0.05	0.966	0.25	0.976	0.57	0.991	0.28	33.9
0.07	0.967	0.27	0.977	0.60	0.993	0.32	32.4
0.08	0.968	0.28	0.978	0.63	0.994	0.41	29.4
0.10	0.969	0.30	0.979	0.67	0.995	0.49	27.2
0.12	0.969	0.32	0.980	0.73	0.997	0.57	25.4
0.13	0.970	0.33	0.981	0.80	0.999	0.66	23.5
0.15	0.971	0.37	0.982	0.87	1.000	0.74	22.1
0.17	0.971	0.40	0.984	0.93	1.017	0.82	20.8
0.18	0.972	0.43	0.986	0.95	1.040	0.91	19.5
				0.96	1.064	0.99	18.4
h_{avg} (μm) =		2492				1.00	18.4

Table C.206: Experimental data for $\mu = 0.192$ N·s/m^2, $h_o = 2.486$ mm, $\Delta T_s = 31.5$°C.

r'	h / h_{avg}	r'	h / h_{avg}	r'	h / h_{avg}	r'	T_s (°C)
0.00	0.954	0.20	0.967	0.47	0.985	0.16	51.0
0.02	0.954	0.22	0.968	0.50	0.987	0.20	47.3
0.03	0.955	0.23	0.969	0.53	0.988	0.24	44.1
0.05	0.956	0.25	0.970	0.57	0.990	0.28	41.1
0.07	0.957	0.27	0.972	0.60	0.992	0.32	39.1
0.08	0.958	0.28	0.973	0.63	0.993	0.41	34.9
0.10	0.960	0.30	0.974	0.67	0.995	0.49	31.7
0.12	0.961	0.32	0.975	0.73	0.998	0.57	29.2
0.13	0.962	0.33	0.976	0.80	1.000	0.66	26.7
0.15	0.963	0.37	0.978	0.87	1.003	0.74	24.7
0.17	0.964	0.40	0.981	0.93	1.020	0.82	22.8
0.18	0.965	0.43	0.983	0.95	1.043	0.91	21.1
				0.96	1.067	0.99	19.5
h_{avg} (μm) =		2503				1.00	19.5

Table C.207: Experimental data for $\mu = 0.192$ N·s/m^2, $h_o = 2.486$ mm, $\Delta T_s = 38.7$°C.

r'	h / h_{avg}	r'	h / h_{avg}	r'	h / h_{avg}	r'	T_s (°C)
0.00	1.084	0.20	1.099	0.47	1.124	0.16	59.2
0.02	1.084	0.22	1.101	0.50	1.127	0.20	54.5
0.03	1.085	0.23	1.102	0.53	1.130	0.24	50.6
0.05	1.086	0.25	1.104	0.57	1.132	0.28	46.8
0.07	1.088	0.27	1.106	0.60	1.135	0.32	44.4
0.08	1.089	0.28	1.107	0.63	1.137	0.41	39.2
0.10	1.090	0.30	1.109	0.67	1.139	0.49	35.3
0.12	1.092	0.32	1.110	0.73	1.144	0.57	32.2
0.13	1.093	0.33	1.113	0.80	1.147	0.66	29.1
0.15	1.095	0.37	1.115	0.87	1.151	0.74	26.7
0.17	1.096	0.40	1.118	0.93	1.171	0.82	24.3
0.18	1.098	0.43	1.121	0.95	1.198	0.91	22.3
						0.99	20.5
h_{avg} (μm) =		2511				1.00	20.5

Table C.208: Experimental data for $\mu = 0.192$ N·s/m^2, $h_o = 2.486$ mm, $\Delta T_s = 46.6$°C.

r'	h / h_{avg}	r'	h / h_{avg}	r'	h / h_{avg}	r'	T_s (°C)
0.00	0.940	0.20	0.955	0.47	0.979	0.16	68.2
0.02	0.941	0.22	0.957	0.50	0.982	0.20	62.6
0.03	0.942	0.23	0.959	0.53	0.985	0.24	57.9
0.05	0.943	0.25	0.960	0.57	0.988	0.28	53.3
0.07	0.944	0.27	0.961	0.60	0.990	0.32	50.3
0.08	0.945	0.28	0.963	0.63	0.992	0.41	44.0
0.10	0.947	0.30	0.965	0.67	0.995	0.49	39.3
0.12	0.948	0.32	0.966	0.73	1.000	0.57	35.7
0.13	0.949	0.33	0.968	0.80	1.004	0.66	32.0
0.15	0.951	0.37	0.971	0.87	1.008	0.74	29.0
0.17	0.952	0.40	0.974	0.93	1.026	0.82	26.2
0.18	0.954	0.43	0.977	0.95	1.048	0.91	23.7
				0.96	1.071	0.99	21.6
h_{avg} (μm) =		2526				1.00	21.6

Table C.209: Experimental data for $\mu = 0.192$ N·s/m^2, $h_o = 2.486$ mm, $\Delta T_s = 53.2$°C.

r'	h / h_{avg}	r'	h / h_{avg}	r'	h / h_{avg}	r'	T_s (°C)
0.00	0.937	0.20	0.953	0.47	0.978	0.16	75.8
0.02	0.938	0.22	0.954	0.50	0.981	0.20	69.4
0.03	0.939	0.23	0.956	0.53	0.984	0.24	64.0
0.05	0.940	0.25	0.958	0.57	0.987	0.28	58.8
0.07	0.941	0.27	0.959	0.60	0.990	0.32	55.4
0.08	0.943	0.28	0.961	0.63	0.992	0.41	48.3
0.10	0.944	0.30	0.962	0.67	0.995	0.49	42.9
0.12	0.945	0.32	0.964	0.73	1.000	0.57	38.7
0.13	0.947	0.33	0.966	0.80	1.004	0.66	34.6
0.15	0.948	0.37	0.969	0.87	1.009	0.74	31.2
0.17	0.949	0.40	0.972	0.93	1.027	0.82	27.9
0.18	0.951	0.43	0.975	0.95	1.049	0.91	25.0
				0.96	1.072	0.99	22.6
h_{avg} (μm) =		2541				1.00	22.6

Table C.210: Experimental data for $\mu = 0.192$ N·s/m^2, $h_o = 2.991$ mm, $\Delta T_s = 0.1$°C.

r'	h / h_{avg}	r'	h / h_{avg}	r'	h / h_{avg}	r'	T_s (°C)
0.00	0.995	0.20	0.995	0.47	0.995	0.16	21.7
0.02	0.995	0.22	0.995	0.50	0.995	0.20	21.6
0.03	0.995	0.23	0.995	0.53	0.995	0.24	21.6
0.05	0.995	0.25	0.995	0.57	0.995	0.28	21.7
0.07	0.995	0.27	0.995	0.60	0.995	0.32	21.6
0.08	0.995	0.28	0.995	0.63	0.995	0.41	21.7
0.10	0.995	0.30	0.995	0.67	0.995	0.49	21.8
0.12	0.995	0.32	0.995	0.73	0.995	0.57	21.8
0.13	0.995	0.33	0.995	0.80	0.995	0.66	21.6
0.15	0.995	0.37	0.995	0.87	0.995	0.74	21.7
0.17	0.995	0.40	0.995	0.93	1.008	0.82	21.8
0.18	0.995	0.43	0.995	0.95	1.026	0.91	21.7
				0.96	1.045	0.99	21.6
h_{avg} (μm) =		3006				1.00	21.6

Table C.211: Experimental data for $\mu = 0.192$ N·s/m^2, $h_o = 2.991$ mm, $\Delta T_s = 37.1$°C.

r'	h / h_{avg}	r'	h / h_{avg}	r'	h / h_{avg}	r'	T_s (°C)
0.00	0.971	0.20	0.977	0.47	0.988	0.16	57.5
0.02	0.971	0.22	0.978	0.50	0.989	0.20	53.0
0.03	0.971	0.23	0.978	0.53	0.991	0.24	49.3
0.05	0.972	0.25	0.979	0.57	0.992	0.28	45.6
0.07	0.972	0.27	0.980	0.60	0.993	0.32	43.3
0.08	0.973	0.28	0.981	0.63	0.994	0.41	38.3
0.10	0.973	0.30	0.982	0.67	0.996	0.49	34.6
0.12	0.974	0.32	0.982	0.73	0.997	0.57	31.7
0.13	0.974	0.33	0.983	0.80	1.000	0.66	28.7
0.15	0.975	0.37	0.984	0.87	1.002	0.74	26.4
0.17	0.975	0.40	0.985	0.93	1.015	0.82	24.1
0.18	0.976	0.43	0.987	0.95	1.034	0.91	22.2
				0.96	1.052	0.99	20.4
h_{avg} (μm) =		3020				1.00	20.4

Table C.212: Experimental data for $\mu = 0.192$ N·s/m^2, $h_o = 2.991$ mm, $\Delta T_s = 45.2$°C.

r'	h / h_{avg}	r'	h / h_{avg}	r'	h / h_{avg}	r'	T_s (°C)
0.00	0.968	0.20	0.975	0.47	0.987	0.16	66.8
0.02	0.968	0.22	0.976	0.50	0.988	0.20	61.3
0.03	0.968	0.23	0.977	0.53	0.990	0.24	56.7
0.05	0.969	0.25	0.977	0.57	0.991	0.28	52.2
0.07	0.969	0.27	0.978	0.60	0.993	0.32	49.3
0.08	0.970	0.28	0.979	0.63	0.994	0.41	43.2
0.10	0.971	0.30	0.980	0.67	0.995	0.49	38.7
0.12	0.971	0.32	0.980	0.73	0.998	0.57	35.1
0.13	0.972	0.33	0.981	0.80	1.000	0.66	31.6
0.15	0.973	0.37	0.983	0.87	1.003	0.74	28.8
0.17	0.974	0.40	0.984	0.93	1.017	0.82	26.0
0.18	0.974	0.43	0.985	0.95	1.035	0.91	23.6
				0.96	1.053	0.99	21.7
h_{avg} (μm) =		3033				1.00	21.7

Table C.213: Experimental data for $\mu = 0.192$ N·s/m^2, $h_o = 2.991$ mm, $\Delta T_s = 51.3$°C.

r'	h / h_{avg}	r'	h / h_{avg}	r'	h / h_{avg}	r'	T_s (°C)
0.00	1.125	0.20	1.134	0.47	1.148	0.16	73.9
0.02	1.128	0.22	1.135	0.50	1.150	0.20	67.6
0.03	1.126	0.23	1.136	0.53	1.152	0.24	62.3
0.05	1.126	0.25	1.137	0.57	1.154	0.28	57.2
0.07	1.127	0.27	1.138	0.60	1.156	0.32	53.9
0.08	1.128	0.28	1.139	0.63	1.157	0.41	46.9
0.10	1.129	0.30	1.140	0.67	1.159	0.49	41.8
0.12	1.130	0.32	1.141	0.73	1.162	0.57	37.8
0.13	1.131	0.33	1.141	0.80	1.165	0.66	33.9
0.15	1.131	0.37	1.143	0.87	1.168	0.74	30.7
0.17	1.132	0.40	1.145	0.93	1.184	0.82	27.5
0.18	1.133	0.43	1.147	0.95	1.205	0.91	24.8
						0.99	22.7
h_{avg} (μm) =		3043				1.00	22.7

Table C.214: Experimental data for $\mu = 0.480$ N·s/m^2, $h_o = 0.999$ mm, $\Delta T_s = 0.0$°C.

r'	h / h_{avg}	r'	h / h_{avg}	r'	h / h_{avg}	r'	T_s (°C)
0.00	0.982	0.20	0.983	0.47	0.983	0.16	20.1
0.02	0.983	0.22	0.983	0.50	0.983	0.20	20.1
0.03	0.983	0.23	0.984	0.53	0.983	0.24	20.1
0.05	0.983	0.25	0.984	0.57	0.983	0.28	20.2
0.07	0.983	0.27	0.983	0.60	0.983	0.32	20.2
0.08	0.983	0.28	0.984	0.63	0.982	0.41	20.3
0.10	0.982	0.30	0.983	0.67	0.983	0.49	20.3
0.12	0.983	0.32	0.983	0.73	0.983	0.57	20.4
0.13	0.983	0.33	0.983	0.80	0.983	0.66	20.2
0.15	0.983	0.37	0.984	0.87	0.982	0.74	20.3
0.17	0.983	0.40	0.984	0.93	1.029	0.82	20.3
0.18	0.983	0.43	0.983	0.95	1.087	0.91	20.3
				0.96	1.150	0.99	20.1
h_{avg} (μm) =		1016				1.00	20.1

Table C.215: Experimental data for $\mu = 0.480$ N·s/m^2, $h_o = 0.999$ mm, $\Delta T_s = 12.3$°C.

r'	h / h_{avg}	r'	h / h_{avg}	r'	h / h_{avg}	r'	T_s (°C)
0.00	0.850	0.20	0.896	0.47	0.960	0.16	29.3
0.02	0.851	0.22	0.901	0.50	0.966	0.20	27.8
0.03	0.853	0.23	0.907	0.53	0.971	0.24	26.6
0.05	0.856	0.25	0.912	0.57	0.975	0.28	25.5
0.07	0.859	0.27	0.916	0.60	0.980	0.32	24.7
0.08	0.862	0.28	0.921	0.63	0.984	0.41	23.1
0.10	0.866	0.30	0.925	0.67	0.988	0.49	21.9
0.12	0.870	0.32	0.930	0.73	0.995	0.57	21.0
0.13	0.875	0.33	0.934	0.80	1.001	0.66	19.8
0.15	0.880	0.37	0.941	0.87	1.008	0.74	19.1
0.17	0.885	0.40	0.948	0.93	1.057	0.82	18.4
0.18	0.891	0.43	0.955	0.95	1.121	0.91	17.8
				0.96	1.181	0.99	17.0
h_{avg} (μm) =		1003				1.00	17.0

Table C.216: Experimental data for $\mu = 0.480$ N·s/m^2, $h_o = 0.999$ mm, $\Delta T_s = 22.7$°C.

r'	h / h_{avg}	r'	h / h_{avg}	r'	h / h_{avg}	r'	T_s (°C)
0.00	0.723	0.20	0.819	0.47	0.944	0.16	41.0
0.02	0.728	0.22	0.829	0.50	0.954	0.20	38.3
0.03	0.732	0.23	0.840	0.53	0.963	0.24	36.0
0.05	0.737	0.25	0.850	0.57	0.972	0.28	33.8
0.07	0.743	0.27	0.859	0.60	0.979	0.32	32.4
0.08	0.751	0.28	0.869	0.63	0.987	0.41	29.3
0.10	0.758	0.30	0.878	0.67	0.994	0.49	27.0
0.12	0.766	0.32	0.886	0.73	1.006	0.57	25.3
0.13	0.776	0.33	0.894	0.80	1.017	0.66	23.4
0.15	0.785	0.37	0.909	0.87	1.028	0.74	22.0
0.17	0.797	0.40	0.922	0.93	1.080	0.82	20.7
0.18	0.807	0.43	0.933	0.95	1.143	0.91	19.5
				0.96	1.204	0.99	18.3
h_{avg} (μm) =		1009				1.00	18.3

Table C.217: Experimental data for $\mu = 0.480$ N·s/m^2, $h_o = 0.999$ mm, $\Delta T_s = 31.5$°C.

r'	h / h_{avg}	r'	h / h_{avg}	r'	h / h_{avg}	r'	T_s (°C)
0.00	0.609	0.20	0.754	0.47	0.932	0.16	51.0
0.02	0.615	0.22	0.771	0.50	0.945	0.20	47.2
0.03	0.623	0.23	0.787	0.53	0.957	0.24	44.1
0.05	0.631	0.25	0.800	0.57	0.969	0.28	41.0
0.07	0.640	0.27	0.815	0.60	0.979	0.32	39.0
0.08	0.651	0.28	0.828	0.63	0.989	0.41	34.7
0.10	0.663	0.30	0.840	0.67	0.998	0.49	31.6
0.12	0.675	0.32	0.852	0.73	1.015	0.57	29.0
0.13	0.690	0.33	0.863	0.80	1.029	0.66	26.5
0.15	0.703	0.37	0.882	0.87	1.045	0.74	24.6
0.17	0.721	0.40	0.901	0.93	1.099	0.82	22.7
0.18	0.737	0.43	0.917	0.95	1.161	0.91	21.0
				0.96	1.220	0.99	19.4
h_{avg} (μm) =		1017				1.00	19.4

Table C.218: Experimental data for $\mu = 0.480$ N·s/m^2, $h_o = 0.999$ mm, $\Delta T_s = 39.4$°C.

r'	h / h_{avg}	r'	h / h_{avg}	r'	h / h_{avg}	r'	T_s (°C)
0.00	0.475	0.20	0.689	0.47	0.920	0.16	60.0
0.02	0.482	0.22	0.711	0.50	0.937	0.20	55.3
0.03	0.495	0.23	0.733	0.53	0.952	0.24	51.3
0.05	0.507	0.25	0.752	0.57	0.967	0.28	47.5
0.07	0.521	0.27	0.771	0.60	0.980	0.32	45.0
0.08	0.540	0.28	0.788	0.63	0.993	0.41	39.6
0.10	0.556	0.30	0.804	0.67	1.003	0.49	35.6
0.12	0.574	0.32	0.820	0.73	1.024	0.57	32.5
0.13	0.597	0.33	0.834	0.80	1.042	0.66	29.3
0.15	0.619	0.37	0.859	0.87	1.060	0.74	26.9
0.17	0.641	0.40	0.882	0.93	1.117	0.82	24.5
0.18	0.665	0.43	0.903	0.95	1.179	0.91	22.4
				0.96	1.235	0.99	20.6
h_{avg} (μm) =		1026				1.00	20.6

Table C.219: Experimental data for $\mu = 0.480$ N·s/m^2, $h_o = 0.999$ mm, $\Delta T_s = 47.3$°C.

r'	h / h_{avg}	r'	h / h_{avg}	r'	h / h_{avg}	r'	T_s (°C)
0.00	0.253	0.20	0.620	0.47	0.911	0.16	68.9
0.02	0.275	0.22	0.650	0.50	0.932	0.20	63.4
0.03	0.307	0.23	0.678	0.53	0.950	0.24	58.7
0.05	0.335	0.25	0.703	0.57	0.967	0.28	54.0
0.07	0.362	0.27	0.726	0.60	0.982	0.32	51.0
0.08	0.395	0.28	0.749	0.63	0.997	0.41	44.6
0.10	0.424	0.30	0.770	0.67	1.010	0.49	39.8
0.12	0.454	0.32	0.788	0.73	1.034	0.57	36.0
0.13	0.486	0.33	0.805	0.80	1.056	0.66	32.2
0.15	0.520	0.37	0.836	0.87	1.076	0.74	29.2
0.17	0.554	0.40	0.864	0.93	1.135	0.82	26.3
0.18	0.587	0.43	0.889	0.95	1.195	0.91	23.7
				0.96	1.253	0.99	21.6
h_{avg} (μm) =		1035				1.00	21.6

Table C.220: Experimental data for $\mu = 0.480$ N·s/m^2, $h_o = 0.999$ mm, $\Delta T_s = 55.6$°C.

r'	h / h_{avg}	r'	h / h_{avg}	r'	h / h_{avg}	r'	T_s (°C)
0.00	0.106	0.20	0.538	0.47	0.907	0.16	78.2
0.02	0.090	0.22	0.580	0.50	0.930	0.20	71.6
0.03	0.081	0.23	0.620	0.53	0.951	0.24	66.1
0.05	0.082	0.25	0.654	0.57	0.970	0.28	60.6
0.07	0.085	0.27	0.684	0.60	0.988	0.32	57.0
0.08	0.081	0.28	0.710	0.63	1.004	0.41	49.4
0.10	0.082	0.30	0.737	0.67	1.019	0.49	43.7
0.12	0.191	0.32	0.758	0.73	1.047	0.57	39.3
0.13	0.292	0.33	0.781	0.80	1.072	0.66	34.9
0.15	0.371	0.37	0.818	0.87	1.095	0.74	31.4
0.17	0.435	0.40	0.852	0.93	1.155	0.82	27.9
0.18	0.490	0.43	0.881	0.95	1.216	0.91	25.0
				0.96	1.271	0.99	22.5
h_{avg} (μm) =		1043				1.00	22.5

Table C.221: Experimental data for $\mu = 0.480$ N·s/m^2, $h_o = 0.999$ mm, $\Delta T_s = 0.1$°C.

r'	h / h_{avg}	r'	h / h_{avg}	r'	h / h_{avg}	r'	T_s (°C)
0.00	0.984	0.20	0.984	0.47	0.984	0.16	20.7
0.02	0.983	0.22	0.984	0.50	0.984	0.20	20.7
0.03	0.984	0.23	0.984	0.53	0.983	0.24	20.7
0.05	0.984	0.25	0.985	0.57	0.983	0.28	20.8
0.07	0.984	0.27	0.984	0.60	0.984	0.32	20.8
0.08	0.984	0.28	0.984	0.63	0.983	0.41	20.9
0.10	0.984	0.30	0.984	0.67	0.983	0.49	20.9
0.12	0.984	0.32	0.985	0.73	0.983	0.57	21.0
0.13	0.984	0.33	0.984	0.80	0.982	0.66	20.8
0.15	0.984	0.37	0.984	0.87	0.983	0.74	20.9
0.17	0.984	0.40	0.984	0.93	1.029	0.82	20.9
0.18	0.984	0.43	0.984	0.95	1.086	0.91	20.9
				0.96	1.144	0.99	20.6
h_{avg} (μm) =		1019				1.00	20.6

Table C.222: Experimental data for $\mu = 0.480$ N·s/m^2, $h_o = 1.981$ mm, $\Delta T_s = 0.0$°C.

r'	h / h_{avg}	r'	h / h_{avg}	r'	h / h_{avg}	r'	T_s (°C)
0.00	0.993	0.20	0.993	0.47	0.992	0.16	20.4
0.02	0.993	0.22	0.993	0.50	0.991	0.20	20.4
0.03	0.993	0.23	0.993	0.53	0.992	0.24	20.5
0.05	0.993	0.25	0.993	0.57	0.992	0.28	20.6
0.07	0.993	0.27	0.993	0.60	0.991	0.32	20.6
0.08	0.993	0.28	0.993	0.63	0.992	0.41	20.7
0.10	0.993	0.30	0.992	0.67	0.992	0.49	20.8
0.12	0.993	0.32	0.992	0.73	0.993	0.57	20.8
0.13	0.993	0.33	0.992	0.80	0.993	0.66	20.7
0.15	0.992	0.37	0.992	0.87	0.993	0.74	20.8
0.17	0.992	0.40	0.992	0.93	1.013	0.82	20.8
0.18	0.993	0.43	0.992	0.95	1.040	0.91	20.8
				0.96	1.066	0.99	20.5
h_{avg} (μm) =		1996				1.00	20.5

Table C.223: Experimental data for $\mu = 0.480$ N·s/m^2, $h_o = 1.981$ mm, $\Delta T_s = 12.4$°C.

r'	h / h_{avg}	r'	h / h_{avg}	r'	h / h_{avg}	r'	T_s (°C)
0.00	0.966	0.20	0.974	0.47	0.987	0.16	29.4
0.02	0.966	0.22	0.976	0.50	0.988	0.20	27.9
0.03	0.967	0.23	0.977	0.53	0.990	0.24	26.7
0.05	0.967	0.25	0.978	0.57	0.991	0.28	25.5
0.07	0.968	0.27	0.979	0.60	0.992	0.32	24.8
0.08	0.968	0.28	0.980	0.63	0.993	0.41	23.2
0.10	0.969	0.30	0.980	0.67	0.993	0.49	22.0
0.12	0.970	0.32	0.981	0.73	0.995	0.57	21.0
0.13	0.971	0.33	0.982	0.80	0.996	0.66	19.9
0.15	0.971	0.37	0.984	0.87	0.998	0.74	19.2
0.17	0.972	0.40	0.985	0.93	1.019	0.82	18.4
0.18	0.974	0.43	0.986	0.95	1.047	0.91	17.7
				0.96	1.073	0.99	17.0
h_{avg} (μm) =		1979				1.00	17.0

Table C.224: Experimental data for $\mu = 0.480$ N·s/m^2, $h_o = 1.981$ mm, $\Delta T_s = 22.6$°C.

r'	h / h_{avg}	r'	h / h_{avg}	r'	h / h_{avg}	r'	T_s (°C)
0.00	0.946	0.20	0.960	0.47	0.984	0.16	41.0
0.02	0.947	0.22	0.962	0.50	0.986	0.20	38.3
0.03	0.947	0.23	0.964	0.53	0.988	0.24	36.0
0.05	0.948	0.25	0.966	0.57	0.989	0.28	33.8
0.07	0.949	0.27	0.967	0.60	0.991	0.32	32.4
0.08	0.950	0.28	0.969	0.63	0.993	0.41	29.4
0.10	0.951	0.30	0.971	0.67	0.994	0.49	27.1
0.12	0.952	0.32	0.973	0.73	0.997	0.57	25.4
0.13	0.954	0.33	0.974	0.80	0.999	0.66	23.5
0.15	0.955	0.37	0.977	0.87	1.002	0.74	22.1
0.17	0.956	0.40	0.980	0.93	1.023	0.82	20.7
0.18	0.958	0.43	0.982	0.95	1.051	0.91	19.5
				0.96	1.078	0.99	18.4
h_{avg} (μm) =		1988				1.00	18.4

Table C.225: Experimental data for $\mu = 0.480$ N·s/m^2, $h_o = 1.981$ mm, $\Delta T_s = 31.3$°C.

r'	h / h_{avg}	r'	h / h_{avg}	r'	h / h_{avg}	r'	T_s (°C)
0.00	0.928	0.20	0.947	0.47	0.981	0.16	50.7
0.02	0.928	0.22	0.949	0.50	0.983	0.20	47.0
0.03	0.930	0.23	0.952	0.53	0.986	0.24	43.9
0.05	0.931	0.25	0.954	0.57	0.989	0.28	40.8
0.07	0.932	0.27	0.956	0.60	0.991	0.32	38.8
0.08	0.933	0.28	0.959	0.63	0.993	0.41	34.6
0.10	0.934	0.30	0.962	0.67	0.995	0.49	31.4
0.12	0.936	0.32	0.964	0.73	0.999	0.57	29.0
0.13	0.938	0.33	0.966	0.80	1.002	0.66	26.4
0.15	0.940	0.37	0.970	0.87	1.005	0.74	24.5
0.17	0.942	0.40	0.974	0.93	1.028	0.82	22.6
0.18	0.944	0.43	0.977	0.95	1.056	0.91	20.9
				0.96	1.082	0.99	19.4
h_{avg} (μm) =		1997				1.00	19.4

Table C.226: Experimental data for $\mu = 0.480$ N·s/m^2, $h_o = 1.981$ mm, $\Delta T_s = 39.4$°C.

r'	h / h_{avg}	r'	h / h_{avg}	r'	h / h_{avg}	r'	T_s (°C)
0.00	0.908	0.20	0.934	0.47	0.978	0.16	60.0
0.02	0.910	0.22	0.937	0.50	0.981	0.20	55.3
0.03	0.911	0.23	0.941	0.53	0.985	0.24	51.3
0.05	0.913	0.25	0.944	0.57	0.987	0.28	47.5
0.07	0.915	0.27	0.946	0.60	0.990	0.32	44.9
0.08	0.917	0.28	0.950	0.63	0.993	0.41	39.6
0.10	0.919	0.30	0.953	0.67	0.996	0.49	35.6
0.12	0.921	0.32	0.956	0.73	1.001	0.57	32.4
0.13	0.923	0.33	0.959	0.80	1.005	0.66	29.3
0.15	0.926	0.37	0.964	0.87	1.009	0.74	26.8
0.17	0.929	0.40	0.969	0.93	1.032	0.82	24.4
0.18	0.931	0.43	0.973	0.95	1.060	0.91	22.3
				0.96	1.086	0.99	20.6
h_{avg} (μm) =		2005				1.00	20.6

Table C.227: Experimental data for $\mu = 0.480$ N·s/m^2, $h_o = 1.981$ mm, $\Delta T_s = 46.9$°C.

r'	h / h_{avg}	r'	h / h_{avg}	r'	h / h_{avg}	r'	T_s (°C)
0.00	0.894	0.20	0.924	0.47	0.974	0.16	68.5
0.02	0.895	0.22	0.928	0.50	0.979	0.20	62.9
0.03	0.897	0.23	0.931	0.53	0.983	0.24	58.2
0.05	0.899	0.25	0.935	0.57	0.987	0.28	53.6
0.07	0.902	0.27	0.938	0.60	0.990	0.32	50.6
0.08	0.904	0.28	0.942	0.63	0.994	0.41	44.2
0.10	0.907	0.30	0.945	0.67	0.996	0.49	39.4
0.12	0.909	0.32	0.949	0.73	1.002	0.57	35.7
0.13	0.911	0.33	0.952	0.80	1.007	0.66	31.9
0.15	0.914	0.37	0.958	0.87	1.012	0.74	29.0
0.17	0.917	0.40	0.964	0.93	1.036	0.82	26.1
0.18	0.920	0.43	0.969	0.95	1.063	0.91	23.6
				0.96	1.090	0.99	21.5
h_{avg} (μm) =		2014				1.00	21.5

Table C.228: Experimental data for $\mu = 0.480$ N·s/m^2, $h_o = 1.981$ mm, $\Delta T_s = 53.9$°C.

r'	h / h_{avg}	r'	h / h_{avg}	r'	h / h_{avg}	r'	T_s (°C)
0.00	0.879	0.20	0.914	0.47	0.971	0.16	76.2
0.02	0.880	0.22	0.918	0.50	0.977	0.20	69.9
0.03	0.882	0.23	0.922	0.53	0.982	0.24	64.5
0.05	0.885	0.25	0.926	0.57	0.986	0.28	59.2
0.07	0.888	0.27	0.930	0.60	0.990	0.32	55.8
0.08	0.890	0.28	0.933	0.63	0.994	0.41	48.5
0.10	0.893	0.30	0.937	0.67	0.998	0.49	42.9
0.12	0.896	0.32	0.941	0.73	1.004	0.57	38.6
0.13	0.899	0.33	0.945	0.80	1.009	0.66	34.4
0.15	0.902	0.37	0.952	0.87	1.016	0.74	30.9
0.17	0.906	0.40	0.959	0.93	1.039	0.82	27.6
0.18	0.910	0.43	0.965	0.95	1.067	0.91	24.8
				0.96	1.093	0.99	22.4
h_{avg} (μm) =		2020				1.00	22.4

Table C.229: Experimental data for $\mu = 0.480$ N·s/m^2, $h_o = 1.981$ mm, $\Delta T_s = 0.0$°C.

r'	h / h_{avg}	r'	h / h_{avg}	r'	h / h_{avg}	r'	T_s (°C)
0.00	0.990	0.20	0.993	0.47	0.993	0.16	19.7
0.02	0.992	0.22	0.993	0.50	0.993	0.20	19.7
0.03	0.992	0.23	0.993	0.53	0.992	0.24	19.8
0.05	0.992	0.25	0.993	0.57	0.993	0.28	19.8
0.07	0.992	0.27	0.993	0.60	0.993	0.32	19.8
0.08	0.992	0.28	0.993	0.63	0.992	0.41	19.9
0.10	0.993	0.30	0.993	0.67	0.993	0.49	20.0
0.12	0.993	0.32	0.993	0.73	0.992	0.57	20.0
0.13	0.993	0.33	0.993	0.80	0.992	0.66	19.9
0.15	0.993	0.37	0.993	0.87	0.993	0.74	19.9
0.17	0.993	0.40	0.993	0.93	1.012	0.82	20.0
0.18	0.993	0.43	0.993	0.95	1.040	0.91	20.0
				0.96	1.067	0.99	19.7
h_{avg} (μm) =		1983				1.00	19.7

Table C.230: Experimental data for $\mu = 0.480$ N·s/m^2, $h_o = 2.985$ mm, $\Delta T_s = 0.0$°C.

r'	h / h_{avg}	r'	h / h_{avg}	r'	h / h_{avg}	r'	T_s (°C)
0.00	0.994	0.20	0.995	0.47	0.995	0.16	19.9
0.02	0.994	0.22	0.995	0.50	0.995	0.20	19.9
0.03	0.995	0.23	0.995	0.53	0.995	0.24	19.9
0.05	0.995	0.25	0.995	0.57	0.995	0.28	20.0
0.07	0.995	0.27	0.995	0.60	0.995	0.32	20.0
0.08	0.995	0.28	0.995	0.63	0.995	0.41	20.0
0.10	0.995	0.30	0.995	0.67	0.995	0.49	20.1
0.12	0.995	0.32	0.995	0.73	0.995	0.57	20.2
0.13	0.995	0.33	0.995	0.80	0.995	0.66	20.0
0.15	0.995	0.37	0.995	0.87	0.995	0.74	20.1
0.17	0.995	0.40	0.995	0.93	1.008	0.82	20.1
0.18	0.995	0.43	0.995	0.95	1.026	0.91	20.1
				0.96	1.046	0.99	19.9
h_{avg} (μm) =		3000				1.00	19.9

Table C.231: Experimental data for $\mu = 0.480$ N·s/m^2, $h_o = 2.985$ mm, $\Delta T_s = 12.5$°C.

r'	h / h_{avg}	r'	h / h_{avg}	r'	h / h_{avg}	r'	T_s (°C)
0.00	0.985	0.20	0.989	0.47	0.993	0.16	29.6
0.02	0.985	0.22	0.989	0.50	0.994	0.20	28.1
0.03	0.986	0.23	0.989	0.53	0.994	0.24	26.9
0.05	0.986	0.25	0.990	0.57	0.994	0.28	25.7
0.07	0.986	0.27	0.990	0.60	0.995	0.32	24.9
0.08	0.986	0.28	0.990	0.63	0.995	0.41	23.3
0.10	0.987	0.30	0.991	0.67	0.995	0.49	22.1
0.12	0.987	0.32	0.991	0.73	0.996	0.57	21.1
0.13	0.987	0.33	0.991	0.80	0.996	0.66	20.0
0.15	0.987	0.37	0.992	0.87	0.997	0.74	19.3
0.17	0.988	0.40	0.992	0.93	1.010	0.82	18.5
0.18	0.988	0.43	0.993	0.95	1.029	0.91	17.8
				0.96	1.048	0.99	17.1
h_{avg} (μm) =		2988				1.00	17.1

Table C.232: Experimental data for $\mu = 0.480$ N·s/m^2, $h_o = 2.985$ mm, $\Delta T_s = 22.7$°C.

r'	h / h_{avg}	r'	h / h_{avg}	r'	h / h_{avg}	r'	T_s (°C)
0.00	0.977	0.20	0.983	0.47	0.992	0.16	41.0
0.02	0.978	0.22	0.983	0.50	0.992	0.20	38.3
0.03	0.978	0.23	0.984	0.53	0.993	0.24	36.1
0.05	0.978	0.25	0.985	0.57	0.994	0.28	33.9
0.07	0.979	0.27	0.985	0.60	0.995	0.32	32.5
0.08	0.980	0.28	0.986	0.63	0.995	0.41	29.4
0.10	0.980	0.30	0.987	0.67	0.996	0.49	27.2
0.12	0.980	0.32	0.987	0.73	0.997	0.57	25.4
0.13	0.981	0.33	0.988	0.80	0.997	0.66	23.5
0.15	0.981	0.37	0.989	0.87	0.998	0.74	22.2
0.17	0.982	0.40	0.990	0.93	1.012	0.82	20.8
0.18	0.982	0.43	0.991	0.95	1.030	0.91	19.5
				0.96	1.050	0.99	18.4
h_{avg} (μm) =		3002				1.00	18.4

Table C.233: Experimental data for $\mu = 0.480$ N·s/m^2, $h_o = 2.985$ mm, $\Delta T_s = 31.0$°C.

r'	h / h_{avg}	r'	h / h_{avg}	r'	h / h_{avg}	r'	T_s (°C)
0.00	0.973	0.20	0.979	0.47	0.990	0.16	50.5
0.02	0.973	0.22	0.980	0.50	0.991	0.20	46.8
0.03	0.973	0.23	0.981	0.53	0.992	0.24	43.7
0.05	0.973	0.25	0.981	0.57	0.993	0.28	40.7
0.07	0.974	0.27	0.982	0.60	0.994	0.32	38.7
0.08	0.974	0.28	0.983	0.63	0.995	0.41	34.5
0.10	0.975	0.30	0.984	0.67	0.996	0.49	31.4
0.12	0.976	0.32	0.984	0.73	0.998	0.57	28.9
0.13	0.976	0.33	0.985	0.80	0.999	0.66	26.4
0.15	0.977	0.37	0.987	0.87	1.000	0.74	24.5
0.17	0.978	0.40	0.988	0.93	1.013	0.82	22.6
0.18	0.978	0.43	0.989	0.95	1.032	0.91	20.9
				0.96	1.051	0.99	19.5
h_{avg} (μm) =		3013				1.00	19.5

Table C.234: Experimental data for $\mu = 0.480$ N·s/m^2, $h_o = 2.985$ mm, $\Delta T_s = 39.4$°C.

r'	h / h_{avg}	r'	h / h_{avg}	r'	h / h_{avg}	r'	T_s (°C)
0.00	0.967	0.20	0.975	0.47	0.988	0.16	60.0
0.02	0.967	0.22	0.976	0.50	0.990	0.20	55.3
0.03	0.968	0.23	0.977	0.53	0.992	0.24	51.4
0.05	0.969	0.25	0.978	0.57	0.993	0.28	47.5
0.07	0.969	0.27	0.979	0.60	0.994	0.32	45.0
0.08	0.970	0.28	0.979	0.63	0.995	0.41	39.7
0.10	0.970	0.30	0.980	0.67	0.996	0.49	35.7
0.12	0.971	0.32	0.981	0.73	0.998	0.57	32.6
0.13	0.972	0.33	0.982	0.80	1.000	0.66	29.4
0.15	0.972	0.37	0.983	0.87	1.002	0.74	26.9
0.17	0.973	0.40	0.985	0.93	1.015	0.82	24.5
0.18	0.974	0.43	0.987	0.95	1.033	0.91	22.4
				0.96	1.053	0.99	20.6
h_{avg} (μm) =		3027				1.00	20.6

Table C.235: Experimental data for $\mu = 0.480$ N·s/m^2, $h_o = 2.985$ mm, $\Delta T_s = 48.1$°C.

r'	h / h_{avg}	r'	h / h_{avg}	r'	h / h_{avg}	r'	T_s (°C)
0.00	0.963	0.20	0.972	0.47	0.987	0.16	70.0
0.02	0.962	0.22	0.972	0.50	0.989	0.20	64.3
0.03	0.963	0.23	0.973	0.53	0.990	0.24	59.5
0.05	0.964	0.25	0.975	0.57	0.992	0.28	54.7
0.07	0.964	0.27	0.975	0.60	0.993	0.32	51.7
0.08	0.965	0.28	0.976	0.63	0.994	0.41	45.2
0.10	0.966	0.30	0.978	0.67	0.996	0.49	40.3
0.12	0.967	0.32	0.978	0.73	0.999	0.57	36.5
0.13	0.968	0.33	0.980	0.80	1.001	0.66	32.7
0.15	0.969	0.37	0.982	0.87	1.003	0.74	29.6
0.17	0.970	0.40	0.983	0.93	1.017	0.82	26.6
0.18	0.971	0.43	0.985	0.95	1.035	0.91	24.0
				0.96	1.054	0.99	21.8
h_{avg} (μm) =		3045				1.00	21.8

Table C.236: Experimental data for $\mu = 0.480$ N·s/m^2, $h_o = 2.985$ mm, $\Delta T_s = 52.3$°C.

r'	h / h_{avg}	r'	h / h_{avg}	r'	h / h_{avg}	r'	T_s (°C)
0.00	0.960	0.20	0.970	0.47	0.986	0.16	74.7
0.02	0.961	0.22	0.971	0.50	0.988	0.20	68.4
0.03	0.961	0.23	0.972	0.53	0.990	0.24	63.2
0.05	0.962	0.25	0.973	0.57	0.991	0.28	58.1
0.07	0.963	0.27	0.974	0.60	0.993	0.32	54.8
0.08	0.964	0.28	0.975	0.63	0.995	0.41	47.7
0.10	0.965	0.30	0.976	0.67	0.996	0.49	42.5
0.12	0.965	0.32	0.977	0.73	0.999	0.57	38.3
0.13	0.967	0.33	0.979	0.80	1.002	0.66	34.2
0.15	0.967	0.37	0.980	0.87	1.003	0.74	30.8
0.17	0.968	0.40	0.982	0.93	1.018	0.82	27.6
0.18	0.969	0.43	0.984	0.95	1.036	0.91	24.7
				0.96	1.054	0.99	22.4
h_{avg} (μm) =		3051				1.00	22.4

Table C.237: Experimental data for $\mu = 0.480$ N·s/m^2, $h_o = 2.985$ mm, $\Delta T_s = 0.1$°C.

r'	h / h_{avg}	r'	h / h_{avg}	r'	h / h_{avg}	r'	T_s (°C)
0.00	0.995	0.20	0.995	0.47	0.995	0.16	21.3
0.02	0.995	0.22	0.995	0.50	0.995	0.20	21.3
0.03	0.995	0.23	0.995	0.53	0.995	0.24	21.4
0.05	0.995	0.25	0.996	0.57	0.995	0.28	21.4
0.07	0.996	0.27	0.995	0.60	0.995	0.32	21.4
0.08	0.996	0.28	0.995	0.63	0.995	0.41	21.5
0.10	0.996	0.30	0.996	0.67	0.995	0.49	21.6
0.12	0.996	0.32	0.995	0.73	0.995	0.57	21.7
0.13	0.995	0.33	0.995	0.80	0.995	0.66	21.5
0.15	0.995	0.37	0.995	0.87	0.995	0.74	21.6
0.17	0.996	0.40	0.995	0.93	1.007	0.82	21.6
0.18	0.995	0.43	0.995	0.95	1.026	0.91	21.6
				0.96	1.045	0.99	21.4
h_{avg} (μm)		3017				1.00	21.4

Table C.238: Experimental data for $\mu = 9.600$ N·s/m^2, $h_o = 0.976$ mm, $\Delta T_s = 0.1$°C.

r'	h / h_{avg}	r'	h / h_{avg}	r'	h / h_{avg}	r'	T_s (°C)
0.00	0.982	0.20	0.983	0.47	0.983	0.16	20.5
0.02	0.982	0.22	0.983	0.50	0.983	0.20	20.5
0.03	0.982	0.23	0.983	0.53	0.983	0.24	20.5
0.05	0.982	0.25	0.983	0.57	0.983	0.28	20.6
0.07	0.982	0.27	0.983	0.60	0.983	0.32	20.6
0.08	0.982	0.28	0.983	0.63	0.982	0.41	20.6
0.10	0.982	0.30	0.983	0.67	0.982	0.49	20.7
0.12	0.982	0.32	0.983	0.73	0.982	0.57	20.7
0.13	0.983	0.33	0.983	0.80	0.982	0.66	20.6
0.15	0.983	0.37	0.983	0.87	0.982	0.74	20.6
0.17	0.982	0.40	0.983	0.93	1.030	0.82	20.7
0.18	0.983	0.43	0.983	0.95	1.089	0.91	20.7
				0.96	1.154	0.99	20.4
h_{avg} (μm) =		993				1.00	20.4

Table C.239: Experimental data for $\mu = 9.600$ N·s/m^2, $h_o = 0.976$ mm, $\Delta T_s = 12.4$°C.

r'	h / h_{avg}	r'	h / h_{avg}	r'	h / h_{avg}	r'	T_s (°C)
0.00	0.846	0.20	0.893	0.47	0.959	0.16	29.4
0.02	0.847	0.22	0.899	0.50	0.965	0.20	27.9
0.03	0.850	0.23	0.905	0.53	0.970	0.24	26.7
0.05	0.852	0.25	0.910	0.57	0.975	0.28	25.5
0.07	0.856	0.27	0.914	0.60	0.979	0.32	24.8
0.08	0.859	0.28	0.919	0.63	0.984	0.41	23.2
0.10	0.863	0.30	0.923	0.67	0.987	0.49	22.0
0.12	0.867	0.32	0.928	0.73	0.995	0.57	21.0
0.13	0.872	0.33	0.932	0.80	1.001	0.66	19.9
0.15	0.877	0.37	0.939	0.87	1.009	0.74	19.2
0.17	0.882	0.40	0.947	0.93	1.058	0.82	18.4
0.18	0.888	0.43	0.953	0.95	1.124	0.91	17.8
				0.96	1.186	0.99	17.0
h_{avg} (μm) =		981				1.00	17.0

Table C.240: Experimental data for $\mu = 9.600$ N·s/m^2, $h_o = 0.976$ mm, $\Delta T_s = 22.5$°C.

r'	h / h_{avg}	r'	h / h_{avg}	r'	h / h_{avg}	r'	T_s (°C)
0.00	0.716	0.20	0.814	0.47	0.943	0.16	40.8
0.02	0.721	0.22	0.825	0.50	0.953	0.20	38.1
0.03	0.726	0.23	0.837	0.53	0.962	0.24	35.9
0.05	0.731	0.25	0.846	0.57	0.971	0.28	33.7
0.07	0.737	0.27	0.856	0.60	0.979	0.32	32.2
0.08	0.745	0.28	0.866	0.63	0.986	0.41	29.2
0.10	0.753	0.30	0.875	0.67	0.994	0.49	27.0
0.12	0.761	0.32	0.884	0.73	1.006	0.57	25.2
0.13	0.771	0.33	0.892	0.80	1.017	0.66	23.3
0.15	0.780	0.37	0.907	0.87	1.029	0.74	22.0
0.17	0.792	0.40	0.920	0.93	1.082	0.82	20.6
0.18	0.803	0.43	0.932	0.95	1.147	0.91	19.4
				0.96	1.209	0.99	18.3
h_{avg} (μm) =		986				1.00	18.3

Table C.241: Experimental data for $\mu = 9.600$ N·s/m^2, $h_o = 0.976$ mm, $\Delta T_s = 31.3$°C.

r'	h / h_{avg}	r'	h / h_{avg}	r'	h / h_{avg}	r'	T_s (°C)
0.00	0.600	0.20	0.748	0.47	0.930	0.16	50.7
0.02	0.607	0.22	0.765	0.50	0.944	0.20	47.0
0.03	0.614	0.23	0.782	0.53	0.956	0.24	43.9
0.05	0.623	0.25	0.796	0.57	0.968	0.28	40.8
0.07	0.632	0.27	0.810	0.60	0.978	0.32	38.8
0.08	0.643	0.28	0.824	0.63	0.989	0.41	34.6
0.10	0.655	0.30	0.836	0.67	0.998	0.49	31.5
0.12	0.668	0.32	0.849	0.73	1.015	0.57	29.0
0.13	0.683	0.33	0.860	0.80	1.030	0.66	26.5
0.15	0.697	0.37	0.880	0.87	1.046	0.74	24.5
0.17	0.714	0.40	0.899	0.93	1.102	0.82	22.6
0.18	0.731	0.43	0.915	0.95	1.165	0.91	21.0
				0.96	1.225	0.99	19.5
h_{avg} (μm) =		994				1.00	19.5

Table C.242: Experimental data for $\mu = 9.600$ N·s/m^2, $h_o = 0.976$ mm, $\Delta T_s = 39.4$°C.

r'	h / h_{avg}	r'	h / h_{avg}	r'	h / h_{avg}	r'	T_s (°C)
0.00	0.463	0.20	0.682	0.47	0.919	0.16	59.9
0.02	0.470	0.22	0.705	0.50	0.935	0.20	55.2
0.03	0.484	0.23	0.727	0.53	0.951	0.24	51.3
0.05	0.496	0.25	0.747	0.57	0.966	0.28	47.5
0.07	0.511	0.27	0.766	0.60	0.980	0.32	45.0
0.08	0.529	0.28	0.783	0.63	0.993	0.41	39.6
0.10	0.546	0.30	0.800	0.67	1.003	0.49	35.7
0.12	0.565	0.32	0.816	0.73	1.024	0.57	32.5
0.13	0.588	0.33	0.830	0.80	1.043	0.66	29.4
0.15	0.610	0.37	0.856	0.87	1.062	0.74	26.9
0.17	0.633	0.40	0.880	0.93	1.119	0.82	24.5
0.18	0.658	0.43	0.900	0.95	1.183	0.91	22.4
				0.96	1.241	0.99	20.5
h_{avg} (μm) =		1004				1.00	20.5

Table C.243: Experimental data for $\mu = 9.600$ N·s/m^2, $h_o = 0.976$ mm, $\Delta T_s = 47.1$°C.

r'	h / h_{avg}	r'	h / h_{avg}	r'	h / h_{avg}	r'	T_s (°C)
0.00	0.236	0.20	0.611	0.47	0.909	0.16	68.7
0.02	0.259	0.22	0.642	0.50	0.930	0.20	63.1
0.03	0.292	0.23	0.670	0.53	0.948	0.24	58.4
0.05	0.320	0.25	0.697	0.57	0.966	0.28	53.8
0.07	0.348	0.27	0.720	0.60	0.981	0.32	50.8
0.08	0.382	0.28	0.744	0.63	0.997	0.41	44.4
0.10	0.412	0.30	0.765	0.67	1.010	0.49	39.6
0.12	0.442	0.32	0.783	0.73	1.035	0.57	35.8
0.13	0.474	0.33	0.801	0.80	1.057	0.66	32.1
0.15	0.509	0.37	0.832	0.87	1.078	0.74	29.1
0.17	0.544	0.40	0.861	0.93	1.138	0.82	26.2
0.18	0.578	0.43	0.886	0.95	1.200	0.91	23.7
				0.96	1.259	0.99	21.6
h_{avg} (μm) =		1013				1.00	21.6

Table C.244: Experimental data for $\mu = 9.600$ N·s/m^2, $h_o = 0.976$ mm, $\Delta T_s = 0.0$°C.

r'	h / h_{avg}	r'	h / h_{avg}	r'	h / h_{avg}	r'	T_s (°C)
0.00	0.983	0.20	0.984	0.47	0.983	0.16	21.4
0.02	0.983	0.22	0.984	0.50	0.983	0.20	21.4
0.03	0.984	0.23	0.984	0.53	0.983	0.24	21.4
0.05	0.984	0.25	0.984	0.57	0.983	0.28	21.5
0.07	0.984	0.27	0.984	0.60	0.983	0.32	21.5
0.08	0.984	0.28	0.984	0.63	0.983	0.41	21.6
0.10	0.984	0.30	0.984	0.67	0.983	0.49	21.6
0.12	0.984	0.32	0.984	0.73	0.982	0.57	21.7
0.13	0.984	0.33	0.984	0.80	0.982	0.66	21.5
0.15	0.984	0.37	0.984	0.87	0.982	0.74	21.6
0.17	0.983	0.40	0.984	0.93	1.030	0.82	21.6
0.18	0.984	0.43	0.983	0.95	1.088	0.91	21.6
				0.96	1.147	0.99	21.4
h_{avg} (μm) =		996				1.00	21.4

Table C.245: Experimental data for $\mu = 9.600$ N·s/m^2, $h_o = 1.964$ mm, $\Delta T_s = 0.2$°C.

r'	h / h_{avg}	r'	h / h_{avg}	r'	h / h_{avg}	r'	T_s (°C)
0.02	0.993	0.22	0.993	0.50	0.992	0.16	21.3
0.03	0.993	0.23	0.993	0.53	0.992	0.20	21.3
0.05	0.993	0.25	0.993	0.57	0.992	0.24	21.3
0.07	0.993	0.27	0.993	0.60	0.992	0.28	21.3
0.08	0.993	0.28	0.993	0.63	0.992	0.32	21.3
0.10	0.993	0.30	0.993	0.67	0.992	0.41	21.3
0.12	0.993	0.32	0.993	0.73	0.993	0.49	21.4
0.13	0.993	0.33	0.993	0.80	0.993	0.57	21.4
0.15	0.993	0.37	0.992	0.87	0.993	0.66	21.3
0.17	0.993	0.40	0.992	0.93	1.013	0.74	21.3
0.18	0.993	0.43	0.992	0.95	1.041	0.82	21.3
0.20	0.993	0.47	0.992	0.96	1.067	0.91	21.3
						0.99	21.1
h_{avg} (μm) =		1977				1.00	21.1

Table C.246: Experimental data for $\mu = 9.600$ N·s/m^2, $h_o = 1.964$ mm, $\Delta T_s = 12.6$°C.

r'	h / h_{avg}	r'	h / h_{avg}	r'	h / h_{avg}	r'	T_s (°C)
0.00	0.966	0.20	0.974	0.47	0.987	0.16	29.7
0.02	0.966	0.22	0.976	0.50	0.988	0.20	28.3
0.03	0.967	0.23	0.977	0.53	0.989	0.24	27.1
0.05	0.967	0.25	0.978	0.57	0.991	0.28	25.9
0.07	0.968	0.27	0.978	0.60	0.992	0.32	25.1
0.08	0.968	0.28	0.979	0.63	0.993	0.41	23.4
0.10	0.969	0.30	0.980	0.67	0.993	0.49	22.2
0.12	0.970	0.32	0.981	0.73	0.995	0.57	21.3
0.13	0.971	0.33	0.982	0.80	0.996	0.66	20.1
0.15	0.971	0.37	0.983	0.87	0.998	0.74	19.4
0.17	0.972	0.40	0.985	0.93	1.019	0.82	18.6
0.18	0.973	0.43	0.986	0.95	1.047	0.91	17.9
				0.96	1.073	0.99	17.1
h_{avg} (μm) =		1960				1.00	17.1

Table C.247: Experimental data for $\mu = 9.600$ N·s/m^2, $h_o = 1.964$ mm, $\Delta T_s = 23.0$°C.

r'	h / h_{avg}	r'	h / h_{avg}	r'	h / h_{avg}	r'	T_s (°C)
0.00	0.946	0.20	0.960	0.47	0.984	0.16	41.4
0.02	0.946	0.22	0.962	0.50	0.986	0.20	38.7
0.03	0.947	0.23	0.964	0.53	0.988	0.24	36.4
0.05	0.948	0.25	0.966	0.57	0.989	0.28	34.1
0.07	0.949	0.27	0.967	0.60	0.991	0.32	32.7
0.08	0.950	0.28	0.969	0.63	0.992	0.41	29.6
0.10	0.951	0.30	0.971	0.67	0.994	0.49	27.3
0.12	0.952	0.32	0.972	0.73	0.997	0.57	25.5
0.13	0.953	0.33	0.974	0.80	0.999	0.66	23.6
0.15	0.955	0.37	0.977	0.87	1.002	0.74	22.2
0.17	0.956	0.40	0.979	0.93	1.024	0.82	20.8
0.18	0.958	0.43	0.982	0.95	1.052	0.91	19.6
				0.96	1.079	0.99	18.4
h_{avg} (μm) =		1970				1.00	18.4

Table C.248: Experimental data for $\mu = 9.600$ N·s/m^2, $h_o = 1.964$ mm, $\Delta T_s = 50.0$°C.

r'	h / h_{avg}	r'	h / h_{avg}	r'	h / h_{avg}	r'	T_s (°C)
0.00	0.927	0.20	0.947	0.47	0.980	0.16	50.0
0.02	0.928	0.22	0.949	0.50	0.983	0.20	46.3
0.03	0.929	0.23	0.951	0.53	0.986	0.24	43.2
0.05	0.931	0.25	0.954	0.57	0.988	0.28	40.2
0.07	0.931	0.27	0.956	0.60	0.991	0.32	38.2
0.08	0.932	0.28	0.959	0.63	0.993	0.41	34.1
0.10	0.934	0.30	0.961	0.67	0.995	0.49	31.0
0.12	0.935	0.32	0.964	0.73	0.999	0.57	28.6
0.13	0.938	0.33	0.966	0.80	1.002	0.66	26.1
0.15	0.939	0.37	0.970	0.87	1.005	0.74	24.2
0.17	0.941	0.40	0.974	0.93	1.028	0.82	22.4
0.18	0.944	0.43	0.977	0.95	1.056	0.91	20.8
				0.96	1.083	1.00	20.8
h_{avg} (μm) =		1979					

Table C.249: Experimental data for $\mu = 9.600$ N·s/m^2, $h_o = 1.964$ mm, $\Delta T_s = 60.6$°C.

r'	h / h_{avg}	r'	h / h_{avg}	r'	h / h_{avg}	r'	T_s (°C)
0.00	0.908	0.20	0.934	0.47	0.977	0.16	60.6
0.02	0.909	0.22	0.936	0.50	0.981	0.20	55.8
0.03	0.910	0.23	0.940	0.53	0.985	0.24	51.8
0.05	0.912	0.25	0.944	0.57	0.987	0.28	47.9
0.07	0.914	0.27	0.946	0.60	0.990	0.32	45.3
0.08	0.916	0.28	0.949	0.63	0.993	0.41	39.9
0.10	0.918	0.30	0.952	0.67	0.996	0.49	35.8
0.12	0.921	0.32	0.956	0.73	1.001	0.57	32.6
0.13	0.923	0.33	0.958	0.80	1.005	0.66	29.4
0.15	0.925	0.37	0.964	0.87	1.009	0.74	26.9
0.17	0.928	0.40	0.969	0.93	1.032	0.82	24.5
0.18	0.930	0.43	0.973	0.95	1.060	0.91	22.4
h_{avg} (μm) =		1987		0.96	1.087	1.00	22.4

Table C.250: Experimental data for $\mu = 9.600$ N·s/m^2, $h_o = 1.964$ mm, $\Delta T_s = 70.9$°C.

r'	h / h_{avg}	r'	h / h_{avg}	r'	h / h_{avg}	r'	T_s (°C)
0.00	0.893	0.20	0.924	0.47	0.974	0.16	70.9
0.02	0.894	0.22	0.927	0.50	0.978	0.20	65.1
0.03	0.897	0.23	0.931	0.53	0.983	0.24	60.2
0.05	0.899	0.25	0.934	0.57	0.987	0.28	55.3
0.07	0.901	0.27	0.937	0.60	0.990	0.32	52.2
0.08	0.903	0.28	0.942	0.63	0.994	0.41	45.5
0.10	0.906	0.30	0.945	0.67	0.996	0.49	40.5
0.12	0.908	0.32	0.948	0.73	1.002	0.57	36.5
0.13	0.911	0.33	0.952	0.80	1.007	0.66	32.7
0.15	0.914	0.37	0.958	0.87	1.012	0.74	29.5
0.17	0.917	0.40	0.964	0.93	1.036	0.82	26.5
0.18	0.919	0.43	0.969	0.95	1.063	0.91	23.9
h_{avg} (μm) =		1996		0.96	1.090	1.00	23.9

Table C.251: Experimental data for $\mu = 9.600$ N·s/m^2, $h_o = 1.964$ mm, $\Delta T_s = 77.9$°C.

r'	h / h_{avg}	r'	h / h_{avg}	r'	h / h_{avg}	r'	T_s (°C)
0.00	0.878	0.20	0.913	0.47	0.971	0.16	77.9
0.02	0.880	0.22	0.917	0.50	0.976	0.20	71.4
0.03	0.881	0.23	0.921	0.53	0.981	0.24	65.9
0.05	0.884	0.25	0.926	0.57	0.986	0.28	60.4
0.07	0.887	0.27	0.929	0.60	0.990	0.32	56.9
0.08	0.889	0.28	0.933	0.63	0.994	0.41	49.3
0.10	0.892	0.30	0.937	0.67	0.998	0.49	43.7
0.12	0.895	0.32	0.941	0.73	1.004	0.57	39.2
0.13	0.898	0.33	0.945	0.80	1.009	0.66	34.9
0.15	0.901	0.37	0.952	0.87	1.016	0.74	31.4
0.17	0.905	0.40	0.959	0.93	1.039	0.82	28.0
0.18	0.909	0.43	0.965	0.95	1.067	0.91	25.0
h_{avg} (μm) =		2002		0.96	1.093	1.00	25.0

Table C.252: Experimental data for $\mu = 9.600$ N·s/m^2, $h_o = 1.964$ mm, $\Delta T_s = 18.6$°C.

r'	h / h_{avg}	r'	h / h_{avg}	r'	h / h_{avg}	r'	T_s (°C)
0.00	0.991	0.20	0.993	0.47	0.993	0.16	18.6
0.02	0.992	0.22	0.993	0.50	0.993	0.20	18.5
0.03	0.992	0.23	0.993	0.53	0.992	0.24	18.6
0.05	0.992	0.25	0.993	0.57	0.993	0.28	18.6
0.07	0.992	0.27	0.993	0.60	0.992	0.32	18.6
0.08	0.992	0.28	0.993	0.63	0.992	0.41	18.6
0.10	0.993	0.30	0.993	0.67	0.992	0.49	18.7
0.12	0.993	0.32	0.993	0.73	0.992	0.57	18.7
0.13	0.993	0.33	0.993	0.80	0.992	0.66	18.5
0.15	0.993	0.37	0.993	0.87	0.993	0.74	18.6
0.17	0.993	0.40	0.993	0.93	1.012	0.82	18.6
0.18	0.993	0.43	0.993	0.95	1.041	0.91	18.6
h_{avg} (μm) =		1964		0.96	1.068	1.00	18.6

Table C.253: Experimental data for $\mu = 9.600$ N·s/m^2, $h_o = 2.957$ mm, $\Delta T_s = 16.0$°C.

r'	h / h_{avg}	r'	h / h_{avg}	r'	h / h_{avg}	r'	T_s (°C)
0.00	0.994	0.20	0.995	0.47	0.995	0.16	16.0
0.02	0.994	0.22	0.995	0.50	0.995	0.20	16.0
0.03	0.995	0.23	0.995	0.53	0.995	0.24	16.0
0.05	0.995	0.25	0.995	0.57	0.995	0.28	16.0
0.07	0.995	0.27	0.995	0.60	0.995	0.32	16.0
0.08	0.995	0.28	0.995	0.63	0.995	0.41	16.0
0.10	0.995	0.30	0.995	0.67	0.995	0.49	16.1
0.12	0.995	0.32	0.995	0.73	0.995	0.57	16.1
0.13	0.995	0.33	0.995	0.80	0.995	0.66	15.8
0.15	0.995	0.37	0.995	0.87	0.995	0.74	15.9
0.17	0.995	0.40	0.995	0.93	1.008	0.82	15.9
0.18	0.995	0.43	0.995	0.95	1.027	0.91	15.8
h_{avg} (μm) =		2972		0.96	1.047	1.00	15.8

Table C.254: Experimental data for $\mu = 9.600$ N·s/m^2, $h_o = 2.957$ mm, $\Delta T_s = 29.6$°C.

r'	h / h_{avg}	r'	h / h_{avg}	r'	h / h_{avg}	r'	T_s (°C)
0.00	0.985	0.20	0.988	0.47	0.993	0.16	29.6
0.02	0.985	0.22	0.989	0.50	0.994	0.20	28.1
0.03	0.985	0.23	0.989	0.53	0.994	0.24	26.9
0.05	0.986	0.25	0.990	0.57	0.994	0.28	25.7
0.07	0.986	0.27	0.990	0.60	0.995	0.32	24.9
0.08	0.986	0.28	0.990	0.63	0.995	0.41	23.2
0.10	0.986	0.30	0.991	0.67	0.995	0.49	22.0
0.12	0.987	0.32	0.991	0.73	0.996	0.57	21.1
0.13	0.987	0.33	0.991	0.80	0.996	0.66	19.9
0.15	0.987	0.37	0.992	0.87	0.997	0.74	19.2
0.17	0.988	0.40	0.992	0.93	1.010	0.82	18.5
0.18	0.988	0.43	0.993	0.95	1.029	0.91	17.8
h_{avg} (μm) =		2960		0.96	1.049	1.00	17.8

Table C.255: Experimental data for $\mu = 9.600$ N·s/m^2, $h_o = 2.957$ mm, $\Delta T_s = 40.8$°C.

r'	h / h_{avg}	r'	h / h_{avg}	r'	h / h_{avg}	r'	T_s (°C)
0.00	0.977	0.20	0.983	0.47	0.992	0.16	40.8
0.02	0.978	0.22	0.983	0.50	0.992	0.20	38.1
0.03	0.978	0.23	0.984	0.53	0.993	0.24	35.9
0.05	0.978	0.25	0.985	0.57	0.994	0.28	33.7
0.07	0.979	0.27	0.985	0.60	0.995	0.32	32.2
0.08	0.979	0.28	0.986	0.63	0.995	0.41	29.2
0.10	0.979	0.30	0.987	0.67	0.996	0.49	26.9
0.12	0.980	0.32	0.987	0.73	0.997	0.57	25.2
0.13	0.981	0.33	0.988	0.80	0.997	0.66	23.3
0.15	0.981	0.37	0.989	0.87	0.998	0.74	22.0
0.17	0.982	0.40	0.990	0.93	1.012	0.82	20.6
0.18	0.982	0.43	0.991	0.95	1.031	0.91	19.4
h_{avg} (μm) =		2973		0.96	1.050	1.00	19.4

Table C.256: Experimental data for $\mu = 9.600$ N·s/m^2, $h_o = 2.957$ mm, $\Delta T_s = 50.6$°C.

r'	h / h_{avg}	r'	h / h_{avg}	r'	h / h_{avg}	r'	T_s (°C)
0.00	0.972	0.20	0.979	0.47	0.990	0.16	50.6
0.02	0.972	0.22	0.979	0.50	0.991	0.20	46.9
0.03	0.972	0.23	0.981	0.53	0.992	0.24	43.8
0.05	0.973	0.25	0.981	0.57	0.993	0.28	40.7
0.07	0.974	0.27	0.982	0.60	0.994	0.32	38.7
0.08	0.974	0.28	0.982	0.63	0.995	0.41	34.5
0.10	0.975	0.30	0.983	0.67	0.996	0.49	31.3
0.12	0.975	0.32	0.984	0.73	0.998	0.57	28.8
0.13	0.976	0.33	0.985	0.80	0.999	0.66	26.3
0.15	0.977	0.37	0.986	0.87	1.000	0.74	24.4
0.17	0.977	0.40	0.988	0.93	1.013	0.82	22.5
0.18	0.978	0.43	0.989	0.95	1.033	0.91	20.9
h_{avg} (μm) =		2985		0.96	1.052	1.00	20.9

Table C.257: Experimental data for $\mu = 9.600$ N·s/m^2, $h_o = 2.957$ mm, $\Delta T_s = 59.0$°C.

r'	h / h_{avg}	r'	h / h_{avg}	r'	h / h_{avg}	r'	T_s (°C)
0.00	0.967	0.20	0.975	0.47	0.988	0.16	59.0
0.02	0.967	0.22	0.976	0.50	0.990	0.20	54.4
0.03	0.968	0.23	0.977	0.53	0.992	0.24	50.6
0.05	0.968	0.25	0.978	0.57	0.993	0.28	46.8
0.07	0.969	0.27	0.978	0.60	0.994	0.32	44.3
0.08	0.970	0.28	0.979	0.63	0.995	0.41	39.1
0.10	0.970	0.30	0.980	0.67	0.996	0.49	35.1
0.12	0.971	0.32	0.981	0.73	0.998	0.57	32.0
0.13	0.972	0.33	0.982	0.80	1.000	0.66	28.9
0.15	0.972	0.37	0.983	0.87	1.002	0.74	26.5
0.17	0.973	0.40	0.985	0.93	1.015	0.82	24.2
0.18	0.974	0.43	0.987	0.95	1.034	0.91	22.2
h_{avg} (μm) =		2999		0.96	1.053	1.00	22.2

Table C.258: Experimental data for $\mu = 9.600$ N·s/m^2, $h_o = 2.957$ mm, $\Delta T_s = 71.0$°C.

r'	h / h_{avg}	r'	h / h_{avg}	r'	h / h_{avg}	r'	T_s (°C)
0.00	0.963	0.20	0.971	0.47	0.987	0.16	71.0
0.02	0.962	0.22	0.972	0.50	0.988	0.20	65.2
0.03	0.963	0.23	0.973	0.53	0.990	0.24	60.3
0.05	0.963	0.25	0.974	0.57	0.992	0.28	55.5
0.07	0.964	0.27	0.975	0.60	0.993	0.32	52.3
0.08	0.965	0.28	0.976	0.63	0.994	0.41	45.7
0.10	0.966	0.30	0.977	0.67	0.996	0.49	40.6
0.12	0.966	0.32	0.978	0.73	0.999	0.57	36.7
0.13	0.968	0.33	0.979	0.80	1.001	0.66	32.8
0.15	0.968	0.37	0.981	0.87	1.003	0.74	29.6
0.17	0.969	0.40	0.983	0.93	1.017	0.82	26.6
0.18	0.970	0.43	0.985	0.95	1.035	0.91	24.0
h_{avg} (μm) =		3017		0.96	1.054	1.00	24.0

Table C.259: Experimental data for $\mu = 9.600$ N·s/m^2, $h_o = 2.957$ mm, $\Delta T_s = 74.7$°C.

r'	h / h_{avg}	r'	h / h_{avg}	r'	h / h_{avg}	r'	T_s (°C)
0.00	0.960	0.20	0.970	0.47	0.986	0.16	74.7
0.02	0.961	0.22	0.971	0.50	0.988	0.20	68.5
0.03	0.961	0.23	0.972	0.53	0.989	0.24	63.3
0.05	0.962	0.25	0.973	0.57	0.991	0.28	58.1
0.07	0.963	0.27	0.974	0.60	0.993	0.32	54.8
0.08	0.964	0.28	0.975	0.63	0.995	0.41	47.7
0.10	0.964	0.30	0.976	0.67	0.996	0.49	42.3
0.12	0.965	0.32	0.977	0.73	0.999	0.57	38.1
0.13	0.966	0.33	0.978	0.80	1.002	0.66	33.9
0.15	0.967	0.37	0.980	0.87	1.003	0.74	30.6
0.17	0.968	0.40	0.982	0.93	1.018	0.82	27.4
0.18	0.969	0.43	0.984	0.95	1.036	0.91	24.6
h_{avg} (μm) =		3023		0.96	1.055	1.00	24.6

C.2.3. Numerical Results

This section presents numerical results obtained for simulations at experimental conditions. The temperatures along the bottom of the liquid layer were distributed using a Gaussian function, as discussed previously in Chapter 4. In all cases shown here, the resolution of the stationary grid was 15 × 30 along the r and z directions, respectively. The presented simulations are organized by viscosity, initial film height, and temperature difference.

Table C.260: Numerical results for $\mu = 0.048$ N·s/m^2, $h_o = 0.438$ mm, $\Delta T_s = 7.6$°C.

r'	***h'***	***r'***	***h'***	***r'***	***h'***	***r'***	***h'***
0.00	0.506	0.27	0.816	0.53	0.963	0.80	1.062
0.02	0.510	0.28	0.831	0.55	0.970	0.82	1.067
0.03	0.519	0.30	0.844	0.57	0.977	0.83	1.071
0.05	0.534	0.32	0.857	0.58	0.984	0.85	1.076
0.07	0.554	0.33	0.868	0.60	0.991	0.87	1.080
0.08	0.576	0.35	0.879	0.62	0.998	0.88	1.084
0.10	0.600	0.37	0.888	0.63	1.005	0.90	1.089
0.12	0.625	0.38	0.897	0.65	1.011	0.92	1.094
0.13	0.650	0.40	0.906	0.67	1.018	0.93	1.099
0.15	0.674	0.42	0.914	0.68	1.024	0.95	1.105
0.17	0.698	0.43	0.921	0.70	1.031	0.97	1.110
0.18	0.721	0.45	0.928	0.72	1.037	0.98	1.114
0.20	0.742	0.47	0.936	0.73	1.042	1.00	1.116
0.22	0.763	0.48	0.943	0.75	1.048		
0.23	0.782	0.50	0.950	0.77	1.053		
0.25	0.800	0.52	0.956	0.78	1.058		

Table C.261: Numerical results for $\mu = 0.048$ N·s/m^2, $h_o = 0.588$ mm, $\Delta T_s = 9.8$°C.

r'	***h'***	***r'***	***h'***	***r'***	***h'***	***r'***	***h'***
0.02	0.745	0.28	0.859	0.55	0.996	0.82	1.048
0.05	0.749	0.32	0.879	0.58	1.007	0.85	1.051
0.08	0.757	0.35	0.898	0.62	1.016	0.88	1.053
0.12	0.769	0.38	0.917	0.65	1.024	0.92	1.054
0.15	0.784	0.42	0.935	0.68	1.031	0.95	1.055
0.18	0.801	0.45	0.952	0.72	1.037	0.98	1.056
0.22	0.819	0.48	0.968	0.75	1.042		
0.25	0.838	0.52	0.983	0.78	1.045		

Table C.262: Numerical results for $\mu = 0.048$ N·s/m^2, $h_o = 0.695$ mm, $\Delta T_s = 13.0$°C.

r'	***h'***	***r'***	***h'***	***r'***	***h'***	***r'***	***h'***
0.00	0.701	0.27	0.883	0.53	0.983	0.80	1.039
0.02	0.703	0.28	0.893	0.55	0.988	0.82	1.041
0.03	0.707	0.30	0.902	0.57	0.992	0.83	1.043
0.05	0.715	0.32	0.911	0.58	0.996	0.85	1.045
0.07	0.725	0.33	0.919	0.60	1.000	0.87	1.047
0.08	0.737	0.35	0.926	0.62	1.004	0.88	1.049
0.10	0.750	0.37	0.933	0.63	1.007	0.90	1.051
0.12	0.764	0.38	0.940	0.65	1.011	0.92	1.053
0.13	0.780	0.40	0.945	0.67	1.015	0.93	1.055
0.15	0.795	0.42	0.950	0.68	1.018	0.95	1.058
0.17	0.810	0.43	0.956	0.70	1.022	0.97	1.060
0.18	0.823	0.45	0.961	0.72	1.025	0.98	1.061
0.20	0.836	0.47	0.966	0.73	1.028	1.00	1.062
0.22	0.849	0.48	0.970	0.75	1.031		
0.23	0.862	0.50	0.975	0.77	1.034		
0.25	0.873	0.52	0.979	0.78	1.037		

Table C.263: Numerical results for $\mu = 0.048$ N·s/m^2, $h_o = 0.695$ mm, $\Delta T_s = 21.7$°C.

r'	***h'***	***r'***	***h'***	***r'***	***h'***	***r'***	***h'***
0.00	0.388	0.27	0.785	0.53	0.972	0.80	1.071
0.02	0.392	0.28	0.805	0.55	0.979	0.82	1.075
0.03	0.404	0.30	0.823	0.57	0.987	0.83	1.079
0.05	0.423	0.32	0.839	0.58	0.994	0.85	1.083
0.07	0.447	0.33	0.854	0.60	1.000	0.87	1.087
0.08	0.475	0.35	0.868	0.62	1.007	0.88	1.091
0.10	0.506	0.37	0.881	0.63	1.014	0.90	1.095
0.12	0.539	0.38	0.893	0.65	1.020	0.92	1.099
0.13	0.571	0.40	0.904	0.67	1.026	0.93	1.103
0.15	0.603	0.42	0.914	0.68	1.032	0.95	1.107
0.17	0.633	0.43	0.923	0.70	1.039	0.97	1.111
0.18	0.662	0.45	0.932	0.72	1.045	0.98	1.114
0.20	0.690	0.47	0.941	0.73	1.050	1.00	1.115
0.22	0.716	0.48	0.949	0.75	1.056		
0.23	0.741	0.50	0.957	0.77	1.061		
0.25	0.764	0.52	0.965	0.78	1.066		

Table C.264: Numerical results0 for $\mu = 0.048$ N·s/m^2, $h_o = 0.695$ mm, $\Delta T_s = 34.40$°C.

r'	***h'***	***r'***	***h'***	***r'***	***h'***	***r'***	***h'***
0.00	-0.149	0.27	0.641	0.53	0.976	0.80	1.125
0.02	-0.126	0.28	0.679	0.55	0.988	0.82	1.132
0.03	-0.102	0.30	0.714	0.57	0.999	0.83	1.138
0.05	-0.083	0.32	0.745	0.58	1.010	0.85	1.143
0.07	-0.058	0.33	0.774	0.60	1.020	0.87	1.149
0.08	-0.031	0.35	0.800	0.62	1.030	0.88	1.154
0.10	-0.001	0.37	0.823	0.63	1.041	0.90	1.158
0.12	0.040	0.38	0.843	0.65	1.051	0.92	1.164
0.13	0.096	0.40	0.863	0.67	1.060	0.93	1.169
0.15	0.174	0.42	0.881	0.68	1.069	0.95	1.173
0.17	0.273	0.43	0.897	0.70	1.078	0.97	1.177
0.18	0.360	0.45	0.911	0.72	1.087	0.98	1.180
0.20	0.430	0.47	0.926	0.73	1.096	1.00	1.182
0.22	0.491	0.48	0.939	0.75	1.104		
0.23	0.547	0.50	0.952	0.77	1.111		
0.25	0.597	0.52	0.964	0.78	1.119		

Table C.265: Numerical results for $\mu = 0.048$ N·s/m^2, $h_o = 1.026$ mm, $\Delta T_s = 38.5$°C.

r'	***h'***	***r'***	***h'***	***r'***	***h'***	***r'***	***h'***
0.00	0.645	0.27	0.790	0.53	0.983	0.80	1.066
0.02	0.645	0.28	0.804	0.55	0.992	0.82	1.067
0.03	0.648	0.30	0.818	0.57	1.000	0.83	1.069
0.05	0.651	0.32	0.832	0.58	1.007	0.85	1.071
0.07	0.656	0.33	0.846	0.60	1.014	0.87	1.072
0.08	0.662	0.35	0.859	0.62	1.021	0.88	1.073
0.10	0.669	0.37	0.872	0.63	1.027	0.90	1.074
0.12	0.677	0.38	0.885	0.65	1.033	0.92	1.075
0.13	0.686	0.40	0.897	0.67	1.038	0.93	1.076
0.15	0.697	0.42	0.909	0.68	1.043	0.95	1.077
0.17	0.708	0.43	0.921	0.70	1.047	0.97	1.077
0.18	0.720	0.45	0.932	0.72	1.051	0.98	1.077
0.20	0.733	0.47	0.943	0.73	1.055	1.00	1.078
0.22	0.747	0.48	0.953	0.75	1.058		
0.23	0.761	0.50	0.964	0.77	1.061		
0.25	0.776	0.52	0.973	0.78	1.063		

Table C.266: Numerical results for $\mu = 0.048$ N·s/m^2, $h_o = 1.026$ mm, $\Delta T_s = 47.3$°C.

r'	***h'***	***r'***	***h'***	***r'***	***h'***	***r'***	***h'***
0.00	0.514	0.27	0.729	0.53	0.980	0.80	1.085
0.02	0.515	0.28	0.748	0.55	0.991	0.82	1.087
0.03	0.519	0.30	0.768	0.57	1.001	0.83	1.089
0.05	0.525	0.32	0.787	0.58	1.011	0.85	1.091
0.07	0.533	0.33	0.805	0.60	1.019	0.87	1.093
0.08	0.544	0.35	0.822	0.62	1.028	0.88	1.094
0.10	0.557	0.37	0.839	0.63	1.036	0.90	1.096
0.12	0.572	0.38	0.856	0.65	1.043	0.92	1.097
0.13	0.587	0.40	0.872	0.67	1.049	0.93	1.098
0.15	0.603	0.42	0.888	0.68	1.055	0.95	1.099
0.17	0.619	0.43	0.902	0.70	1.061	0.97	1.099
0.18	0.637	0.45	0.916	0.72	1.066	0.98	1.100
0.20	0.655	0.47	0.930	0.73	1.071	1.00	1.100
0.22	0.673	0.48	0.943	0.75	1.075		
0.23	0.691	0.50	0.956	0.77	1.078		
0.25	0.710	0.52	0.968	0.78	1.082		

Table C.267: Numerical results for $\mu = 0.048$ N·s/m^2, $h_o = 1.026$ mm, $\Delta T_s = 53.8$°C.

r'	***h'***	***r'***	***h'***	***r'***	***h'***	***r'***	***h'***
0.00	0.427	0.27	0.690	0.53	0.978	0.80	1.097
0.02	0.429	0.28	0.712	0.55	0.990	0.82	1.099
0.03	0.433	0.30	0.734	0.57	1.002	0.83	1.102
0.05	0.440	0.32	0.757	0.58	1.012	0.85	1.104
0.07	0.450	0.33	0.778	0.60	1.022	0.87	1.106
0.08	0.462	0.35	0.799	0.62	1.031	0.88	1.108
0.10	0.477	0.37	0.819	0.63	1.040	0.90	1.110
0.12	0.494	0.38	0.838	0.65	1.049	0.92	1.111
0.13	0.512	0.40	0.856	0.67	1.056	0.93	1.112
0.15	0.533	0.42	0.874	0.68	1.063	0.95	1.113
0.17	0.554	0.43	0.891	0.70	1.069	0.97	1.114
0.18	0.576	0.45	0.907	0.72	1.075	0.98	1.114
0.20	0.599	0.47	0.922	0.73	1.080	1.00	1.114
0.22	0.622	0.48	0.937	0.75	1.085		
0.23	0.645	0.50	0.951	0.77	1.089		
0.25	0.667	0.52	0.965	0.78	1.093		

Table C.268: Numerical results for $\mu = 0.048$ N·s/m^2, $h_o = 1.026$ mm, $\Delta T_s = 57.9$°C.

r'	***h'***	***r'***	***h'***	***r'***	***h'***	***r'***	***h'***
0.00	-0.023	0.27	0.676	0.53	0.956	0.80	1.105
0.02	-0.009	0.28	0.704	0.55	0.967	0.82	1.112
0.03	0.027	0.30	0.730	0.57	0.978	0.83	1.119
0.05	0.070	0.32	0.754	0.58	0.989	0.85	1.126
0.07	0.120	0.33	0.777	0.60	0.999	0.87	1.132
0.08	0.183	0.35	0.797	0.62	1.009	0.88	1.138
0.10	0.245	0.37	0.816	0.63	1.018	0.90	1.144
0.12	0.300	0.38	0.834	0.65	1.028	0.92	1.149
0.13	0.353	0.40	0.851	0.67	1.038	0.93	1.154
0.15	0.405	0.42	0.867	0.68	1.047	0.95	1.159
0.17	0.454	0.43	0.881	0.70	1.056	0.97	1.163
0.18	0.499	0.45	0.895	0.72	1.065	0.98	1.166
0.20	0.540	0.47	0.908	0.73	1.073	1.00	1.167
0.22	0.578	0.48	0.920	0.75	1.082		
0.23	0.614	0.50	0.933	0.77	1.090		
0.25	0.647	0.52	0.944	0.78	1.098		

Table C.269: Numerical results for $\mu = 0.048$ N·s/m^2, $h_o = 1.026$ mm, $\Delta T_s = 68.6$°C.

r'	***h'***	***r'***	***h'***	***r'***	***h'***	***r'***	***h'***
0.00	-0.133	0.27	0.648	0.53	0.941	0.80	1.100
0.02	-0.087	0.28	0.677	0.55	0.953	0.82	1.108
0.03	-0.047	0.30	0.704	0.57	0.964	0.83	1.115
0.05	-0.010	0.32	0.729	0.58	0.976	0.85	1.123
0.07	0.039	0.33	0.753	0.60	0.987	0.87	1.129
0.08	0.096	0.35	0.775	0.62	0.998	0.88	1.136
0.10	0.163	0.37	0.795	0.63	1.008	0.90	1.142
0.12	0.236	0.38	0.814	0.65	1.018	0.92	1.148
0.13	0.299	0.40	0.831	0.67	1.028	0.93	1.154
0.15	0.353	0.42	0.847	0.68	1.038	0.95	1.159
0.17	0.405	0.43	0.863	0.70	1.048	0.97	1.164
0.18	0.455	0.45	0.878	0.72	1.057	0.98	1.167
0.20	0.500	0.47	0.891	0.73	1.066	1.00	1.168
0.22	0.542	0.48	0.904	0.75	1.075		
0.23	0.580	0.50	0.917	0.77	1.084		
0.25	0.616	0.52	0.929	0.78	1.092		

Table C.270: Numerical results for $\mu = 0.048$ N·s/m^2, $h_o = 1.134$ mm, $\Delta T_s = 32.6$°C.

r'	***h'***	***r'***	***h'***	***r'***	***h'***	***r'***	***h'***
0.00	0.695	0.27	0.866	0.52	0.975	0.77	1.033
0.03	0.700	0.28	0.876	0.53	0.979	0.78	1.036
0.05	0.707	0.30	0.886	0.55	0.984	0.80	1.039
0.07	0.716	0.32	0.895	0.57	0.988	0.82	1.042
0.08	0.726	0.33	0.904	0.58	0.993	0.83	1.044
0.10	0.738	0.35	0.913	0.60	0.997	0.85	1.047
0.12	0.751	0.37	0.920	0.62	1.001	0.87	1.049
0.13	0.765	0.38	0.928	0.63	1.005	0.88	1.051
0.15	0.779	0.40	0.935	0.65	1.009	0.90	1.053
0.17	0.793	0.42	0.941	0.67	1.012	0.92	1.056
0.18	0.806	0.43	0.948	0.68	1.016	0.93	1.058
0.20	0.819	0.45	0.954	0.70	1.020	0.95	1.060
0.22	0.831	0.47	0.959	0.72	1.023	0.97	1.062
0.23	0.843	0.48	0.965	0.73	1.027	0.98	1.063
0.25	0.855	0.50	0.970	0.75	1.030	1.00	1.064

Table C.271: Numerical results for $\mu = 0.048$ N·s/m^2, $h_o = 1.134$ mm, $\Delta T_s = 59.9$°C.

r'	***h'***	***r'***	***h'***	***r'***	***h'***	***r'***	***h'***
0.00	0.377	0.27	0.746	0.53	0.962	0.80	1.078
0.02	0.381	0.28	0.767	0.55	0.971	0.82	1.083
0.03	0.390	0.30	0.786	0.57	0.980	0.83	1.088
0.05	0.406	0.32	0.805	0.58	0.988	0.85	1.093
0.07	0.426	0.33	0.821	0.60	0.996	0.87	1.098
0.08	0.450	0.35	0.837	0.62	1.004	0.88	1.102
0.10	0.477	0.37	0.852	0.63	1.012	0.90	1.106
0.12	0.505	0.38	0.866	0.65	1.019	0.92	1.110
0.13	0.536	0.40	0.879	0.67	1.026	0.93	1.114
0.15	0.566	0.42	0.891	0.68	1.034	0.95	1.117
0.17	0.596	0.43	0.903	0.70	1.041	0.97	1.120
0.18	0.624	0.45	0.914	0.72	1.047	0.98	1.122
0.20	0.651	0.47	0.924	0.73	1.054	1.00	1.123
0.22	0.677	0.48	0.934	0.75	1.060		
0.23	0.701	0.50	0.944	0.77	1.066		
0.25	0.724	0.52	0.953	0.78	1.072		

Table C.272: Numerical results for $\mu = 0.192$ N·s/m^2, $h_o = 0.271$ mm, $\Delta T_s = 3.6$°C.

r'	***h'***	***r'***	***h'***	***r'***	***h'***	***r'***	***h'***
0.00	0.642	0.27	0.873	0.53	0.970	0.80	1.045
0.02	0.645	0.28	0.883	0.55	0.975	0.82	1.048
0.03	0.652	0.30	0.892	0.57	0.980	0.83	1.051
0.05	0.663	0.32	0.900	0.58	0.985	0.85	1.054
0.07	0.677	0.33	0.908	0.60	0.991	0.87	1.056
0.08	0.694	0.35	0.914	0.62	0.996	0.88	1.060
0.10	0.712	0.37	0.920	0.63	1.001	0.90	1.063
0.12	0.731	0.38	0.926	0.65	1.007	0.92	1.068
0.13	0.750	0.40	0.931	0.67	1.012	0.93	1.073
0.15	0.769	0.42	0.936	0.68	1.016	0.95	1.078
0.17	0.788	0.43	0.941	0.70	1.021	0.97	1.084
0.18	0.805	0.45	0.946	0.72	1.026	0.98	1.088
0.20	0.821	0.47	0.950	0.73	1.030	1.00	1.090
0.22	0.835	0.48	0.955	0.75	1.034		
0.23	0.849	0.50	0.960	0.77	1.038		
0.25	0.862	0.52	0.965	0.78	1.042		

Table C.273: Numerical results for $\mu = 0.192$ N·s/m^2, $h_o = 0.271$ mm, $\Delta T_s = 5.0$°C.

r'	***h'***	***r'***	***h'***	***r'***	***h'***	***r'***	***h'***
0.00	0.325	0.27	0.796	0.53	0.962	0.80	1.071
0.02	0.331	0.28	0.814	0.55	0.969	0.82	1.075
0.03	0.347	0.30	0.830	0.57	0.977	0.83	1.080
0.05	0.373	0.32	0.845	0.58	0.986	0.85	1.084
0.07	0.406	0.33	0.859	0.60	0.993	0.87	1.088
0.08	0.443	0.35	0.871	0.62	1.000	0.88	1.093
0.10	0.483	0.37	0.882	0.63	1.008	0.90	1.098
0.12	0.523	0.38	0.892	0.65	1.016	0.92	1.104
0.13	0.562	0.40	0.901	0.67	1.023	0.93	1.111
0.15	0.600	0.42	0.910	0.68	1.029	0.95	1.117
0.17	0.635	0.43	0.918	0.70	1.037	0.97	1.124
0.18	0.667	0.45	0.925	0.72	1.044	0.98	1.129
0.20	0.697	0.47	0.933	0.73	1.050	1.00	1.131
0.22	0.725	0.48	0.940	0.75	1.055		
0.23	0.751	0.50	0.948	0.77	1.061		
0.25	0.775	0.52	0.955	0.78	1.066		

Table C.274: Numerical results for $\mu = 0.480$ N·s/m^2, $h_o = 0.467$ mm, $\Delta T_s = 8.5$°C.

r'	***h'***	***r'***	***h'***	***r'***	***h'***	***r'***	***h'***
0.00	0.589	0.27	0.862	0.53	0.976	0.80	1.047
0.02	0.592	0.28	0.875	0.55	0.981	0.82	1.050
0.03	0.600	0.30	0.886	0.57	0.986	0.83	1.053
0.05	0.613	0.32	0.896	0.58	0.991	0.85	1.055
0.07	0.629	0.33	0.905	0.60	0.996	0.87	1.058
0.08	0.649	0.35	0.914	0.62	1.001	0.88	1.061
0.10	0.670	0.37	0.921	0.63	1.006	0.90	1.064
0.12	0.691	0.38	0.928	0.65	1.011	0.92	1.068
0.13	0.713	0.40	0.935	0.67	1.016	0.93	1.072
0.15	0.736	0.42	0.941	0.68	1.021	0.95	1.077
0.17	0.758	0.43	0.946	0.70	1.025	0.97	1.081
0.18	0.779	0.45	0.952	0.72	1.029	0.98	1.084
0.20	0.798	0.47	0.957	0.73	1.034	1.00	1.086
0.22	0.816	0.48	0.962	0.75	1.037		
0.23	0.832	0.50	0.967	0.77	1.041		
0.25	0.848	0.52	0.971	0.78	1.044		

Table C.275: Numerical results for $\mu = 0.480$ N·s/m^2, $h_o = 0.956$ mm, $\Delta T_s = 35.0$°C.

r'	***h'***	***r'***	***h'***	***r'***	***h'***	***r'***	***h'***
0.00	0.489	0.27	0.824	0.53	0.979	0.80	1.059
0.02	0.492	0.28	0.840	0.55	0.985	0.82	1.062
0.03	0.502	0.30	0.855	0.57	0.991	0.83	1.065
0.05	0.518	0.32	0.870	0.58	0.997	0.85	1.068
0.07	0.539	0.33	0.882	0.60	1.002	0.87	1.071
0.08	0.563	0.35	0.894	0.62	1.008	0.88	1.073
0.10	0.588	0.37	0.904	0.63	1.013	0.90	1.076
0.12	0.615	0.38	0.914	0.65	1.019	0.92	1.079
0.13	0.641	0.40	0.923	0.67	1.024	0.93	1.081
0.15	0.668	0.42	0.932	0.68	1.029	0.95	1.084
0.17	0.694	0.43	0.939	0.70	1.034	0.97	1.087
0.18	0.719	0.45	0.946	0.72	1.039	0.98	1.088
0.20	0.742	0.47	0.954	0.73	1.043	1.00	1.089
0.22	0.765	0.48	0.960	0.75	1.047		
0.23	0.787	0.50	0.967	0.77	1.051		
0.25	0.807	0.52	0.973	0.78	1.055		

Table C.276: Numerical results for $\mu = 0.480$ N·s/m^2, $h_o = 0.956$ mm, $\Delta T_s = 44.3$°C.

r'	***h'***	***r'***	***h'***	***r'***	***h'***	***r'***	***h'***
0.00	0.231	0.27	0.767	0.53	0.974	0.80	1.077
0.02	0.237	0.28	0.791	0.55	0.982	0.82	1.082
0.03	0.256	0.30	0.811	0.57	0.990	0.83	1.086
0.05	0.286	0.32	0.830	0.58	0.997	0.85	1.089
0.07	0.324	0.33	0.847	0.60	1.004	0.87	1.093
0.08	0.367	0.35	0.862	0.62	1.011	0.88	1.097
0.10	0.411	0.37	0.877	0.63	1.018	0.90	1.100
0.12	0.457	0.38	0.890	0.65	1.025	0.92	1.104
0.13	0.500	0.40	0.901	0.67	1.032	0.93	1.108
0.15	0.542	0.42	0.912	0.68	1.038	0.95	1.112
0.17	0.582	0.43	0.922	0.70	1.045	0.97	1.115
0.18	0.620	0.45	0.932	0.72	1.051	0.98	1.117
0.20	0.654	0.47	0.941	0.73	1.057	1.00	1.118
0.22	0.685	0.48	0.950	0.75	1.062		
0.23	0.715	0.50	0.958	0.77	1.068		
0.25	0.742	0.52	0.966	0.78	1.073		

Table C.277: Numerical results for $\mu = 0.480$ N·s/m^2, $h_o = 0.956$ mm, $\Delta T_s = 54.1$°C.

r'	***h'***	***r'***	***h'***	***r'***	***h'***	***r'***	***h'***
0.00	0.016	0.27	0.713	0.53	0.964	0.80	1.098
0.02	0.023	0.28	0.740	0.55	0.974	0.82	1.104
0.03	0.044	0.30	0.765	0.57	0.984	0.83	1.109
0.05	0.080	0.32	0.788	0.58	0.994	0.85	1.114
0.07	0.133	0.33	0.809	0.60	1.003	0.87	1.119
0.08	0.198	0.35	0.827	0.62	1.012	0.88	1.123
0.10	0.264	0.37	0.844	0.63	1.021	0.90	1.128
0.12	0.325	0.38	0.859	0.65	1.030	0.92	1.132
0.13	0.383	0.40	0.874	0.67	1.038	0.93	1.136
0.15	0.438	0.42	0.888	0.68	1.047	0.95	1.140
0.17	0.490	0.43	0.900	0.70	1.055	0.97	1.143
0.18	0.536	0.45	0.912	0.72	1.063	0.98	1.145
0.20	0.578	0.47	0.923	0.73	1.071	1.00	1.146
0.22	0.617	0.48	0.934	0.75	1.078		
0.23	0.652	0.50	0.944	0.77	1.085		
0.25	0.684	0.52	0.954	0.78	1.092		

Table C.278: Numerical results for $\mu = 0.480$ N·s/m^2, $h_o = 1.461$ mm, $\Delta T_s = 62.6$°C.

r'	***h'***	***r'***	***h'***	***r'***	***h'***	***r'***	***h'***
0.00	-0.067	0.27	0.662	0.53	0.953	0.80	1.117
0.02	-0.060	0.28	0.692	0.55	0.965	0.82	1.125
0.03	-0.040	0.30	0.720	0.57	0.977	0.83	1.132
0.05	-0.013	0.32	0.746	0.58	0.989	0.85	1.138
0.07	0.019	0.33	0.769	0.60	1.000	0.87	1.144
0.08	0.059	0.35	0.791	0.62	1.011	0.88	1.150
0.10	0.117	0.37	0.811	0.63	1.022	0.90	1.155
0.12	0.193	0.38	0.829	0.65	1.033	0.92	1.160
0.13	0.271	0.40	0.845	0.67	1.044	0.93	1.165
0.15	0.340	0.42	0.861	0.68	1.054	0.95	1.169
0.17	0.400	0.43	0.876	0.70	1.064	0.97	1.173
0.18	0.455	0.45	0.890	0.72	1.074	0.98	1.175
0.20	0.506	0.47	0.903	0.73	1.084	1.00	1.176
0.22	0.552	0.48	0.916	0.75	1.093		
0.23	0.592	0.50	0.929	0.77	1.101		
0.25	0.629	0.52	0.941	0.78	1.110		

Table C.279: Numerical results for $\mu = 0.480$ N·s/m^2, $h_o = 1.461$ mm, $\Delta T_s = 63.7$°C.

r'	***h'***	***r'***	***h'***	***r'***	***h'***	***r'***	***h'***
0.00	0.802	0.26	0.902	0.52	0.979	0.78	1.029
0.02	0.803	0.28	0.910	0.54	0.983	0.80	1.032
0.04	0.806	0.30	0.918	0.56	0.987	0.82	1.035
0.06	0.811	0.32	0.925	0.58	0.992	0.84	1.037
0.08	0.818	0.34	0.932	0.60	0.996	0.86	1.040
0.10	0.826	0.36	0.939	0.62	1.000	0.88	1.042
0.12	0.835	0.38	0.945	0.64	1.004	0.90	1.044
0.14	0.845	0.40	0.950	0.66	1.008	0.92	1.046
0.16	0.854	0.42	0.956	0.68	1.012	0.94	1.047
0.18	0.864	0.44	0.961	0.70	1.015	0.96	1.048
0.20	0.874	0.46	0.965	0.72	1.019	0.98	1.049
0.22	0.884	0.48	0.970	0.74	1.022	1.00	1.049
0.24	0.893	0.50	0.974	0.76	1.026		

Table C.280: Numerical results for $\mu = 0.480$ N·s/m^2, $h_o = 1.461$ mm, $\Delta T_s = 89.7$°C.

r'	***h'***	***r'***	***h'***	***r'***	***h'***	***r'***	***h'***
0.00	0.509	0.26	0.787	0.52	0.957	0.78	1.061
0.02	0.512	0.28	0.807	0.54	0.966	0.80	1.067
0.04	0.523	0.30	0.826	0.56	0.975	0.82	1.073
0.06	0.541	0.32	0.842	0.58	0.984	0.84	1.079
0.08	0.563	0.34	0.857	0.60	0.992	0.86	1.084
0.10	0.587	0.36	0.872	0.62	1.001	0.88	1.089
0.12	0.613	0.38	0.886	0.64	1.009	0.90	1.093
0.14	0.640	0.40	0.898	0.66	1.017	0.92	1.098
0.16	0.666	0.42	0.909	0.68	1.025	0.94	1.102
0.18	0.692	0.44	0.919	0.70	1.032	0.96	1.105
0.20	0.717	0.46	0.930	0.72	1.040	0.98	1.107
0.22	0.741	0.48	0.939	0.74	1.047	1.00	1.108
0.24	0.765	0.50	0.948	0.76	1.054		

Table C.281: Numerical results for $\mu = 0.480$ N·s/m^2, $h_o = 1.461$ mm, $\Delta T_s = 125.4$°C.

r'	***h'***	***r'***	***h'***	***r'***	***h'***	***r'***	***h'***
0.00	0.256	0.27	0.641	0.53	0.983	0.80	1.110
0.05	0.280	0.32	0.723	0.58	1.021	0.85	1.119
0.03	0.267	0.30	0.696	0.57	1.009	0.83	1.116
0.08	0.319	0.35	0.774	0.62	1.042	0.88	1.123
0.07	0.297	0.33	0.749	0.60	1.032	0.87	1.121
0.12	0.370	0.38	0.821	0.65	1.060	0.92	1.126
0.10	0.343	0.37	0.798	0.63	1.052	0.90	1.124
0.15	0.429	0.42	0.863	0.68	1.076	0.95	1.128
0.13	0.399	0.40	0.842	0.67	1.068	0.93	1.127
0.18	0.490	0.45	0.901	0.72	1.088	0.98	1.129
0.17	0.459	0.43	0.882	0.70	1.082	0.97	1.128
0.22	0.551	0.48	0.936	0.75	1.099	1.02	1.129
0.20	0.520	0.47	0.919	0.73	1.094	1.00	1.129
0.25	0.612	0.52	0.968	0.78	1.107		
0.23	0.582	0.50	0.952	0.77	1.103		
0.28	0.669	0.55	0.996	0.82	1.113		

Table C.282: Numerical results for $\mu = 0.480$ N·s/m^2, $h_o = 1.461$ mm, $\Delta T_s = 203$°C.

r'	***h'***	***r'***	***h'***	***r'***	***h'***	***r'***	***h'***
0.00	-0.143	0.27	0.338	0.53	0.997	0.80	1.203
0.02	-0.140	0.28	0.416	0.55	1.018	0.82	1.208
0.03	-0.132	0.30	0.482	0.57	1.037	0.83	1.214
0.05	-0.121	0.32	0.540	0.58	1.056	0.85	1.218
0.07	-0.109	0.33	0.594	0.60	1.073	0.87	1.222
0.08	-0.096	0.35	0.644	0.62	1.089	0.88	1.225
0.10	-0.083	0.37	0.689	0.63	1.104	0.90	1.228
0.12	-0.069	0.38	0.730	0.65	1.117	0.92	1.231
0.13	-0.053	0.40	0.769	0.67	1.130	0.93	1.233
0.15	-0.035	0.42	0.805	0.68	1.142	0.95	1.234
0.17	-0.014	0.43	0.838	0.70	1.153	0.97	1.235
0.18	0.013	0.45	0.869	0.72	1.163	0.98	1.236
0.20	0.047	0.47	0.898	0.73	1.173	1.00	1.236
0.22	0.090	0.48	0.925	0.75	1.182		
0.23	0.154	0.50	0.950	0.77	1.190		
0.25	0.244	0.52	0.975	0.78	1.197		

C.2.4. Asymptotic Solution

This section details the results of the asymptotic analysis for cases simulating experimental parameters. In the asymptotic equation derived in Chapter 4, the initial film height and the radial temperature difference were the only experimental variables that affected the solution. Therefore, the following tables are ordered by initial film height first and then by temperature difference. The solutions provided are thus applicable for any viscosity because of it was assumed $A \ll 1$. In all solutions of the asymptotic equation, the resolution along r was 1000 grid points. For brevity, the following tables only show 100 radial locations for each case.

Table C.283: Asymptotic results for $h_o = 0.271$ mm, $\Delta T_s = 2.7°C$.

r'	***h'***	***r'***	***h'***	***r'***	***h'***	***r'***	***h'***
0.00	0.383	0.26	0.809	0.52	0.948	0.78	1.060
0.01	0.386	0.27	0.818	0.53	0.953	0.79	1.063
0.02	0.395	0.28	0.827	0.54	0.957	0.80	1.066
0.03	0.408	0.29	0.836	0.55	0.962	0.81	1.069
0.04	0.424	0.30	0.843	0.56	0.966	0.82	1.071
0.05	0.443	0.31	0.850	0.57	0.971	0.83	1.073
0.06	0.463	0.32	0.857	0.58	0.976	0.84	1.076
0.07	0.485	0.33	0.863	0.59	0.980	0.85	1.078
0.08	0.507	0.34	0.869	0.60	0.985	0.86	1.081
0.09	0.530	0.35	0.875	0.61	0.990	0.87	1.083
0.10	0.552	0.36	0.880	0.62	0.995	0.88	1.086
0.11	0.573	0.37	0.885	0.63	1.000	0.89	1.089
0.12	0.595	0.38	0.890	0.64	1.004	0.90	1.092
0.13	0.615	0.39	0.894	0.65	1.009	0.91	1.096
0.14	0.635	0.40	0.899	0.66	1.014	0.92	1.100
0.15	0.654	0.41	0.903	0.67	1.018	0.93	1.105
0.16	0.673	0.42	0.907	0.68	1.023	0.94	1.111
0.17	0.690	0.43	0.911	0.69	1.027	0.95	1.118
0.18	0.706	0.44	0.915	0.70	1.032	0.96	1.125
0.19	0.722	0.45	0.919	0.71	1.036	0.97	1.134
0.20	0.737	0.46	0.923	0.72	1.040	0.98	1.145
0.21	0.751	0.47	0.927	0.73	1.044	0.99	1.157
0.22	0.764	0.48	0.932	0.74	1.047	1.00	1.171
0.23	0.776	0.49	0.936	0.75	1.051		
0.24	0.788	0.50	0.940	0.76	1.054		
0.25	0.799	0.51	0.944	0.77	1.057		

Table C.284: Asymptotic results for h_o = 0.271 mm, ΔT_s = 5.0°C.

r'	***h'***	***r'***	***h'***	***r'***	***h'***	***r'***	***h'***
0.00	-0.120	0.26	0.745	0.52	0.944	0.78	1.078
0.01	-0.062	0.27	0.759	0.53	0.949	0.79	1.082
0.02	-0.007	0.28	0.772	0.54	0.955	0.80	1.085
0.03	0.046	0.29	0.784	0.55	0.960	0.81	1.089
0.04	0.096	0.30	0.796	0.56	0.966	0.82	1.092
0.05	0.144	0.31	0.806	0.57	0.971	0.83	1.095
0.06	0.191	0.32	0.816	0.58	0.977	0.84	1.098
0.07	0.234	0.33	0.825	0.59	0.983	0.85	1.100
0.08	0.276	0.34	0.834	0.60	0.988	0.86	1.103
0.09	0.316	0.35	0.842	0.61	0.994	0.87	1.106
0.10	0.354	0.36	0.850	0.62	1.000	0.88	1.109
0.11	0.391	0.37	0.857	0.63	1.005	0.89	1.113
0.12	0.425	0.38	0.864	0.64	1.011	0.90	1.116
0.13	0.457	0.39	0.871	0.65	1.017	0.91	1.120
0.14	0.488	0.40	0.877	0.66	1.022	0.92	1.125
0.15	0.517	0.41	0.884	0.67	1.028	0.93	1.130
0.16	0.545	0.42	0.889	0.68	1.033	0.94	1.136
0.17	0.571	0.43	0.895	0.69	1.038	0.95	1.143
0.18	0.595	0.44	0.901	0.70	1.043	0.96	1.151
0.19	0.618	0.45	0.906	0.71	1.048	0.97	1.160
0.20	0.640	0.46	0.912	0.72	1.053	0.98	1.170
0.21	0.661	0.47	0.917	0.73	1.058	0.99	1.182
0.22	0.680	0.48	0.922	0.74	1.062	1.00	1.196
0.23	0.698	0.49	0.928	0.75	1.067		
0.24	0.715	0.50	0.933	0.76	1.071		
0.25	0.730	0.51	0.938	0.77	1.075		

Table C.285: Asymptotic results for h_o = 0.271 mm, ΔT_s = 4.4°C.

r'	***h'***	***r'***	***h'***	***r'***	***h'***	***r'***	***h'***
0.00	-0.030	0.26	0.761	0.52	0.939	0.78	1.065
0.01	0.023	0.27	0.773	0.53	0.944	0.79	1.069
0.02	0.074	0.28	0.785	0.54	0.949	0.80	1.072
0.03	0.122	0.29	0.795	0.55	0.954	0.81	1.075
0.04	0.169	0.30	0.806	0.56	0.959	0.82	1.077
0.05	0.213	0.31	0.815	0.57	0.965	0.83	1.080
0.06	0.256	0.32	0.824	0.58	0.970	0.84	1.083
0.07	0.296	0.33	0.832	0.59	0.975	0.85	1.085
0.08	0.335	0.34	0.840	0.60	0.981	0.86	1.088
0.09	0.371	0.35	0.847	0.61	0.986	0.87	1.091
0.10	0.406	0.36	0.854	0.62	0.992	0.88	1.094
0.11	0.439	0.37	0.861	0.63	0.997	0.89	1.097
0.12	0.470	0.38	0.867	0.64	1.002	0.90	1.100
0.13	0.500	0.39	0.873	0.65	1.008	0.91	1.104
0.14	0.528	0.40	0.878	0.66	1.013	0.92	1.109
0.15	0.555	0.41	0.884	0.67	1.018	0.93	1.114
0.16	0.580	0.42	0.889	0.68	1.023	0.94	1.119
0.17	0.603	0.43	0.894	0.69	1.028	0.95	1.126
0.18	0.625	0.44	0.899	0.70	1.033	0.96	1.134
0.19	0.646	0.45	0.904	0.71	1.038	0.97	1.143
0.20	0.666	0.46	0.909	0.72	1.042	0.98	1.154
0.21	0.685	0.47	0.914	0.73	1.047	0.99	1.166
0.22	0.702	0.48	0.919	0.74	1.051	1.00	1.180
0.23	0.718	0.49	0.924	0.75	1.055		
0.24	0.733	0.50	0.929	0.76	1.058		
0.25	0.747	0.51	0.934	0.77	1.062		

Table C.286: Asymptotic results for h_o = 0.313 mm, ΔT_s = 6.2°C.

r'	***h'***	***r'***	***h'***	***r'***	***h'***	***r'***	***h'***
0.00	-0.120	0.26	0.755	0.52	0.954	0.78	1.070
0.01	-0.063	0.27	0.769	0.53	0.959	0.79	1.073
0.02	-0.007	0.28	0.783	0.54	0.964	0.80	1.075
0.03	0.045	0.29	0.795	0.55	0.969	0.81	1.078
0.04	0.096	0.30	0.807	0.56	0.974	0.82	1.080
0.05	0.145	0.31	0.818	0.57	0.979	0.83	1.082
0.06	0.191	0.32	0.828	0.58	0.984	0.84	1.084
0.07	0.235	0.33	0.838	0.59	0.989	0.85	1.086
0.08	0.277	0.34	0.847	0.60	0.994	0.86	1.087
0.09	0.318	0.35	0.856	0.61	0.999	0.87	1.089
0.10	0.356	0.36	0.864	0.62	1.004	0.88	1.091
0.11	0.392	0.37	0.871	0.63	1.009	0.89	1.093
0.12	0.427	0.38	0.878	0.64	1.013	0.90	1.095
0.13	0.460	0.39	0.885	0.65	1.018	0.91	1.098
0.14	0.491	0.40	0.891	0.66	1.023	0.92	1.100
0.15	0.521	0.41	0.897	0.67	1.028	0.93	1.104
0.16	0.549	0.42	0.903	0.68	1.032	0.94	1.108
0.17	0.575	0.43	0.909	0.69	1.037	0.95	1.112
0.18	0.600	0.44	0.914	0.70	1.041	0.96	1.118
0.19	0.624	0.45	0.920	0.71	1.045	0.97	1.124
0.20	0.646	0.46	0.925	0.72	1.049	0.98	1.132
0.21	0.667	0.47	0.930	0.73	1.053	0.99	1.140
0.22	0.687	0.48	0.935	0.74	1.057	1.00	1.151
0.23	0.706	0.49	0.940	0.75	1.060		
0.24	0.723	0.50	0.945	0.76	1.064		
0.25	0.740	0.51	0.950	0.77	1.067		

Table C.287: Asymptotic results for h_o = 0.313 mm, ΔT_s = 3.5°C.

r'	***h'***	***r'***	***h'***	***r'***	***h'***	***r'***	***h'***
0.00	0.628	0.26	0.871	0.52	0.966	0.78	1.042
0.01	0.629	0.27	0.877	0.53	0.969	0.79	1.044
0.02	0.633	0.28	0.883	0.54	0.972	0.80	1.046
0.03	0.639	0.29	0.889	0.55	0.975	0.81	1.047
0.04	0.646	0.30	0.894	0.56	0.978	0.82	1.049
0.05	0.655	0.31	0.899	0.57	0.981	0.83	1.050
0.06	0.665	0.32	0.904	0.58	0.984	0.84	1.052
0.07	0.676	0.33	0.908	0.59	0.987	0.85	1.053
0.08	0.688	0.34	0.912	0.60	0.991	0.86	1.055
0.09	0.699	0.35	0.916	0.61	0.994	0.87	1.057
0.10	0.712	0.36	0.920	0.62	0.997	0.88	1.058
0.11	0.724	0.37	0.923	0.63	1.000	0.89	1.060
0.12	0.736	0.38	0.927	0.64	1.004	0.90	1.062
0.13	0.748	0.39	0.930	0.65	1.007	0.91	1.064
0.14	0.760	0.40	0.933	0.66	1.010	0.92	1.067
0.15	0.771	0.41	0.936	0.67	1.013	0.93	1.070
0.16	0.783	0.42	0.939	0.68	1.016	0.94	1.073
0.17	0.793	0.43	0.941	0.69	1.019	0.95	1.078
0.18	0.804	0.44	0.944	0.70	1.022	0.96	1.082
0.19	0.814	0.45	0.947	0.71	1.025	0.97	1.088
0.20	0.823	0.46	0.950	0.72	1.028	0.98	1.094
0.21	0.832	0.47	0.952	0.73	1.030	0.99	1.102
0.22	0.841	0.48	0.955	0.74	1.033	1.00	1.111
0.23	0.849	0.49	0.958	0.75	1.035		
0.24	0.857	0.50	0.961	0.76	1.038		
0.25	0.864	0.51	0.963	0.77	1.040		

Table C.288: Asymptotic results for h_o = 0.313 mm, ΔT_s = 3.5°C.

r'	***h'***	***r'***	***h'***	***r'***	***h'***	***r'***	***h'***
0.00	0.296	0.26	0.698	0.52	1.003	0.78	1.081
0.01	0.297	0.27	0.715	0.53	1.010	0.79	1.082
0.02	0.301	0.28	0.732	0.54	1.015	0.80	1.083
0.03	0.307	0.29	0.748	0.55	1.021	0.81	1.084
0.04	0.315	0.30	0.764	0.56	1.026	0.82	1.084
0.05	0.325	0.31	0.780	0.57	1.031	0.83	1.085
0.06	0.337	0.32	0.795	0.58	1.035	0.84	1.086
0.07	0.351	0.33	0.810	0.59	1.039	0.85	1.086
0.08	0.366	0.34	0.824	0.60	1.043	0.86	1.086
0.09	0.381	0.35	0.838	0.61	1.047	0.87	1.087
0.10	0.398	0.36	0.851	0.62	1.050	0.88	1.087
0.11	0.416	0.37	0.864	0.63	1.054	0.89	1.088
0.12	0.434	0.38	0.876	0.64	1.057	0.90	1.088
0.13	0.453	0.39	0.888	0.65	1.059	0.91	1.088
0.14	0.472	0.40	0.900	0.66	1.062	0.92	1.088
0.15	0.491	0.41	0.911	0.67	1.064	0.93	1.089
0.16	0.510	0.42	0.921	0.68	1.067	0.94	1.089
0.17	0.530	0.43	0.931	0.69	1.069	0.95	1.089
0.18	0.549	0.44	0.941	0.70	1.071	0.96	1.089
0.19	0.568	0.45	0.950	0.71	1.072	0.97	1.089
0.20	0.588	0.46	0.959	0.72	1.074	0.98	1.089
0.21	0.607	0.47	0.967	0.73	1.076	0.99	1.089
0.22	0.625	0.48	0.975	0.74	1.077	1.00	1.089
0.23	0.644	0.49	0.983	0.75	1.078		
0.24	0.662	0.50	0.990	0.76	1.079		
0.25	0.680	0.51	0.997	0.77	1.080		

Table C.289: Asymptotic results for h_o = 0.438 mm, ΔT_s = 7.6°C.

r'	***h'***	***r'***	***h'***	***r'***	***h'***	***r'***	***h'***
0.00	0.486	0.26	0.814	0.52	0.958	0.78	1.057
0.01	0.488	0.27	0.823	0.53	0.962	0.79	1.060
0.02	0.493	0.28	0.831	0.54	0.967	0.80	1.062
0.03	0.501	0.29	0.840	0.55	0.971	0.81	1.065
0.04	0.511	0.30	0.847	0.56	0.975	0.82	1.068
0.05	0.523	0.31	0.855	0.57	0.979	0.83	1.070
0.06	0.537	0.32	0.862	0.58	0.983	0.84	1.072
0.07	0.552	0.33	0.869	0.59	0.987	0.85	1.075
0.08	0.567	0.34	0.875	0.60	0.991	0.86	1.077
0.09	0.583	0.35	0.881	0.61	0.995	0.87	1.080
0.10	0.599	0.36	0.887	0.62	0.999	0.88	1.082
0.11	0.615	0.37	0.892	0.63	1.003	0.89	1.084
0.12	0.632	0.38	0.897	0.64	1.007	0.90	1.087
0.13	0.648	0.39	0.903	0.65	1.011	0.91	1.090
0.14	0.663	0.40	0.907	0.66	1.015	0.92	1.093
0.15	0.678	0.41	0.912	0.67	1.019	0.93	1.096
0.16	0.693	0.42	0.917	0.68	1.023	0.94	1.100
0.17	0.708	0.43	0.921	0.69	1.027	0.95	1.104
0.18	0.722	0.44	0.926	0.70	1.031	0.96	1.109
0.19	0.735	0.45	0.930	0.71	1.034	0.97	1.114
0.20	0.748	0.46	0.934	0.72	1.038	0.98	1.120
0.21	0.760	0.47	0.938	0.73	1.041	0.99	1.127
0.22	0.772	0.48	0.942	0.74	1.045	1.00	1.135
0.23	0.783	0.49	0.946	0.75	1.048		
0.24	0.794	0.50	0.950	0.76	1.051		
0.25	0.804	0.51	0.954	0.77	1.054		

Table C.290: Asymptotic results for h_o = 0.438mm, ΔT_s = 13.4°C.

r'	***h'***	***r'***	***h'***	***r'***	***h'***	***r'***	***h'***
0.00	0.000	0.26	0.879	0.52	1.118	0.78	1.247
0.01	0.056	0.27	0.895	0.53	1.123	0.79	1.251
0.02	0.109	0.28	0.911	0.54	1.129	0.80	1.254
0.03	0.160	0.29	0.925	0.55	1.135	0.81	1.258
0.04	0.210	0.30	0.938	0.56	1.140	0.82	1.261
0.05	0.257	0.31	0.951	0.57	1.145	0.83	1.264
0.06	0.302	0.32	0.963	0.58	1.151	0.84	1.267
0.07	0.346	0.33	0.975	0.59	1.156	0.85	1.270
0.08	0.387	0.34	0.986	0.60	1.162	0.86	1.273
0.09	0.427	0.35	0.996	0.61	1.167	0.87	1.276
0.10	0.466	0.36	1.006	0.62	1.172	0.88	1.279
0.11	0.502	0.37	1.015	0.63	1.178	0.89	1.282
0.12	0.537	0.38	1.024	0.64	1.183	0.90	1.285
0.13	0.570	0.39	1.032	0.65	1.188	0.91	1.289
0.14	0.602	0.40	1.040	0.66	1.193	0.92	1.292
0.15	0.632	0.41	1.048	0.67	1.198	0.93	1.296
0.16	0.661	0.42	1.055	0.68	1.203	0.94	1.301
0.17	0.688	0.43	1.062	0.69	1.208	0.95	1.305
0.18	0.714	0.44	1.069	0.70	1.213	0.96	1.310
0.19	0.739	0.45	1.076	0.71	1.217	0.97	1.316
0.20	0.762	0.46	1.082	0.72	1.222	0.98	1.323
0.21	0.785	0.47	1.088	0.73	1.227	0.99	1.331
0.22	0.806	0.48	1.095	0.74	1.231	1.00	1.339
0.23	0.826	0.49	1.100	0.75	1.235		
0.24	0.845	0.50	1.106	0.76	1.239		
0.25	0.863	0.51	1.112	0.77	1.243		

Table C.291: Asymptotic results for h_o = 0.467 mm, ΔT_s = 8.5°C.

r'	***h'***	***r'***	***h'***	***r'***	***h'***	***r'***	***h'***
0.00	0.491	0.26	0.828	0.52	0.969	0.78	1.054
0.01	0.493	0.27	0.838	0.53	0.972	0.79	1.056
0.02	0.498	0.28	0.846	0.54	0.976	0.80	1.058
0.03	0.507	0.29	0.855	0.55	0.980	0.81	1.060
0.04	0.517	0.30	0.862	0.56	0.983	0.82	1.062
0.05	0.530	0.31	0.870	0.57	0.987	0.83	1.064
0.06	0.544	0.32	0.877	0.58	0.991	0.84	1.065
0.07	0.559	0.33	0.883	0.59	0.994	0.85	1.067
0.08	0.575	0.34	0.890	0.60	0.998	0.86	1.068
0.09	0.592	0.35	0.896	0.61	1.002	0.87	1.070
0.10	0.609	0.36	0.901	0.62	1.005	0.88	1.072
0.11	0.625	0.37	0.907	0.63	1.009	0.89	1.073
0.12	0.642	0.38	0.912	0.64	1.012	0.90	1.075
0.13	0.658	0.39	0.917	0.65	1.016	0.91	1.077
0.14	0.675	0.40	0.921	0.66	1.019	0.92	1.079
0.15	0.690	0.41	0.926	0.67	1.023	0.93	1.082
0.16	0.706	0.42	0.930	0.68	1.026	0.94	1.085
0.17	0.720	0.43	0.934	0.69	1.029	0.95	1.088
0.18	0.735	0.44	0.938	0.70	1.032	0.96	1.092
0.19	0.748	0.45	0.942	0.71	1.036	0.97	1.096
0.20	0.762	0.46	0.946	0.72	1.039	0.98	1.102
0.21	0.774	0.47	0.950	0.73	1.041	0.99	1.108
0.22	0.786	0.48	0.954	0.74	1.044	1.00	1.115
0.23	0.797	0.49	0.958	0.75	1.047		
0.24	0.808	0.50	0.961	0.76	1.049		
0.25	0.819	0.51	0.965	0.77	1.052		

Table C.292: Asymptotic results for h_o = 0.467 mm, ΔT_s = 14.0°C.

r'	***h'***	***r'***	***h'***	***r'***	***h'***	***r'***	***h'***
0.00	0.000	0.26	0.782	0.52	0.983	0.78	1.103
0.01	0.050	0.27	0.796	0.53	0.988	0.79	1.106
0.02	0.099	0.28	0.809	0.54	0.993	0.80	1.110
0.03	0.145	0.29	0.821	0.55	0.998	0.81	1.113
0.04	0.190	0.30	0.832	0.56	1.003	0.82	1.116
0.05	0.232	0.31	0.843	0.57	1.008	0.83	1.119
0.06	0.273	0.32	0.853	0.58	1.012	0.84	1.122
0.07	0.312	0.33	0.863	0.59	1.017	0.85	1.125
0.08	0.350	0.34	0.872	0.60	1.022	0.86	1.128
0.09	0.385	0.35	0.880	0.61	1.027	0.87	1.131
0.10	0.419	0.36	0.888	0.62	1.032	0.88	1.134
0.11	0.452	0.37	0.896	0.63	1.037	0.89	1.137
0.12	0.483	0.38	0.903	0.64	1.042	0.90	1.141
0.13	0.512	0.39	0.910	0.65	1.047	0.91	1.144
0.14	0.540	0.40	0.917	0.66	1.052	0.92	1.148
0.15	0.567	0.41	0.923	0.67	1.057	0.93	1.152
0.16	0.592	0.42	0.929	0.68	1.061	0.94	1.157
0.17	0.617	0.43	0.935	0.69	1.066	0.95	1.162
0.18	0.639	0.44	0.941	0.70	1.070	0.96	1.168
0.19	0.661	0.45	0.947	0.71	1.075	0.97	1.174
0.20	0.681	0.46	0.952	0.72	1.079	0.98	1.181
0.21	0.701	0.47	0.957	0.73	1.083	0.99	1.190
0.22	0.719	0.48	0.962	0.74	1.088	1.00	1.199
0.23	0.736	0.49	0.968	0.75	1.092		
0.24	0.752	0.50	0.973	0.76	1.095		
0.25	0.768	0.51	0.978	0.77	1.099		

Table C.293: Asymptotic results for h_o = 0.502 mm, ΔT_s = 7.6°C.

r'	***h'***	***r'***	***h'***	***r'***	***h'***	***r'***	***h'***
0.00	0.628	0.26	0.862	0.52	0.968	0.78	1.041
0.01	0.629	0.27	0.869	0.53	0.971	0.79	1.043
0.02	0.633	0.28	0.876	0.54	0.974	0.80	1.045
0.03	0.638	0.29	0.882	0.55	0.977	0.81	1.047
0.04	0.645	0.30	0.888	0.56	0.980	0.82	1.049
0.05	0.653	0.31	0.893	0.57	0.983	0.83	1.051
0.06	0.662	0.32	0.898	0.58	0.986	0.84	1.052
0.07	0.672	0.33	0.903	0.59	0.989	0.85	1.054
0.08	0.683	0.34	0.908	0.60	0.992	0.86	1.056
0.09	0.694	0.35	0.912	0.61	0.995	0.87	1.058
0.10	0.705	0.36	0.916	0.62	0.998	0.88	1.060
0.11	0.717	0.37	0.920	0.63	1.001	0.89	1.062
0.12	0.728	0.38	0.924	0.64	1.004	0.90	1.064
0.13	0.740	0.39	0.928	0.65	1.007	0.91	1.067
0.14	0.751	0.40	0.931	0.66	1.010	0.92	1.069
0.15	0.762	0.41	0.935	0.67	1.013	0.93	1.072
0.16	0.773	0.42	0.938	0.68	1.016	0.94	1.076
0.17	0.784	0.43	0.941	0.69	1.018	0.95	1.080
0.18	0.794	0.44	0.944	0.70	1.021	0.96	1.084
0.19	0.804	0.45	0.947	0.71	1.024	0.97	1.089
0.20	0.813	0.46	0.950	0.72	1.027	0.98	1.095
0.21	0.823	0.47	0.953	0.73	1.029	0.99	1.101
0.22	0.831	0.48	0.956	0.74	1.032	1.00	1.109
0.23	0.840	0.49	0.959	0.75	1.034		
0.24	0.848	0.50	0.962	0.76	1.036		
0.25	0.855	0.51	0.965	0.77	1.039		

Table C.294: Asymptotic results for h_o = 0.502 mm, ΔT_s = 10.7°C.

r'	***h'***	***r'***	***h'***	***r'***	***h'***	***r'***	***h'***
0.00	0.522	0.26	0.734	0.52	0.980	0.78	1.076
0.01	0.522	0.27	0.746	0.53	0.987	0.79	1.077
0.02	0.524	0.28	0.757	0.54	0.993	0.80	1.079
0.03	0.526	0.29	0.769	0.55	0.998	0.81	1.080
0.04	0.529	0.30	0.780	0.56	1.004	0.82	1.081
0.05	0.533	0.31	0.792	0.57	1.009	0.83	1.082
0.06	0.538	0.32	0.803	0.58	1.014	0.84	1.084
0.07	0.543	0.33	0.814	0.59	1.019	0.85	1.085
0.08	0.549	0.34	0.825	0.60	1.024	0.86	1.085
0.09	0.556	0.35	0.835	0.61	1.028	0.87	1.086
0.10	0.564	0.36	0.846	0.62	1.032	0.88	1.087
0.11	0.572	0.37	0.856	0.63	1.036	0.89	1.088
0.12	0.581	0.38	0.866	0.64	1.040	0.90	1.089
0.13	0.590	0.39	0.876	0.65	1.044	0.91	1.089
0.14	0.599	0.40	0.885	0.66	1.047	0.92	1.090
0.15	0.609	0.41	0.895	0.67	1.050	0.93	1.090
0.16	0.620	0.42	0.904	0.68	1.053	0.94	1.091
0.17	0.630	0.43	0.913	0.69	1.056	0.95	1.091
0.18	0.641	0.44	0.921	0.70	1.059	0.96	1.092
0.19	0.653	0.45	0.929	0.71	1.061	0.97	1.092
0.20	0.664	0.46	0.937	0.72	1.064	0.98	1.093
0.21	0.675	0.47	0.945	0.73	1.066	0.99	1.093
0.22	0.687	0.48	0.953	0.74	1.068	1.00	1.093
0.23	0.699	0.49	0.960	0.75	1.070		
0.24	0.711	0.50	0.967	0.76	1.072		
0.25	0.722	0.51	0.974	0.77	1.074		

Table C.295: Asymptotic results for h_o = 0.502 mm, ΔT_s = 13.4°C.

r'	***h'***	***r'***	***h'***	***r'***	***h'***	***r'***	***h'***
0.00	0.313	0.26	0.657	0.52	0.979	0.78	1.097
0.01	0.314	0.27	0.673	0.53	0.987	0.79	1.099
0.02	0.317	0.28	0.689	0.54	0.995	0.80	1.101
0.03	0.321	0.29	0.705	0.55	1.002	0.81	1.103
0.04	0.327	0.30	0.720	0.56	1.009	0.82	1.104
0.05	0.335	0.31	0.736	0.57	1.015	0.83	1.106
0.06	0.345	0.32	0.751	0.58	1.022	0.84	1.107
0.07	0.355	0.33	0.765	0.59	1.028	0.85	1.108
0.08	0.367	0.34	0.780	0.60	1.033	0.86	1.110
0.09	0.380	0.35	0.794	0.61	1.039	0.87	1.111
0.10	0.393	0.36	0.808	0.62	1.044	0.88	1.112
0.11	0.408	0.37	0.821	0.63	1.049	0.89	1.113
0.12	0.423	0.38	0.834	0.64	1.054	0.90	1.113
0.13	0.438	0.39	0.847	0.65	1.058	0.91	1.114
0.14	0.454	0.40	0.859	0.66	1.062	0.92	1.115
0.15	0.471	0.41	0.871	0.67	1.066	0.93	1.116
0.16	0.487	0.42	0.883	0.68	1.070	0.94	1.116
0.17	0.504	0.43	0.894	0.69	1.074	0.95	1.117
0.18	0.521	0.44	0.905	0.70	1.077	0.96	1.117
0.19	0.538	0.45	0.915	0.71	1.080	0.97	1.118
0.20	0.556	0.46	0.925	0.72	1.083	0.98	1.118
0.21	0.573	0.47	0.935	0.73	1.086	0.99	1.119
0.22	0.590	0.48	0.945	0.74	1.088	1.00	1.119
0.23	0.607	0.49	0.954	0.75	1.091		
0.24	0.623	0.50	0.963	0.76	1.093		
0.25	0.640	0.51	0.971	0.77	1.095		

Table C.296: Asymptotic results for h_o = 0.537 mm, ΔT_s = 5.6°C.

r'	***h'***	***r'***	***h'***	***r'***	***h'***	***r'***	***h'***
0.00	0.780	0.26	0.856	0.52	0.978	0.78	1.043
0.10	0.793	0.27	0.861	0.53	0.982	0.79	1.045
0.20	0.828	0.28	0.866	0.54	0.985	0.80	1.046
0.30	0.876	0.29	0.871	0.55	0.989	0.81	1.047
0.40	0.926	0.30	0.876	0.56	0.992	0.82	1.048
0.50	0.970	0.31	0.881	0.57	0.996	0.83	1.049
0.60	1.005	0.32	0.886	0.58	0.999	0.84	1.050
0.70	1.030	0.33	0.891	0.59	1.002	0.85	1.051
0.80	1.046	0.34	0.896	0.60	1.005	0.86	1.052
0.90	1.055	0.35	0.901	0.61	1.008	0.87	1.053
1.00	1.061	0.36	0.906	0.62	1.011	0.88	1.054
0.11	0.796	0.37	0.911	0.63	1.013	0.89	1.055
0.12	0.799	0.38	0.916	0.64	1.016	0.90	1.055
0.13	0.802	0.39	0.921	0.65	1.019	0.91	1.056
0.14	0.805	0.40	0.926	0.66	1.021	0.92	1.057
0.15	0.809	0.41	0.931	0.67	1.023	0.93	1.057
0.16	0.812	0.42	0.935	0.68	1.026	0.94	1.058
0.17	0.816	0.43	0.940	0.69	1.028	0.95	1.058
0.18	0.820	0.44	0.944	0.70	1.030	0.96	1.059
0.19	0.824	0.45	0.949	0.71	1.032	0.97	1.059
0.20	0.828	0.46	0.953	0.72	1.034	0.98	1.060
0.21	0.833	0.47	0.958	0.73	1.035	0.99	1.060
0.22	0.837	0.48	0.962	0.74	1.037	1.00	1.061
0.23	0.842	0.49	0.966	0.75	1.039		
0.24	0.847	0.50	0.970	0.76	1.040		
0.25	0.851	0.51	0.974	0.77	1.042		

Table C.297: Asymptotic results for h_o = 0.537 mm, ΔT_s = 8.3°C.

r'	***h'***	***r'***	***h'***	***r'***	***h'***	***r'***	***h'***
0.00	0.635	0.26	0.771	0.52	0.968	0.78	1.068
0.01	0.635	0.27	0.779	0.53	0.974	0.79	1.070
0.02	0.636	0.28	0.788	0.54	0.979	0.80	1.072
0.03	0.637	0.29	0.796	0.55	0.985	0.81	1.073
0.04	0.639	0.30	0.805	0.56	0.990	0.82	1.075
0.05	0.641	0.31	0.813	0.57	0.995	0.83	1.077
0.06	0.644	0.32	0.821	0.58	1.000	0.84	1.078
0.07	0.647	0.33	0.830	0.59	1.005	0.85	1.080
0.08	0.651	0.34	0.838	0.60	1.010	0.86	1.081
0.09	0.655	0.35	0.846	0.61	1.014	0.87	1.082
0.10	0.659	0.36	0.854	0.62	1.018	0.88	1.084
0.11	0.664	0.37	0.862	0.63	1.023	0.89	1.085
0.12	0.670	0.38	0.870	0.64	1.027	0.90	1.086
0.13	0.675	0.39	0.878	0.65	1.030	0.91	1.087
0.14	0.681	0.40	0.886	0.66	1.034	0.92	1.088
0.15	0.688	0.41	0.894	0.67	1.038	0.93	1.089
0.16	0.694	0.42	0.901	0.68	1.041	0.94	1.090
0.17	0.701	0.43	0.908	0.69	1.044	0.95	1.090
0.18	0.708	0.44	0.916	0.70	1.047	0.96	1.091
0.19	0.715	0.45	0.923	0.71	1.050	0.97	1.092
0.20	0.723	0.46	0.930	0.72	1.053	0.98	1.092
0.21	0.731	0.47	0.936	0.73	1.056	0.99	1.093
0.22	0.738	0.48	0.943	0.74	1.058	1.00	1.094
0.23	0.746	0.49	0.950	0.75	1.061		
0.24	0.755	0.50	0.956	0.76	1.063		
0.25	0.763	0.51	0.962	0.77	1.066		

Table C.298: Asymptotic results for h_o = 0.537 mm, ΔT_s = 10.7°C.

r'	***h'***	***r'***	***h'***	***r'***	***h'***	***r'***	***h'***
0.00	0.536	0.26	0.719	0.52	0.963	0.78	1.083
0.01	0.536	0.27	0.730	0.53	0.970	0.79	1.085
0.02	0.537	0.28	0.740	0.54	0.977	0.80	1.087
0.03	0.539	0.29	0.751	0.55	0.984	0.81	1.089
0.04	0.542	0.30	0.762	0.56	0.990	0.82	1.091
0.05	0.545	0.31	0.772	0.57	0.996	0.83	1.093
0.06	0.549	0.32	0.783	0.58	1.002	0.84	1.095
0.07	0.553	0.33	0.794	0.59	1.008	0.85	1.097
0.08	0.558	0.34	0.804	0.60	1.014	0.86	1.098
0.09	0.564	0.35	0.814	0.61	1.019	0.87	1.100
0.10	0.570	0.36	0.824	0.62	1.024	0.88	1.101
0.11	0.577	0.37	0.834	0.63	1.029	0.89	1.103
0.12	0.584	0.38	0.844	0.64	1.034	0.90	1.104
0.13	0.592	0.39	0.854	0.65	1.038	0.91	1.105
0.14	0.600	0.40	0.863	0.66	1.043	0.92	1.106
0.15	0.609	0.41	0.873	0.67	1.047	0.93	1.107
0.16	0.618	0.42	0.882	0.68	1.051	0.94	1.108
0.17	0.627	0.43	0.891	0.69	1.055	0.95	1.109
0.18	0.637	0.44	0.900	0.70	1.058	0.96	1.110
0.19	0.646	0.45	0.909	0.71	1.062	0.97	1.111
0.20	0.656	0.46	0.917	0.72	1.065	0.98	1.112
0.21	0.666	0.47	0.925	0.73	1.069	0.99	1.113
0.22	0.677	0.48	0.933	0.74	1.072	1.00	1.113
0.23	0.687	0.49	0.941	0.75	1.075		
0.24	0.698	0.50	0.949	0.76	1.077		
0.25	0.708	0.51	0.956	0.77	1.080		

Table C.299: Asymptotic results for h_o = 0.537 mm, ΔT_s = 13.2°C.

r'	***h'***	***r'***	***h'***	***r'***	***h'***	***r'***	***h'***
0.00	0.345	0.26	0.637	0.52	0.959	0.78	1.106
0.01	0.346	0.27	0.652	0.53	0.968	0.79	1.109
0.02	0.348	0.28	0.667	0.54	0.976	0.80	1.112
0.03	0.351	0.29	0.682	0.55	0.984	0.81	1.115
0.04	0.356	0.30	0.697	0.56	0.992	0.82	1.117
0.05	0.362	0.31	0.711	0.57	1.000	0.83	1.119
0.06	0.369	0.32	0.725	0.58	1.007	0.84	1.122
0.07	0.378	0.33	0.739	0.59	1.015	0.85	1.124
0.08	0.387	0.34	0.753	0.60	1.021	0.86	1.126
0.09	0.397	0.35	0.767	0.61	1.028	0.87	1.128
0.10	0.408	0.36	0.780	0.62	1.034	0.88	1.129
0.11	0.420	0.37	0.794	0.63	1.040	0.89	1.131
0.12	0.432	0.38	0.806	0.64	1.046	0.90	1.133
0.13	0.445	0.39	0.819	0.65	1.052	0.91	1.134
0.14	0.459	0.40	0.832	0.66	1.057	0.92	1.135
0.15	0.473	0.41	0.844	0.67	1.063	0.93	1.137
0.16	0.487	0.42	0.856	0.68	1.068	0.94	1.138
0.17	0.501	0.43	0.867	0.69	1.072	0.95	1.139
0.18	0.516	0.44	0.879	0.70	1.077	0.96	1.140
0.19	0.531	0.45	0.890	0.71	1.081	0.97	1.141
0.20	0.546	0.46	0.900	0.72	1.085	0.98	1.142
0.21	0.561	0.47	0.911	0.73	1.089	0.99	1.143
0.22	0.576	0.48	0.921	0.74	1.093	1.00	1.144
0.23	0.592	0.49	0.931	0.75	1.097		
0.24	0.607	0.50	0.941	0.76	1.100		
0.25	0.622	0.51	0.950	0.77	1.103		

Table C.300: Asymptotic results for h_o = 0.537 mm, ΔT_s = 13.8°C.

r'	***h'***	***r'***	***h'***	***r'***	***h'***	***r'***	***h'***
0.00	0.201	0.26	0.596	0.52	0.958	0.78	1.118
0.01	0.202	0.27	0.613	0.53	0.967	0.79	1.122
0.02	0.206	0.28	0.630	0.54	0.977	0.80	1.125
0.03	0.213	0.29	0.648	0.55	0.986	0.81	1.127
0.04	0.221	0.30	0.664	0.56	0.994	0.82	1.130
0.05	0.232	0.31	0.681	0.57	1.003	0.83	1.133
0.06	0.244	0.32	0.697	0.58	1.011	0.84	1.135
0.07	0.257	0.33	0.713	0.59	1.019	0.85	1.137
0.08	0.272	0.34	0.729	0.60	1.026	0.86	1.139
0.09	0.288	0.35	0.744	0.61	1.033	0.87	1.141
0.10	0.304	0.36	0.760	0.62	1.040	0.88	1.143
0.11	0.321	0.37	0.774	0.63	1.047	0.89	1.145
0.12	0.338	0.38	0.789	0.64	1.053	0.90	1.147
0.13	0.356	0.39	0.803	0.65	1.059	0.91	1.148
0.14	0.375	0.40	0.817	0.66	1.065	0.92	1.150
0.15	0.393	0.41	0.831	0.67	1.071	0.93	1.151
0.16	0.412	0.42	0.844	0.68	1.076	0.94	1.153
0.17	0.430	0.43	0.857	0.69	1.082	0.95	1.154
0.18	0.449	0.44	0.869	0.70	1.086	0.96	1.155
0.19	0.468	0.45	0.881	0.71	1.091	0.97	1.156
0.20	0.486	0.46	0.893	0.72	1.096	0.98	1.157
0.21	0.505	0.47	0.905	0.73	1.100	0.99	1.158
0.22	0.523	0.48	0.916	0.74	1.104	1.00	1.159
0.23	0.542	0.49	0.927	0.75	1.108		
0.24	0.560	0.50	0.938	0.76	1.112		
0.25	0.578	0.51	0.948	0.77	1.115		

Table C.301: Asymptotic results for h_o = 0.588 mm, ΔT_s = 8.5°C.

r'	***h'***	***r'***	***h'***	***r'***	***h'***	***r'***	***h'***
0.00	0.762	0.26	0.856	0.52	0.987	0.78	1.042
0.01	0.762	0.27	0.862	0.53	0.991	0.79	1.043
0.02	0.763	0.28	0.868	0.54	0.994	0.80	1.044
0.03	0.764	0.29	0.873	0.55	0.997	0.81	1.045
0.04	0.765	0.30	0.879	0.56	1.000	0.82	1.046
0.05	0.766	0.31	0.885	0.57	1.003	0.83	1.046
0.06	0.768	0.32	0.891	0.58	1.006	0.84	1.047
0.07	0.770	0.33	0.896	0.59	1.009	0.85	1.047
0.08	0.773	0.34	0.902	0.60	1.012	0.86	1.048
0.09	0.776	0.35	0.908	0.61	1.014	0.87	1.049
0.10	0.779	0.36	0.913	0.62	1.017	0.88	1.049
0.11	0.782	0.37	0.919	0.63	1.019	0.89	1.049
0.12	0.786	0.38	0.924	0.64	1.021	0.90	1.050
0.13	0.790	0.39	0.929	0.65	1.023	0.91	1.050
0.14	0.794	0.40	0.934	0.66	1.025	0.92	1.051
0.15	0.798	0.41	0.939	0.67	1.027	0.93	1.051
0.16	0.803	0.42	0.944	0.68	1.029	0.94	1.051
0.17	0.808	0.43	0.949	0.69	1.031	0.95	1.052
0.18	0.812	0.44	0.954	0.70	1.032	0.96	1.052
0.19	0.818	0.45	0.958	0.71	1.034	0.97	1.052
0.20	0.823	0.46	0.963	0.72	1.035	0.98	1.052
0.21	0.828	0.47	0.967	0.73	1.037	0.99	1.052
0.22	0.834	0.48	0.971	0.74	1.038	1.00	1.053
0.23	0.839	0.49	0.976	0.75	1.039		
0.24	0.845	0.50	0.979	0.76	1.040		
0.25	0.850	0.51	0.983	0.77	1.041		

Table C.302: Asymptotic results for h_o = 0.588 mm, ΔT_s = 9.8°C.

r'	***h'***	***r'***	***h'***	***r'***	***h'***	***r'***	***h'***
0.00	0.717	0.26	0.831	0.52	0.985	0.78	1.049
0.01	0.717	0.27	0.838	0.53	0.989	0.79	1.050
0.02	0.718	0.28	0.845	0.54	0.993	0.80	1.051
0.03	0.719	0.29	0.852	0.55	0.997	0.81	1.052
0.04	0.720	0.30	0.859	0.56	1.001	0.82	1.053
0.05	0.722	0.31	0.865	0.57	1.004	0.83	1.054
0.06	0.725	0.32	0.872	0.58	1.008	0.84	1.054
0.07	0.727	0.33	0.879	0.59	1.011	0.85	1.055
0.08	0.730	0.34	0.886	0.60	1.014	0.86	1.056
0.09	0.734	0.35	0.892	0.61	1.017	0.87	1.056
0.10	0.738	0.36	0.899	0.62	1.020	0.88	1.057
0.11	0.742	0.37	0.905	0.63	1.022	0.89	1.057
0.12	0.746	0.38	0.911	0.64	1.025	0.90	1.058
0.13	0.751	0.39	0.918	0.65	1.027	0.91	1.058
0.14	0.756	0.40	0.924	0.66	1.030	0.92	1.059
0.15	0.761	0.41	0.930	0.67	1.032	0.93	1.059
0.16	0.767	0.42	0.935	0.68	1.034	0.94	1.059
0.17	0.773	0.43	0.941	0.69	1.036	0.95	1.060
0.18	0.779	0.44	0.946	0.70	1.038	0.96	1.060
0.19	0.785	0.45	0.952	0.71	1.039	0.97	1.060
0.20	0.791	0.46	0.957	0.72	1.041	0.98	1.060
0.21	0.797	0.47	0.962	0.73	1.043	0.99	1.061
0.22	0.804	0.48	0.967	0.74	1.044	1.00	1.061
0.23	0.811	0.49	0.972	0.75	1.045		
0.24	0.817	0.50	0.976	0.76	1.047		
0.25	0.824	0.51	0.981	0.77	1.048		

Table C.303: Asymptotic results for h_o = 0.695 mm, ΔT_s = 13.0°C.

r'	***h'***	***r'***	***h'***	***r'***	***h'***	***r'***	***h'***
0.00	0.695	0.26	0.883	0.52	0.981	0.78	1.036
0.01	0.696	0.27	0.889	0.53	0.983	0.79	1.037
0.02	0.698	0.28	0.895	0.54	0.985	0.80	1.039
0.03	0.702	0.29	0.901	0.55	0.988	0.81	1.040
0.04	0.707	0.30	0.906	0.56	0.990	0.82	1.041
0.05	0.713	0.31	0.911	0.57	0.993	0.83	1.043
0.06	0.720	0.32	0.916	0.58	0.995	0.84	1.044
0.07	0.727	0.33	0.921	0.59	0.997	0.85	1.045
0.08	0.736	0.34	0.925	0.60	1.000	0.86	1.046
0.09	0.744	0.35	0.929	0.61	1.002	0.87	1.047
0.10	0.753	0.36	0.933	0.62	1.004	0.88	1.048
0.11	0.762	0.37	0.937	0.63	1.007	0.89	1.049
0.12	0.771	0.38	0.941	0.64	1.009	0.90	1.050
0.13	0.780	0.39	0.944	0.65	1.011	0.91	1.051
0.14	0.789	0.40	0.948	0.66	1.013	0.92	1.052
0.15	0.798	0.41	0.951	0.67	1.016	0.93	1.054
0.16	0.807	0.42	0.954	0.68	1.018	0.94	1.055
0.17	0.816	0.43	0.957	0.69	1.020	0.95	1.057
0.18	0.824	0.44	0.960	0.70	1.022	0.96	1.059
0.19	0.833	0.45	0.962	0.71	1.024	0.97	1.061
0.20	0.841	0.46	0.965	0.72	1.026	0.98	1.064
0.21	0.848	0.47	0.968	0.73	1.028	0.99	1.067
0.22	0.856	0.48	0.971	0.74	1.030	1.00	1.070
0.23	0.863	0.49	0.973	0.75	1.031		
0.24	0.870	0.50	0.976	0.76	1.033		
0.25	0.877	0.51	0.978	0.77	1.035		

Table C.304: Asymptotic results for h_o = 0.695 mm, ΔT_s = 21.7°C.

r'	***h'***	***r'***	***h'***	***r'***	***h'***	***r'***	***h'***
0.00	0.345	0.26	0.785	0.52	0.967	0.78	1.064
0.01	0.348	0.27	0.797	0.53	0.971	0.79	1.067
0.02	0.356	0.28	0.808	0.54	0.975	0.80	1.070
0.03	0.368	0.29	0.819	0.55	0.979	0.81	1.073
0.04	0.383	0.30	0.829	0.56	0.984	0.82	1.075
0.05	0.401	0.31	0.839	0.57	0.988	0.83	1.078
0.06	0.420	0.32	0.848	0.58	0.992	0.84	1.080
0.07	0.441	0.33	0.857	0.59	0.996	0.85	1.082
0.08	0.462	0.34	0.865	0.60	1.000	0.86	1.085
0.09	0.484	0.35	0.873	0.61	1.004	0.87	1.087
0.10	0.506	0.36	0.880	0.62	1.008	0.88	1.089
0.11	0.528	0.37	0.887	0.63	1.012	0.89	1.091
0.12	0.549	0.38	0.894	0.64	1.016	0.90	1.094
0.13	0.570	0.39	0.901	0.65	1.020	0.91	1.096
0.14	0.590	0.40	0.907	0.66	1.023	0.92	1.098
0.15	0.610	0.41	0.913	0.67	1.027	0.93	1.101
0.16	0.630	0.42	0.919	0.68	1.031	0.94	1.103
0.17	0.648	0.43	0.924	0.69	1.035	0.95	1.106
0.18	0.666	0.44	0.929	0.70	1.038	0.96	1.110
0.19	0.684	0.45	0.935	0.71	1.042	0.97	1.113
0.20	0.700	0.46	0.939	0.72	1.045	0.98	1.117
0.21	0.716	0.47	0.944	0.73	1.049	0.99	1.122
0.22	0.731	0.48	0.949	0.74	1.052	1.00	1.127
0.23	0.745	0.49	0.954	0.75	1.055		
0.24	0.759	0.50	0.958	0.76	1.058		
0.25	0.772	0.51	0.962	0.77	1.061		

Table C.305: Asymptotic results for h_o = 0.695 mm, ΔT_s = 34.4°C.

r'	***h'***	***r'***	***h'***	***r'***	***h'***	***r'***	***h'***
0.00	0.000	0.26	0.907	0.52	1.162	0.78	1.289
0.01	0.056	0.27	0.924	0.53	1.168	0.79	1.293
0.02	0.110	0.28	0.940	0.54	1.173	0.80	1.296
0.03	0.162	0.29	0.955	0.55	1.179	0.81	1.299
0.04	0.213	0.30	0.970	0.56	1.184	0.82	1.303
0.05	0.261	0.31	0.984	0.57	1.190	0.83	1.306
0.06	0.307	0.32	0.997	0.58	1.195	0.84	1.308
0.07	0.352	0.33	1.009	0.59	1.201	0.85	1.311
0.08	0.394	0.34	1.021	0.60	1.206	0.86	1.314
0.09	0.435	0.35	1.032	0.61	1.211	0.87	1.316
0.10	0.474	0.36	1.043	0.62	1.216	0.88	1.319
0.11	0.512	0.37	1.053	0.63	1.221	0.89	1.321
0.12	0.548	0.38	1.062	0.64	1.226	0.90	1.323
0.13	0.582	0.39	1.071	0.65	1.232	0.91	1.326
0.14	0.615	0.40	1.080	0.66	1.236	0.92	1.328
0.15	0.646	0.41	1.088	0.67	1.241	0.93	1.331
0.16	0.676	0.42	1.096	0.68	1.246	0.94	1.333
0.17	0.705	0.43	1.104	0.69	1.251	0.95	1.336
0.18	0.732	0.44	1.111	0.70	1.256	0.96	1.339
0.19	0.758	0.45	1.118	0.71	1.260	0.97	1.343
0.20	0.783	0.46	1.125	0.72	1.265	0.98	1.347
0.21	0.806	0.47	1.132	0.73	1.269	0.99	1.351
0.22	0.828	0.48	1.138	0.74	1.273	1.00	1.356
0.23	0.849	0.49	1.144	0.75	1.278		
0.24	0.870	0.50	1.150	0.76	1.282		
0.25	0.889	0.51	1.156	0.77	1.285		

Table C.306: Asymptotic results for h_o = 0.956 mm, ΔT_s = 35.0°C.

r'	***h'***	***r'***	***h'***	***r'***	***h'***	***r'***	***h'***
0.00	0.461	0.26	0.822	0.52	0.975	0.78	1.055
0.01	0.463	0.27	0.832	0.53	0.978	0.79	1.057
0.02	0.469	0.28	0.842	0.54	0.982	0.80	1.059
0.03	0.477	0.29	0.851	0.55	0.985	0.81	1.061
0.04	0.489	0.30	0.860	0.56	0.989	0.82	1.063
0.05	0.502	0.31	0.868	0.57	0.992	0.83	1.064
0.06	0.517	0.32	0.876	0.58	0.995	0.84	1.066
0.07	0.533	0.33	0.883	0.59	0.999	0.85	1.068
0.08	0.550	0.34	0.890	0.60	1.002	0.86	1.069
0.09	0.567	0.35	0.897	0.61	1.005	0.87	1.071
0.10	0.585	0.36	0.903	0.62	1.009	0.88	1.072
0.11	0.603	0.37	0.909	0.63	1.012	0.89	1.074
0.12	0.620	0.38	0.915	0.64	1.015	0.90	1.075
0.13	0.638	0.39	0.921	0.65	1.018	0.91	1.076
0.14	0.655	0.40	0.926	0.66	1.021	0.92	1.078
0.15	0.672	0.41	0.931	0.67	1.025	0.93	1.080
0.16	0.688	0.42	0.935	0.68	1.028	0.94	1.082
0.17	0.704	0.43	0.940	0.69	1.031	0.95	1.084
0.18	0.720	0.44	0.944	0.70	1.034	0.96	1.086
0.19	0.734	0.45	0.949	0.71	1.037	0.97	1.088
0.20	0.749	0.46	0.953	0.72	1.039	0.98	1.092
0.21	0.762	0.47	0.957	0.73	1.042	0.99	1.095
0.22	0.775	0.48	0.960	0.74	1.045	1.00	1.099
0.23	0.788	0.49	0.964	0.75	1.047		
0.24	0.800	0.50	0.968	0.76	1.050		
0.25	0.811	0.51	0.971	0.77	1.052		

Table C.307: Asymptotic results for h_o = 0.956 mm, ΔT_s = 44.3°C.

r'	***h'***	***r'***	***h'***	***r'***	***h'***	***r'***	***h'***
0.00	0.020	0.26	0.766	0.52	0.970	0.78	1.072
0.01	0.052	0.27	0.780	0.53	0.974	0.79	1.075
0.02	0.097	0.28	0.794	0.54	0.979	0.80	1.078
0.03	0.140	0.29	0.806	0.55	0.983	0.81	1.081
0.04	0.183	0.30	0.818	0.56	0.987	0.82	1.083
0.05	0.224	0.31	0.829	0.57	0.992	0.83	1.086
0.06	0.263	0.32	0.840	0.58	0.996	0.84	1.088
0.07	0.301	0.33	0.849	0.59	1.000	0.85	1.090
0.08	0.337	0.34	0.859	0.60	1.005	0.86	1.092
0.09	0.372	0.35	0.868	0.61	1.009	0.87	1.094
0.10	0.405	0.36	0.876	0.62	1.013	0.88	1.096
0.11	0.437	0.37	0.884	0.63	1.017	0.89	1.098
0.12	0.467	0.38	0.892	0.64	1.021	0.90	1.100
0.13	0.496	0.39	0.899	0.65	1.025	0.91	1.102
0.14	0.524	0.40	0.905	0.66	1.030	0.92	1.104
0.15	0.550	0.41	0.912	0.67	1.034	0.93	1.107
0.16	0.575	0.42	0.918	0.68	1.038	0.94	1.109
0.17	0.599	0.43	0.924	0.69	1.041	0.95	1.112
0.18	0.622	0.44	0.930	0.70	1.045	0.96	1.115
0.19	0.644	0.45	0.935	0.71	1.049	0.97	1.118
0.20	0.664	0.46	0.941	0.72	1.053	0.98	1.122
0.21	0.684	0.47	0.946	0.73	1.056	0.99	1.127
0.22	0.702	0.48	0.951	0.74	1.060	1.00	1.132
0.23	0.719	0.49	0.956	0.75	1.063		
0.24	0.736	0.50	0.960	0.76	1.066		
0.25	0.752	0.51	0.965	0.77	1.069		

Table C.308: Asymptotic results for h_o = 0.975 mm, ΔT_s = 43.3°C.

r'	***h'***	***r'***	***h'***	***r'***	***h'***	***r'***	***h'***
0.00	0.250	0.26	0.781	0.52	0.968	0.78	1.068
0.01	0.254	0.27	0.793	0.53	0.972	0.79	1.071
0.02	0.266	0.28	0.806	0.54	0.976	0.80	1.074
0.03	0.284	0.29	0.817	0.55	0.980	0.81	1.076
0.04	0.306	0.30	0.828	0.56	0.985	0.82	1.079
0.05	0.330	0.31	0.838	0.57	0.989	0.83	1.081
0.06	0.356	0.32	0.848	0.58	0.993	0.84	1.084
0.07	0.383	0.33	0.857	0.59	0.997	0.85	1.086
0.08	0.410	0.34	0.865	0.60	1.001	0.86	1.088
0.09	0.437	0.35	0.874	0.61	1.005	0.87	1.090
0.10	0.464	0.36	0.881	0.62	1.009	0.88	1.092
0.11	0.490	0.37	0.889	0.63	1.013	0.89	1.094
0.12	0.515	0.38	0.895	0.64	1.017	0.90	1.096
0.13	0.540	0.39	0.902	0.65	1.021	0.91	1.098
0.14	0.564	0.40	0.908	0.66	1.025	0.92	1.100
0.15	0.587	0.41	0.914	0.67	1.029	0.93	1.102
0.16	0.609	0.42	0.920	0.68	1.033	0.94	1.105
0.17	0.630	0.43	0.926	0.69	1.037	0.95	1.107
0.18	0.650	0.44	0.931	0.70	1.040	0.96	1.110
0.19	0.669	0.45	0.936	0.71	1.044	0.97	1.113
0.20	0.688	0.46	0.941	0.72	1.048	0.98	1.116
0.21	0.705	0.47	0.946	0.73	1.051	0.99	1.120
0.22	0.722	0.48	0.950	0.74	1.055	1.00	1.125
0.23	0.738	0.49	0.955	0.75	1.058		
0.24	0.753	0.50	0.959	0.76	1.062		
0.25	0.767	0.51	0.964	0.77	1.065		

Table C.309: Asymptotic results for h_o = 1.026 mm, ΔT_s = 38.5°C.

r'	***h'***	***r'***	***h'***	***r'***	***h'***	***r'***	***h'***
0.00	0.610	0.26	0.775	0.52	0.982	0.78	1.064
0.01	0.610	0.27	0.785	0.53	0.987	0.79	1.066
0.02	0.611	0.28	0.795	0.54	0.993	0.80	1.067
0.03	0.613	0.29	0.804	0.55	0.998	0.81	1.068
0.04	0.615	0.30	0.813	0.56	1.002	0.82	1.069
0.05	0.618	0.31	0.823	0.57	1.007	0.83	1.070
0.06	0.622	0.32	0.832	0.58	1.011	0.84	1.071
0.07	0.626	0.33	0.841	0.59	1.015	0.85	1.072
0.08	0.630	0.34	0.850	0.60	1.019	0.86	1.073
0.09	0.635	0.35	0.859	0.61	1.023	0.87	1.074
0.10	0.641	0.36	0.868	0.62	1.027	0.88	1.075
0.11	0.647	0.37	0.876	0.63	1.030	0.89	1.075
0.12	0.654	0.38	0.885	0.64	1.034	0.90	1.076
0.13	0.661	0.39	0.893	0.65	1.037	0.91	1.076
0.14	0.668	0.40	0.901	0.66	1.040	0.92	1.077
0.15	0.676	0.41	0.909	0.67	1.042	0.93	1.077
0.16	0.684	0.42	0.917	0.68	1.045	0.94	1.078
0.17	0.693	0.43	0.924	0.69	1.048	0.95	1.078
0.18	0.701	0.44	0.931	0.70	1.050	0.96	1.079
0.19	0.710	0.45	0.939	0.71	1.052	0.97	1.079
0.20	0.719	0.46	0.945	0.72	1.054	0.98	1.079
0.21	0.728	0.47	0.952	0.73	1.056	0.99	1.079
0.22	0.737	0.48	0.958	0.74	1.058	1.00	1.080
0.23	0.747	0.49	0.965	0.75	1.060		
0.24	0.756	0.50	0.971	0.76	1.061		
0.25	0.766	0.51	0.976	0.77	1.063		

Table C.310: Asymptotic results for h_o = 1.026 mm, ΔT_s = 47.3°C.

r'	***h'***	***r'***	***h'***	***r'***	***h'***	***r'***	***h'***
0.00	0.465	0.26	0.710	0.52	0.980	0.78	1.083
0.01	0.466	0.27	0.723	0.53	0.987	0.79	1.084
0.02	0.467	0.28	0.736	0.54	0.993	0.80	1.086
0.03	0.470	0.29	0.749	0.55	0.999	0.81	1.087
0.04	0.474	0.30	0.762	0.56	1.005	0.82	1.089
0.05	0.478	0.31	0.774	0.57	1.011	0.83	1.090
0.06	0.484	0.32	0.786	0.58	1.017	0.84	1.091
0.07	0.490	0.33	0.799	0.59	1.022	0.85	1.092
0.08	0.498	0.34	0.811	0.60	1.027	0.86	1.093
0.09	0.506	0.35	0.822	0.61	1.032	0.87	1.094
0.10	0.515	0.36	0.834	0.62	1.036	0.88	1.095
0.11	0.525	0.37	0.845	0.63	1.040	0.89	1.096
0.12	0.535	0.38	0.856	0.64	1.044	0.90	1.097
0.13	0.546	0.39	0.867	0.65	1.048	0.91	1.097
0.14	0.557	0.40	0.877	0.66	1.052	0.92	1.098
0.15	0.568	0.41	0.887	0.67	1.055	0.93	1.099
0.16	0.580	0.42	0.897	0.68	1.059	0.94	1.099
0.17	0.593	0.43	0.907	0.69	1.062	0.95	1.100
0.18	0.605	0.44	0.916	0.70	1.065	0.96	1.100
0.19	0.618	0.45	0.925	0.71	1.067	0.97	1.101
0.20	0.631	0.46	0.934	0.72	1.070	0.98	1.101
0.21	0.644	0.47	0.942	0.73	1.073	0.99	1.101
0.22	0.657	0.48	0.950	0.74	1.075	1.00	1.102
0.23	0.670	0.49	0.958	0.75	1.077		
0.24	0.684	0.50	0.966	0.76	1.079		
0.25	0.697	0.51	0.973	0.77	1.081		

Table C.311: Asymptotic results for h_o = 1.026 mm, ΔT_s = 47.3°C.

r'	***h'***	***r'***	***h'***	***r'***	***h'***	***r'***	***h'***
0.00	0.465	0.26	0.710	0.52	0.980	0.78	1.083
0.01	0.466	0.27	0.723	0.53	0.987	0.79	1.084
0.02	0.467	0.28	0.736	0.54	0.993	0.80	1.086
0.03	0.470	0.29	0.749	0.55	0.999	0.81	1.087
0.04	0.474	0.30	0.762	0.56	1.005	0.82	1.089
0.05	0.478	0.31	0.774	0.57	1.011	0.83	1.090
0.06	0.484	0.32	0.786	0.58	1.017	0.84	1.091
0.07	0.490	0.33	0.799	0.59	1.022	0.85	1.092
0.08	0.498	0.34	0.811	0.60	1.027	0.86	1.093
0.09	0.506	0.35	0.822	0.61	1.032	0.87	1.094
0.10	0.515	0.36	0.834	0.62	1.036	0.88	1.095
0.11	0.525	0.37	0.845	0.63	1.040	0.89	1.096
0.12	0.535	0.38	0.856	0.64	1.044	0.90	1.097
0.13	0.546	0.39	0.867	0.65	1.048	0.91	1.097
0.14	0.557	0.40	0.877	0.66	1.052	0.92	1.098
0.15	0.568	0.41	0.887	0.67	1.055	0.93	1.099
0.16	0.580	0.42	0.897	0.68	1.059	0.94	1.099
0.17	0.593	0.43	0.907	0.69	1.062	0.95	1.100
0.18	0.605	0.44	0.916	0.70	1.065	0.96	1.100
0.19	0.618	0.45	0.925	0.71	1.067	0.97	1.101
0.20	0.631	0.46	0.934	0.72	1.070	0.98	1.101
0.21	0.644	0.47	0.942	0.73	1.073	0.99	1.101
0.22	0.657	0.48	0.950	0.74	1.075	1.00	1.102
0.23	0.670	0.49	0.958	0.75	1.077		
0.24	0.684	0.50	0.966	0.76	1.079		
0.25	0.697	0.51	0.973	0.77	1.081		

Table C.312: Asymptotic results for h_o = 1.026 mm, ΔT_s = 53.8°C.

r'	***h'***	***r'***	***h'***	***r'***	***h'***	***r'***	***h'***
0.00	0.352	0.26	0.669	0.52	0.979	0.78	1.094
0.01	0.353	0.27	0.684	0.53	0.987	0.79	1.096
0.02	0.355	0.28	0.700	0.54	0.994	0.80	1.098
0.03	0.359	0.29	0.715	0.55	1.001	0.81	1.099
0.04	0.365	0.30	0.730	0.56	1.008	0.82	1.101
0.05	0.371	0.31	0.744	0.57	1.014	0.83	1.102
0.06	0.380	0.32	0.759	0.58	1.020	0.84	1.104
0.07	0.389	0.33	0.773	0.59	1.026	0.85	1.105
0.08	0.399	0.34	0.787	0.60	1.032	0.86	1.106
0.09	0.411	0.35	0.800	0.61	1.037	0.87	1.107
0.10	0.423	0.36	0.813	0.62	1.042	0.88	1.108
0.11	0.436	0.37	0.826	0.63	1.047	0.89	1.109
0.12	0.450	0.38	0.839	0.64	1.051	0.90	1.110
0.13	0.464	0.39	0.851	0.65	1.056	0.91	1.110
0.14	0.479	0.40	0.863	0.66	1.060	0.92	1.111
0.15	0.494	0.41	0.874	0.67	1.064	0.93	1.112
0.16	0.509	0.42	0.886	0.68	1.067	0.94	1.112
0.17	0.525	0.43	0.897	0.69	1.071	0.95	1.113
0.18	0.541	0.44	0.907	0.70	1.074	0.96	1.113
0.19	0.557	0.45	0.917	0.71	1.077	0.97	1.114
0.20	0.573	0.46	0.927	0.72	1.080	0.98	1.114
0.21	0.589	0.47	0.937	0.73	1.083	0.99	1.115
0.22	0.605	0.48	0.946	0.74	1.085	1.00	1.115
0.23	0.621	0.49	0.955	0.75	1.088		
0.24	0.637	0.50	0.963	0.76	1.090		
0.25	0.653	0.51	0.972	0.77	1.092		

Table C.313: Asymptotic results for h_o = 1.026 mm, ΔT_s = 57.9°C.

r'	***h'***	***r'***	***h'***	***r'***	***h'***	***r'***	***h'***
0.00	-0.040	0.26	0.593	0.52	0.977	0.78	1.113
0.01	-0.014	0.27	0.613	0.53	0.986	0.79	1.115
0.02	0.013	0.28	0.633	0.54	0.995	0.80	1.117
0.03	0.039	0.29	0.652	0.55	1.003	0.81	1.119
0.04	0.065	0.30	0.671	0.56	1.011	0.82	1.121
0.05	0.092	0.31	0.690	0.57	1.019	0.83	1.122
0.06	0.118	0.32	0.708	0.58	1.026	0.84	1.124
0.07	0.144	0.33	0.725	0.59	1.033	0.85	1.125
0.08	0.170	0.34	0.743	0.60	1.039	0.86	1.127
0.09	0.195	0.35	0.760	0.61	1.046	0.87	1.128
0.10	0.221	0.36	0.776	0.62	1.052	0.88	1.129
0.11	0.246	0.37	0.792	0.63	1.057	0.89	1.130
0.12	0.271	0.38	0.807	0.64	1.063	0.90	1.131
0.13	0.296	0.39	0.822	0.65	1.068	0.91	1.132
0.14	0.321	0.40	0.837	0.66	1.072	0.92	1.133
0.15	0.345	0.41	0.851	0.67	1.077	0.93	1.134
0.16	0.369	0.42	0.864	0.68	1.081	0.94	1.134
0.17	0.393	0.43	0.878	0.69	1.085	0.95	1.135
0.18	0.417	0.44	0.890	0.70	1.089	0.96	1.136
0.19	0.440	0.45	0.903	0.71	1.093	0.97	1.136
0.20	0.463	0.46	0.915	0.72	1.096	0.98	1.137
0.21	0.486	0.47	0.926	0.73	1.100	0.99	1.137
0.22	0.508	0.48	0.937	0.74	1.103	1.00	1.137
0.23	0.530	0.49	0.948	0.75	1.105		
0.24	0.551	0.50	0.958	0.76	1.108		
0.25	0.572	0.51	0.968	0.77	1.111		

Table C.314: Asymptotic results for h_o = 1.134 mm, ΔT_s = 32.6°C.

r'	***h'***	***r'***	***h'***	***r'***	***h'***	***r'***	***h'***
0.00	0.698	0.26	0.881	0.52	0.980	0.78	1.036
0.01	0.699	0.27	0.887	0.53	0.983	0.79	1.038
0.02	0.701	0.28	0.893	0.54	0.985	0.80	1.039
0.03	0.705	0.29	0.899	0.55	0.987	0.81	1.041
0.04	0.709	0.30	0.904	0.56	0.990	0.82	1.042
0.05	0.715	0.31	0.910	0.57	0.992	0.83	1.043
0.06	0.722	0.32	0.915	0.58	0.994	0.84	1.045
0.07	0.729	0.33	0.919	0.59	0.997	0.85	1.046
0.08	0.737	0.34	0.924	0.60	0.999	0.86	1.047
0.09	0.745	0.35	0.928	0.61	1.001	0.87	1.048
0.10	0.753	0.36	0.932	0.62	1.004	0.88	1.049
0.11	0.762	0.37	0.936	0.63	1.006	0.89	1.051
0.12	0.771	0.38	0.940	0.64	1.008	0.90	1.052
0.13	0.779	0.39	0.943	0.65	1.010	0.91	1.053
0.14	0.788	0.40	0.947	0.66	1.013	0.92	1.054
0.15	0.797	0.41	0.950	0.67	1.015	0.93	1.055
0.16	0.806	0.42	0.953	0.68	1.017	0.94	1.057
0.17	0.814	0.43	0.956	0.69	1.019	0.95	1.058
0.18	0.823	0.44	0.959	0.70	1.021	0.96	1.060
0.19	0.831	0.45	0.962	0.71	1.023	0.97	1.062
0.20	0.839	0.46	0.965	0.72	1.025	0.98	1.064
0.21	0.847	0.47	0.967	0.73	1.027	0.99	1.067
0.22	0.854	0.48	0.970	0.74	1.029	1.00	1.069
0.23	0.861	0.49	0.973	0.75	1.031		
0.24	0.868	0.50	0.975	0.76	1.033		
0.25	0.875	0.51	0.978	0.77	1.034		

Table C.315: Asymptotic results for h_o = 1.134 mm, ΔT_s = 59.9°C.

r'	***h'***	***r'***	***h'***	***r'***	***h'***	***r'***	***h'***
0.00	0.300	0.26	0.765	0.52	0.963	0.78	1.074
0.01	0.303	0.27	0.778	0.53	0.968	0.79	1.077
0.02	0.312	0.28	0.790	0.54	0.973	0.80	1.080
0.03	0.325	0.29	0.801	0.55	0.977	0.81	1.083
0.04	0.342	0.30	0.812	0.56	0.982	0.82	1.086
0.05	0.361	0.31	0.822	0.57	0.987	0.83	1.088
0.06	0.382	0.32	0.832	0.58	0.991	0.84	1.091
0.07	0.405	0.33	0.841	0.59	0.996	0.85	1.093
0.08	0.427	0.34	0.850	0.60	1.001	0.86	1.095
0.09	0.451	0.35	0.859	0.61	1.005	0.87	1.098
0.10	0.474	0.36	0.867	0.62	1.010	0.88	1.100
0.11	0.496	0.37	0.875	0.63	1.014	0.89	1.102
0.12	0.519	0.38	0.882	0.64	1.019	0.90	1.104
0.13	0.541	0.39	0.889	0.65	1.023	0.91	1.105
0.14	0.562	0.40	0.896	0.66	1.027	0.92	1.107
0.15	0.583	0.41	0.903	0.67	1.032	0.93	1.109
0.16	0.603	0.42	0.909	0.68	1.036	0.94	1.111
0.17	0.622	0.43	0.915	0.69	1.040	0.95	1.113
0.18	0.641	0.44	0.921	0.70	1.044	0.96	1.115
0.19	0.659	0.45	0.927	0.71	1.048	0.97	1.117
0.20	0.676	0.46	0.932	0.72	1.052	0.98	1.120
0.21	0.693	0.47	0.938	0.73	1.056	0.99	1.122
0.22	0.709	0.48	0.943	0.74	1.060	1.00	1.125
0.23	0.724	0.49	0.948	0.75	1.063		
0.24	0.738	0.50	0.953	0.76	1.067		
0.25	0.752	0.51	0.958	0.77	1.070		

REFERENCES

Abdou, M. A., (1999), "Exploring Novel High Power Density Concepts for Attractive Fusion Systems," *Fusion Engineering and Design*, **45**, 2,

Ajaev, V. S. and Willis, D. A., (2003), "Thermocapillary Flow and Rupture in Films of Molten Metal on a Substrate," *Physics of Fluids*, **15**, 10,

Ajaev, V. S. and Willis, D. A., (2006), "Heat Transfer, Phase Change, and Thermocapillary Flow in Films of Molten Metal on a Substrate," *Numerical Heat Transfer; Part A: Applications*, **50**, 4,

Atherton, R. W. and Homsy, G. M., (1976), "On the Derivation of Evolution Equations for Interfacial Waves," *Chemical Engineering Communications*, **2**, 2,

Bastasz, R. and Eckstein, W., (2001), "Plasma-Surface Interactions on Liquids," *Journal of Nuclear Materials*, **290**,

Bénard, H., (1900), "Les Tourbillons Cellulaires Dans Une Nappe Liquide," *Revue Gen.Sci. Pure Appl.*, **11**,

Block, M. J., (1956), "Surface Tension as the Cause of Bénard Cells and Surface Deformation in a Liquid Film," *Nature*, **178**, 4534,

Braunsfurth, M. G. and Homsy, G. M., (1997), "Combined Thermocapillary-Buoyancy Convection in a Cavity .2. An Experimental Study," *Physics of Fluids*, **9**, 5,

Burelbach, J. P., Bankoff, S. G. and Davis, S. H., (1988), "Nonlinear Stability of Evaporating/Condensing Liquid-Films," *Journal of Fluid Mechanics*, **195**,

Burelbach, J. P., Bankoff, S. G. and Davis, S. H., (1990), "Steady Thermocapillary Flows of Thin Liquid Layers .2. Experiment," *Physics of Fluids A-Fluid Dynamics*, **2**, 3,

Chorin, A. J., (1968), "Numerical Solution of the Navier-Stokes Equations," *Math. Comp.*, **22**,

Davis, S. H., (1987), "Thermocapillary Instabilities," *Annual Review of Fluid Mechanics*, **19**,

DeSaedeleer, C., Garcimartin, A., Chavepeyer, G., Platten, J. K. and Lebon, G., (1996), "The Instability of a Liquid Layer Heated from the Side When the Upper Surface Is Open to Air," *Physics of Fluids*, **8**, 3,

Ezersky, A. B., Garcimartin, A., Burguete, J., Mancini, H. L. and Perez-Garcia, C., (1993), "Hydrothermal Coupling Waves in Marangoni Convection in a

Cylindrical Container," *Physical Review E. Statistical Physics, Plasmas, Fluids, and Related Interdisciplinary Topics*, **47**, 2,

Ezersky, A. B., Garcimartin, A., Mancini, H. L. and Perez-Garcia, C., (1993), "Spatiotemporal Structure of Hydrothermal Waves in Marangoni Convection," *Physical Review E. Statistical Physics, Plasmas, Fluids, and Related Interdisciplinary Topics*, **48**, 6,

Favre, E., Blumenfeld, L. and Daviaud, F., (1997), "Instabilities of a Liquid Layer Locally Heated on Its Free Surface," *Physics of Fluids*, **9**, 5,

Garnier, N. and Chiffaudel, A., (2001), "Two Dimensional Hydrothermal Waves in an Extended Cylindrical Vessel," *European Physical Journal B*, **19**, 1,

Gillon, P. and Homsy, G. M., (1996), "Combined Thermocapillary-Buoyancy Convection in a Cavity: An Experimental Study," *Physics of Fluids*, **8**, 11,

Goussis, D. A. and Kelly, R. E., (1990), "On the Thermocapillary Instabilities in a Liquid Layer Heated from Below," *International Journal of Heat and Mass Transfer*, **33**, 10,

Hitt, D. L. and Smith, M. K., (1993), "Radiation-Driven Thermocapillary Flows in Optically Thick Liquid Films," *Physics of Fluids A-Fluid Dynamics*, **5**, 11,

Hoyas, S., Mancho, A. M., Herrero, H., Garnier, N. and Chiffaudel, A., (2005), "Benard-Marangoni Convection in a Differentially Heated Cylindrical Cavity," *Physics of Fluids*, **17**, 5,

Juric, D. and Tryggvason, G., (1998), "Computations of Boiling Flows," *International Journal of Multiphase Flow*, **24**, 3,

Kamotani, Y., Ostrach, S. and Masud, J., (1999), "Oscillatory Thermocapillary Flows in Open Cylindrical Containers Induced by Co2 Laser Heating," *International Journal of Heat and Mass Transfer*, **42**, 3,

Kirdyashkin, A. G., (1984), "Thermogravitational and Thermocapillary Flows in a Horizontal Liquid Layer under the Conditions of a Horizontal Temperature-Gradient," *International Journal of Heat and Mass Transfer*, **27**, 8,

Koschmieder, E. L. and Biggerstaff, M. I., (1986), "Onset of Surface-Tension-Driven Bénard Convection," *Journal of Fluid Mechanics*, **167**,

Li, Y.-R., Peng, L., Akiyama, Y. and Imaishi, N., (2003), "Three-Dimensional Numerical Simulation of Thermocapillary Flow of Moderate Prandtl Number Fluid in an Annular Pool," *Journal of Crystal Growth*, **259**, 4,

Li, Y.-R., Imaishi, N., Azami, T. and Hibiya, T., (2004), "Three-Dimensional Oscillatory Flow in a Thin Annular Pool of Silicon Melt," *Journal of Crystal Growth*, **260**, 1-2,

Majeski, R., Kaita, R., Boaz, M., Efthimion, P., Gray, T., Jones, B., Hoffman, D., Kugel, H., Menard, J., Munsat, T., Post-Zwicker, A., Spaleta, J., Taylor, G., Timberlake, J., Woolley, R., Zakharov, L., Finkenthal, M., Stutman, D., Antar, G., Doerner, R., Luckhardt, S., Seraydarian, R., Maingi, R., Maiorano, M., Smith, S., Rodgers, D. and Soukhanovskii, V., (2004), "Testing of Liquid Lithium Limiters in Cdx-U," *Fusion Engineering and Design*, **72**, 1-3 SPEC ISS,

Majeski, R., Jardin, S., Kaita, R., Gray, T., Marfuta, P., Spaleta, J., Timberlake, J., Zakharov, L., Antar, G., Doerner, R., Luckhardt, S., Seraydarian, R., Soukhanovskii, V., Maingi, R., Finkenthal, M., Stutman, D., Rodgers, D. and Angelini, S., (2005), "Recent Liquid Lithium Limiter Experiments in Cdx-U," *Nuclear Fusion*, **45**, 6,

Mattas, R. F., (1998), "The Potential for Advanced Limiter/Divertor Systems," *Journal of Fusion Energy*, **17**, 3,

Mattas, R. F., Allain, J. P., Bastasz, R., Brooks, J. N., Evans, T., Hassanein, A., Luckhardt, S., McCarthy, K., Mioduszewski, P., Maingi, R., Mogahed, E., Moir, R., Molokov, S., Morely, N., Nygren, R., Rognlien, T., Reed, C., Ruzic, D., Sviatoslavsky, I., Sze, D., Tillack, M., Ulrickson, M., Wade, P. M., Wooley, R. and Wong, C., (2000), "Alps - Advanced Limiter-Divertor Plasma-Facing Systems," *Fusion Engineering and Design*, **49**,

Mercier, J. F. and Normand, C., (1996), "Buoyant-Thermocapillary Instabilities of Differentially Heated Liquid Layers," *Physics of Fluids*, **8**, 6,

Merzkirch, W., (1987), "Flow Visualization," Academic Press, Orlando,

Nield, D. A., (1964), "Surface Tension and Buoyancy Effects in Cellular Convection," *Journal of Fluid Mechanics*, **19**, 3,

Nygren, R. E., Rognlien, T. D., Rensink, M. E., Smolentsev, S. S., Youssef, M. Z., Sawan, M. E., Merrill, B. J., Eberle, C., Fogarty, P. J., Nelson, B. E., Sze, D. K. and Majeski, R., (2004), "A Fusion Reactor Design with a Liquid First Wall and Divertor," *Fusion Engineering and Design*, **72**, 1-3,

Oron, A., Davis, S. H. and Bankoff, S. G., (1997), "Long-Scale Evolution of Thin Liquid Films," *Reviews of Modern Physics*, **69**, 3,

Pearson, J. R. A., (1958), "On Convection Cells Induced by Surface Tension," *Journal of Fluid Mechanics*, **4**, 5,

Peng, L., Li, Y.-R., Shi, W.-Y. and Imaishi, N., (2007), "Three-Dimensional Thermocapillary-Buoyancy Flow of Silicone Oil in a Differentially Heated Annular Pool," *International Journal of Heat and Mass Transfer*, **50**, 5-6,

Perez-Garcia, C., Madruga, S., Echebarria, B., Lebon, G. and Burguete, J., (2004), "Hydrothermal Waves and Corotating Rolls in Laterally Heated Convection in Simple Liquids," *Journal of Non-Equilibrium Thermodynamics*, **29**, 4,

Peskin, C. S., (1977), "Numerical Analysis of Blood Flow in the Heart," *Journal of Computational Physics*, **25**, 3,

Popinet, S. and Zaleski, S., (1999), "Front-Tracking Algorithm for Accurate Representation of Surface Tension," *International Journal for Numerical Methods in Fluids*, **30**, 6,

Priede, J., Cramer, A., Bojarevics, A., Gelfgat, A. Y., Bar-Yoseph, P. Z., Yarin, A. L. and Gerbeth, G., (1999), "Experimental and Numerical Study of Anomalous Thermocapillary Convection in Liquid Gallium," *Physics of Fluids*, **11**, 11,

Rayleigh, L., (1916), "On Convection Currents in a Horizontal Layer of Fluid, When the Higher Temperature Is on the under Side," *Philosophical Magazine*, **6**, 32,

Riley, R. J. and Neitzel, G. P., (1998), "Instability of Thermocapillary-Buoyancy Convection in Shallow Layers. Part 1. Characterization of Steady and Oscillatory Instabilities," *Journal of Fluid Mechanics*, **359**,

Rognlien, T. D. and Rensink, M. E., (2001), "Interactions between Liquid-Wall Vapor and Edge Plasmas," *Journal of Nuclear Materials*, **290-293**,

Ruckenstein E and Jain, R. K., (1974), "Spontaneous Rupture of Thin Liquid-Films," *Journal of The Chemical Society-Faraday Transactions Ii*, **70**,

Schatz, M. F. and Neitzel, G. P., (2001), "Experiments on Thermocapillary Instabilities," *Annual Review of Fluid Mechanics*, **33**,

Schlichting, H., (1960), "Boundary Layer Theory," McGraw-Hill, New York,

Schwabe, D., Moller, U., Schneider, J. and Scharmann, A., (1992), "Instabilities of Shallow Dynamic Thermocapillary Liquid Layers," *Physics of Fluids A-Fluid Dynamics*, **4**, 11,

Schwabe, D., Cramer, A., Schneider, J., Benz, S. and Metzger, J., (1999), "Experiments on the Multi-Roll-Structure of Thermocapillary Flow in Side-Heated Thin Liquid Layers," *Advances in Space Research*, **24**, 10,

Schwabe, D. and Benz, S., (2002), "Thermocapillary Flow Instabilities in an Annulus under Microgravity - Results of the Experiment Magia," *Advances in Space Research*, **29**, 4,

Scriven, L. E. and Sternling, C. V., (1960), "Marangoni Effects," *Nature*, **187**, 4733,

Scriven, L. E. and Sternling, C. V., (1964), "On Cellular Convection Driven by Surface-Tension Gradients - Effects of Mean Surface Tension and Surface Viscosity," *Journal of Fluid Mechanics*, **19**, 3,

Sen, A. K. and Davis, S. H., (1982), "Steady Thermocapillary Flows in Two-Dimensional Slots," **121**,

Settles, G. S., (2001), "Schlieren and Shadowgraph Techniques : Visualizing Phenomena in Transparent Media," *Experimental Fluid Mechanics*, Springer, New York

Sheth, K. S. and Pozrikidis, C., (1995), "Effects of Inertia on the Deformation of Liquid Drops in Simple Shear Flow," *Computers & Fluids*, **24**, 2,

Shevtsova, V. M. and Legros, J. C., (2003), "Instability in Thin Layer of Liquid Confined between Rigid Walls at Different Temperatures," *Acta Astronautica*, **52**, 7,

Shin, S. and Juric, D., (2002), "Modeling Three-Dimensional Multiphase Flow Using a Level Contour Reconstruction Method for Front Tracking without Connectivity," *Journal of Computational Physics*, **180**, 2,

Shin, S., Abdel-Khalik, S. I. and Yoda, M., (2005), "Design Constraints for Liquid-Protected Divertors," *Fusion Science and Technology*, **47**, 3,

Sim, B.-C. and Zebib, A., (2002), "Thermocapillary Convection with Underformable Curved Surfaces in Open Cylinders," *International Journal of Heat and Mass Transfer*, **45**, 25,

Sim, B.-C., Kim, W.-S. and Zebib, A., (2004), "Axisymmetric Thermocapillary Convection in Open Cylindrical Annuli with Deforming Interfaces," *International Journal of Heat and Mass Transfer*, **47**, 24,

Smith, M. K. and Davis, S. H., (1983), "Instabilities of Dynamic Thermocapillary Liquid Layers. Part 1. Convective Instabilities," *Journal of Fluid Mechanics*, **132**,

Smith, M. K. and Davis, S. H., (1983), "Instabilities of Dynamic Thermocapillary Liquid Layers. Part 2. Surface-Wave Instabilities," *Journal of Fluid Mechanics*, **132**,

Smith, M. K., (1986), "Instability Mechanisms in Dynamic Thermocapillary Liquid Layers," *Physics Of Fluids*, **29**, 10,

Takashima, M., (1981), "Surface-Tension Driven Instability in a Horizontal Liquid Layer with a Deformable Free-Surface .1. Stationary Convection," *Journal of The Physical Society of Japan*, **50**, 8,

Tan, M. J., Bankoff, S. G. and Davis, S. H., (1990), "Steady Thermocapillary Flows of Thin Liquid Layers .1. Theory," *Physics of Fluids A-Fluid Dynamics*, **2**, 3,

Torres, D. J. and Brackbill, J. U., (2000), "The Point-Set Method: Front-Tracking without Connectivity," *Journal of Computational Physics*, **165**, 2,

Unverdi, S. O. and Tryggvason, G., (1992), "A Front-Tracking Method for Viscous, Incompressible, Multi-Fluid Flows," *Journal of Computational Physics*, **100**, 1,

Unverdi, S. O. and Tryggvason, G., (1992), "Computations of Multifluid Flows," *Physica D*, **60**, 1-4,

Vanhook, S. J., Schatz, M. F., Swift, J. B., McCormick, W. D. and Swinney, H. L., (1997), "Long-Wavelength Surface-Tension-Driven Bénard Convection: Experiment and Theory," *Journal of Fluid Mechanics*, **345**,

Villers, D. and Platten, J. K., (1992), "Coupled Buoyancy and Marangoni Convection in Acetone - Experiments and Comparison with Numerical Simulations," *Journal Of Fluid Mechanics*, **234**,

Wells, W. M., (1981), "System for Handling Divertor Ion and Energy Flux Based on a Lithium Droplet Cloud," *Nuclear Technology/Fusion*

1, 1,

Williams, M. B. and Davis, S. H., (1982), "Nonlinear Theory of Film Rupture," *Journal of Colloid and Interface Science*, **90**, 1,

Yeo, L. Y., Craster, R. V. and Matar, O. K., (2003), "Marangoni Instability of a Thin Liquid Film Resting on a Locally Heated Horizontal Wall," *Physical Review E*, **67**, 5,